INFORMATION TO USERS

This material was produced from a microfilm copy of the original document. While the most advanced technological means to photograph and reproduce this document have been used, the quality is heavily dependent upon the quality of the original submitted.

The following explanation of techniques is provided to help you understand markings or patterns which may appear on this reproduction.

1. The sign or "target" for pages apparently lacking from the document photographed is "Missing Page(s)". If it was possible to obtain the missing page(s) or section, they are spliced into the film along with adjacent pages. This may have necessitated cutting thru an image and duplicating adjacent pages to insure you complete continuity.

2. When an image on the film is obliterated with a large round black mark, it is an indication that the photographer suspected that the copy may have moved during exposure and thus cause a blurred image. You will find a good image of the page in the adjacent frame.

3. When a map, drawing or chart, etc., was part of the material being photographed the photographer followed a definite method in "sectioning" the material. It is customary to begin photoing at the upper left hand corner of a large sheet and to continue photoing from left to right in equal sections with a small overlap. If necessary, sectioning is continued again — beginning below the first row and continuing on until complete.

4. The majority of users indicate that the textual content is of greatest value, however, a somewhat higher quality reproduction could be made from "photographs" if essential to the understanding of the dissertation. Silver prints of "photographs" may be ordered at additional charge by writing the Order Department, giving the catalog number, title, author and specific pages you wish reproduced.

5. PLEASE NOTE: Some pages may have indistinct print. Filmed as received.

Xerox University Microfilms
300 North Zeeb Road
Ann Arbor, Michigan 48106

THE EMISSION FROM PULSARS:

I. A GENERALIZED SINGLE-VECTOR POLARIZATION MODEL

II. A MODEL FOR THE SUB-PULSE AND INTEGRATED PULSE BEHAVIOR

by

Dale Curtis Ferguson

A Dissertation Submitted to the Faculty of the

DEPARTMENT OF ASTRONOMY

In Partial Fulfillment of the Requirements
For the Degree of

DOCTOR OF PHILOSOPHY

In the Graduate College

THE UNIVERSITY OF ARIZONA

1 9 7 4

THE UNIVERSITY OF ARIZONA

GRADUATE COLLEGE

I hereby recommend that this dissertation prepared under my direction by Dale Curtis Ferguson

entitled The Emission From Pulsars: I. A Generalized Single-Vector Polarization Model II. A Model for the Sub-Pulse and Integrated Pulse Behavior

be accepted as fulfilling the dissertation requirement of the degree of Doctor of Philosophy

William J. Cocke — November 12, 1974
Dissertation Director — Date

After inspection of the final copy of the dissertation, the following members of the Final Examination Committee concur in its approval and recommend its acceptance:*

B. J. Rickett	November 6th 1974
T. A. Scott	Nov. 12, 1974
[illegible]	Nov. 12, 1974
[illegible]	" " "

*This approval and acceptance is contingent on the candidate's adequate performance and defense of this dissertation at the final oral examination. The inclusion of this sheet bound into the library copy of the dissertation is evidence of satisfactory performance at the final examination.

STATEMENT BY AUTHOR

This dissertation has been submitted in partial fulfillment of requirements for an advanced degree at The University of Arizona and is deposited in the University Library to be made available to borrowers under rules of the Library.

Brief quotations from this dissertation are allowable without special permission, provided that accurate acknowledgment of source is made. Requests for permission for extended quotation from or reproduction of this manuscript in whole or in part may be granted by the head of the major department or the Dean of the Graduate College when in his judgment the proposed use of the material is in the interests of scholarship. In all other instances, however, permission must be obtained from the author.

SIGNED: Dale C. Ferguson

DEDICATION

I would like to dedicate this dissertation to my grandfather, Curby Wheeler, who died in 1974. He was a natural philosopher and sceptic of science, and he knew the sky as well as anyone. To him I owe a healthy scepticism of scientific dogma. I will remember him always.

ACKNOWLEDGMENTS

I would like to thank Dr. W. J. Cocke for his unlimited encouragement and helpful discussions about my pulsar work, as well as for his efforts to observationally verify many of its predictions. Alice Ferguson deserves much of the credit for my ability to persevere to the completion of this dissertation, because of her help in typing the rough draft, her command of the English language in helping me edit it, and her infinite amounts of good advice and encouragement when I sorely needed them.

I would also like to thank Dr. R. N. Manchester and Dr. John M. Rankin for making certain papers and data available before publication.

TABLE OF CONTENTS

LIST OF TABLES

LIST OF ILLUSTRATIONS

LIST OF ILLUSTRATIONS--Continued

LIST OF ILLUSTRATIONS--Continued

LIST OF ILLUSTRATIONS--Continued

LIST OF ILLUSTRATIONS--Continued

LIST OF ILLUSTRATIONS--Continued

LIST OF ILLUSTRATIONS--Continued

LIST OF ILLUSTRATIONS--Continued

LIST OF ILLUSTRATIONS--Continued

LIST OF ILLUSTRATIONS--Continued

LIST OF ILLUSTRATIONS--Continued

ABSTRACT

In Part I, the properties of models for pulsar polarization which incorporate localized emission regions corotating with a neutron star are investigated. The formulae applicable to the case where emission comes from near the neutron star surface are derived and compared with those applicable for emission from further out in the magnetosphere. In all the models investigated, it is assumed that the instantaneous polarization position angle is given by the apparent projection of a corotating magnetic field vector on the plane of the sky, and that the percentage of linear polarization is proportional to some power of the apparent projected length of the vector along the line of sight.

Relativistic effects which become important for emission from far out in the magnetosphere are thoroughly discussed and related to the polarization behavior predicted by the models. The relativistic vector model proposed by the author in 1973 is generalized so that arbitrary orientations of the magnetic field vector may be incorporated. Extensive illustrations show the properties of models with widely varying parameters.

In Part II, the pulsar observations believed important for an understanding of their physical nature are discussed. Afterward comes a critical discussion of two previous models for pulsar emissions.

Pulsar PSR 0329+54 provides a detailed look at properties of a typical pulsar. It is shown that if the radiation is cyclotron or single electron synchrotron radiation then the emission frame is in rapid motion relative to the observer. Physical arguments are used to derive properties of an emission region. If the radiation is of the single electron synchrotron pattern, the magnetic field strength is lower than the most likely dipole field strength at the radius of the speed-of-light cylinder. If the radiation is cyclotron, the emission region is too large to produce coherence by a single bunch.

Possible mechanisms for producing broad band individual pulse (sub-pulse) radiation are discussed. Evidence that two different emission mechanisms might be in operation is reviewed. The interesting marching sub-pulses find a possible explanation in terms of a changing distance of emission regions from the neutron star, and multiple integrated pulse profiles may be cases where both ends of a magnetic vector sweep past our line of sight in a short time, because of relativistic effects.

Also, the relativistic vector model is fit to several pulsars which represent different classes in a popular classification scheme. The Crab Nebula pulsar is discussed in detail. Using the several model fits, based only on polarization behavior, a tentative relation between the corotational velocity of an emission region and the period of its rotation is found. This relation yields a possible theoretical period-sub-pulse-width distribution. Further discussion of the period-sub-pulse-width diagram lends credence to the idea that the emission from pulsars is beamed even in the corotating emission frame. Finally, guidelines for possible theoretical models of the emission are presented.

THE GENERALIZED SINGLE VECTOR POLARIZATION MODEL

The currently accepted theory that pulsars are rotating neutron stars of strong magnetic field is based on three important pieces of evidence. One is that the Crab nebula pulsar exhibits light variations on a time scale of a fraction of a millisecond. Since any varying source must have dimensions smaller than the distance light can travel in the time of variation, this restricts the size of the emission region of the Crab Nebula pulsar to something less than a few tens of kilometers in diameter. This is about the size of a neutron star.

The second piece of evidence is the high regularity of the period of pulsation of all pulsars, combined with the fact that all pulsars seem to be slowing down. Such behavior seems consistent with an interpretation that pulsars are rotating objects, gradually slowing down due to a loss of rotational energy.

The third piece of evidence is the smooth variation of the position angle of linear polarization through the pulse, which the radiation from many pulsars exhibits. This is consistent with a variation of the aspect of a magnetic field vector as it is carried by rotation past the

line of sight. The polarizations observed would be due to alignment of radiating particles by the strong magnetic field.

It is with the third basic piece of evidence that this dissertation is concerned. It is an investigation of the properties of polarization models based on single magnetic (or other) particle alignment vectors which are carried by rotation past the line of sight. In Part I, the single vector model which was originally proposed for emission assumed to come from the surface of the neutron star is generalized to the case where the emission might come from a localized region located anywhere in the magnetonsphere of the neutron star and for an arbitrary field line direction in the reference frame of the emission region. In Part II, an attempt is made to see whether a single vector model or a combination of several single vector models might account for the polarization behavior observed in the radiation from pulsars. Physical arguments will be used to investigate the plausibility of such models, and whether our physical knowledge at present enables us to narrow down the possible location and physical characteristics of the regions from which the radiation comes.

A. The Non-Relativistic Model

Radhakrishnan and Cooke (1969) proposed the non-relativistic single vector model to explain the regular variation of position angle of the polarization of radio signals from the Vela pulsar. The variation had been observed by Radhakrishnan et al. (1969) at a frequency of 1720 MHz in the previous year. In order to understand any single vector model, one should start his studies with theirs.

In their model, which was later also applied to the Crab Nebula pulsar (Wampler et al. 1969, Disney 1971, Kristian et al. 1970), the radiation comes from the region of a magnetic polar cap near the surface of a neutron star. The narrow pulse of radiation is observed when this polar cap of diverging magnetic field lines is swept by the rotation of the neutron star past the observer's line of sight. The radiation presumably comes in a narrow pulse because the radiating particles are constrained to certain preferred magnetic field lines very near the magnetic pole and beam their radiation outward along these field lines. At any given time, the radiation we see comes mainly from particles streaming along the field lines which are pointing most nearly along our line of sight. If the pulsar's magnetic field near the surface is a nearly perfect dipole field, the resultant position angle of the

radiation observed at a given time is then either parallel (in the case of curvature radiation) or perpendicular (in the case of synchrotron radiation) to the apparent direction of the dipole axis at that time. See Figure 1, adapted from Radhakrishnan and Cooke (1969). As the neutron star rotates, this position angle varies, always so as to keep step with the apparent direction of the dipole axis. Clearly, in such a model, the "single vector" (see Lyne, Smith and Graham, 1971) is the dipole axis of the pulsar's magnetic field.

The quantitative result for the variation of the position angle can be found from looking at Figure 2 of Ferguson (1973) which is reproduced as Figure 2 here. In this figure and in all of the dissertation to follow, L is the angle between the pulsar rotation equator and the magnetic field line, T is the angle between the plane of the sky and the rotation axis, Ψ is the apparent position angle of the alignment axis $\vec{B}$ on the plane of the sky relative to the rotation axis $\vec{\Omega}$, θ is defined as Ωt, where Ω is the angular frequency and t is the time after the point of emission (or the magnetic pole) was travelling most nearly toward us. b is an intermediate angle.

One can find, from the law of cosines, that

$$\sin L = \sin T \cos b + \sin b \cos T \cos \Psi \qquad (1)$$

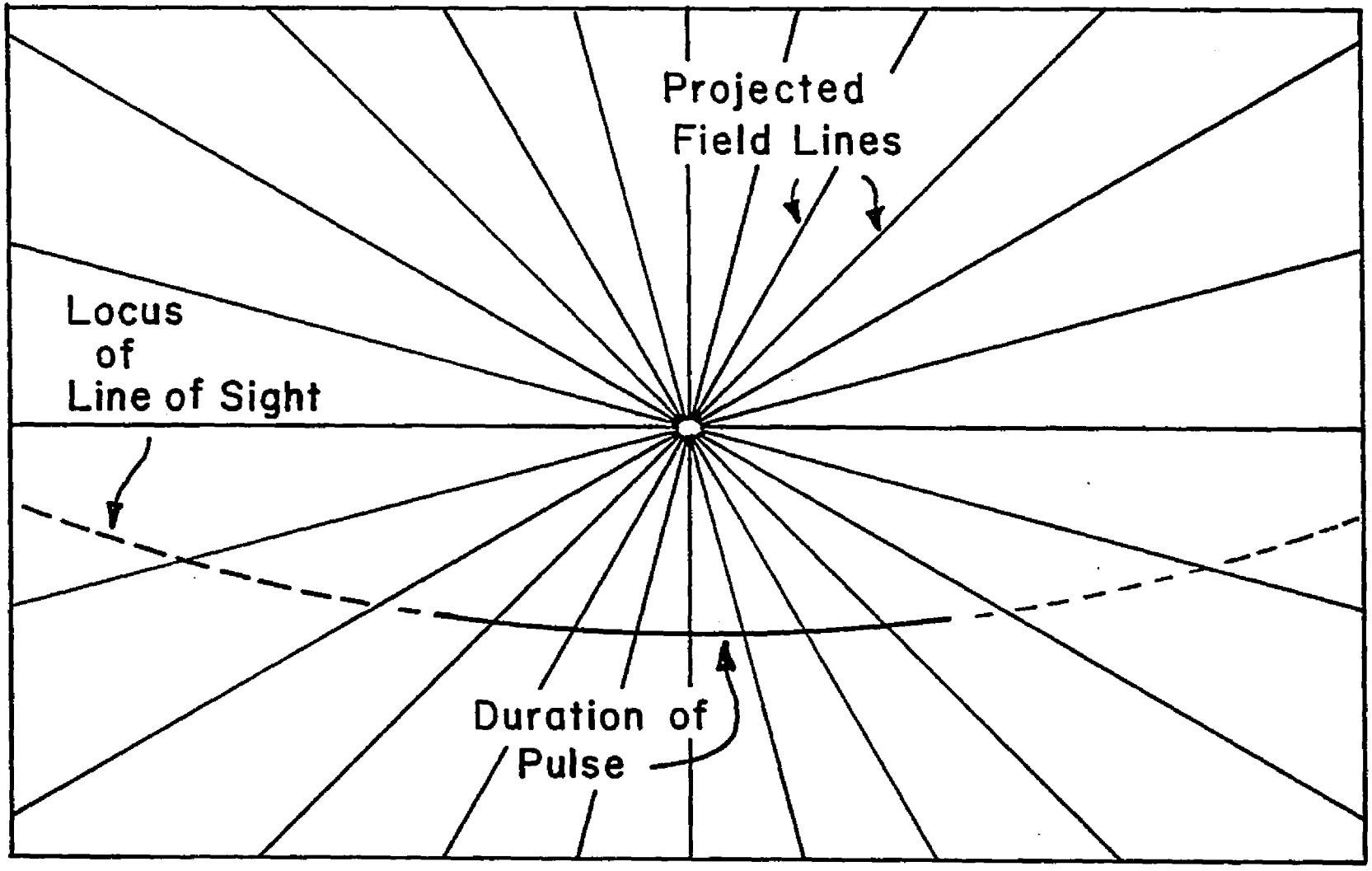

Figure 1. Magnetic Field Lines Near the Neutron Star Magnetic Polar "Cap"

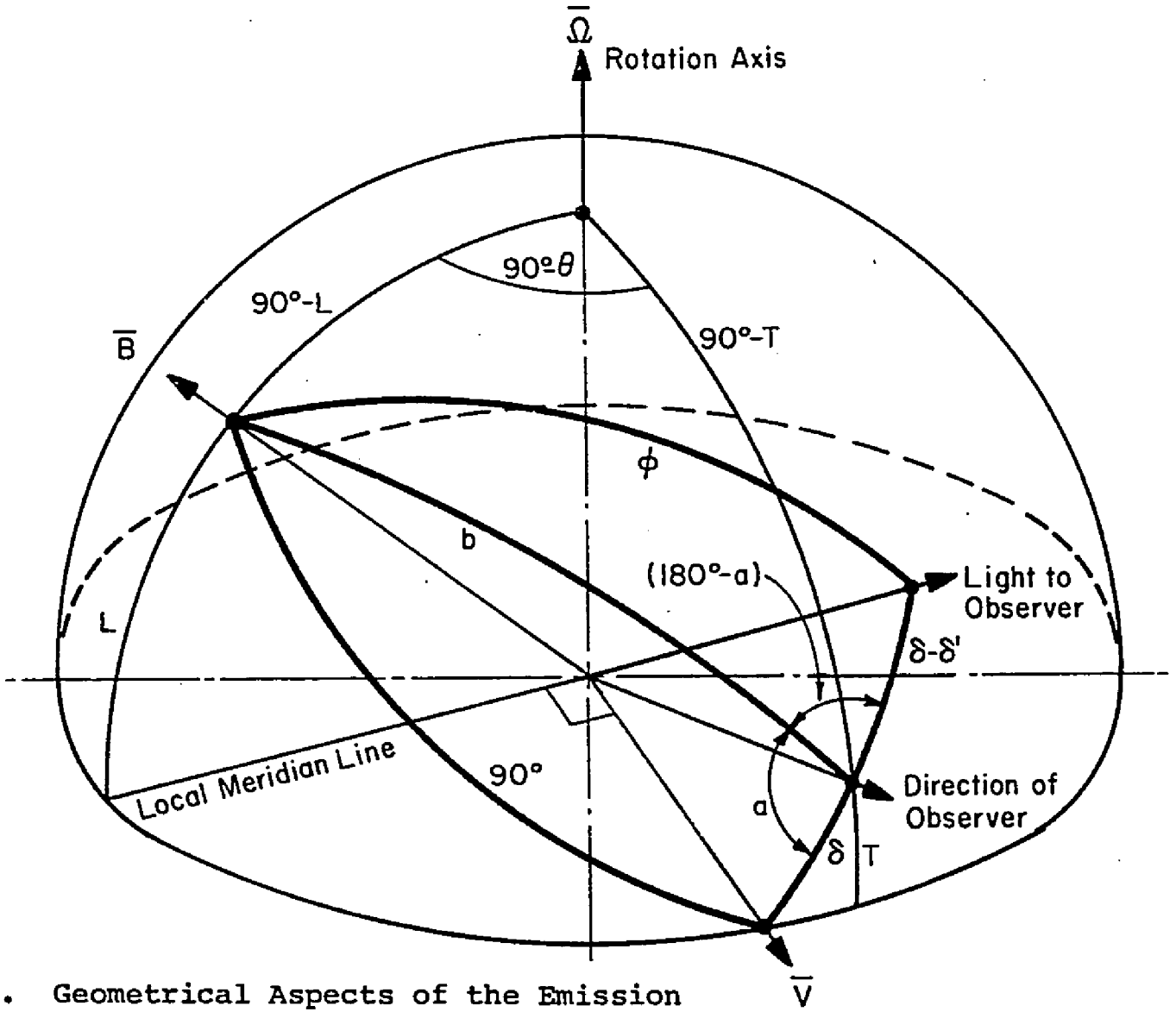

Figure 2. Geometrical Aspects of the Emission

and

$$\cos b = \sin T \sin L + \cos T \cos L \sin \theta \qquad (2)$$

and from the law of sines that

$$\frac{\sin b}{\cos \theta} = \frac{\cos L}{\sin \Psi} \quad . \qquad (3)$$

From (1) and (3) we find that

$$\sin L = \sin T \cos b + \frac{\cos L \cos \theta \cos \Psi \cos T}{\sin \Psi}$$

or that

$$\operatorname{ctn} \Psi = \frac{\sin L - \sin T \cos b}{\cos L \cos \theta \cos T} \quad , \qquad (4)$$

but using (2) and (4) we find that

$$\operatorname{ctn} \Psi = \frac{\sin L - \sin^2 T \sin L - \sin T \cos T \cos L \sin \theta}{\cos L \cos \theta \cos T}$$

$$= \frac{\sin L \cos^2 T - \sin T \cos T \cos L \sin \theta}{\cos L \cos \theta \cos T}$$

$$= \frac{\sin L \cos T - \sin T \cos L \sin \theta}{\cos L \cos \theta}$$

$$= (\tan L \cos T - \sin T \sin \theta)/\cos \theta \quad ,$$

or

$$\tan(90°-\Psi) = (\tan L \cos T - \sin T \sin \theta)/\cos \theta \quad , \tag{5}$$

which is in agreement with Wampler, Scargle, and Miller (1969), where the polarization of the radiation is assumed perpendicular to the apparent projection of the magnetic axis.

As Disney (1971) points out, in such a model, the polarization should be greatest when the magnetic axis is furthest from the observer's line of sight, for then the limited range of magnetic field lines from which emission is coming are apparently lined up in projection upon the sky, and the linear polarization Stokes parameters for the emission will add up to a large amount. Unless, of course, Q and U for the emission process are very small for large angles from the magnetic axis. When we are looking straight down into the magnetic polar cap, however, the field lines will have radial projections, and their linear polarization Stokes parameters should largely cancel. Thus, one might expect a linear polarization behavior to go as $P \simeq P_o \sin^n \phi$ (6) (see Ferguson, 1973) where ϕ is the angle between the line of sight and the magnetic axis, P_o is a scale factor, and n is a parameter depending on peculiarities of the emission.

For cyclotron radiation, which has the intrinsic $P \approx \sin^3 \phi$, this relation is good, as it is for synchrotron radiation from an isotropic electron distribution, which has an intrinsic linear polarization which does not depend on ϕ. However, for synchrotron radiation from particles with very small pitch angles (pitch angle $<< \frac{1}{\gamma}$ of the particles), and for curvature radiation from ultra-relativistic particles, the intrinsic linear polarization amount depends on the angle the observer makes with the plane containing the velocity and acceleration vectors of the radiating particles at the source, and thus cannot really be specified by a single vector. We will discuss the applicability of the model in such cases in Section I.C.1.

It should be mentioned at this stage that this non-relativistic single vector model for pulsar polarizations is identical in every quantitative respect with the oblique rotator model for the polarization of magnetic Ap stars. (See for example, Kemp and Wolstencroft, 1974). Later in this dissertation, plots of polarization angle and amount versus fraction of period and versus each other are presented, as calculated on the basis of the single vector model. The non-relativistic plots in that section will be applicable to the interpretation of the polarizations of magnetic Ap stars as well as pulsars.

B. The Generalized Relativistic Vector Model

If the emission from pulsars does not come from the surface, but instead comes from regions of the magnetosphere co-rotating with the neutron star, certain relativistic effects may become important. First of all, the aberration of light becomes significant, producing an apparent rotation of the emission frame of reference. Second, the time interval of observation of a signal from a small region becomes compressed as compared to the time interval of emission, due to the effects of changing light travel times as the emission region co-rotates with the star. Third, the observed intensity of the radiation from the source will differ from that which would be measured in the reference frame of the emission region. This is because of the aberration of light and the Doppler effect in special relativity. These factors make dealing with radiation from a relativistically orbiting source both complicated to calculate and interesting in the effects produced.

In this section, we will deal with radiation coming from a localized region in the magnetosphere of the neutron star. By "localized", we mean small enough that the light travel time across it is short compared to the time of change of observed quantities, and which may be said to have a magnetic field characterized by a single vector.

Now, instead of considering the radiation to be coming from whatever field line is pointing most directly toward us, we will assume that it comes only from one spot on one field line, and that the sweep of position angle of the observed radiation is due to the varying apparent projection of that field line on the plane of the sky as the source co-rotates with the neutron star. We will think of the local magnetic field direction at that point as if it were a rod, rigidly fixed in the co-rotating frame.

First, let us deal with the change in intensity between the frames of source and observer. If we let θ now be the phase angle of the emission region in its orbit (measured from when the source is moving most nearly towards the observer) and δ be the angle between source motion and the radiation we observe, δ' be the angle between source motion and the emitted radiation in the emission frame, $I(\nu)$ be the intensity we observe at the frequency ν, $I'(\nu')$ be the intensity emitted at the frequency ν' in the emission frame, we find from Pacholczyk (1970) that

$$\frac{I(\nu)}{I'(\nu')} = \frac{1}{\gamma^3(1-\beta\cos\delta)^3}$$

where $\gamma = (1-\beta^2)^{-\frac{1}{2}}$ and $\beta = v/c$, v being the speed of

co-rotation. The relation between ν' and ν is given in the theory of relativity by

$$\nu = \nu'/\gamma\ (1-\beta \cos \delta) \ .$$

However, we want $\frac{I(\nu)}{I'(\nu)}$. Since

$$R \equiv \frac{I(\nu)}{I'(\nu)} = \frac{I(\nu)}{I'(\nu')} \frac{I'(\nu')}{I'(\nu)}$$

we must find $\frac{I'(\nu')}{I'(\nu)} = Y$ for the source, and this depends only on the emission spectrum. Let us call

$$\frac{1}{\gamma(1-\beta \cos \delta)} = X \ .$$

Then,

$$R = YX^3 \ .$$

For a power law spectrum $I \propto \nu^{-\varepsilon}$,

$$Y = X^{\varepsilon}$$

so that

$$R = X^{3+\varepsilon} = [\gamma(1-\beta \cos \delta)]^{-3-\varepsilon} \qquad (7)$$

(See Ferguson, 1971a.) For a black body spectrum

$$I \propto \frac{\nu^3/c^2}{e^{h\nu/kT} - 1} \ ,$$

$$Y = \frac{I'(\nu')}{I'(\nu)} = \frac{(\nu')^3/c^2}{(\nu)^3/c^2} \quad \frac{e^{h\nu/kT} - 1}{e^{h\nu'/kT} - 1}$$

$$= \frac{\nu^3}{X^3\ \nu^3} \quad \frac{e^{h\nu/kT} - 1}{e^{h\nu/XkT} - 1}$$

$$= \frac{1}{X^3} \quad \frac{e^{h\nu/kT} - 1}{e^{h\nu/XkT} - 1}$$

and

$$R = X^3 Y = \frac{e^{h\nu/kT} - 1}{e^{h\nu/XkT} - 1} \quad . \qquad (8)$$

Now, what is R in terms of θ and T, where T is defined again as the tilt of the rotation axis of the neutron star out of the plane of the sky? In this case,

$$\cos \delta = \cos \theta \cos T$$

so that

$$X = \frac{1}{\gamma(1-\beta \cos \delta)} = \frac{1}{\gamma(1-\beta \cos \theta \cos T)}$$

and the formulae (7) and (8) apply with X as defined above.

For an excellent discussion of the relativistic beaming formula and its derivation, see McCrea (1972).

Now let us enter into a discussion of the time of observation versus the time of emission. For a non-relativistic rotator, $t = \theta/\Omega$ where t is a time of

observation, counting the observation of radiation from the source at $\theta = 0$ (when the source is travelling most nearly toward us) as $t = 0$. For a relativistic rotator, one must worry about light travel times across the orbit. Since the light travel time from the position which the emission region occupies at $\theta = 0$ is $(r \sin\theta \cos T)/c$, and $v = \Omega r$, the light travel time is $(\beta \sin\theta \cos T)/\Omega$, making the time of observation (relative to the time of observation of light from the $\theta = 0$ position)

$$t = (\theta - \beta \sin\theta \cos T)/\Omega \ , \qquad (8.5)$$

(see Smith, 1970) whereas the time of emission remains $t = \theta/\Omega$.

Now we have derived the effects which are easily seen to result from relativistic orbiting of an emission region. The effects which are caused by the apparent rotation of a moving reference frame (see Ferguson, 1971b) are more difficult to derive. These effects manifest themselves in a change of the angle and amount of polarization of radiation as seen by the observer and the emitter. A detailed discussion of these effects for the case where the magnetic field (or other) particle alignment vector lies in the meridian plane of the emission region is given in Ferguson (1973) and corrected in Ferguson et al. (1974).

It is applied to the optical observations of the Crab Nebula pulsar in Cocke et al. (1973), and Ferguson et al. (1974).

In the general case, the magnetic field line is not constrained to the meridian plane of the emission frame. This is the problem we will consider now.

I choose to look at the geometrical problems in the following way: I will assume that the amount and angle of polarization observed by an outside observer is the same as would be seen by an observer in the reference frame of the emission if he were looking down along the line that light must take in that frame to reach the outside observer. Later on, I will justify this procedure. Thus, I will mainly deal with pictures and derivations based on the reference frame in which the emission takes place, only at the last step making the transition from the emission frame to the observer's frame.

As before, let $\vec{\Omega}$ be the axis of neutron star rotation (or of the assumed circular orbit of the emission frame), $\vec{B}$ be the direction of the magnetic field vector, L be the angle $\vec{B}$ makes with the rotation equator, T be the angle the rotation axis makes with the plane of the sky, θ be the phase angle in the orbit since the emission region was travelling most directly toward the observer, $\vec{v}$ be the instantaneous velocity vector and now let A be the angle

in the emission frame between the meridian plane ($\perp$ to the velocity vector) and the plane containing $\vec{\Omega}$ and $\vec{B}$, counted positive if $\vec{B}$ points more toward $\vec{v}$ and negative if away from $\vec{v}$. We let A take on values only between -90° and +90°, since $\vec{B}$ would otherwise be ambiguous. (See Figure 3.)

Let the "common vector" be defined as it was in Ferguson (1973) to be the direction perpendicular both to the velocity vector and the direction which light must take to reach the observer. This "common vector" is the axis of the instantaneous apparent rotation of the moving reference frame, and thus is the only vector whose direction is not apparently distorted by the aberration of light. It lies an angle M away from the rotation axis. Now let δ be the angle between the velocity $\vec{v}$ and the true direction of the observer, and δ' be the angle between $\vec{v}$ and the direction in which light must be emitted to reach the observer in the emission frame. Again, let ϕ be the angle between $\vec{B}$ and the light to the observer. From Ferguson (1973) we find that

$$\cos \delta = \cos T \cos \theta \tag{9}$$

and

$$\tan \delta' = \frac{\sin \delta}{\gamma(\cos \delta - \beta)} \tag{10}$$

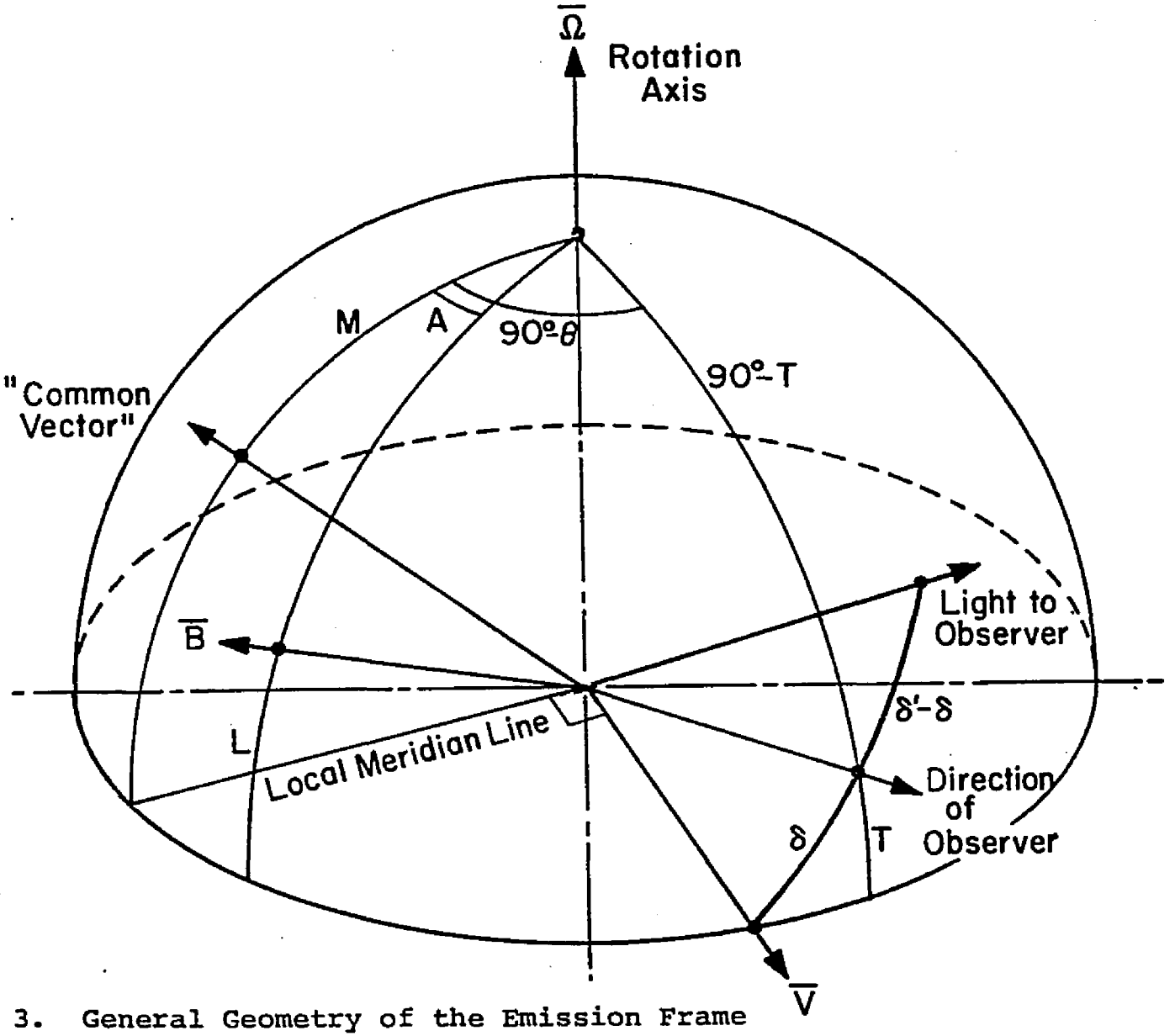

Figure 3. General Geometry of the Emission Frame

where γ and β have the definitions given previously in this dissertation.

We may find ϕ from Figure 4 and the law of cosines (hereafter called LOC). Here, C, b and a are intermediate quantities. By LOC,

$$\cos b = \sin L \sin T + \cos L \cos T \cos(90°-\theta-A) \tag{11}$$

Now $\cos C = \cos L \sin A + \sin L \cos A \cos 90°$ by LOC and thus

$$\cos C = \cos L \sin A$$

but

$$\cos C = \cos \delta \cos b + \sin b \sin \delta \cos a$$

or

$$\cos a = \frac{\cos C - \cos \delta \cos b}{\sin b \sin \delta} = - \cos (180°-a) \quad .$$

Now again by LOC,

$$\cos \phi = \cos b \cos (\delta'-\delta) + [\sin b \sin (\delta'-\delta) \cos (180°-a)] \tag{12}$$

which reduces to

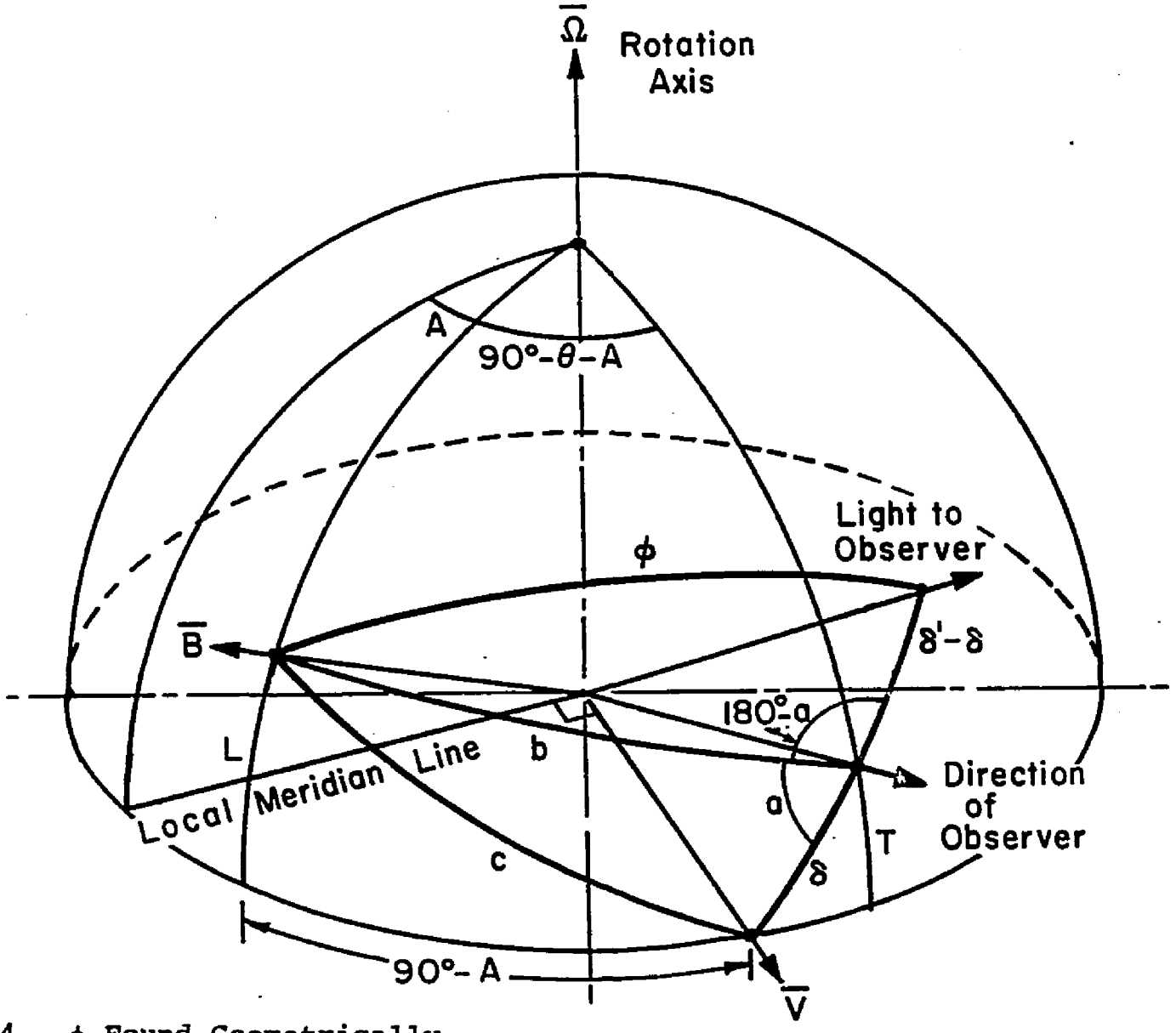

Figure 4. ϕ Found Geometrically

$$\cos \phi = \cos b \cos (\delta'-\delta) - [\frac{\sin(\delta'-\delta)}{\sin \delta}$$

$$(\cos L \sin A - \cos \delta \cos b)]$$

which may be evaluated through Equations (9), (10) and (11) for ϕ in terms of θ, β, T, A and L.

For A = 0°, Equation (12) reduces to

$$\cos \phi = \cos b \cos (\delta'-\delta) + \frac{\sin(\delta'-\delta)}{\sin \delta} \cos \delta \cos b$$

$$= \cos b[\cos(\delta'-\delta) + \frac{\sin(\delta'-\delta)}{\tan \delta}]$$

which agrees with Equation (6) of Ferguson (1973).

M (the angle the common vector makes with the rotation axis in the emission frame) may be found from Figure 5 (taken from Ferguson 1973) and the LOC thusly:

$$\cos(90°-T) = \cos \delta \cos 90° + \sin \delta \sin 90° \cos(90°-M)$$

$$\sin T = \sin \delta \sin M$$

and

$$\sin M = \frac{\sin T}{\sin \delta}$$

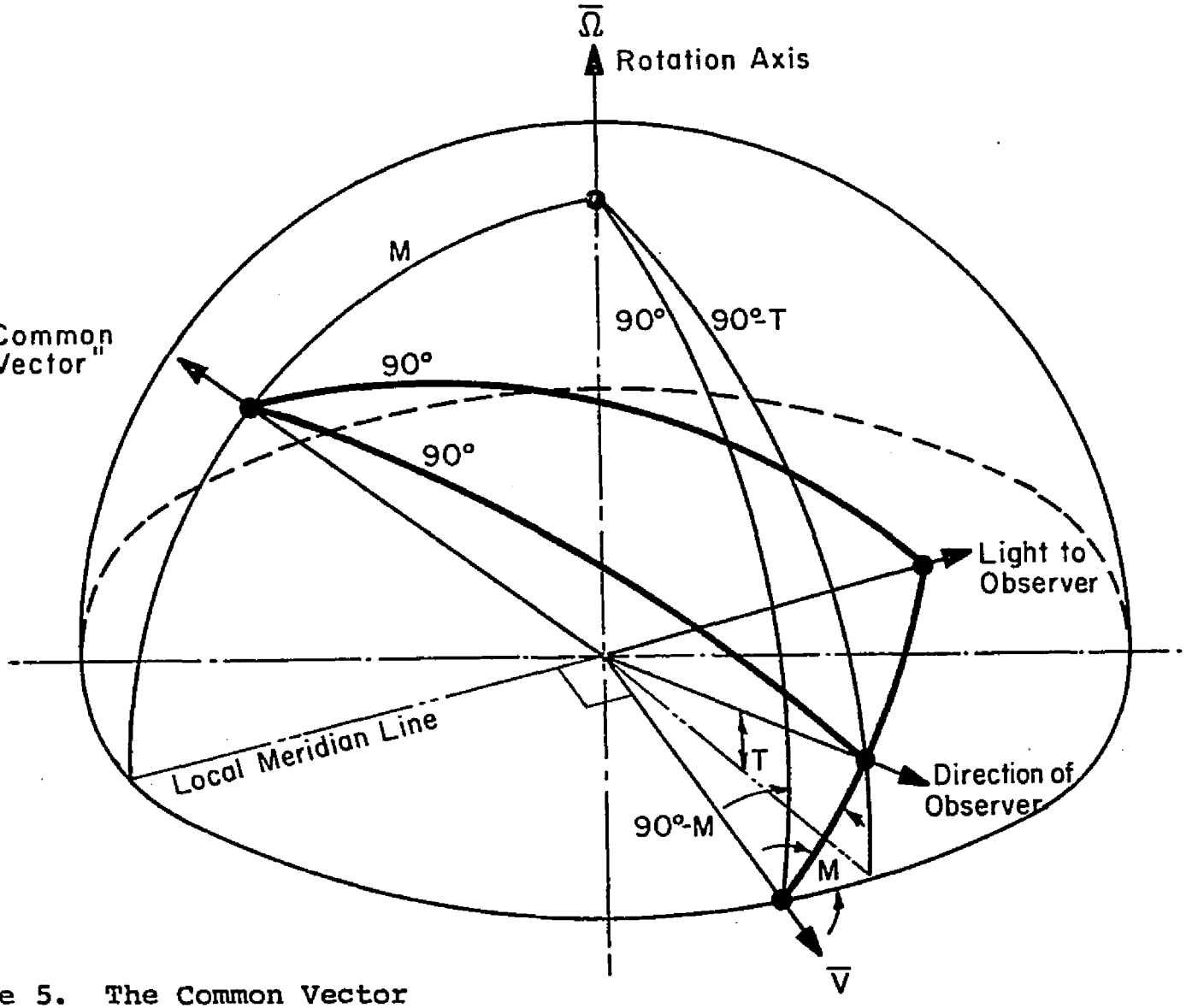

Figure 5. The Common Vector

and it may be seen that for θ greater than zero the common vector will be on the other side of the rotation axis from its depiction in Figure 5.

We now want to find the observed position angle of polarization Ψ relative to the axis of rotation. In general, for an emission mechanism of polarization perpendicular to the projected magnetic field line,

$$(\Psi - 90°) = \pm(\chi \pm N)$$

where χ is the angle the field line appears to make with the common vector in the emission frame, and N is the angle the common vector appears to make with the rotation axis in the observer's frame. For an emission mechanism producing polarization parallel to the projection of the magnetic field,

$$\Psi = \pm(\chi \pm N)$$

so a solution for Ψ, the projection of the field line, will trivially give us the angle of polarization for either type of emission.

Now what is χ, the angle $\vec{B}$ appears to make with the common vector in the emission frame as viewed from the direction in which light must be emitted to reach the

observer? Because of the aberration of light, this is the correct direction from which to look at the emission frame to see it in its properly "rotated" orientation. See Ferguson (1971b). χ may be found from Figure 6 and LOC as follows. The intermediate quantity

$$\cos g = \cos M \cos (90°-L) + \sin M \sin (90°-L) \cos A$$

$$= \cos M \sin L + \sin M \cos L \cos A$$

for the case where θ is less than zero. Since M is on the other side of the rotation axis for θ greater than zero, in that case

$$\cos g = - \cos M \sin L + \sin M \cos L \cos A \qquad (13)$$

or, in general,

$$\cos g = \mp \cos M \sin L + \sin M \cos L \cos A$$

where the + sign applies for $180° < \theta < 360°$ and the - sign for $0° < \theta < 180°$.

Again, from Figure 6 and LOC,

$$\cos g = \cos 90° \cos \phi + \sin 90° \sin \phi \cos \chi$$

or

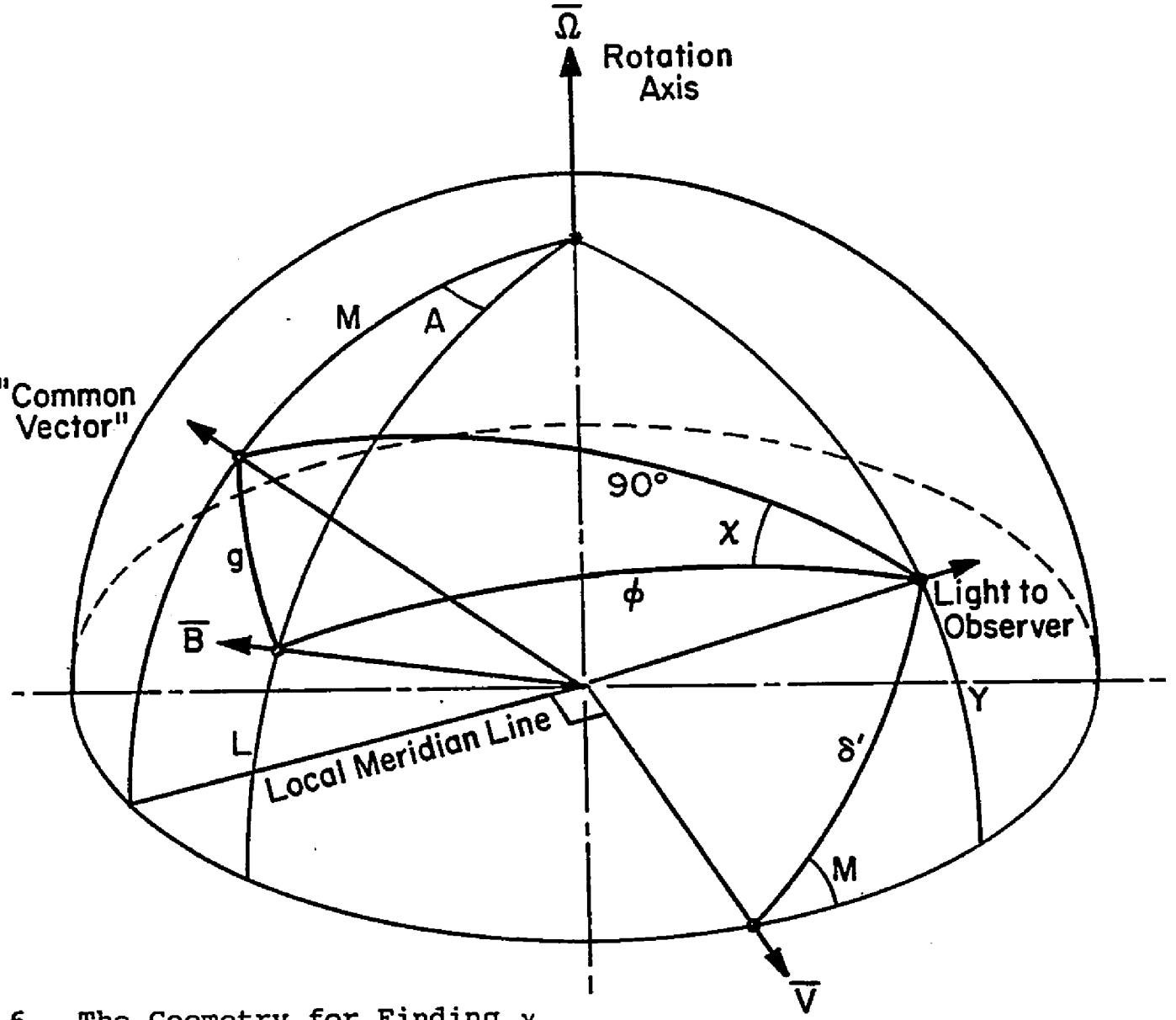

Figure 6. The Geometry for Finding χ

$$\cos \chi = \frac{\cos g}{\sin \phi} \quad . \tag{14}$$

Finally, using (13) and (14), we have

$$\cos \chi = \frac{\sin M \cos L \cos A \pm \cos M \sin L}{\sin \phi} \quad . \tag{15}$$

Notice that the sign of χ is not yet determined. To find it, we must find out whether the magnetic axis is seen clockwise or counterclockwise of the common vector in the emission frame. We will take the counterclockwise direction to be positive.

To find the sign of χ which should be used, we look at Figure 7. Here we can see that for $A > 0$, $L > 0$, and $\theta < 0$, χ will be positive if $90° - L > h$ and negative for $90° - L < h$, where h is the angle between the apparent direction of the common vector and $\vec{\Omega}$, along the line through $\vec{\Omega}$ and $\vec{B}$, as seen from the direction of the light which reaches the observer. We find h from the four parts formula;

$$\cos M \cos A = \sin M \cot h - \sin A \cot \rho$$

or

$$\cot h = \frac{\cos M \cos A + \sin A \cot \rho}{\sin M}$$

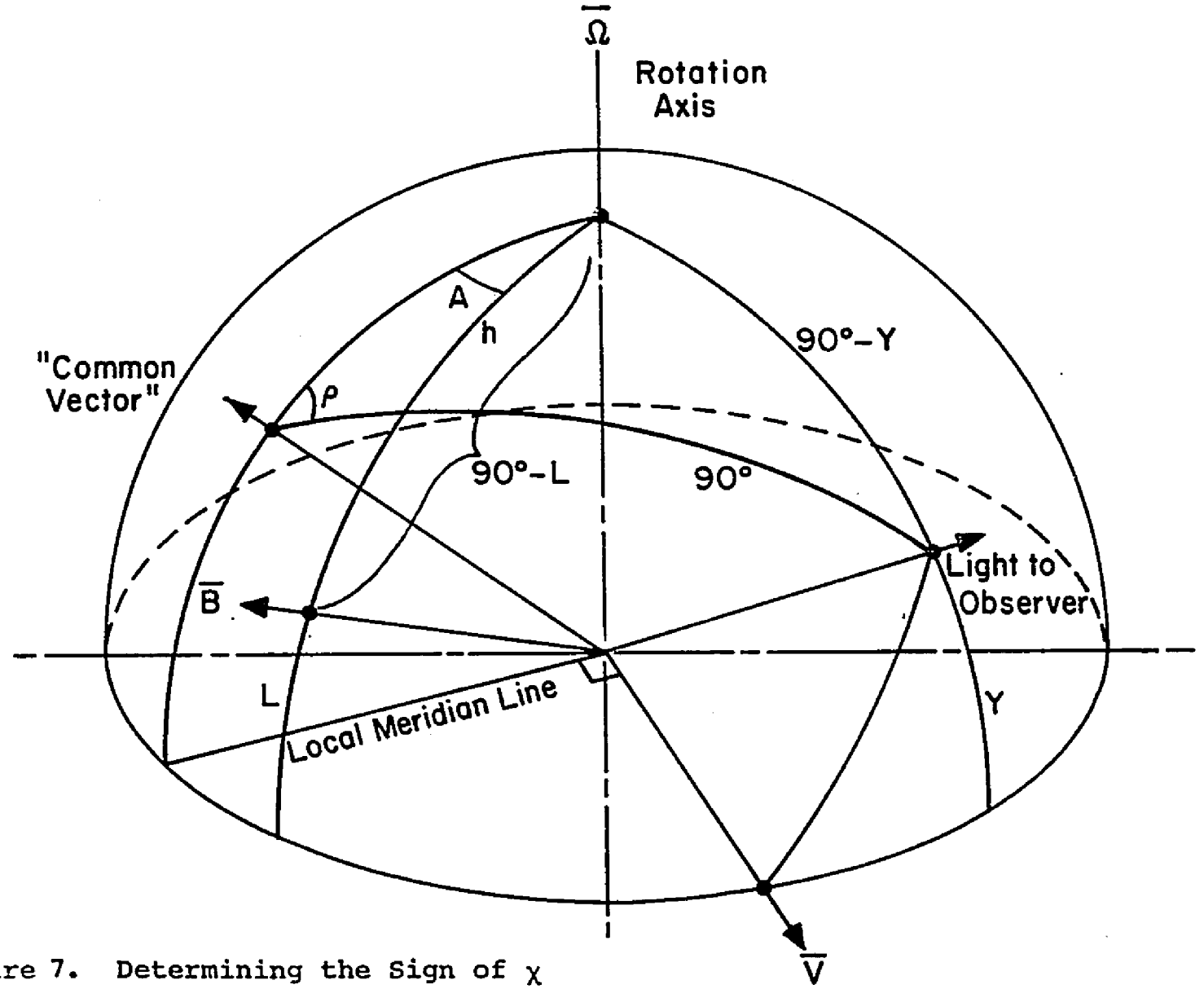

Figure 7. Determining the Sign of χ

or

$$\tan h = \frac{\sin M}{\cos M \cos A + \frac{\sin A}{\tan \rho}} \quad .$$

Now what is ρ? From LOC and Figure 7,

$$\cos (90°-Y) = \cos M \cos 90° + \sin M \sin 90° \cos \rho$$

or

$$\cos \rho = \frac{\sin Y}{\sin M} \quad . \tag{16}$$

But, from Figure 6, and LOC

$$\cos (90°-Y) = \cos \delta' \cos 90° + [\sin \delta' \sin 90° \cos (90°-M)]$$

$$\sin Y = \sin \delta' \sin M \tag{17}$$

and using (16) and (17) we find that

$$\cos \rho = \sin \delta' \quad .$$

Using a blackboard sphere and plotting the various configurations of δ, δ', A, T, and L, the author was able

to verify that the following table obtains as to the signs of ρ and χ to be used in computing Ψ.

TABLE 1

Signs of χ and ρ Used in Computing Ψ

θ	$90°+L<h$		$90°+L>h$	
	$\delta'>90°$	$\delta'<90°$	$\delta'>90°$	$\delta'<90°$
0° to 180°	χ neg. ρ pos.	χ pos. ρ neg.	χ pos. ρ pos.	χ neg. ρ neg.
	$90°-L<h$		$90°-L>h$	
	$\delta'>90°$	$\delta'<90°$	$\delta'>90°$	$\delta'<90°$
180° to 360°	χ pos. ρ neg.	χ neg. ρ pos.	χ neg. ρ neg	χ pos. ρ pos.

In order to find Ψ, we still must find N. This is done in Ferguson (1973) and will be repeated here. From Figure 8, showing the observer's reference frame, we see that, by LOC

$$\cos M = \cos 90° \cos (90°-T) + [\sin 90° \sin (90°-T) \cos N]$$

or

$$\cos N = \cos M / \cos T \quad .$$

The following table gives the correct signs to be used for N.

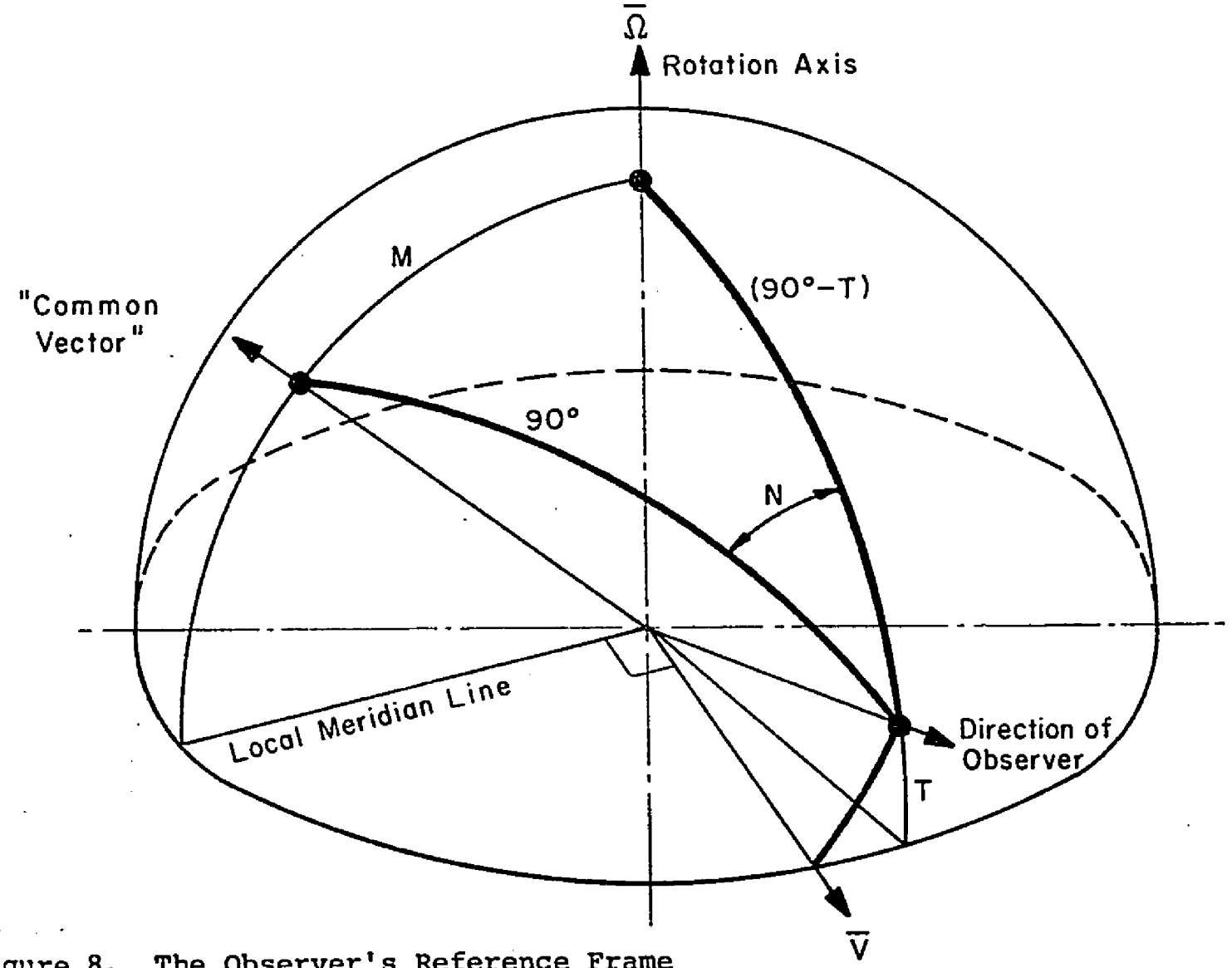

Figure 8. The Observer's Reference Frame

TABLE 2

Signs of N Used in Computing Ψ

θ	$90°+L<h$		$90°+L>h$	
	$\delta'>90°$	$\delta'<90°$	$\delta'>90°$	$\delta'<90°$
0° to 90° 90° to 180°	N neg. N pos.	N neg. -----	N neg. N pos.	N neg. -----
	$90°-L<h$		$90°-L>h$	
	$\delta'>90°$	$\delta'<90°$	$\delta'>90°$	$\delta'<90°$
180° to 270° 270° to 360°	N neg. N pos.	----- N pos.	N neg. N pos.	----- N pos.

Finally, the combination of Tables 1 and 2 gives the following table to be used with the reminder that the sign of ρ to be used in calculating h in order to in turn calculate χ is to be as given in Table 1.

TABLE 3

Ψ or $(\Psi-90°)$

θ	$90°+L<h$		$90°+L>h$	
	$\delta'>90°$	$\delta'<90°$	$\delta'>90°$	$\delta'<90°$
0° to 90° 90° to 180°	$-\chi-N$ $-\chi+N$	$+\chi-N$ ----	$+\chi-N$ $+\chi+N$	$-\chi-N$ ----
	$90°-L<h$		$90°-L>h$	
	$\delta'>90°$	$\delta'<90°$	$\delta'>90°$	$\delta'<90°$
180° to 270° 270° to 360°	$+\chi-N$ $+\chi+N$	---- $-\chi+N$	$-\chi-N$ $-\chi+N$	---- $+\chi+N$

It is unfortunate that no closed form for the solution to Ψ as a function of θ, β, A, T and L could be found. However, the formulae given here are readily evaluated for β, A, T and L for any value of θ on a digital computer. More about this will be found later in this thesis.

However, one can find some expressions for interesting cases. For instance, when $\sin \phi = 0$,

$$\cos \delta' = \cos L \sin A \tag{18}$$

as may be readily verified using Figure 4 and requiring $C = \delta'$. But

$$\cos \delta = \cos T \cos \theta \quad . \tag{9}$$

From Equation (10) it can be found that

$$\cos \delta = \frac{\cos \delta' + \beta}{1 + \beta \cos \delta'} \tag{18.5}$$

so that

$$\cos \theta \cos T = \frac{\cos L \sin A + \beta}{1 + \beta \cos L \sin A}$$

for $\sin \phi = \phi = 0$. This can be turned into the form

$$\cos\theta = \frac{\cos L \sin A+\beta}{\cos T(1+\beta \cos L \sin A)} \qquad (19)$$

and so L, A, T, and β being given, the value of θ when the linear polarization will go to zero may be found. Conversely, if cos θ calculated by Equation (19) has an absolute value greater than 1, we can be sure that the combination of L, A, T and β used will produce no point of zero linear polarization for any θ.

For the special case of A = 0, Equation (19) obviously reduces to

$$\cos\theta = \beta/\cos T \qquad (20)$$

in agreement with Equation (15) of Ferguson (1973).

From Equation (12), with A = 0, and evaluating the sine and cosine of the aberration angle (δ'-δ), we find that

$$\cos\phi = \frac{\cos b}{\gamma(1-\beta \cos \delta)} \quad . \qquad (20.5)$$

Using Equation (18.5) and setting cos φ = 1 and cos δ' = 0, we find that

$$\cos b = \frac{1}{\gamma}$$

if the linear polarization is to go to zero. Putting this result and Equation (20) into Equation (11) with A = 0, we have

$$\gamma^{-1} = \sin T \sin L \pm (\gamma^{-2} - \sin^2 T)^{\frac{1}{2}}$$

which is satisfied when

$$\sin L = \pm \gamma \sin T \tag{21}$$

in agreement with Equation (16) of Ferguson (1973). This is a condition on L which must be met if sin ϕ can equal zero for the special case of A = 0.

For this case of A = 0, θ of sin ϕ = 1, or of maximum linear polarization, comes when cos b = 0, or by simple algebra, when

$$\sin \theta = - \tan L \tan T \quad . \tag{22}$$

For the special case of A = 90°, Equation (19) for θ of linear polarization equal to zero becomes

$$\cos \theta = \frac{\cos L + \beta}{\cos T (1 + \beta \cos L)} \tag{23}$$

but this must also come when cos θ = 1, because only then

does the light to the observer lie in the plane of the rotation axis and the velocity vector. Thus, a condition for sin ϕ = 0 for A = 90° is, from (23),

$$1 = \frac{\cos L+\beta}{\cos T(1+\beta \cos L)}$$

$$\cos T(1+\beta \cos L) = \cos L+\beta$$

$$\cos L(\beta \cos T-1) = \beta - \cos T$$

$$\cos L = \frac{\beta-\cos T}{\beta \cos T-1} \quad . \tag{24}$$

And finally, for this special case, the linear polarization maximum, when cos ϕ = 0, may be found in the following way. Using Equation (20.5) we find that

$$\cos \phi = \frac{\cos b}{\gamma(1-\beta \cos \delta)} - \frac{\sin(\delta'-\delta)}{\sin \delta} \cos L \sin A \quad .$$

Evaluating sin($\delta'-\delta$) and setting sin A = 1 and cos ϕ = 0, we have

$$0 = \frac{\cos b - [\cos \delta-\gamma(\cos \delta -\beta)] \cos L}{\gamma(1-\beta \cos \delta)}$$

which becomes, after evaluating cos b,

$$\sin L \sin T = -\gamma(\cos \delta - \beta) \cos L \quad ,$$

and evaluating cos δ from Equation (9) and rearranging, this is

$$\cos \theta = \frac{\beta}{\cos T} - \frac{\tan L \tan T}{\gamma} \quad . \tag{25}$$

Thus, we have found the value of θ for which sin ϕ = 1 for A = 90°, if sin ϕ is ever equal to 1 for the given values of L and T.

Of course, for intermediate values of A, all of these criteria for sin ϕ = 0 and sin ϕ = 1 will depend in a complicated way upon sin A, and thus, numerical solutions are the best which can be reasonably hoped for.

We have now essentially completed the derivation of formulae which are useful and important in the generalized relativistic single vector model. It is appropriate now to say a few words about the approach to the problem which is taken in this dissertation.

The approach taken here, using the apparent rotation of a moving reference frame, "common" vectors, etc. grew out of the author's studies of the apparent rotation of moving reference frames, which led up to a paper on the subject (see Ferguson 1971b). I believe this to be a correct approach for relating the polarization parameters

of emitted radiation to those observed. It is different from that taken by Smith (1970) and in most cases leads to different results. I believe that Smith is in error, and the following discussion will justify my approach.

Figure 9 shows a schematic diagram of the orbit of, and apparent configuration of, an orbiting reference frame, as seen from a great distance. Since the moving reference frame appears, due to the aberration of light, to be rotated in the direction of its motion, it appears to be rotated around the common vector, which is perpendicular both to the observer's line of sight and the velocity v. Furthermore, the apparent rotation of the emission frame's $\vec{\Omega}$ axis is counterclockwise at t_1, when the emission frame is at $180° < \theta < 360°$, and clockwise at t_2 and t_3, when $0° < \theta < 180°$. The amount of the apparent rotation is always varying as θ changes.

Smith's (1970) approach, which is apparently that of taking the Stokes parameters to be invariant under a Lorentz transformation, and of defining the Stokes parameters with respect to the axis of rotation in the emission frame, is correct only for a source in uniform linear motion. Then the apparent rotation at any one time is the same as at any other time (the source being infinitely distant) and the difference between the projection of the real axis $\vec{\Omega}$ and the apparent direction of $\vec{\Omega}$ of the emission

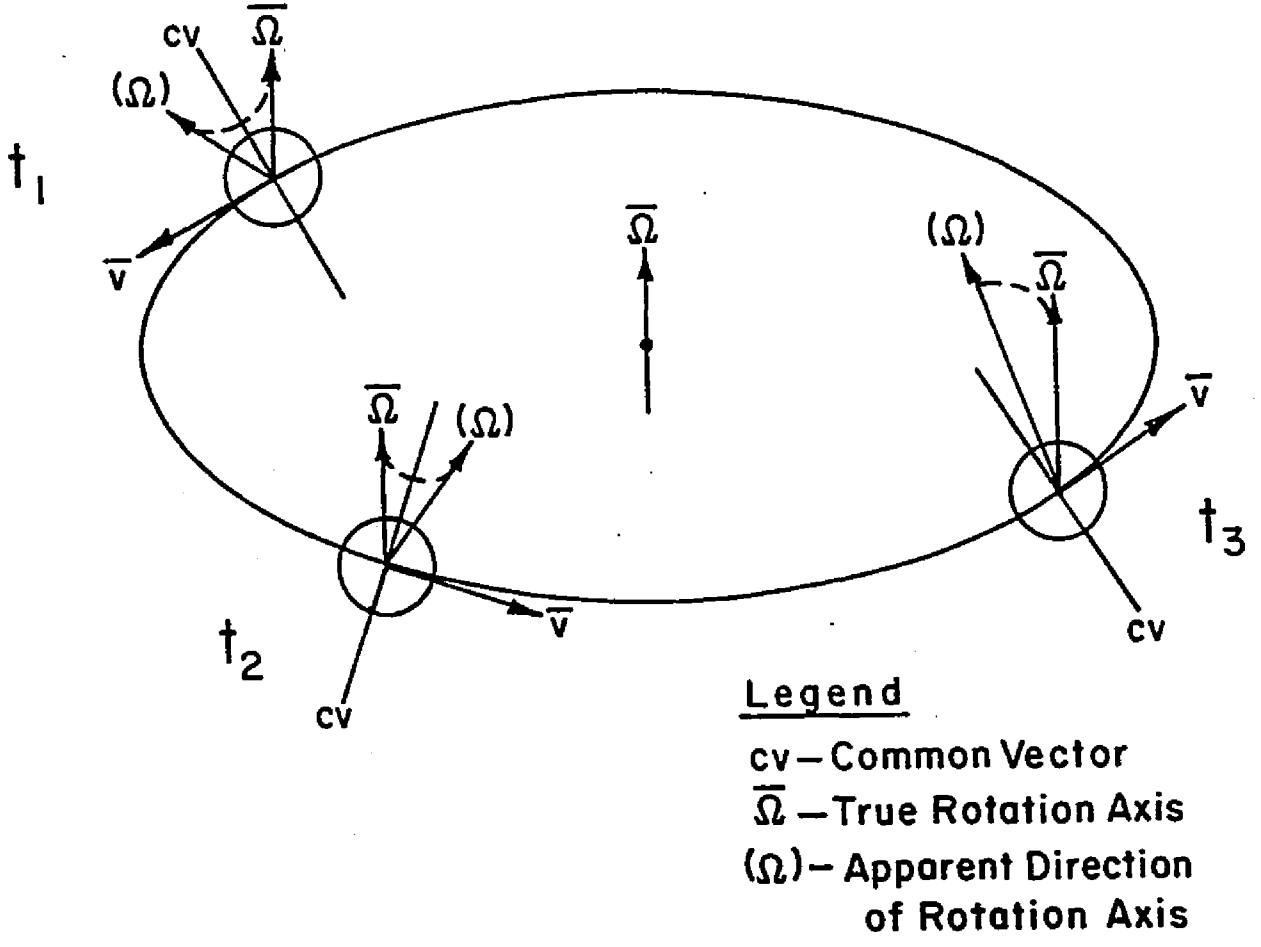

Figure 9. The Orbiting Reference Frame

frame is a constant angle, which may be corrected for by a simple redefinition of the Stokes parameters in the observer's frame.

However, for an accelerated source, as we have postulated for pulsars, the amount of apparent rotation is always changing, and even changes sign, so the difference between the real direction of $\vec{\Omega}$ and the apparent direction cannot be corrected once and for all by a simple redefinition by the observer. Now the observer should keep track of apparent angles with respect to the common vector's apparent direction, which is not affected by aberration, and which is a simple function of θ and T. If the observer measures the apparent angle between the common vector and $\vec{\Omega}$ in his frame, the angle N, and between the common vector and $\vec{B}$ in the rotated emission frame (the emission frame as seen in the observer's frame), the angle χ, and adds them together with the appropriate sign, he will surely have the correct angle he observes with respect to the real projection of $\vec{\Omega}$ on the sky. In contrast, in Smith's procedure, all angles are measured with respect to the instantaneous apparent direction of $\vec{\Omega}$ of the emission frame, which is in reality constantly changing, and allows no comparison with a constant direction in the sky.

The validity of my assumption that polarization angles transform in the same way as the apparent angles

between rigid rods under a Lorentz transformation is borne out by the work of W. J. Cocke and D. A. Holm (1972) who found the Lorentz transformation properties of the Stokes parameters. Essentially, they showed that the polarization position angle and amount viewed by an observer in motion relative to the source were unchanged by the Lorentz transformation if the angles were measured from the direction perpendicular both to the direction of motion and the propagation direction. In their work this axis was the y and y' axes. In mine it is called the common vector. Thus, their work substantiates my approach of referring polarization angles in all cases to the common vector, and of treating the polarization position angles as if they were apparent angles between rigid rods. Since the axis of rotation $\vec{\Omega}$ does not correspond to their y and y' axes, the Lorentz parameters defined with it as a zero point in angle will not, in general, be invariant, as Smith (1970) apparently assumes them to be.

It should be noted that in the limit of small T, Smith's procedure becomes correct, as then the common vector points always along $\vec{\Omega}$. For even a small finite value of T, however, Smith's procedure is in error near $\theta = 0°$ and $180°$.

The entire foregoing discussion is based upon the assumption that the light travel time across the source is

small compared to observed times of light variation. For a good discussion of the inaccuracy of speaking of only the apparent rotation of a moving object when its linear size is not negligible, see McCrea (1973).

C. Properties of Single Vector Models

Many of the conclusions of this section are based upon computer calculations of single vector models which the author performed on the University of Arizona CDC 6400 computer. In these calculations, the formulae of Section IB were used in a Fortran program to make polarization maps. These showed Ψ and sin ϕ for 90 equally spaced values of θ, and for 21 values of L (positive and negative multiples of 9°), for each combination of T, A, and β specified. Values of T, β, and A for which all combinations were tried are given in Table 4.

TABLE 4

Values of Parameters for Which Polarization Maps Were Made

T	cos T	β	γ	A	sin A
18°	.95	0	1.0	0°	0
26	.90	.55	1.2	19	.33
37	.80	.74	1.5	42	.67
53	.60	.87	2.0	89 or 90	1.00
66	.41≃.4	.94	2.9≃3.0		
78	.21≃.2	.98	5.0		

Negative values of A were not necessary, since all of the information in those maps is contained in the maps for positive values.

For selected values of L, such maps were made into plots of polarization throughout the pulse period. For this purpose, the data in the maps were transferred onto punched cards, and the CDC 6400 computer, in conjunction with a CALCOMP plotter, was used to make the final plots.

1. The Non-Relativistic Model

In the non-relativistic model ($\beta=0$), $t = \theta/\Omega = \theta p/2\pi$ (p being the period) always, so one can rightly speak of the longitude on the stellar surface of emission connected with a time t. Many observers (Manchester, 1971a for instance) plot their observations of flux and polarization versus longitude, where LONG.° $= \frac{180}{\pi} \frac{t_1}{p}$, t_1 is taken from an arbitrary starting time, and p is the period.

Plots of polarization amount versus time in the non-relativistic models are symmetric about the time when the vector is pointing most nearly along our line of sight. Position angle plots are symmetric about this time if the sign of Ψ is reversed.

The linear polarization in non-relativistic models can only go to zero if $L = \pm T$, and the maximum rate of

position angle swing comes when the linear polarization amount is at a minimum, at t = 0.25 p. This maximum sweep rate is easily found by differentiating Equation (5) with respect to θ and substituting $\theta = 90°$. We find

$$- \cos^2 \Psi \frac{d\Psi}{d\theta} = \frac{\sin \theta \tan L \cos T - \sin T}{\cos^2 \theta}$$

but

$$\csc^2 \Psi = 1 + \operatorname{ctn}^2 \Psi$$

so that

$$\frac{d\Psi}{d\theta} = \left[\frac{-\sin \theta \tan L \cos T - \sin T}{\cos^2 \theta} \right] x$$

$$\left[\frac{\cos^2 \theta}{\cos^2 \theta + (\tan L \cos T - \sin T \sin \theta)^2} \right]$$

or

$$\frac{d\Psi}{d\theta} = - \frac{\sin \theta \tan L \cos T - \sin T}{\cos^2 \theta + (\tan L \cos T - \sin T \sin \theta)^2}$$

Evaluating at $\theta = 90°$, we have

$$\frac{d\Psi}{d\theta} = - \frac{\tan L \cos T - \sin T}{(\tan L \cos T - \sin T)^2} = - \frac{1}{\tan L \cos T - \sin T}$$

and by rearranging,

$$\frac{d\Psi}{d\theta} = - \frac{\cos L}{\sin(T-L)}$$

which becomes infinite for T = L. This agrees with Lyne, Smith and Graham (1971).

In the non-relativistic model, the vector swings near to the observer's line of sight at $\theta = 90°$ and 270°, and so linear polarization minima would come ½ period apart if both polar caps were seen. Distortions in the field would change this somewhat, but not drastically. Furthermore, the times between maxima and minima of linear polarization are approximately the times between $\cos \phi = 0$ and $\cos \phi = 1$ (see however, discussion following Equation (6)) which from Equation (12) are given by

$$0 = \sin L \sin T + \cos L \cos T \cos(90° - \theta_0) \qquad (26)$$

and

$$1 = \sin L \sin T + \cos L \cos T \cos(90° - \theta_1) \qquad (27)$$

where θ_0 is (θ+A) of polarization maximum and θ_1 is (θ+A) of polarization minimum (assuming L≃T). Now we already know that $\sin \theta_1 = 1$, so that (27) becomes 1≃cos(L-T), or L≃T, as per our assumption.

Now, knowing that $\theta_1 = 90°$, what is θ_0 from (26)?

$$\sin \theta_0 = - \tan L \tan T$$

$$\simeq - \tan^2 T$$

and

$$\cos \theta_0 \sim \sqrt{1 + \tan^4 T}$$

and finally,

$$\sin(\theta_1 - \theta_0) \simeq \sin \theta_1 \cos \theta_0 - \cos \theta_1 \sin \theta_0$$

$$\sin(\theta_1 - \theta_0) \simeq \sqrt{1 + \tan^4 T} \quad .$$

Notice that in the non-relativistic case, since θ always appears added to A, that the combination acts to change the absolute rotational phase of polarization properties, but does not change their character. Thus, a plot of polarization for any A will be the same as one for $A = 0$, but shifted in time.

In Figures 10 through 16 are shown plots of the polarization position angle Ψ versus time (plotted as fraction of pulse period) for various non-relativistic single vector models. Similar plots of the linear polarization determinant, sin ϕ, calculated and plotted in the same way, form Figures 17 through 23. Finally,

Figures 24 through 30 are plots of Ψ versus sin ϕ at identical times in the pulse, 2Ψ being plotted counter-clockwise and sin ϕ being plotted radially. In such a plot, as is indicated thereon, one cartesian coordinate becomes sin ϕ sin 2Ψ and the other coordinate sin ψ cos 2Ψ. If $n = 1$ in Equation (6), then $P \propto \sin \phi$ and the relative Stokes parameters $Q/I = P \cos 2\Psi$ and $U/I = P \sin 2\Psi$ may be picked from the Cartesian coordinates. In other cases, where $n \neq 1$, the qualitative behavior will be the same, i.e., the angles of linear polarization maximum and minimum will be identical. Thus, Figures 24 through 30 are linear polarization plots with the time dependence reduced to a direction of travel along the line.

All of these figures show only cases of interest, i.e., where the magnetic vector comes very near our line of sight, so that radiation (which must be beamed in the non-relativistic emission frame) may be seen. Care must be taken in the interpretation of such diagrams. If the emission is stimulated linear acceleration radiation (Cocke, 1973), curvature radiation, or low pitch angle ($< 1/\gamma$) synchrotron radiation, the approximation $P \propto \sin^n \phi$ may not hold. In such cases, one should use only the polarization position angle plots to determine model parameters. For ordinary synchrotron radiation, cyclotron radiation, or similar types of radiation,

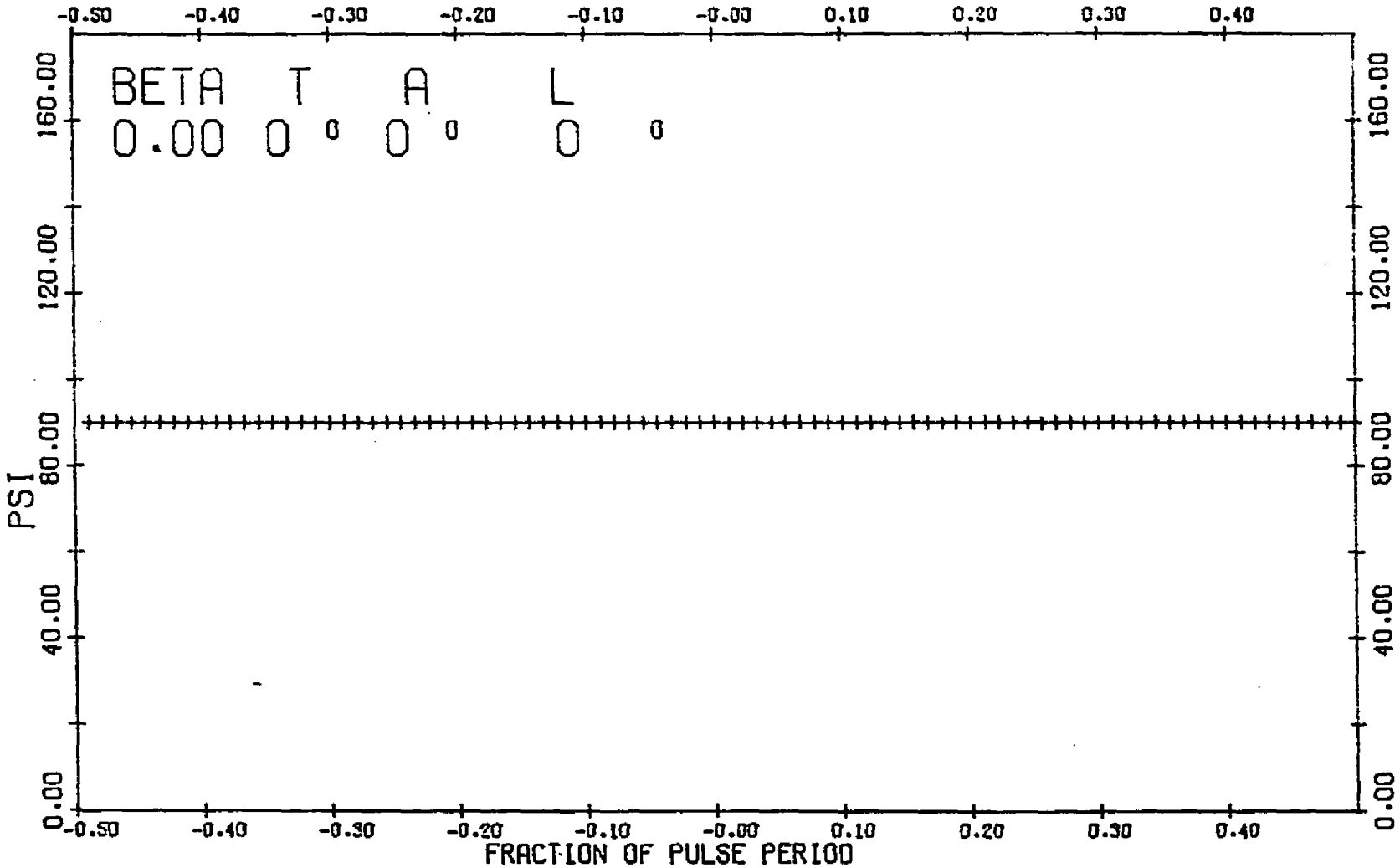

Figure 10. Ψ Versus Time for β=0, T=0°, L=0°

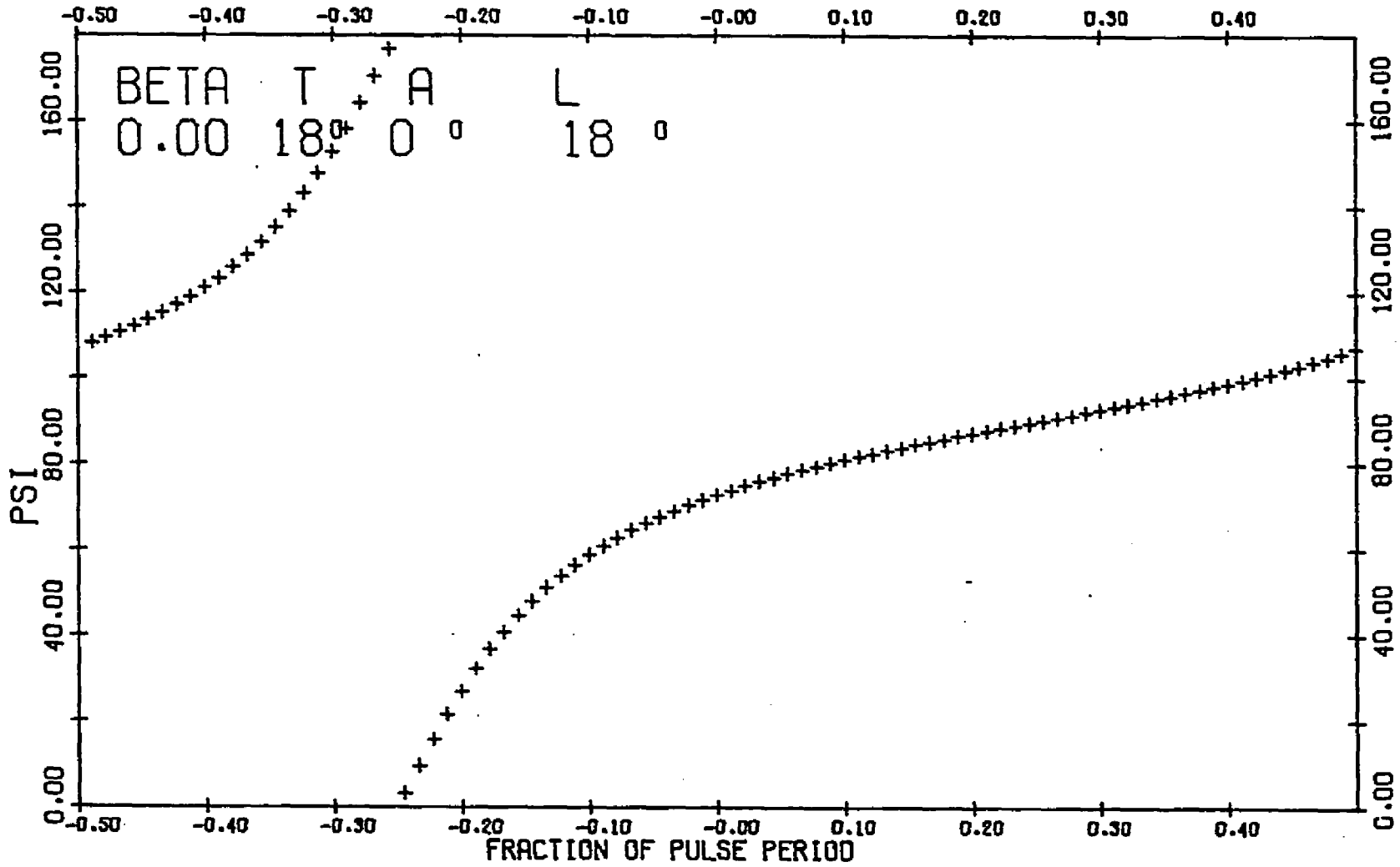

Figure 11. Ψ Versus Time for β=0, T=18°, L=18°

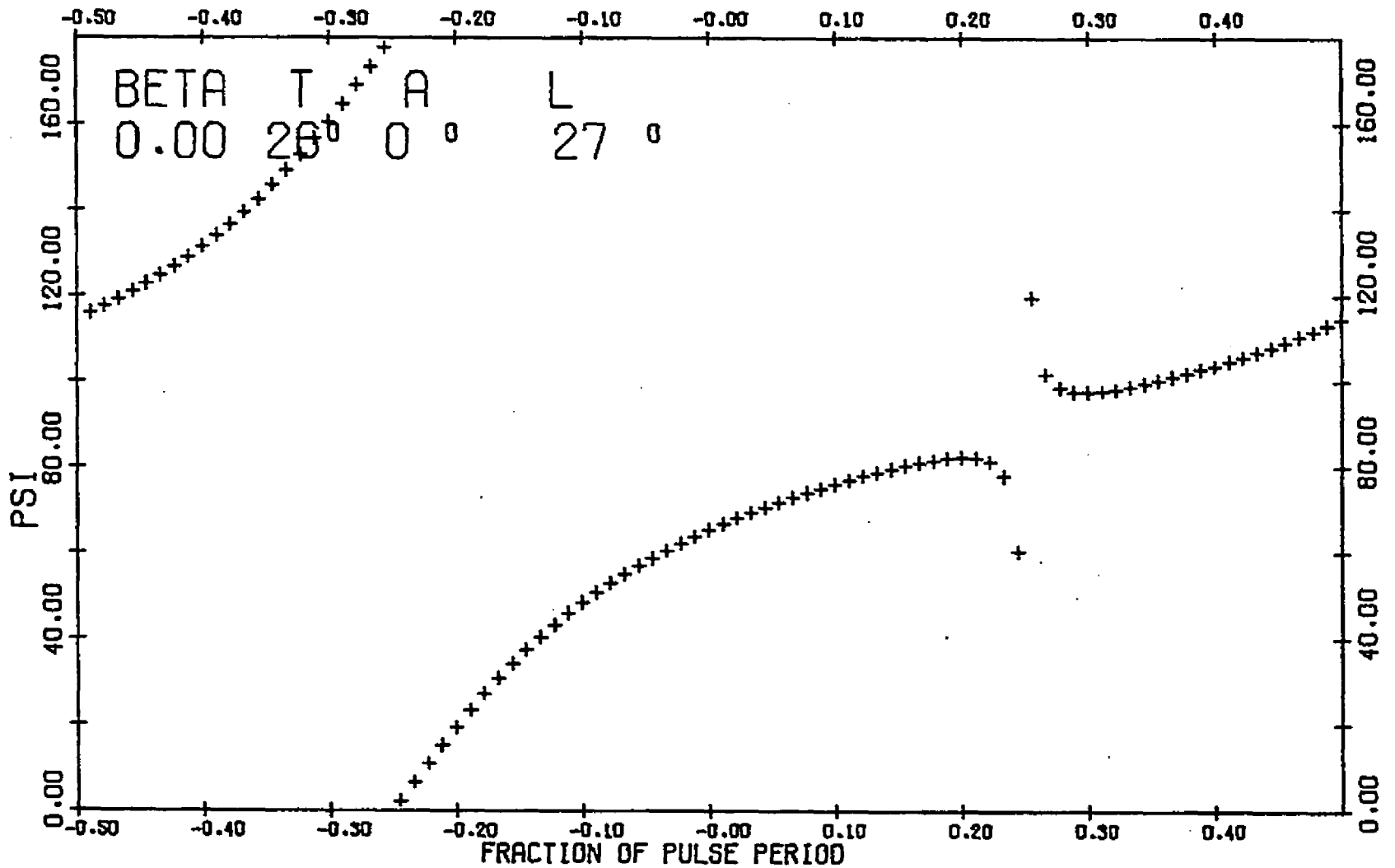

Figure 12. Ψ Versus Time for β=0, T=26°, L=27°

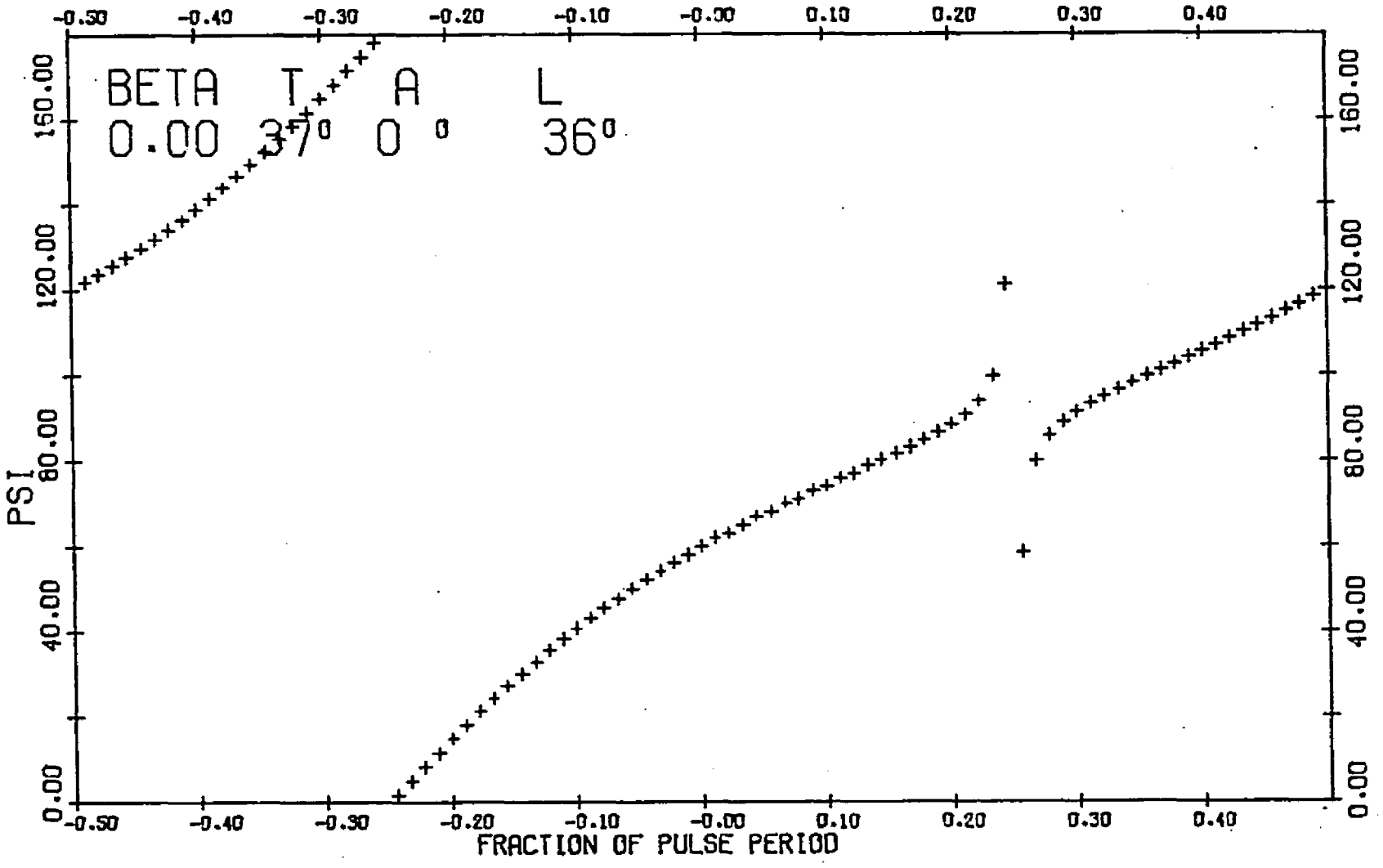

Figure 13. Ψ Versus Time for β=0, T=37°, L=36°

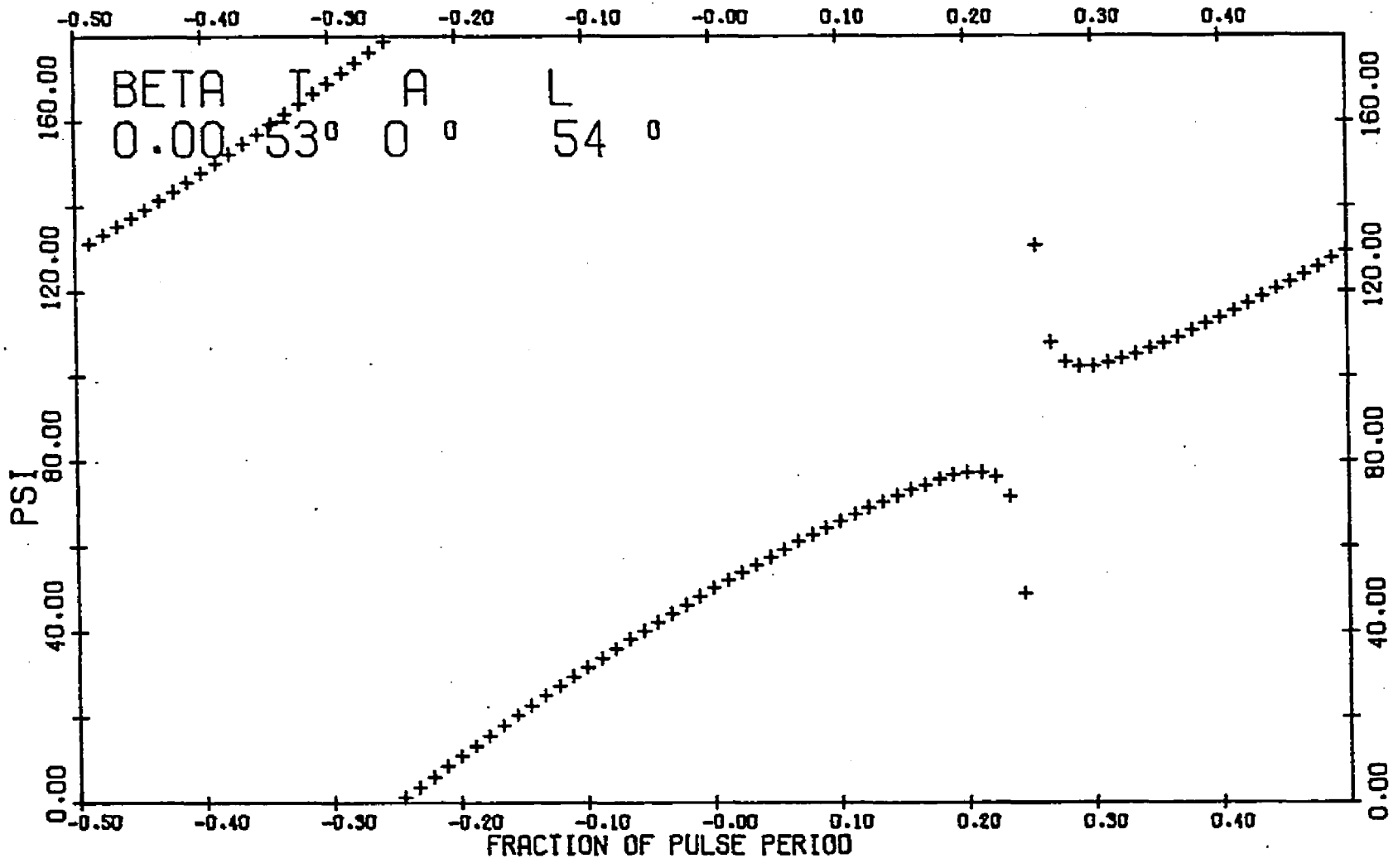

Figure 14. Ψ Versus Time for β=0, T=53°, L=54°

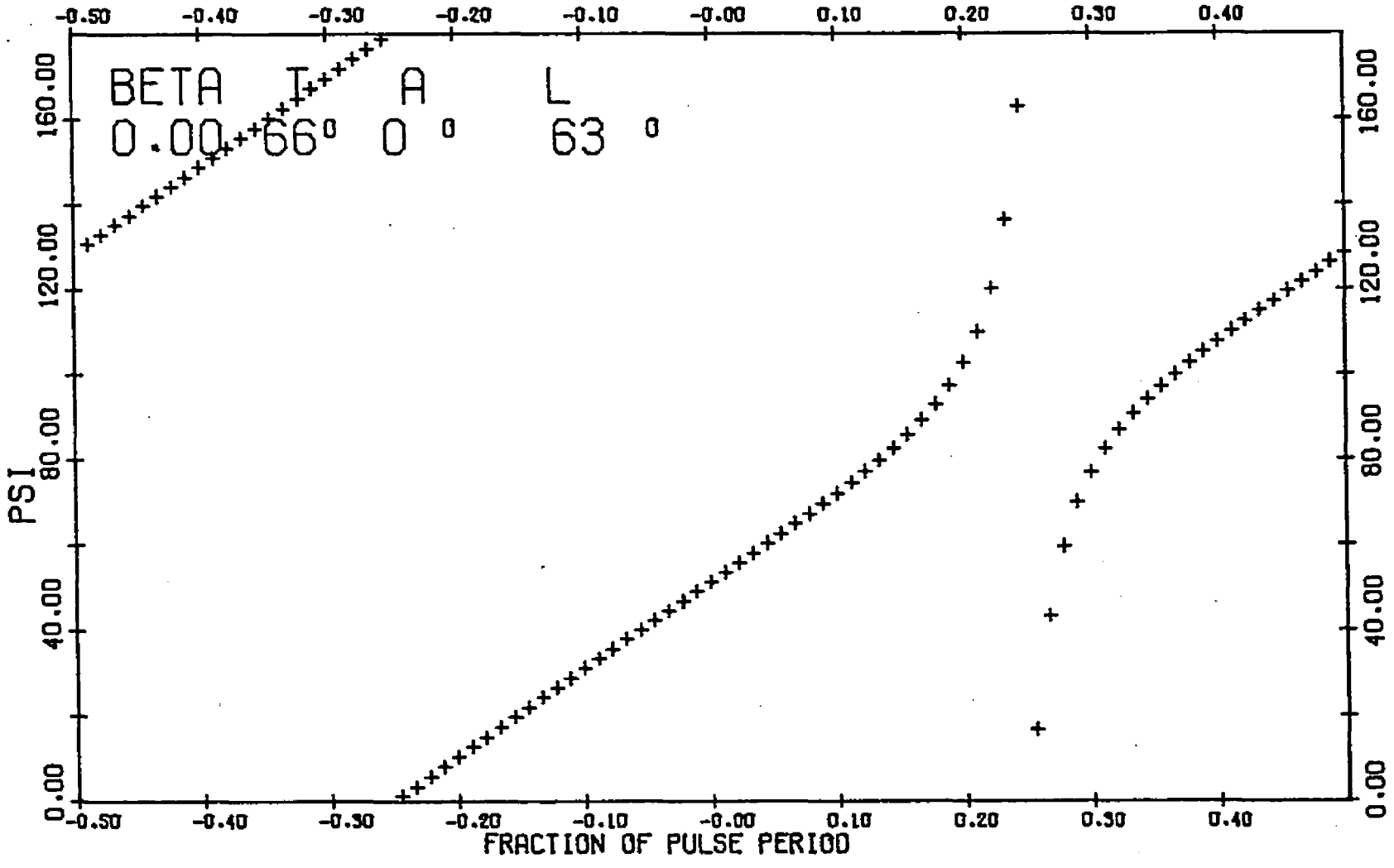

Figure 15. Ψ Versus Time for β=0, T=66°, L=63°

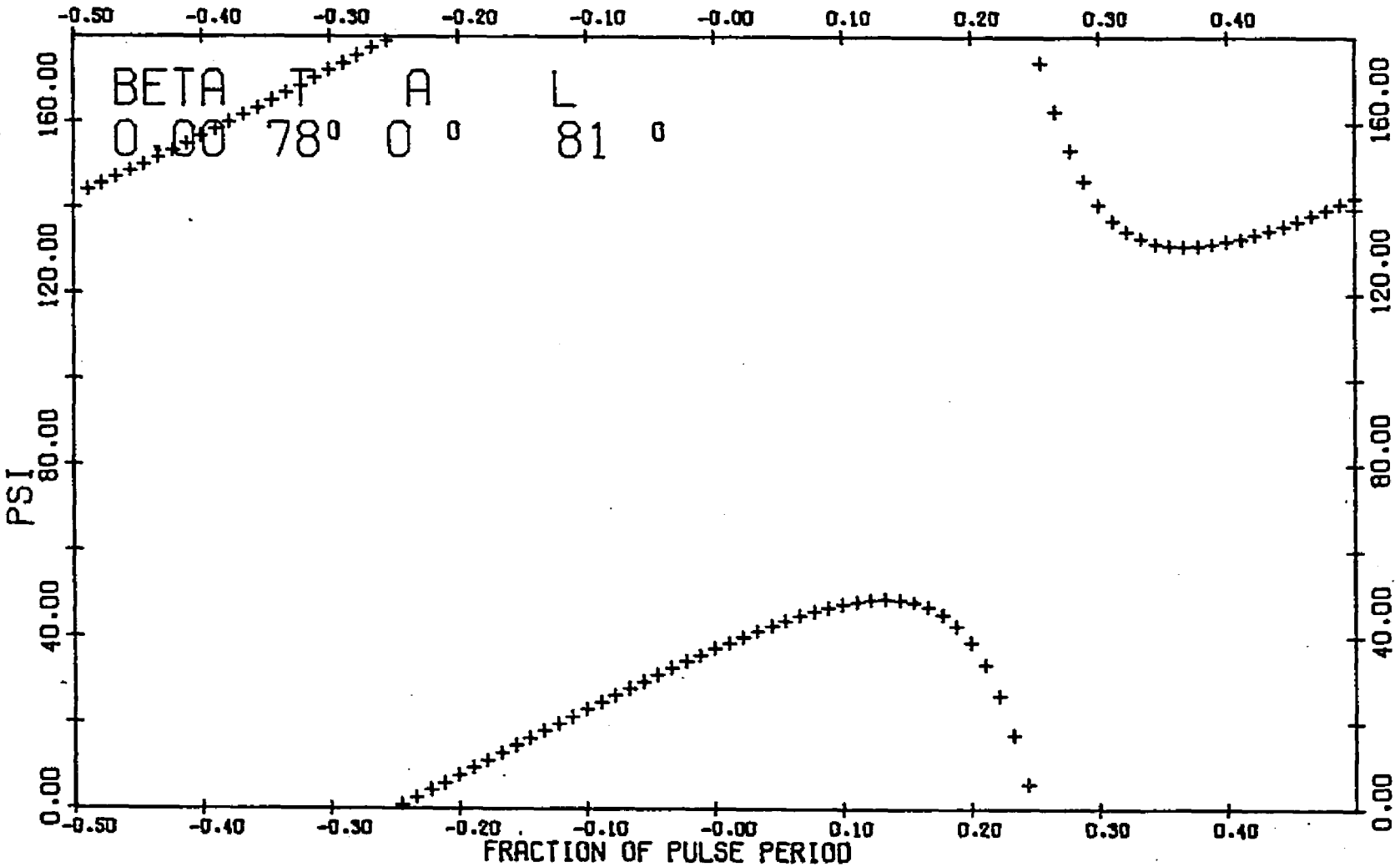

Figure 16. Ψ Versus Time for β=0, T=78°, L=81°

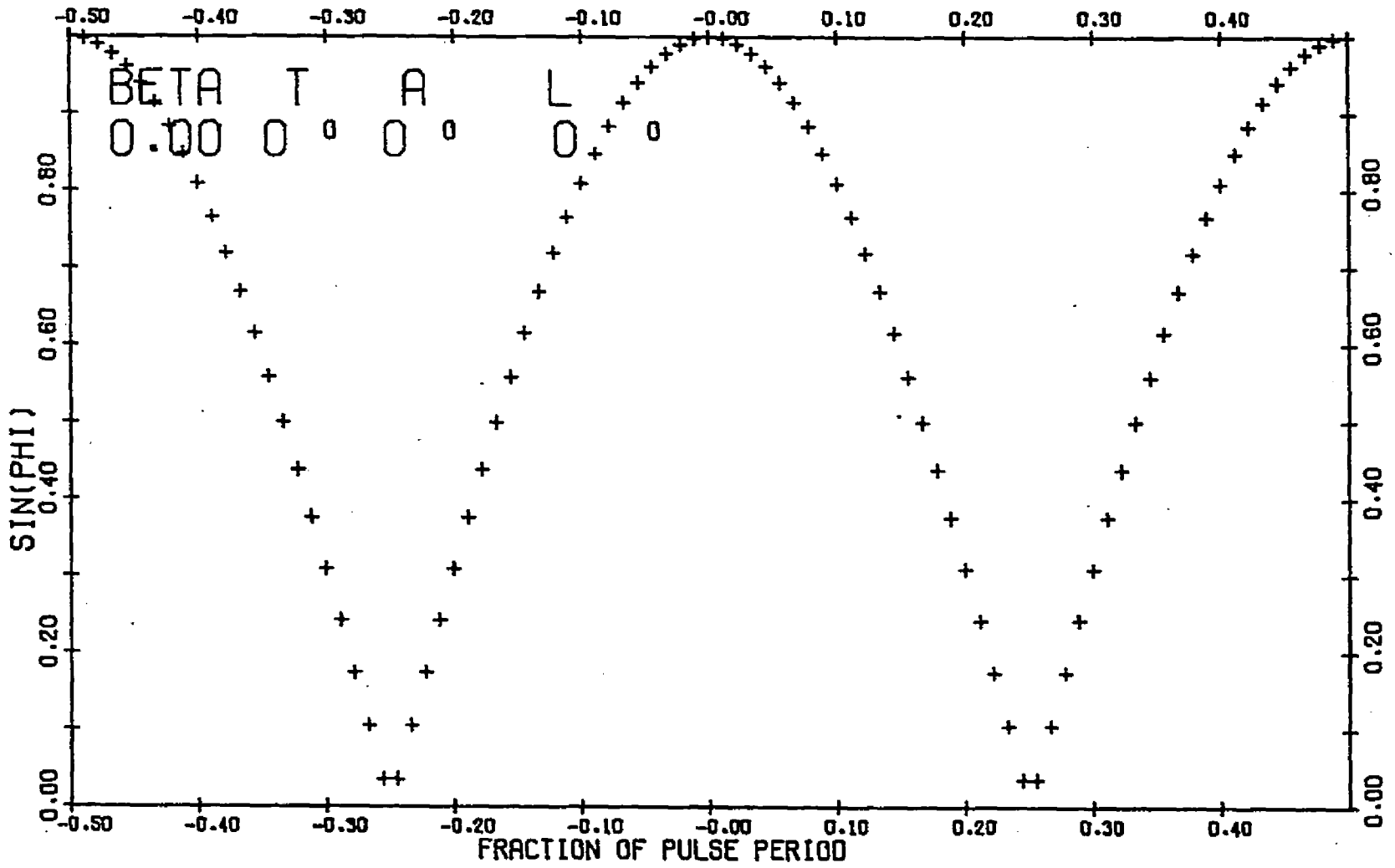

Figure 17. sin ϕ Versus Time for β=0, T=0°, L=0°

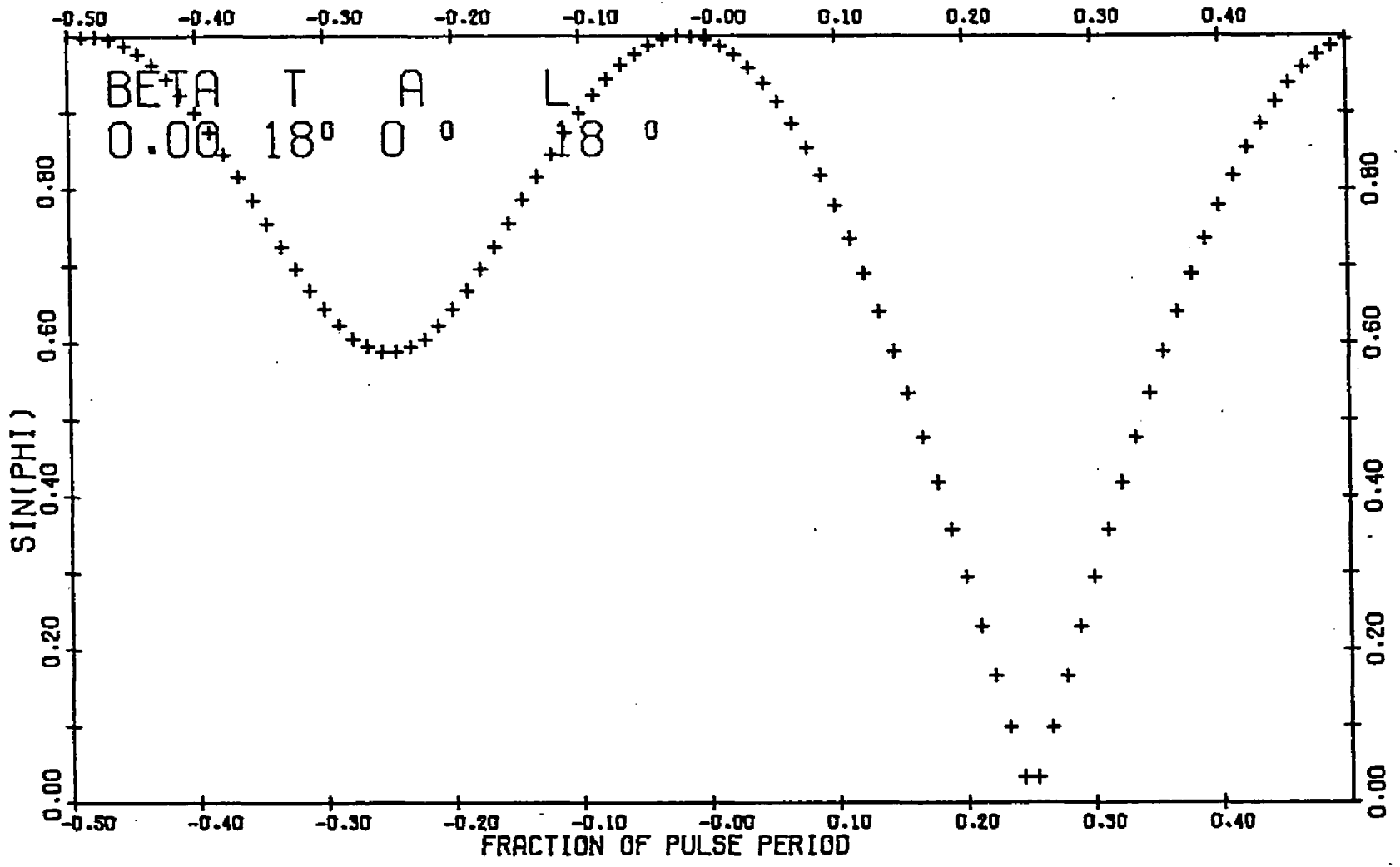

Figure 18. sin ϕ Versus Time for β=0, T=18°, L=18°

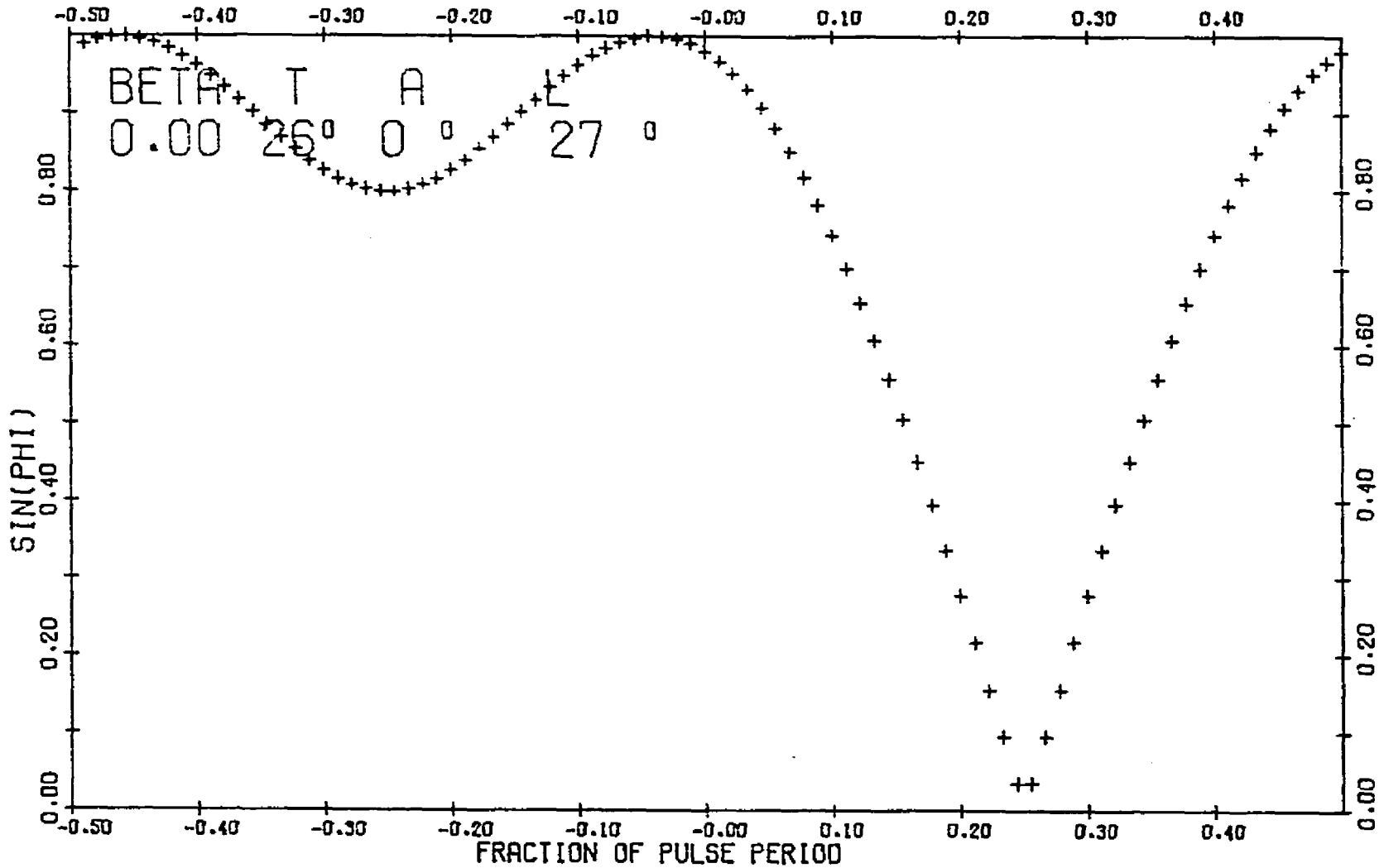

Figure 19. sin ϕ Versus Time for β=0, T=26°, L=27°

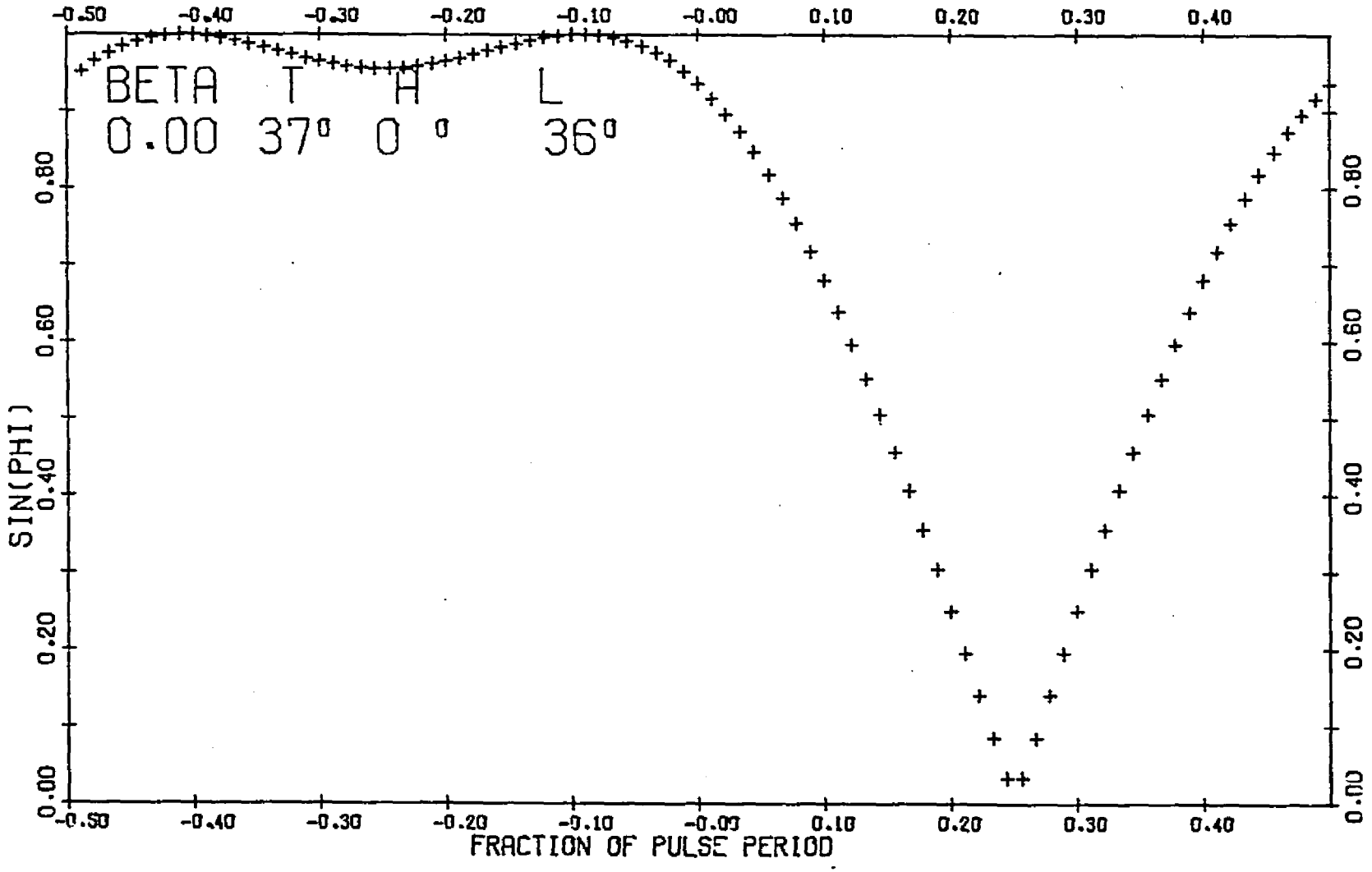

Figure 20. sin ϕ Versus Time for β=0, T=37°, L=36°

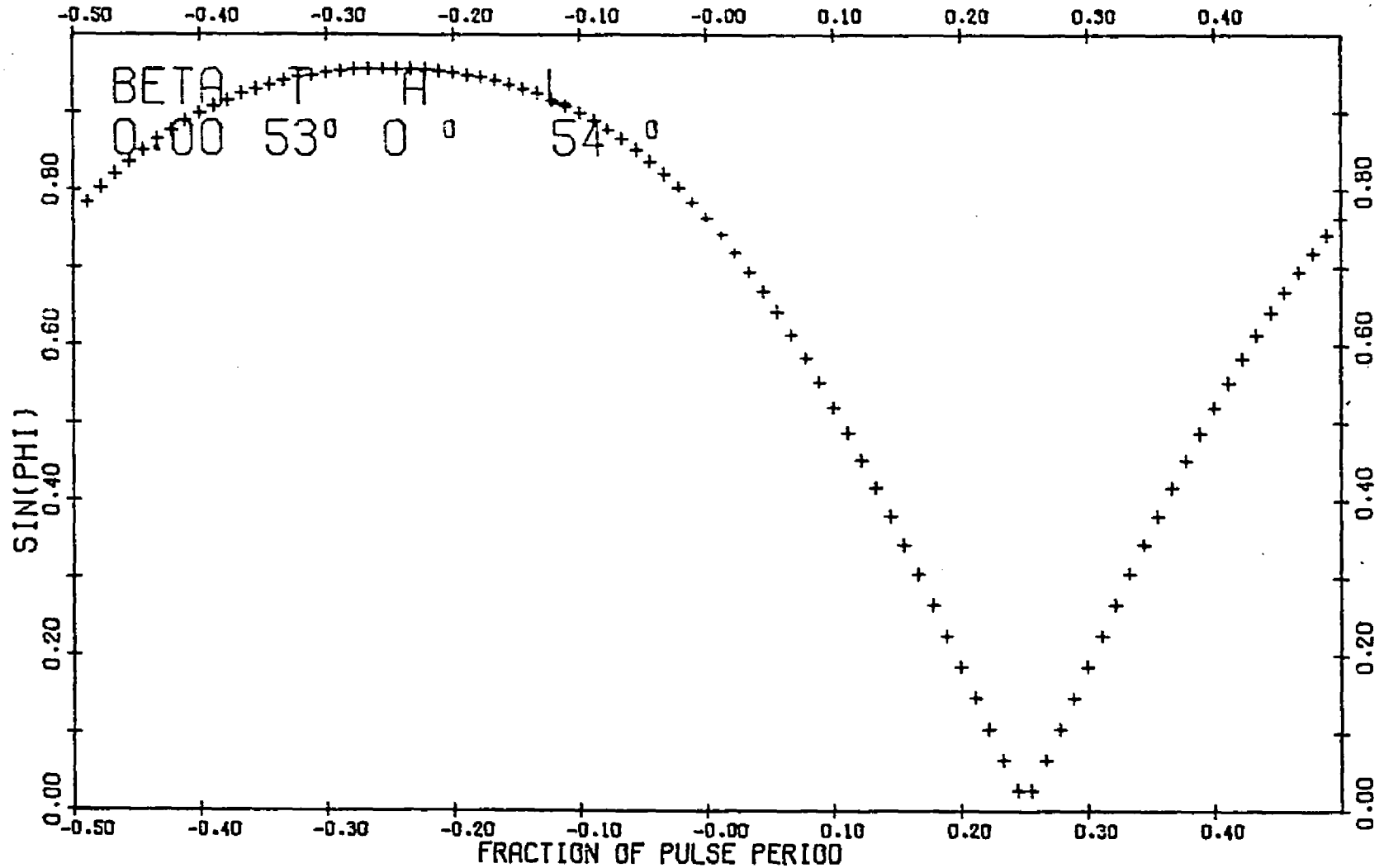

Figure 21. sin ϕ Versus Time for β=0, T=53°, L=54°

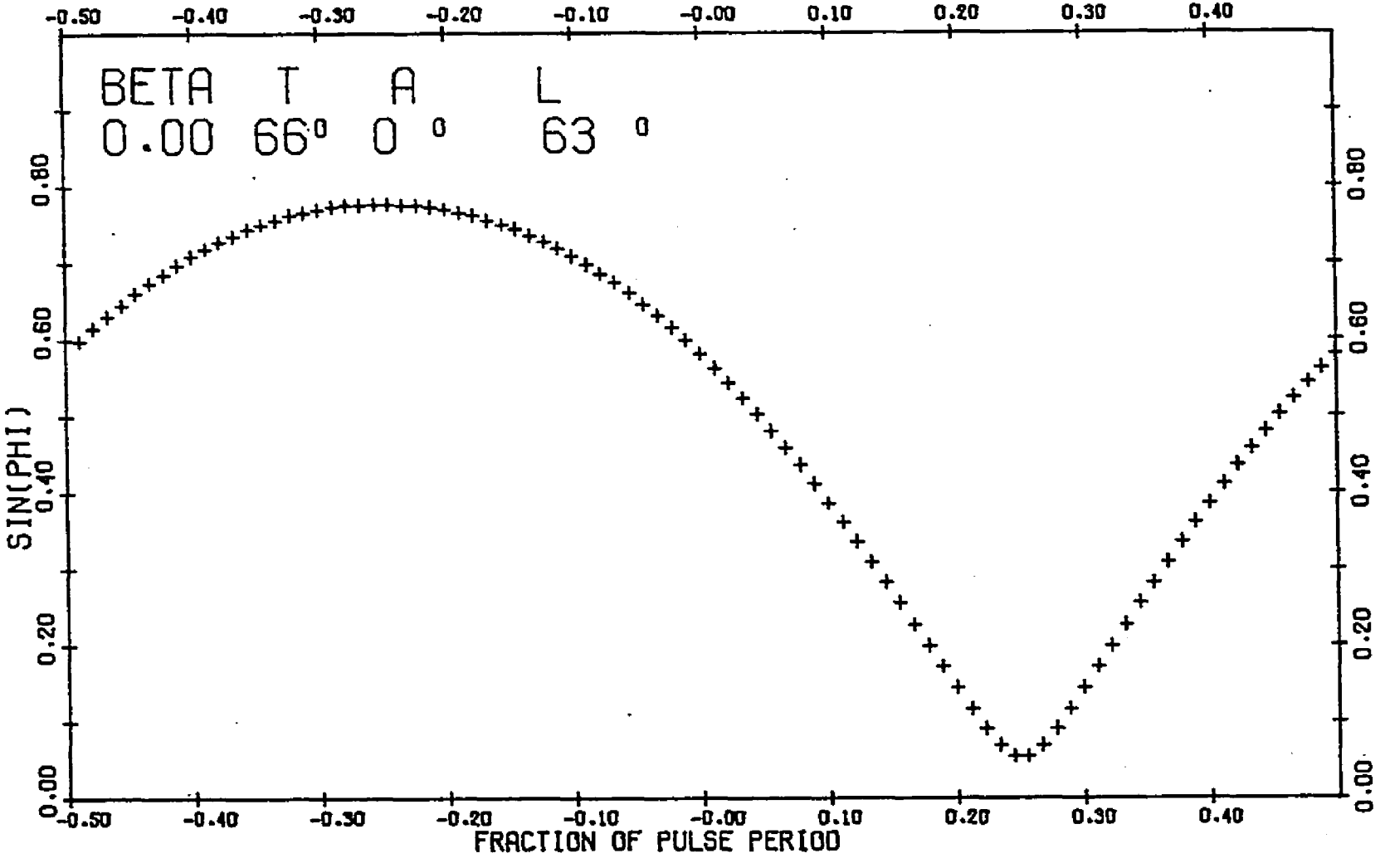

Figure 22. sin ϕ Versus Time for β=0, T=66°, L=63°

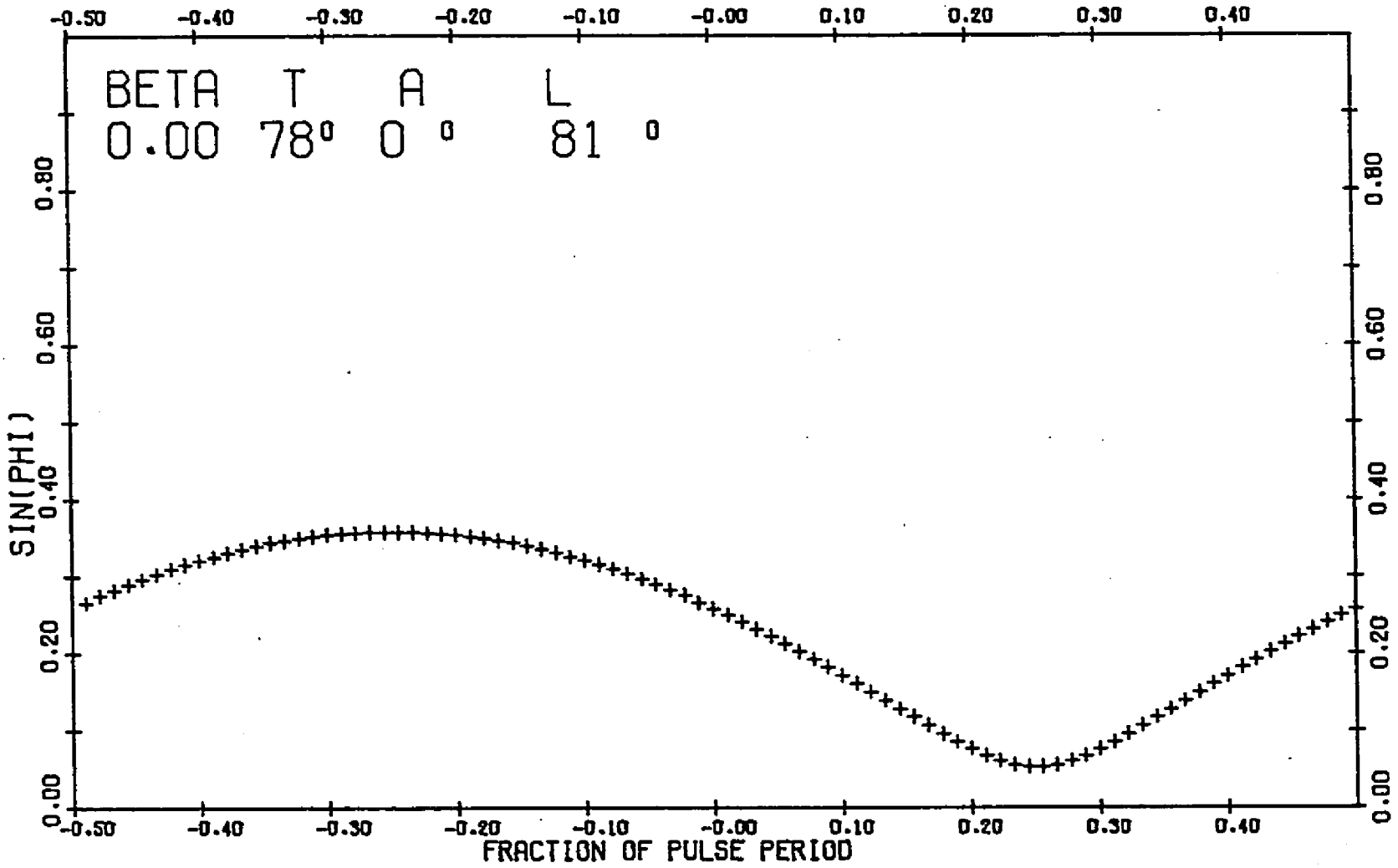

Figure 23. sin ϕ Versus Time for β=0, T=78°, L=81°

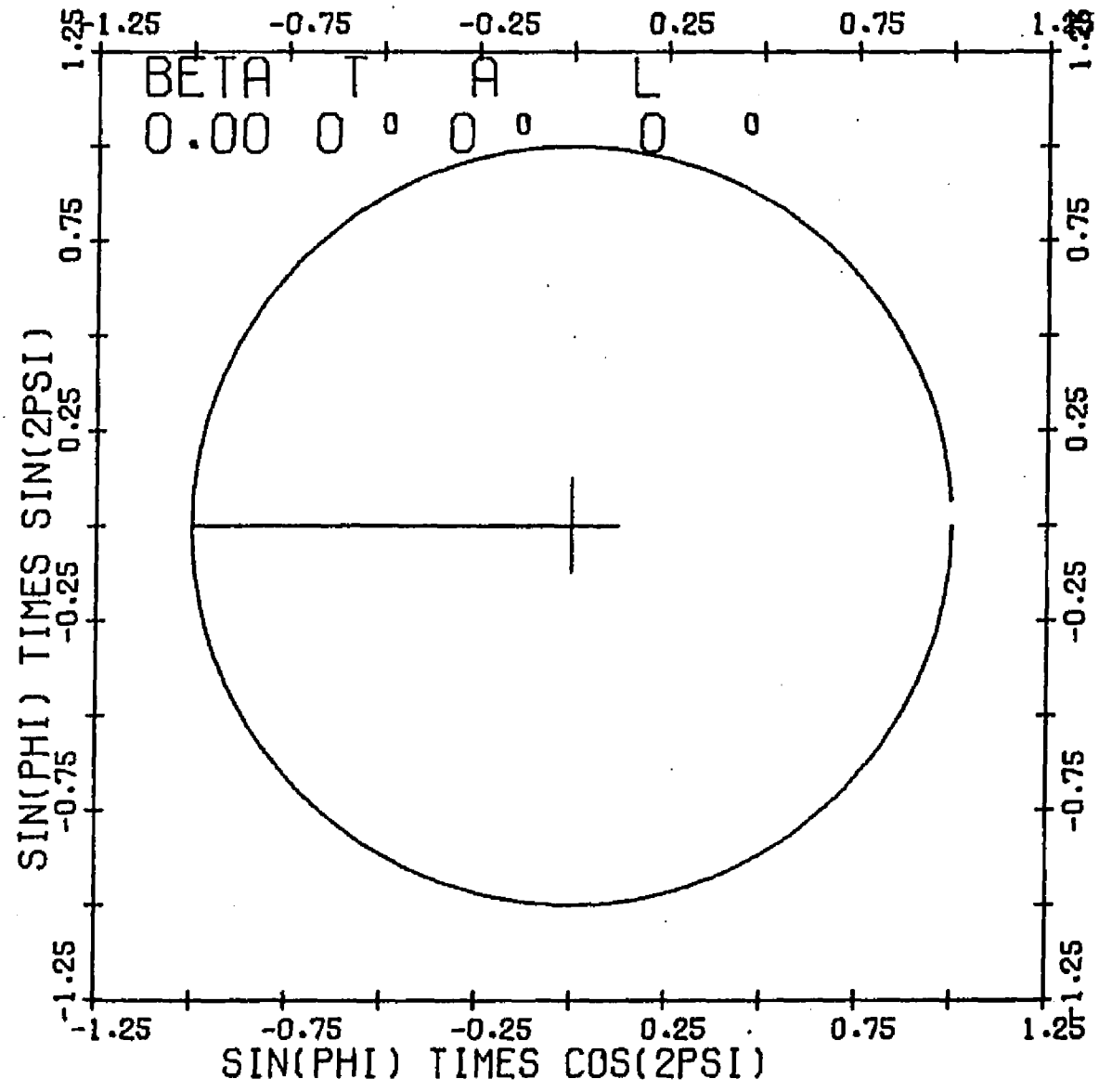

Figure 24. 2Ψ Versus sin ϕ for β=0, T=0°, L=0°

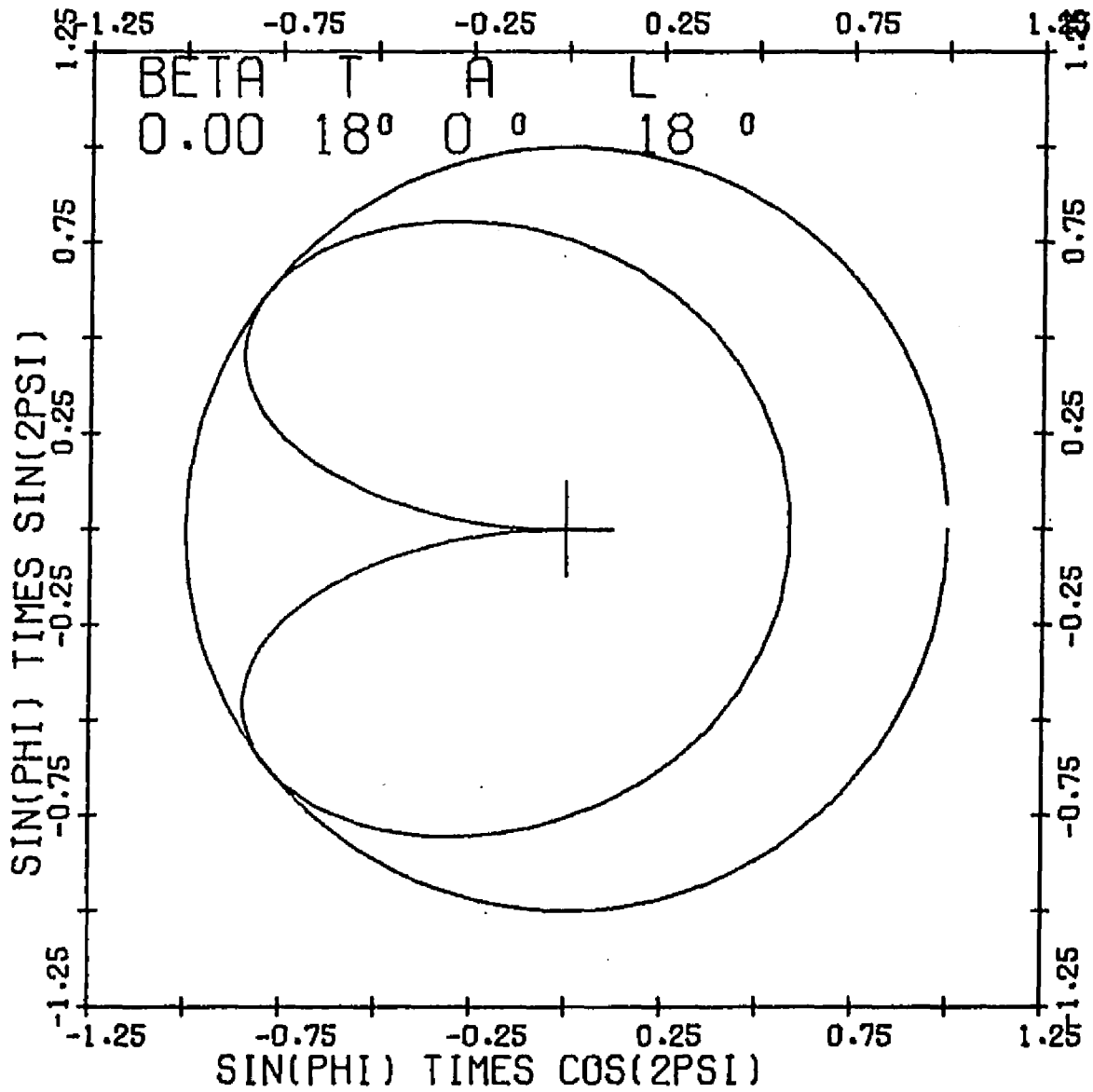

Figure 25. 2Ψ Versus sin ϕ for β=0, T=18°, L=18°

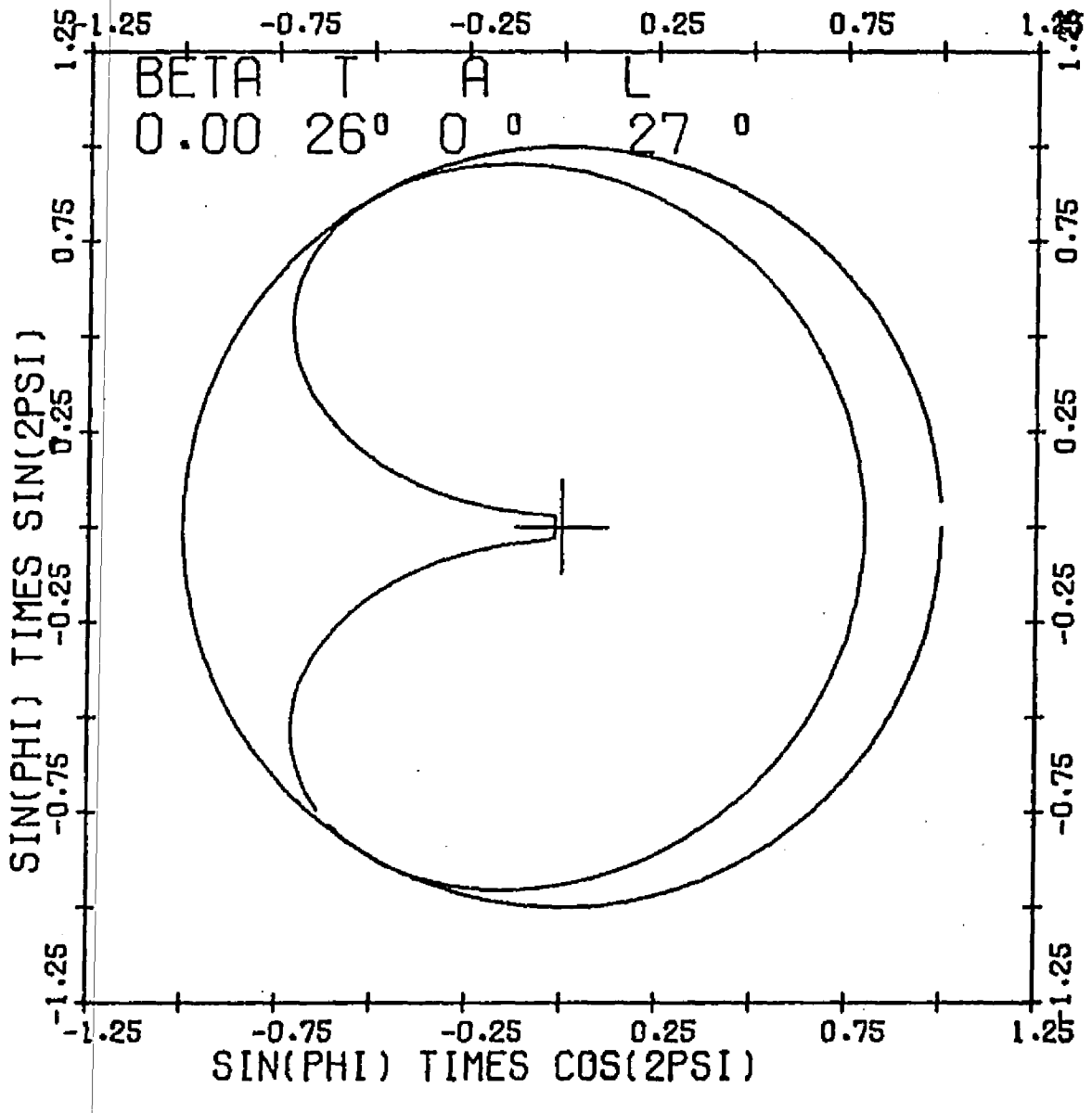

Figure 26. 2Ψ Versus sin ϕ for β=0, T=26°, L=27°

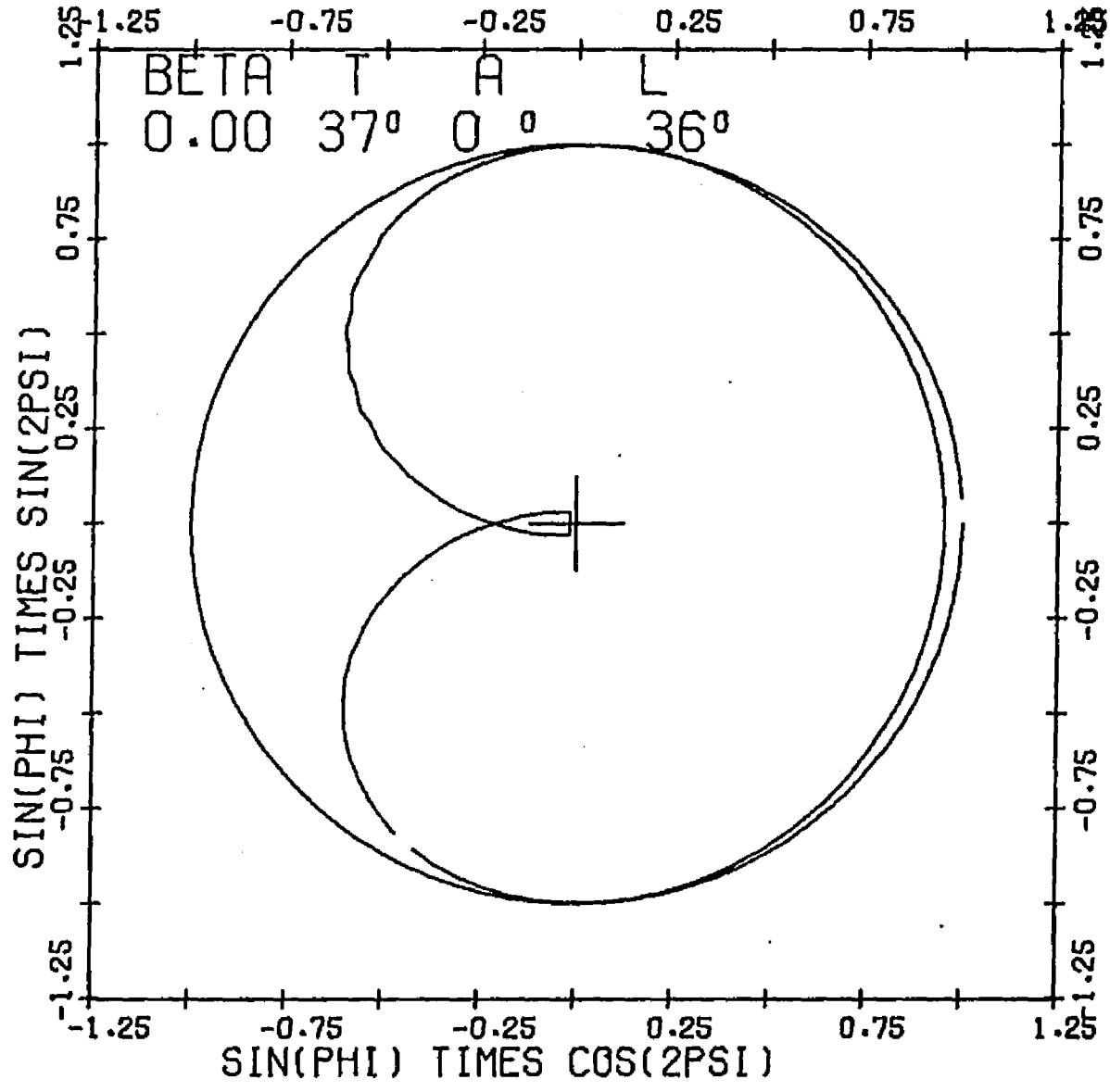

Figure 27. 2Ψ Versus sin ϕ for β=0, T=37°, L=36°

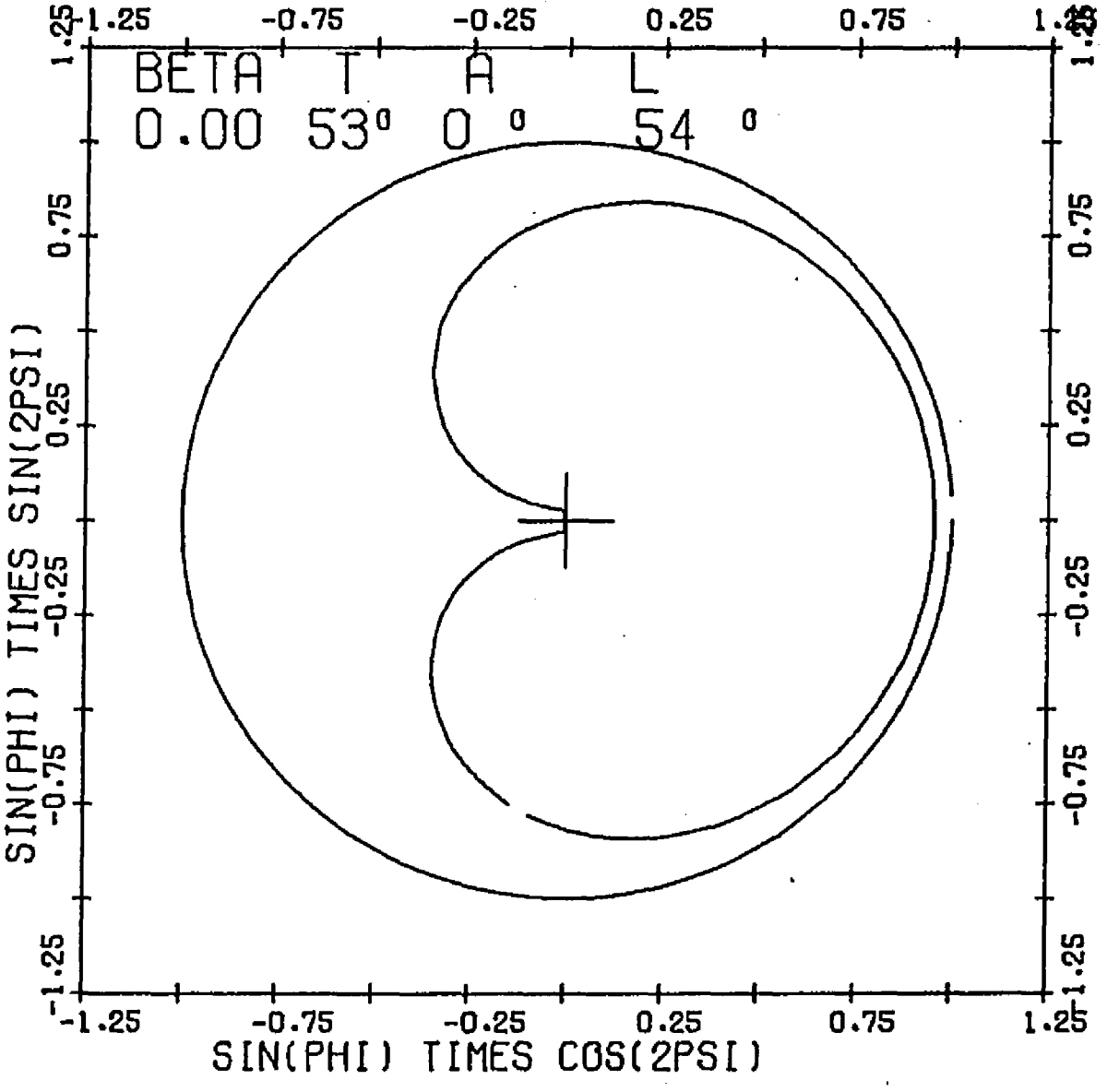

Figure 28. 2Ψ Versus sin ϕ for β=0, T=53°, L=54°

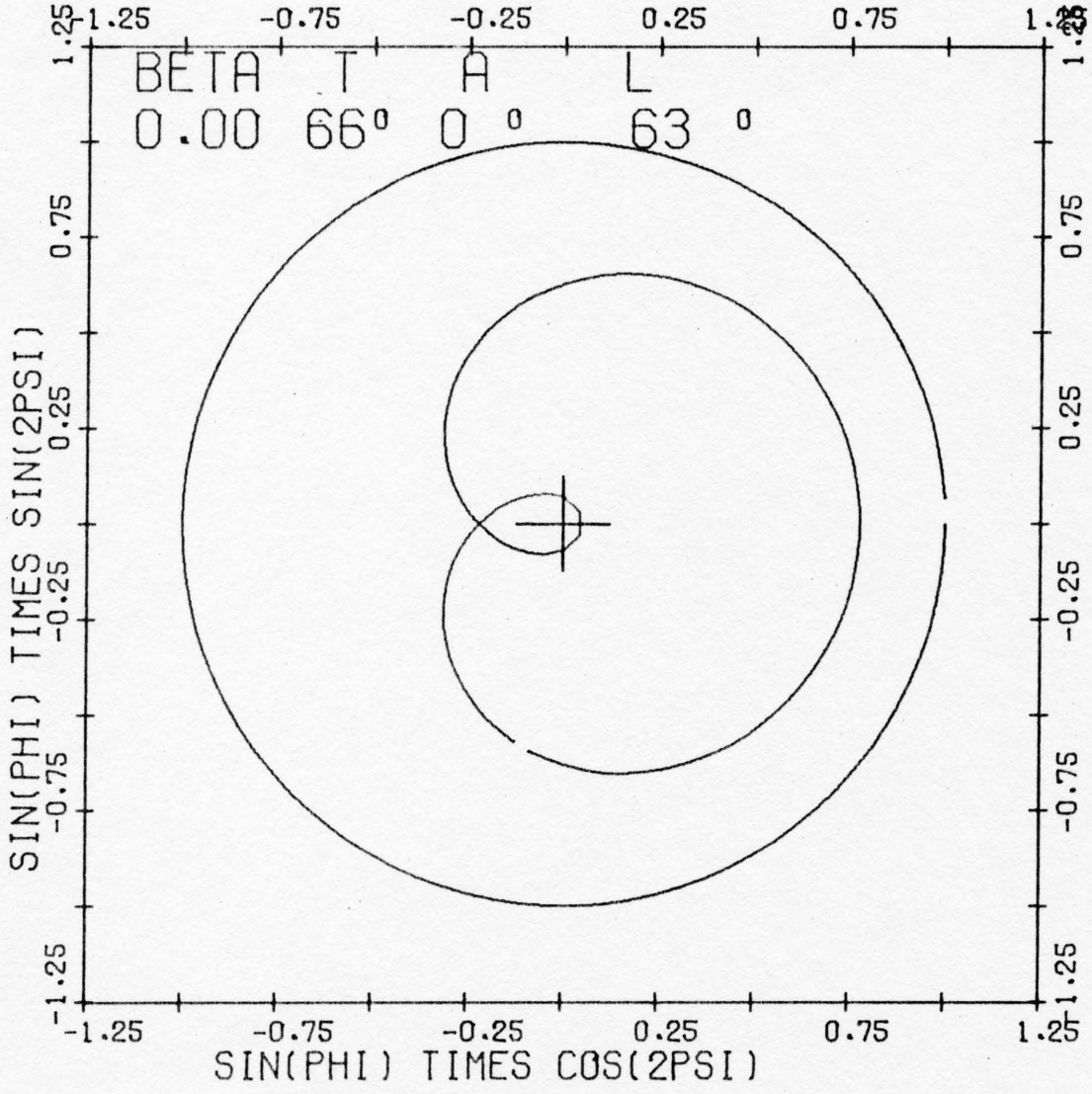

Figure 29. 2Ψ Versus sin ϕ for β=0, T=66°, L=63°

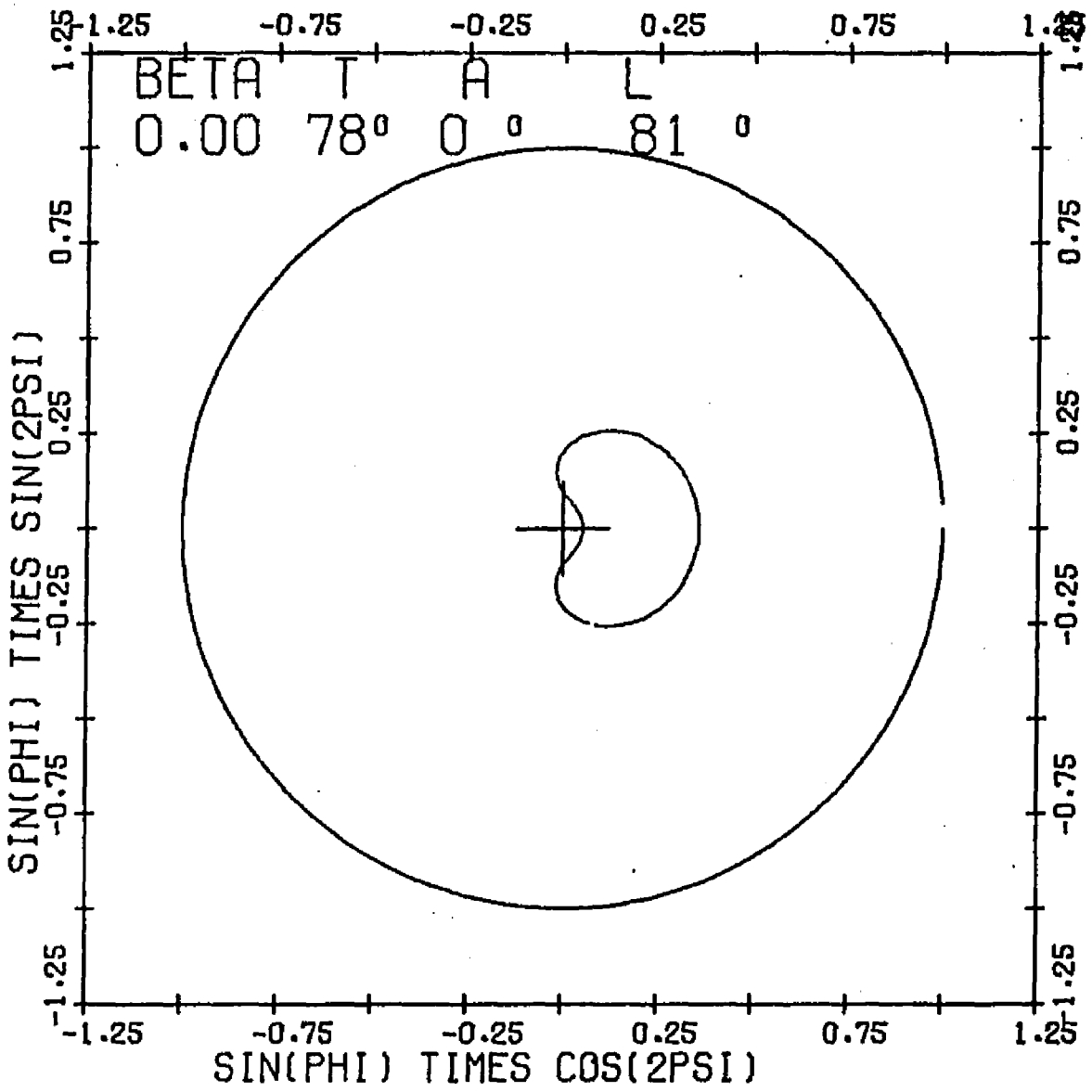

Figure 30. 2Ψ Versus sin ϕ for β=0, T=78°, L=81°

however, the approximation is good and all of the plots are applicable, as was discussed in Section I.A..

In the radial plots of sin ϕ versus 2Ψ, a loop around the original means that the magnetic field vector passed above (nearer to rotation axis) our line of sight, while a bend around the origin indicates that it passed below our line of sight.

2. The Relativistic Models

In relativistic models, one cannot properly speak of a longitude connected with emission observed at time t. This is because $t \neq \theta/\Omega$ but is given by Equation (8.5). Of course, if each emission region were seen only at one θ and there were an ensemble of emission regions distributed longitudinally, then it would be correct to talk of a longitude of emission seen at any time t. However, such models are not single vector models and will not be discussed further in this section.

In general, relativistic polarization plots of observed position angle and amount versus time will be asymmetrical, except for the special case $A = 90°$, when they become symmetrical about the times $t = 0$ and $t = p/2$, or when $L = 0°$ and $A = 0°$, when the same symmetries hold. In these models, the maximum position angle sweep rate is

no simple function of T and L, but depends on all parameters, and is most easily found from calculated plots.

Certain symmetries, however, do appear in polarization plots and maps made for relativistic models, and these are very important. For instance, the polarization remains the same under a simultaneous change of the signs of A, t, L, and Ψ. Thus, it is not necessary to plot the polarizations for negative values of A, as they may be obtained from the plots of positive A by the sign changes mentioned. Also, when A = 0, the above property insures that the polarizations at L and -L will be the same except for time and position angle sign reversals.

It is also interesting that all plots of sin ϕ sin 2Ψ versus sin ϕ cos 2Ψ are symmetrical about $\Psi = 0°$, no matter what the time rate of their traversal. Figure 31 shows this for one combination of parameters.

Also, in plots of sin ϕ sin 2Ψ versus sin ϕ cos 2Ψ, for a given set of values of β and T, the plots will be exactly the same for all combinations of A and L which have sin ϕ going to zero at some point in time. This property is not easy to understand, but is borne out by Figures 31 and 32, which show these "heart-shaped" diagrams for $\beta = 0.87$, $T = 18°$, for $A = 42°$, $L = 54°$ (Figure 31) and for $A = 0°$, $L = 36°$ (Figure 32). If laid atop each other, these "heart-shaped" diagrams nearly exactly coincide.

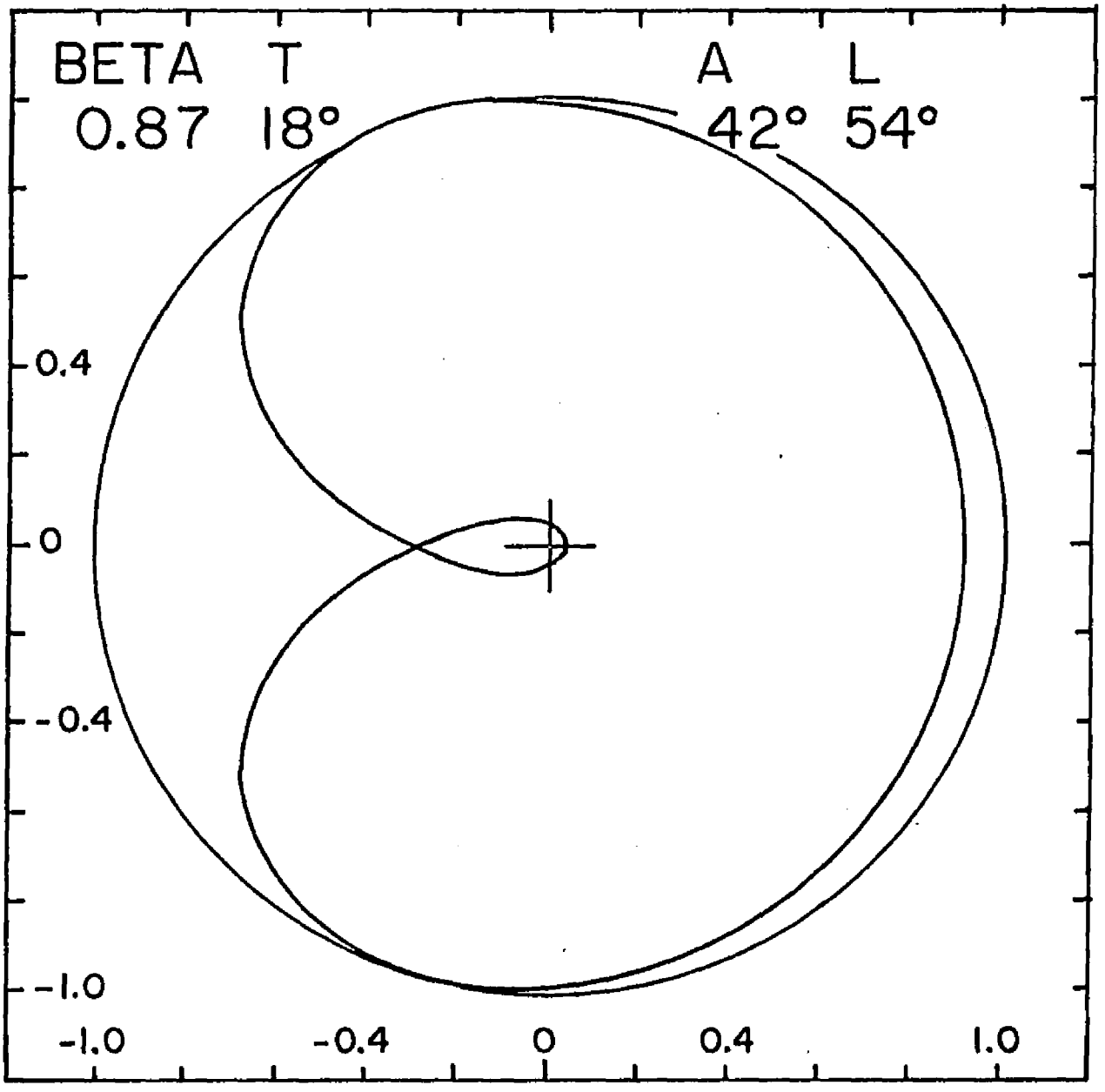

Figure 31. 2Ψ Versus sin ϕ for β=0.87, T=18°, A=42°, L=54°

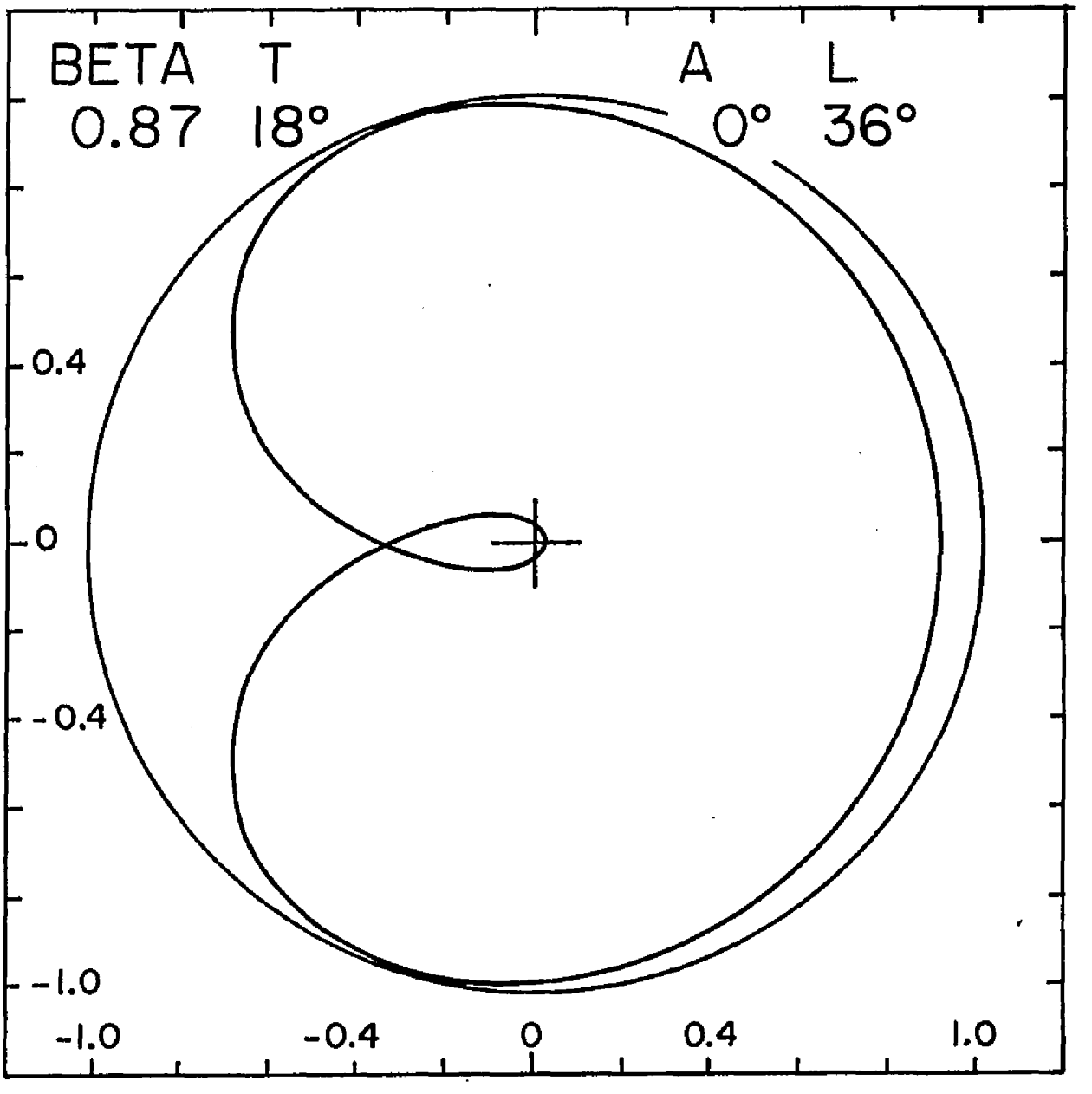

Figure 32. 2Ψ Versus sin ϕ for β=0.87, T=18°, A=0°, L=36°

Thus, in calculating sin ϕ versus Ψ for cases where sin ϕ goes nearly to zero, one need not worry about all possible values of A. One calculation will suffice. Also, in general, there may be two values of L for each combination of β, T, and A which will result in sin ϕ going to zero. Now the heart-shaped diagrams are symmetrical about $\Psi = 0°$, and for $A = 0°$, the polarization behavior of -L is the same as that for L, neglecting the time dependence and the sign of Ψ. Thus, the heart-shaped diagram which describes sin ϕ versus Ψ for the positive L of $P = 0$ is the same as for the negative L of $P = 0$ for $A = 0°$, and thus for any A, by the arguments above! These remarkable and as yet analytically unproven properties, found empirically by inspection of calculated results, will make it easy to determine β and T for any pulsar which displays pulses wherein the linear polarization goes to zero. Then, using plots of angle and amount versus time, the necessary combination of A and L can be found.

In Figures 33 through 64 are heart-shaped diagrams for cases of sin $\phi \simeq 0$ for β of 0.55, 0.74, 0.87, 0.94, and 0.98 and various values of T.

Figures 63 and 64 are especially interesting, as they show that for small values of T and $L = 0°$ there can be two minima in sin ϕ of equal and very small amount. Figures 65 through 68 show the time behavior of these

polarizations, and it becomes clear that the linear polarization minima can appear to be very close together in time, so that the minima would appear as double.

In order to find out where double linear polarization minima are possible, we will combine, for A = 0°, the requirement on T and L for sin ϕ to go to zero with the requirement for cos ϕ to go to zero (as there cannot be two linear polarization minima if sin ϕ does not go to 1 in between). The first requirement is (Equation 21) sin L = $\pm$ γ sin T, or $|\sin L| = |\gamma \sin T|$. The second requirement is that (Equation 22)

$$\sin \theta = - \tan L \tan T,$$

or

$$|\tan L \tan T| < 1 ,$$

or

$$|\sin L| < |\cos T| .$$

Thus,

$$|\gamma \sin T| < |\cos T| ,$$

or

$$\tan T < 1/\gamma .$$

Table 5 gives the approximate maximum values of T for which double linear polarization minima are possible for various values of β.

TABLE 5

Maximum Values of T for Which Double Linear Polarization Minima are Possible

β	$\sim\gamma$	$\sim\tan T_{max}$	$\sim T_{max}$
0.00	1.0	1.0	45°
0.55	1.2	0.83	40
0.75	1.5	0.67	34
0.87	2.0	0.50	27
0.94	3.0	0.33	18
0.98	5.0	0.20	11
0.995	10.0	0.10	6

More about this will come in Section II.C.1..

Finally, in Figures 69 through 121 are shown the time behavior of the polarization position angle for some of the values of β, T and A given in Table 4, and for L which yields the smallest value of sin ϕ. Also in these figures the corresponding time behavior of sin ϕ is shown. Tables 6 and 7 will be very useful for help in finding specific cases among the illustrations.

TABLE 6

Illustrations of sin ϕ cos 2Ψ vs. sin ϕ sin 2Ψ
For Cases When sin ϕ Goes Approximately to Zero

		T							
	Figure Number	0°	6°	18°	26°	37°	53°	66°	78°
β	0.00	24	--	25	26	27	28	29	30
	0.55	--	--	33	38	43	48	53	58
	0.75	--	63	34	39	44	49	54	59
	0.87	--	64	31, 32, 35	40	45	50	55	60
	0.94	--	--	36	41	46	51	56	61
	0.98	--	--	37	42	47	52	57	62

TABLE 7

Illustrations of sin ϕ and ψ vs. Fraction
of Pulse Period for L of Minimum sin ϕ

		T					
	Figure Number	18°	26°	37°	53°	66°	78°
β	0.55	69 70 71 72	83	90 91	100	107 108	116
	0.74	73	84 85	92	101 102	109	117 118
	0.87	74 75 76 77	86	93 94 95 96	103	110 111 112 113	119
	0.94	78	87 88	97	104 105	114	120
	0.98	79 80 81 82	89	98 99	106	115	121

When four figure numbers are given, plots for A = 0°, 19°, 42°, and 90° are shown.

When two figure numbers are given, plots for A = 0° or 90° and 42° are shown.

When one figure number is given, a plot for A = 0° or 90° is shown.

Finally, in Figures 122 through 148 are shown plots of the polarization properties of some models which do not have L such that sin ϕ will go to zero. These are included so that the general properties of such models may be inferred. It will be noticed that the "heart-shaped" diagrams are always convex outward at the secondary minimum of sin ϕ, if there is one. The primary minimum may either loop or bend around the origin, but in any case, the origin is within the average envelope of the "heart-shaped diagram near polarization minimum.

This concludes the first section of this dissertation, and essentially specifies the generalized single vector model in all important aspects.

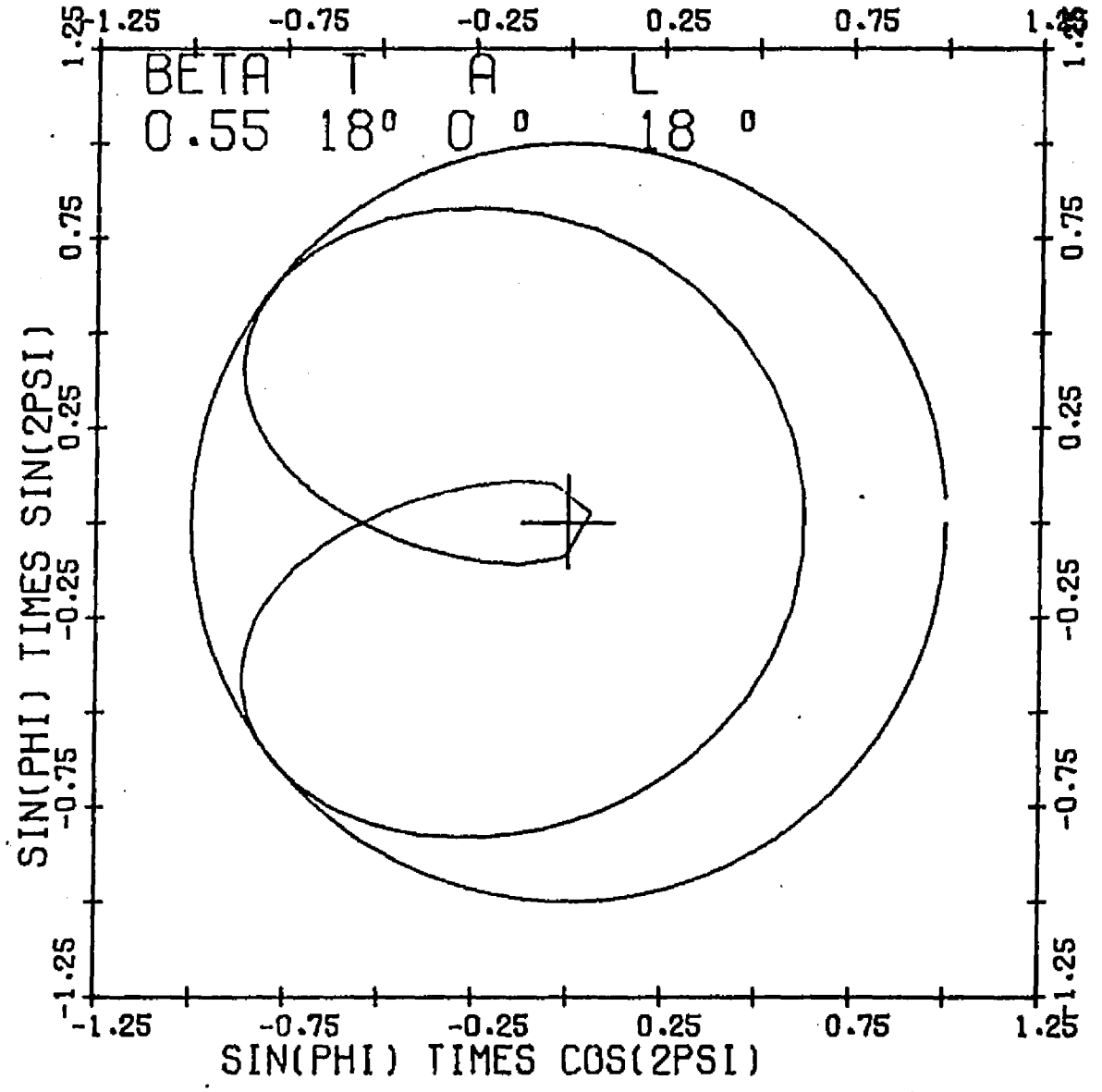

Figure 33. 2Ψ Versus sin ϕ for β=0.55, T=18°, P→0

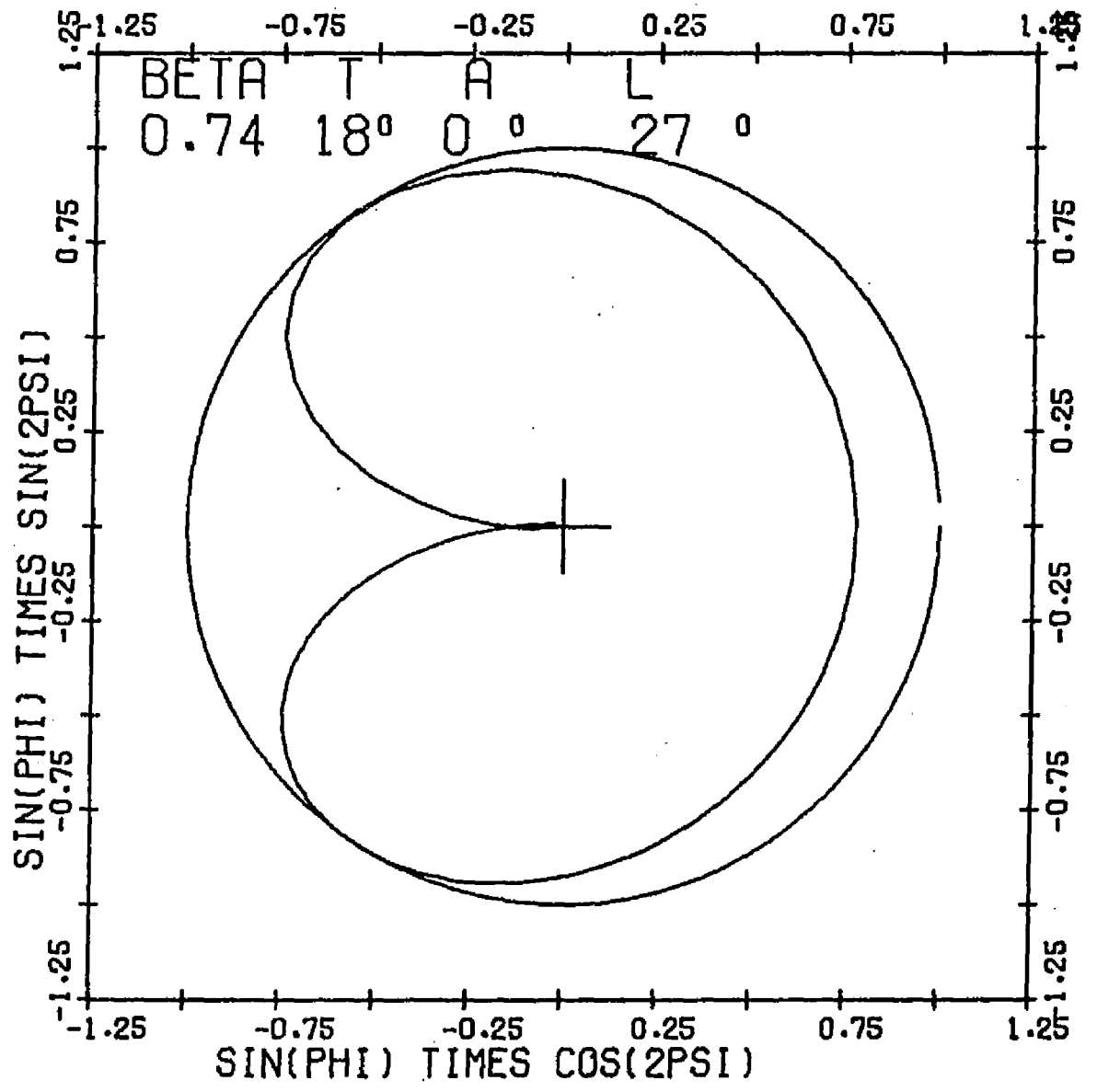

Figure 34. 2Ψ Versus sin ϕ for β=0.74, T=18°, $P_{\sim}^{+}0$

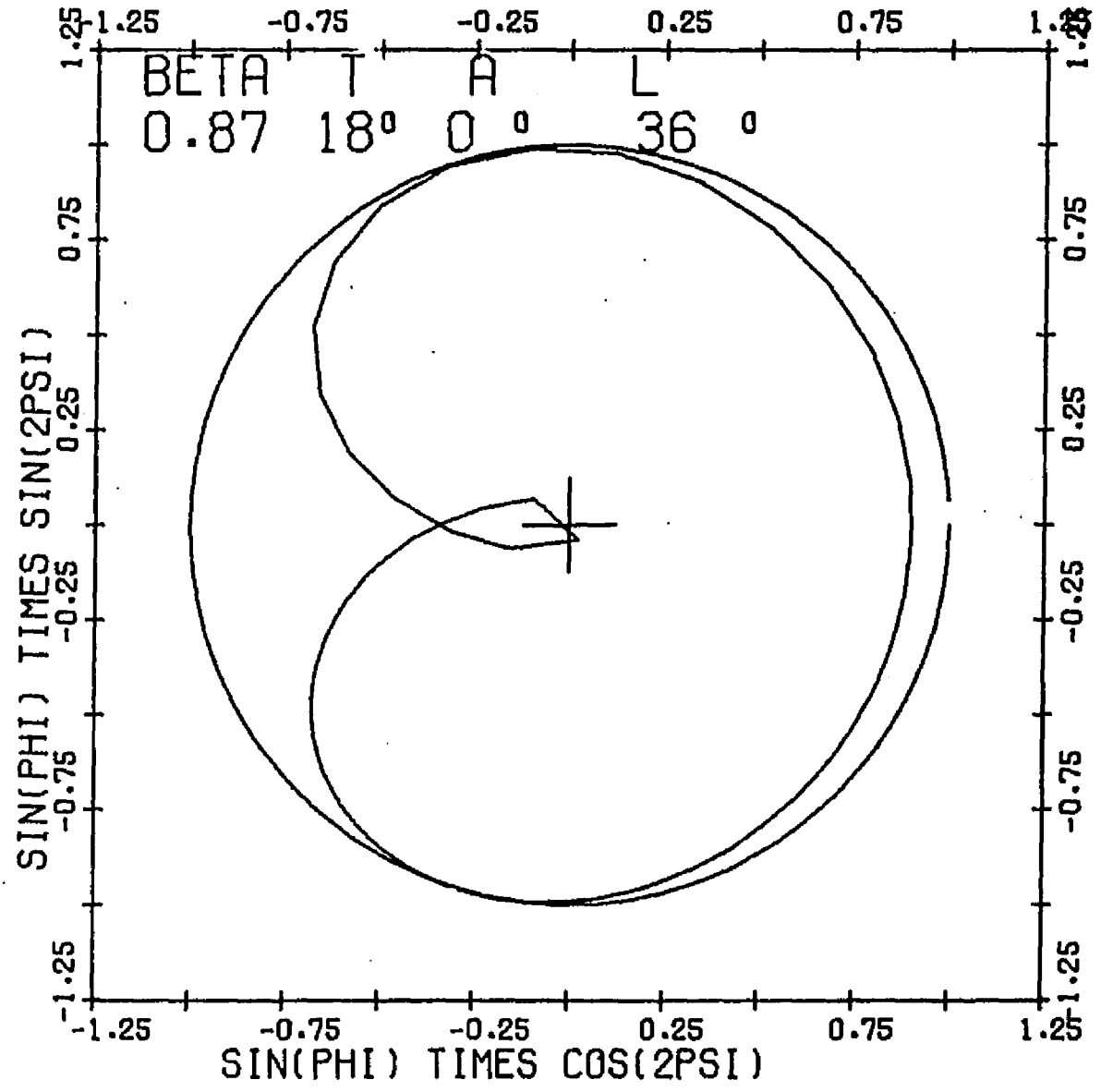

Figure 35. 2ψ Versus sin ϕ for β=0.87, T=18°, $P_{\sim}$0

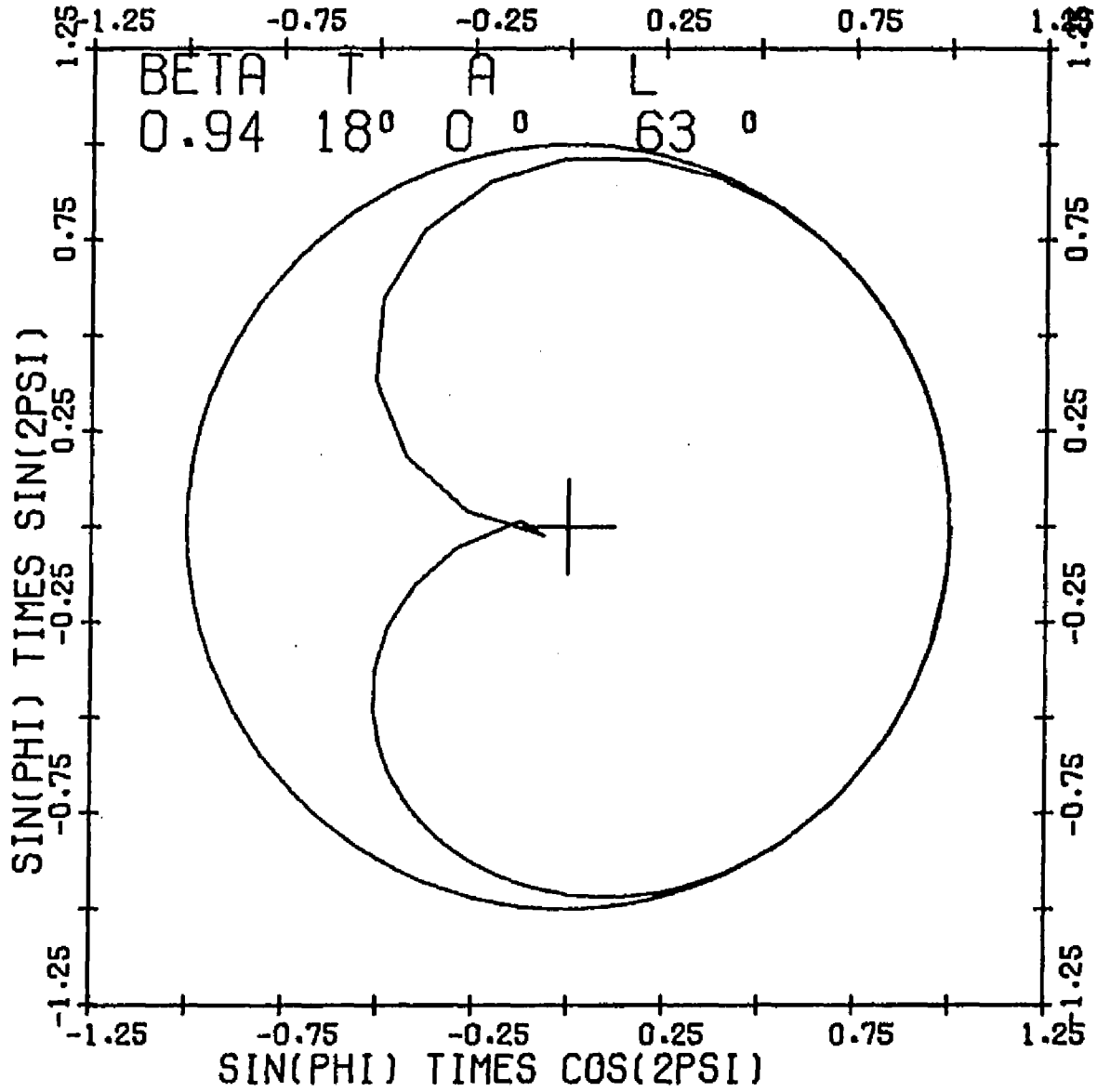

Figure 36. 2Ψ Versus sin ϕ for β=0.94, T=18°, $P_{\sim}$0

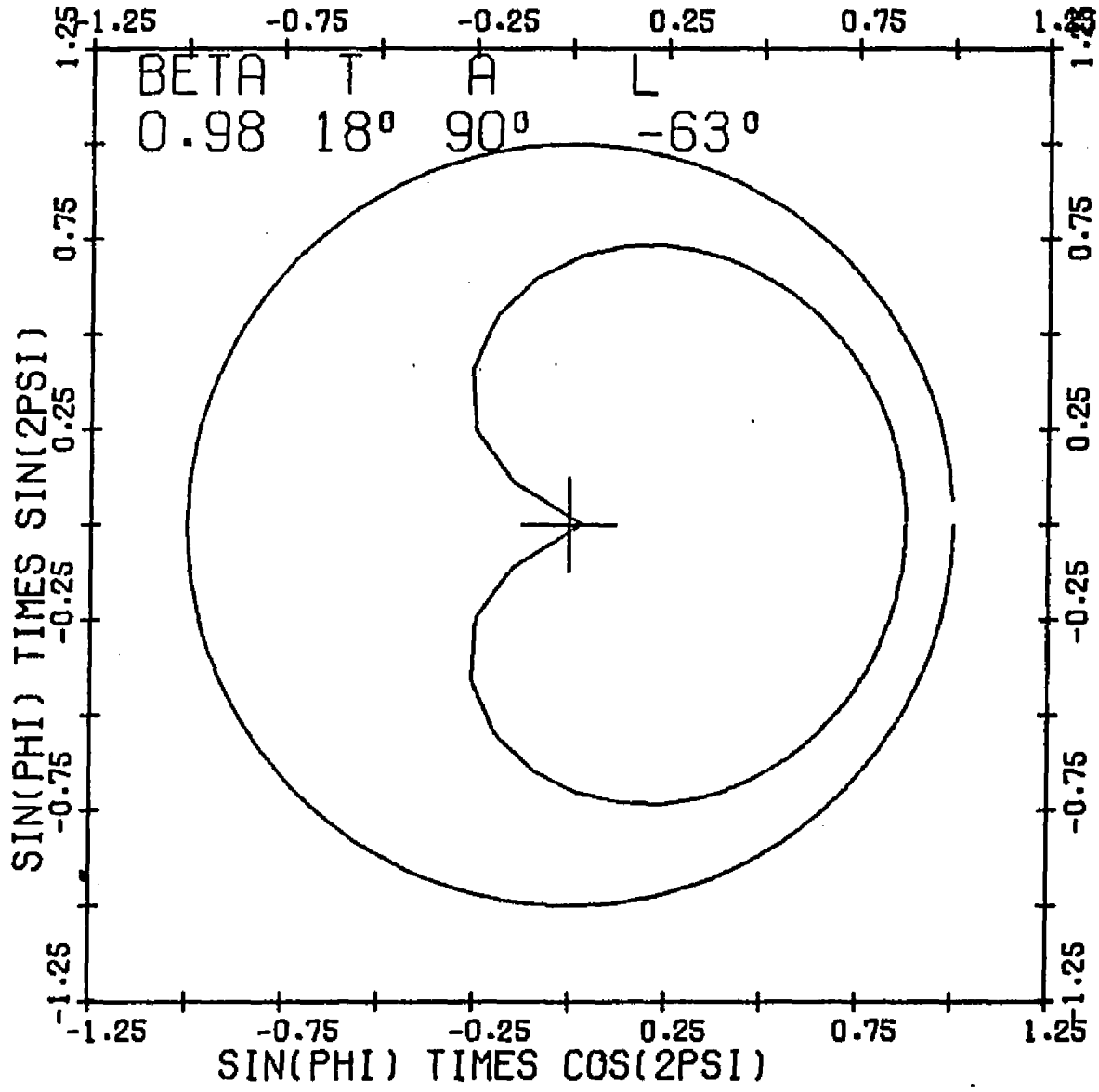

Figure 37. 2ψ Versus sin ϕ for β=0.98, T=18°, P≠0

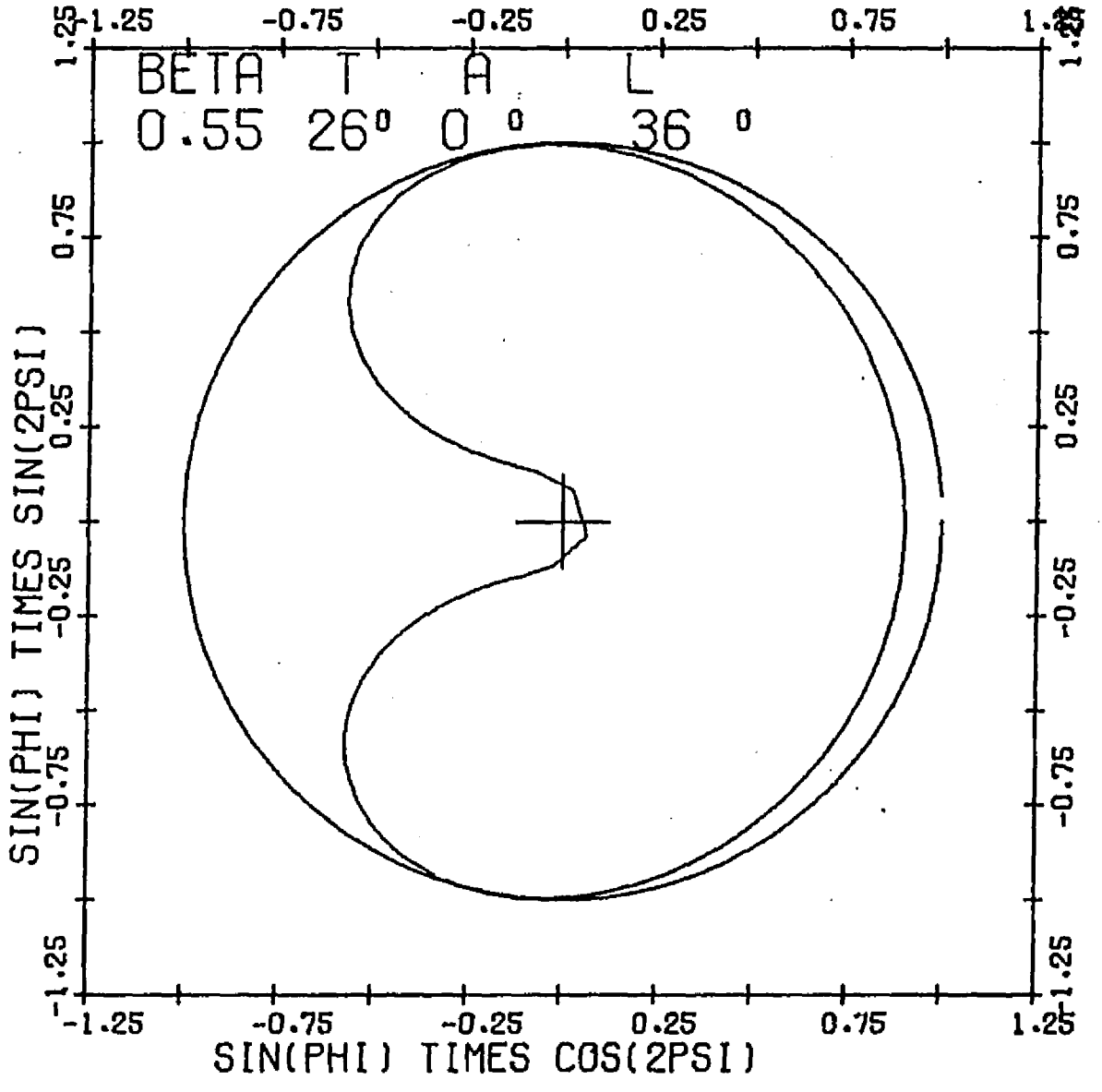

Figure 38. 2ψ Versus sin ϕ for β=0.55, T=26°, $P_{\pm}$0

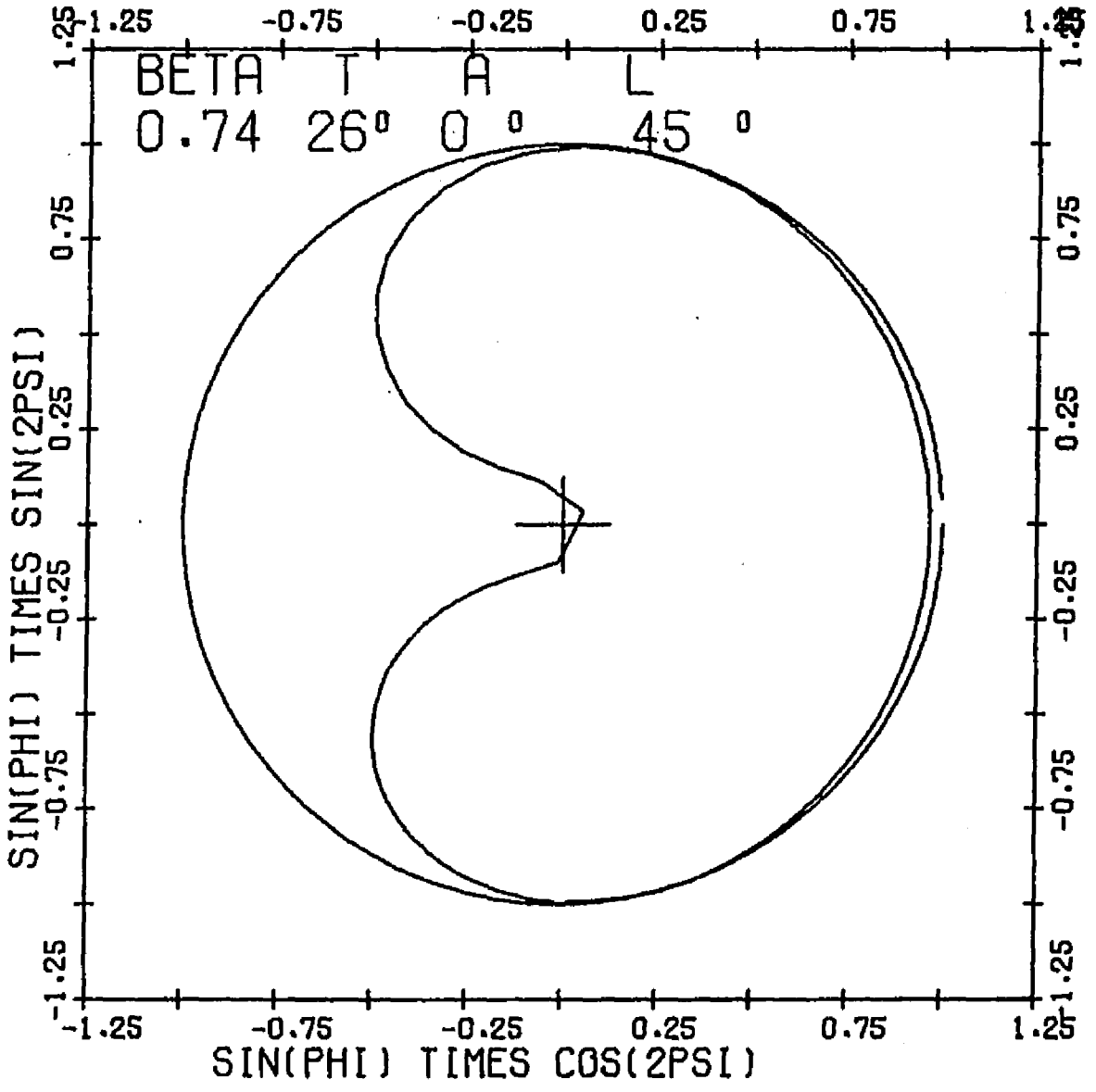

Figure 39. 2ψ Versus sin ϕ for β=0.74, T=26°, $P_{\pm}$0

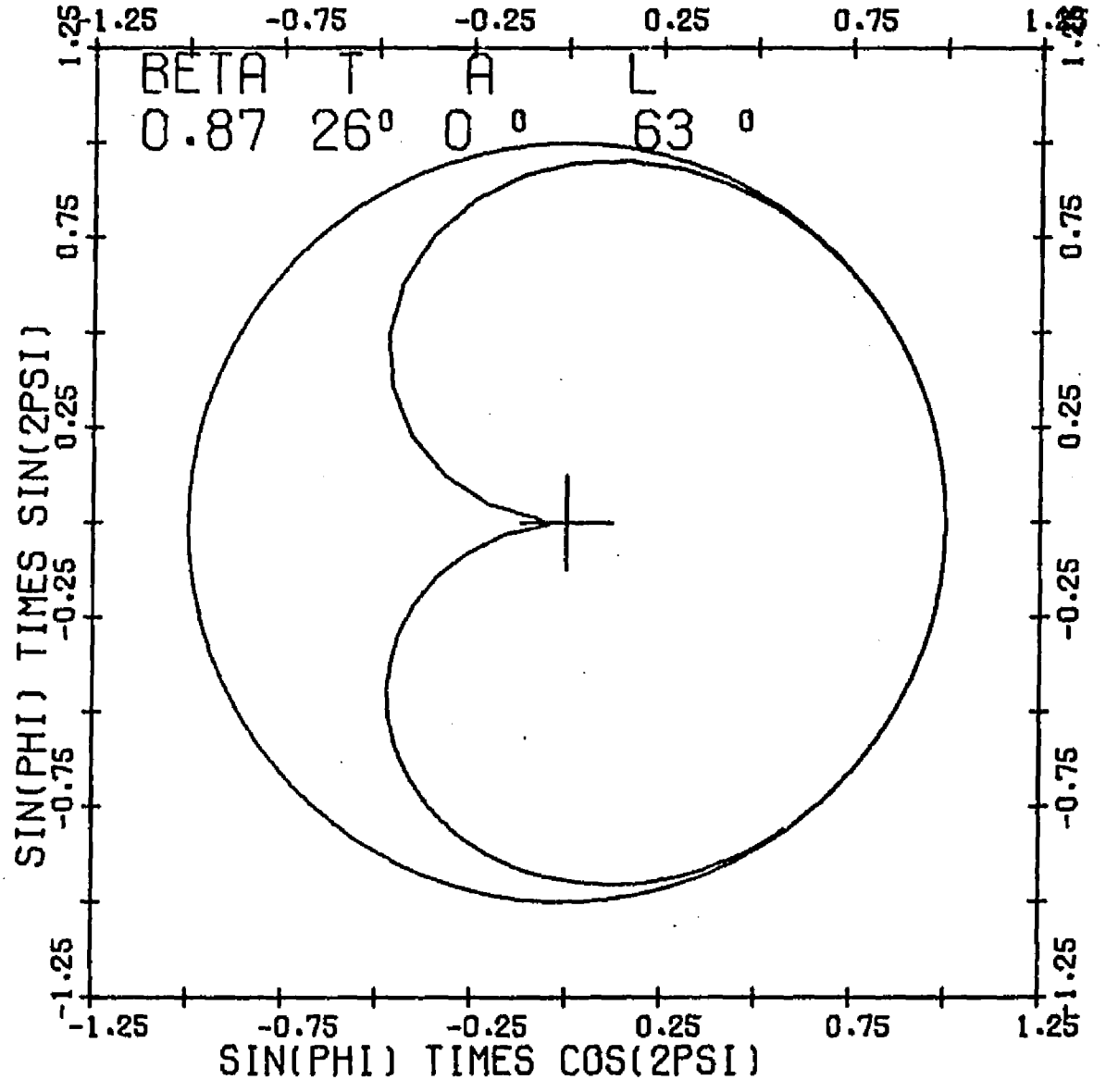

Figure 40. 2ψ Versus sin ϕ for β=0.87, T=26°, $P_{\sim}$0

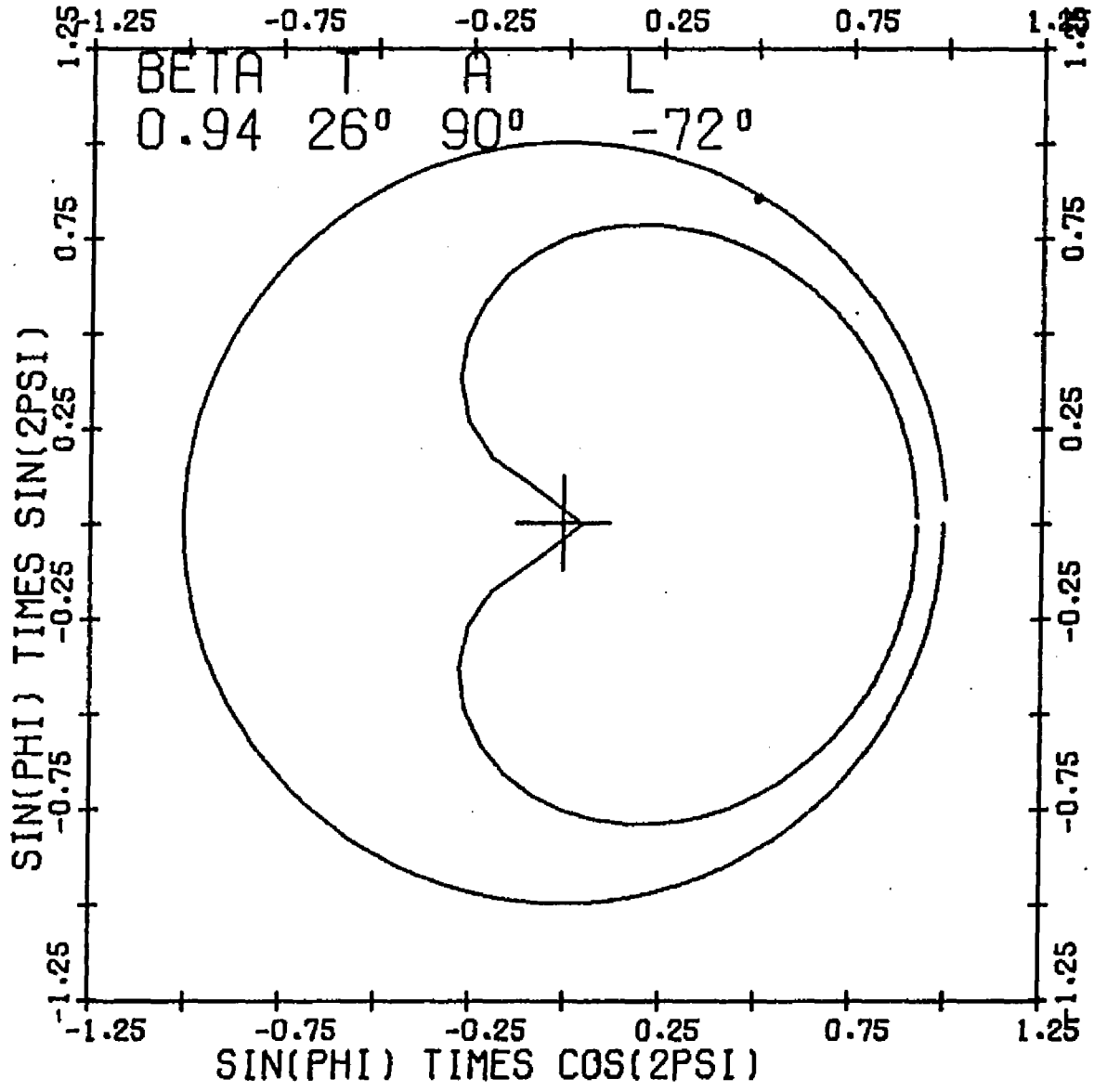

Figure 41. 2ψ Versus sin ϕ for β=0.94, T=26°, P$\doteq$0

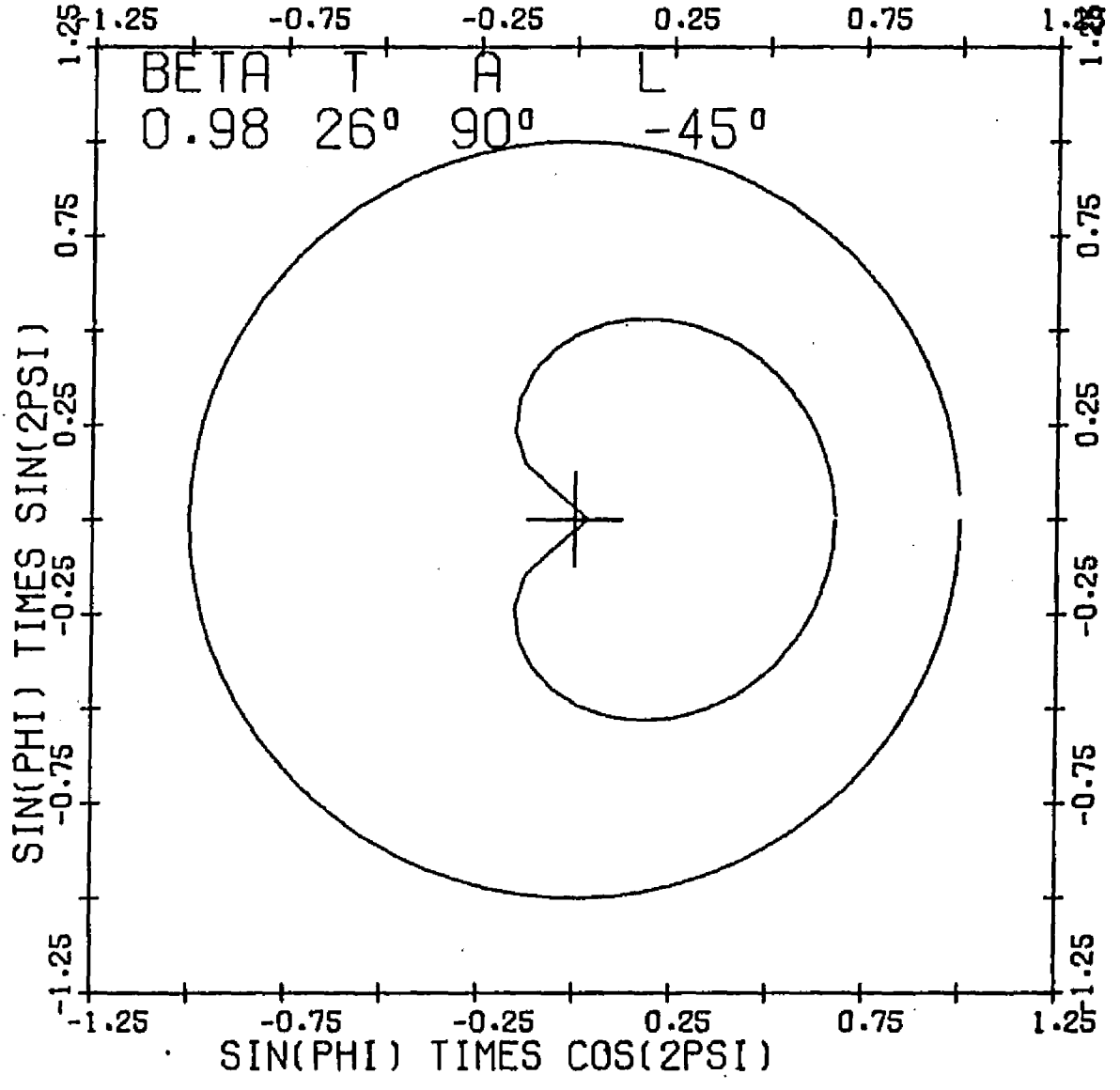

Figure 42. 2Ψ Versus sin ϕ for β=0.98, T=26°, P$\tilde{}$0

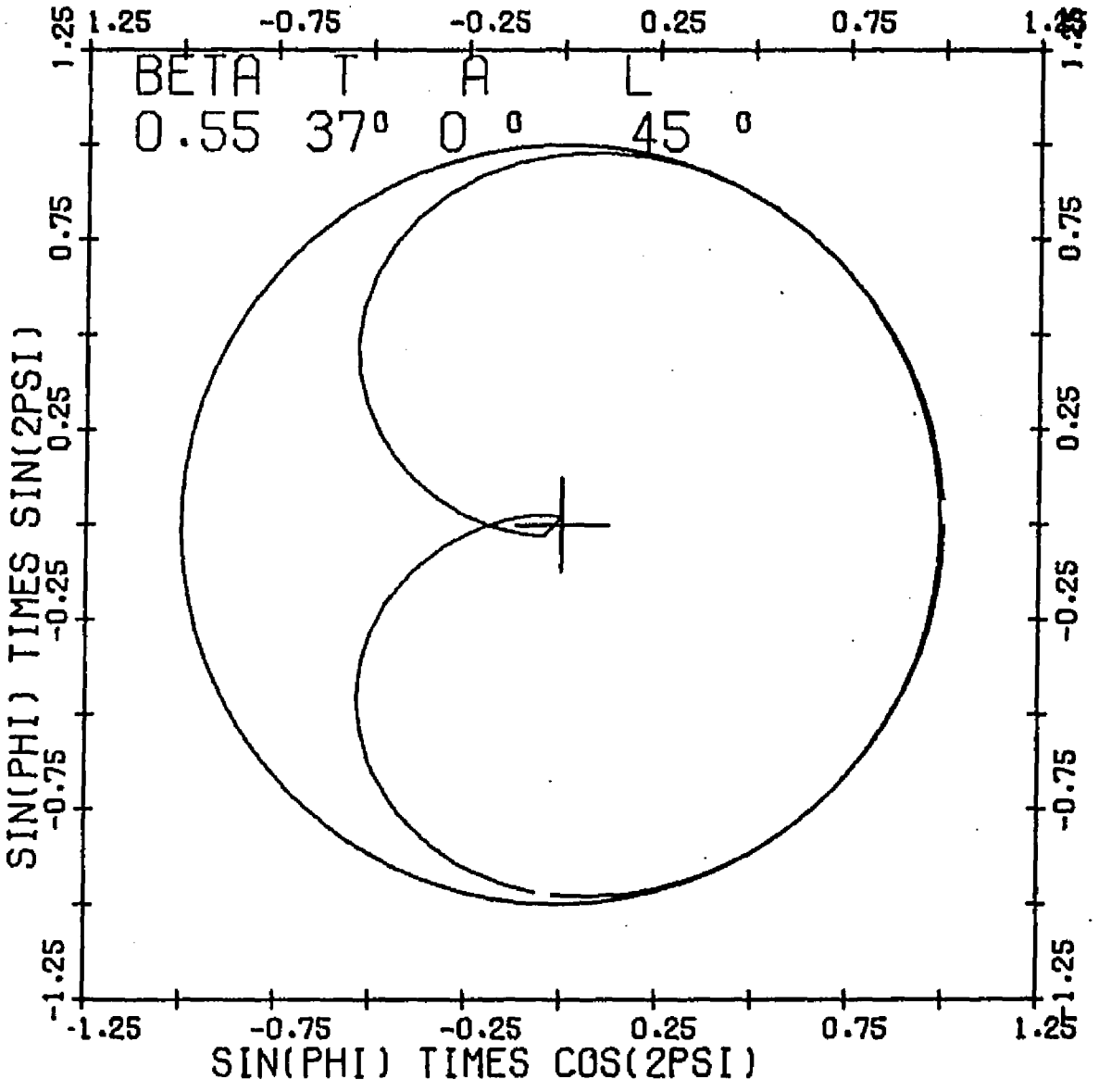

Figure 43. 2Ψ Versus sin ϕ for β=0.55, T=37°, P±0

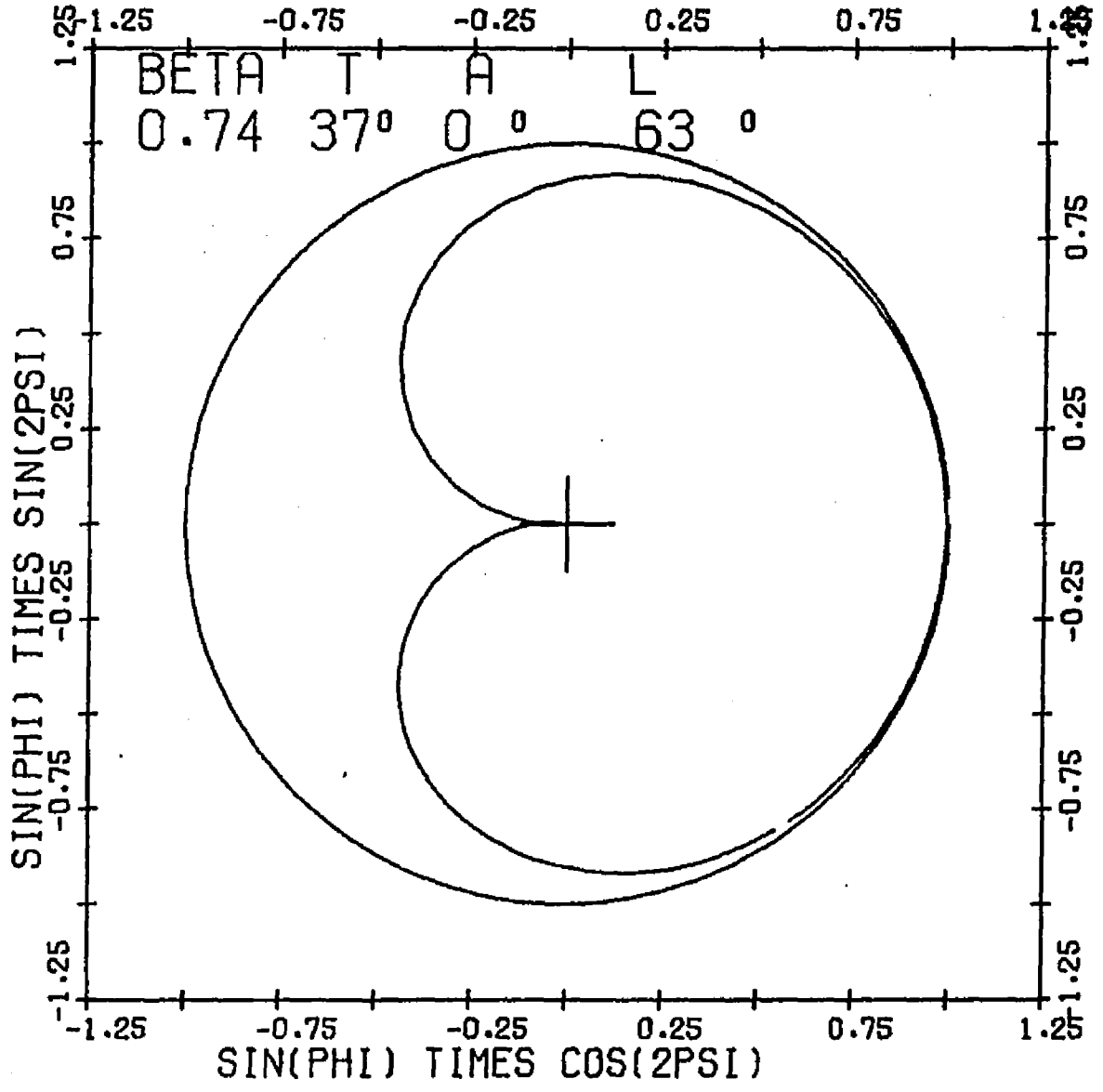

Figure 44. 2Ψ Versus sin ϕ for β=0.74, T=37°, P±0

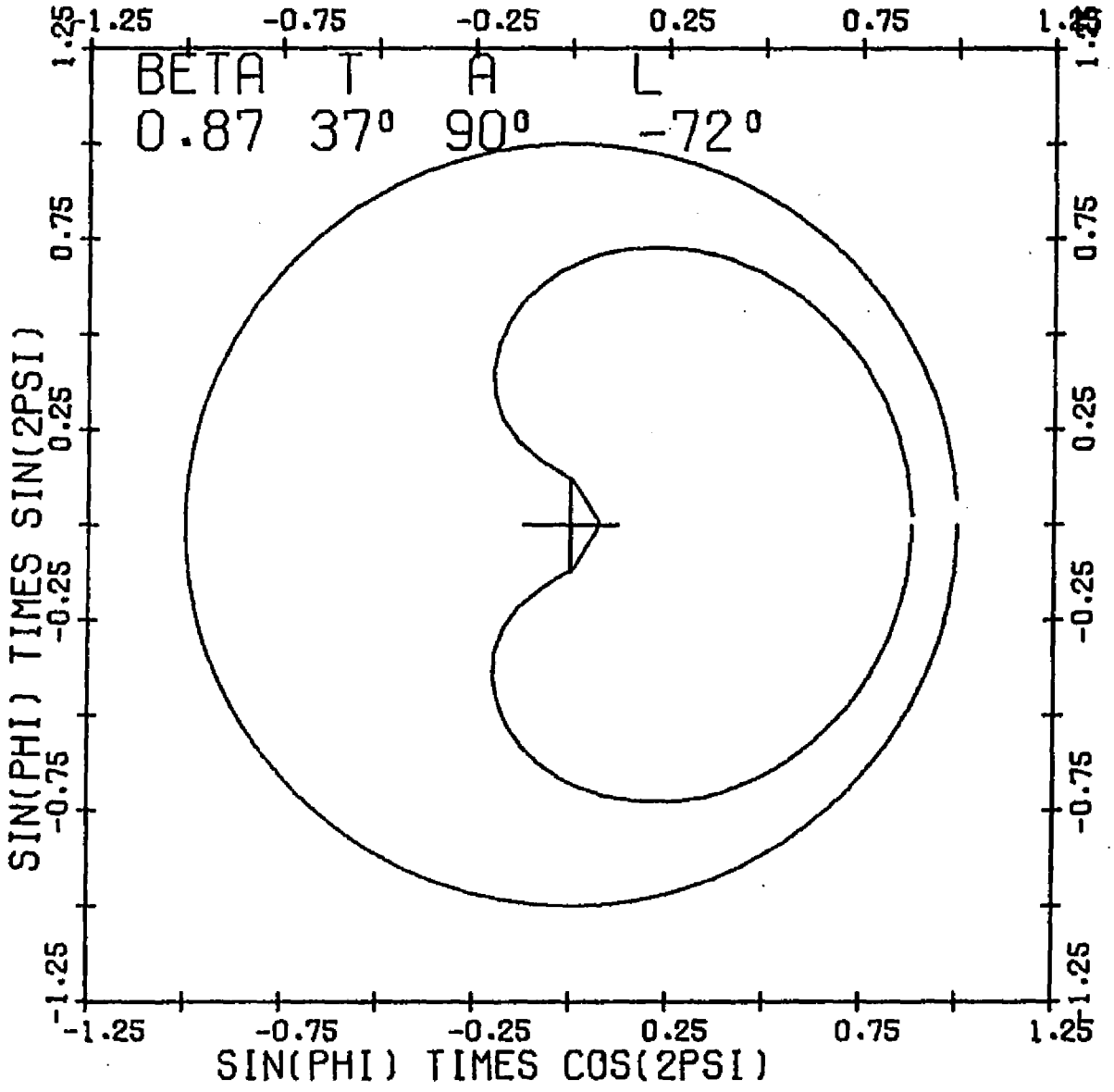

Figure 45. 2Ψ Versus sin ϕ for β=0.87, T=37°, $P_{\tilde{}}$0

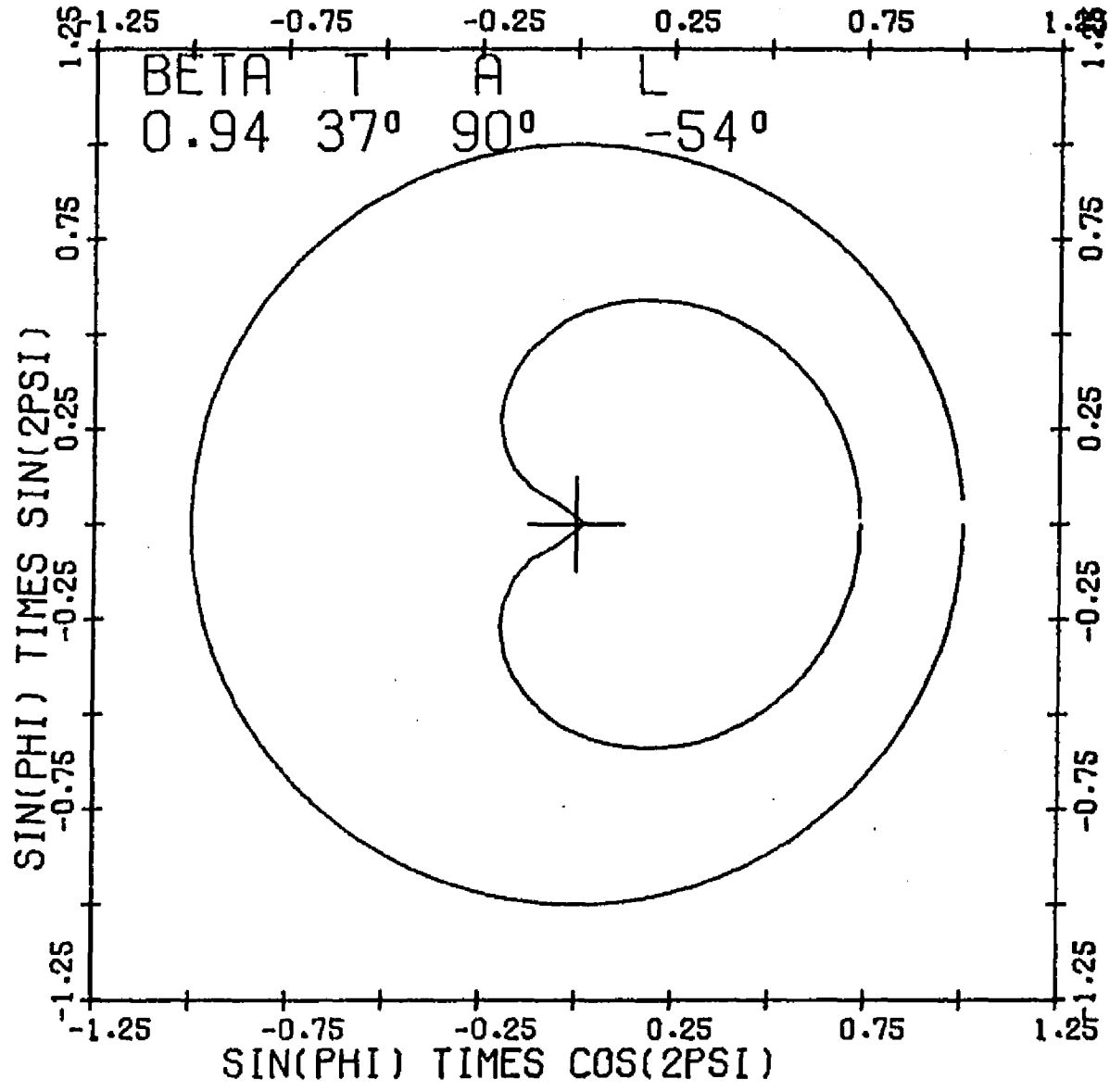

Figure 46. 2Ψ Versus sin ϕ for β=0.94, T=37°, P+0

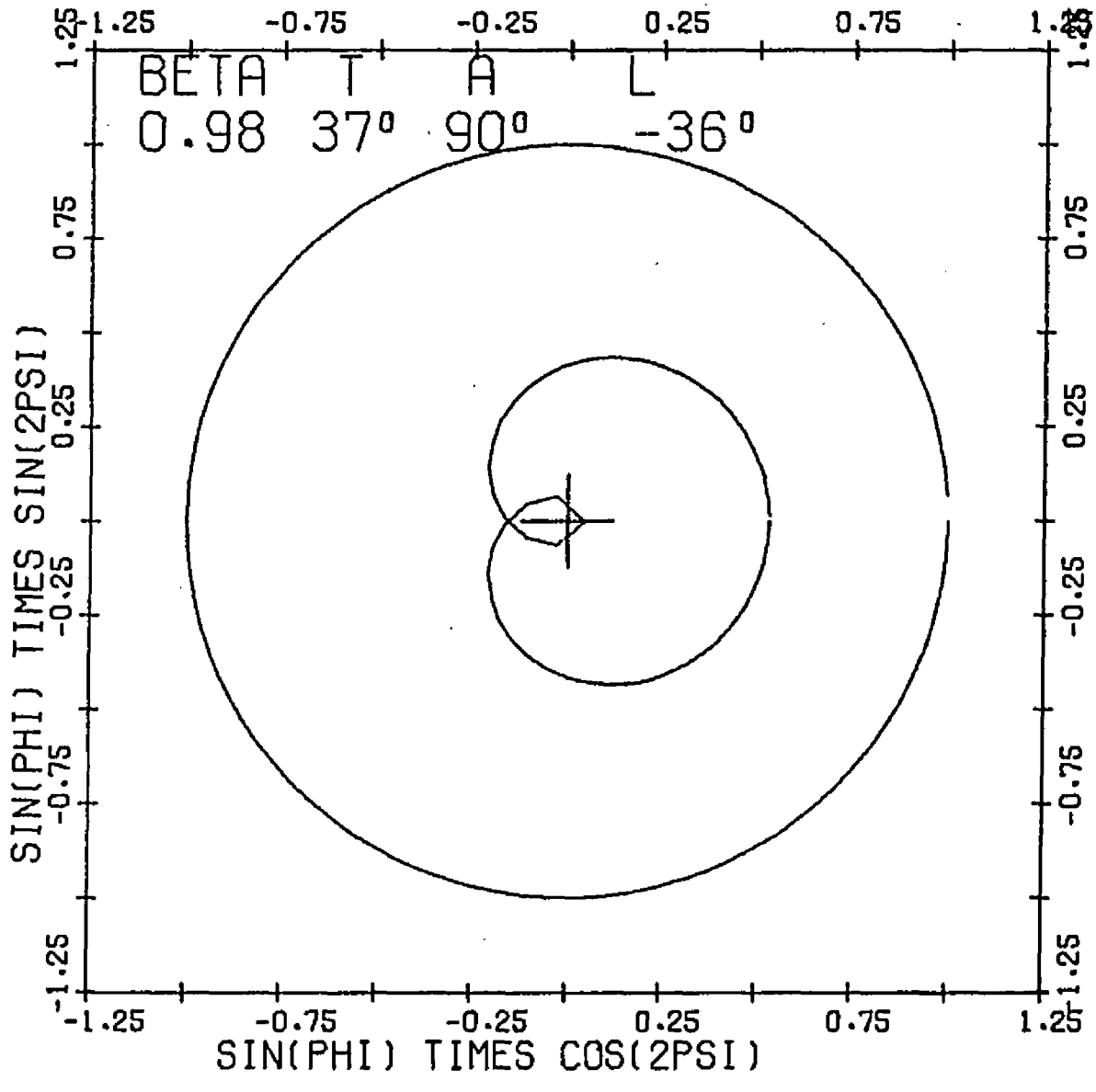

Figure 47. 2Ψ Versus sin ϕ for β=0.98, T=37°, P=0

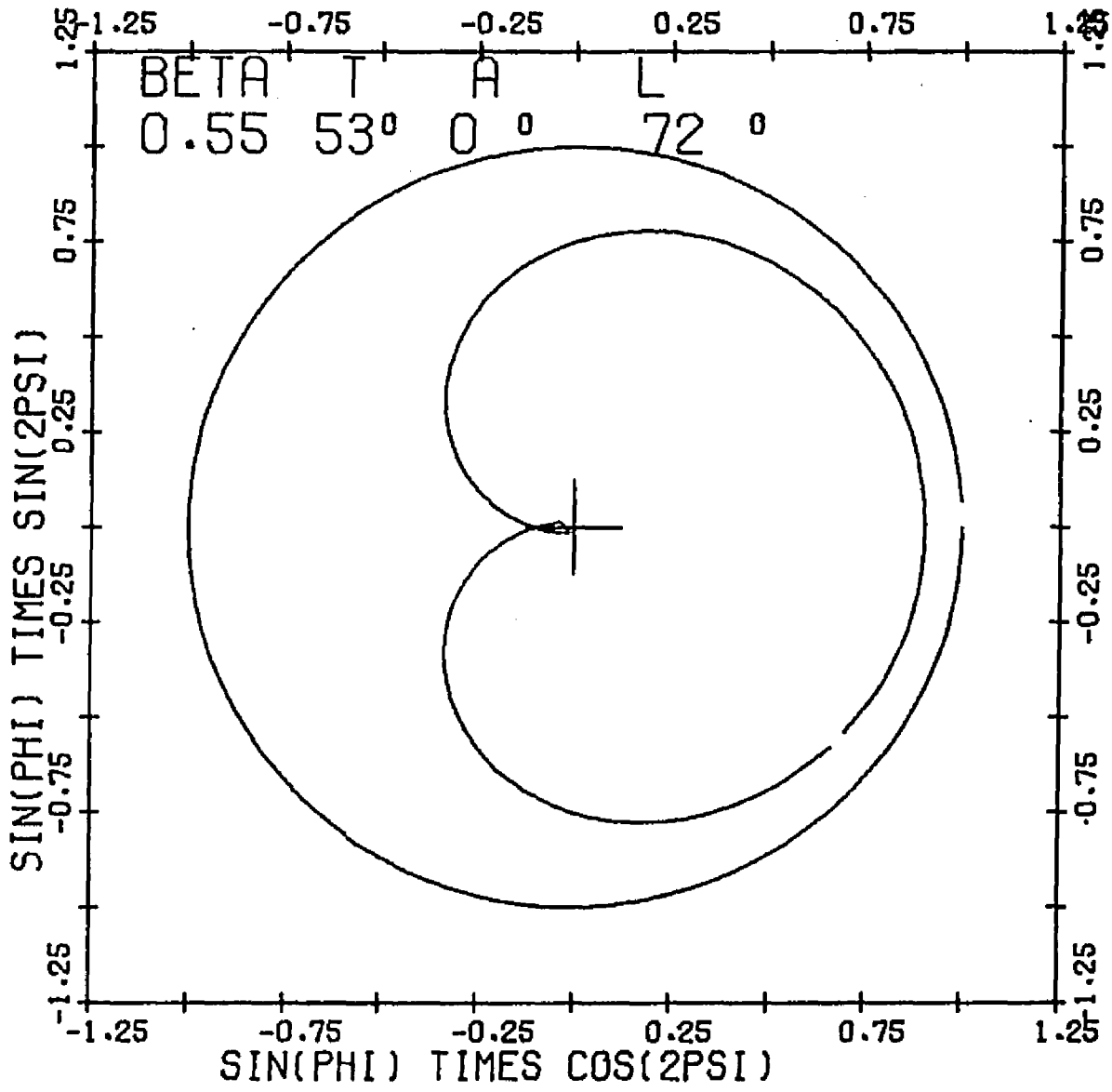

Figure 48. 2Ψ Versus sin ϕ for β=0.55, T=53°, P$\doteq$0

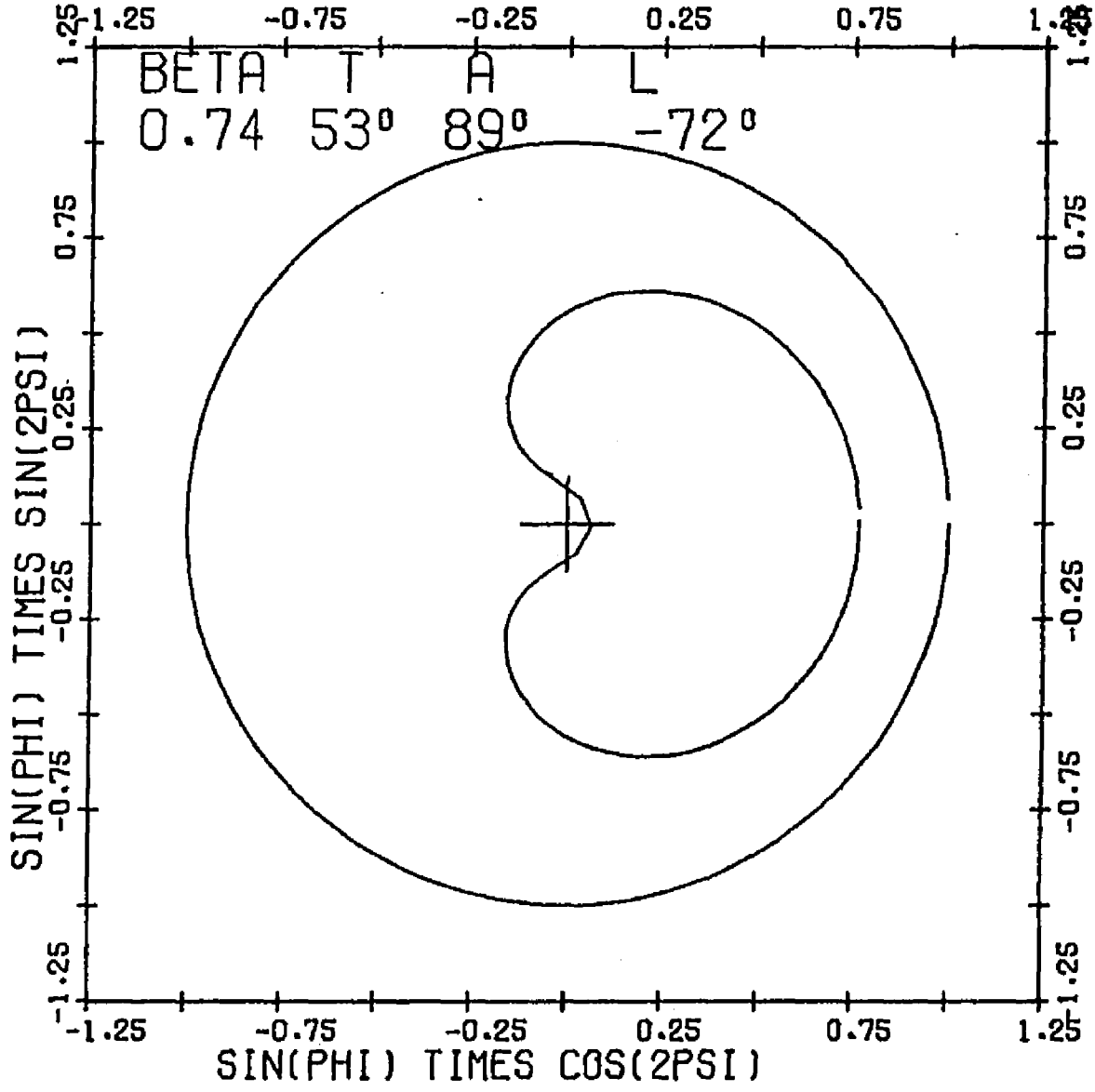

Figure 49. 2Ψ Versus sin ϕ for β=0.74, T=53°, P±0

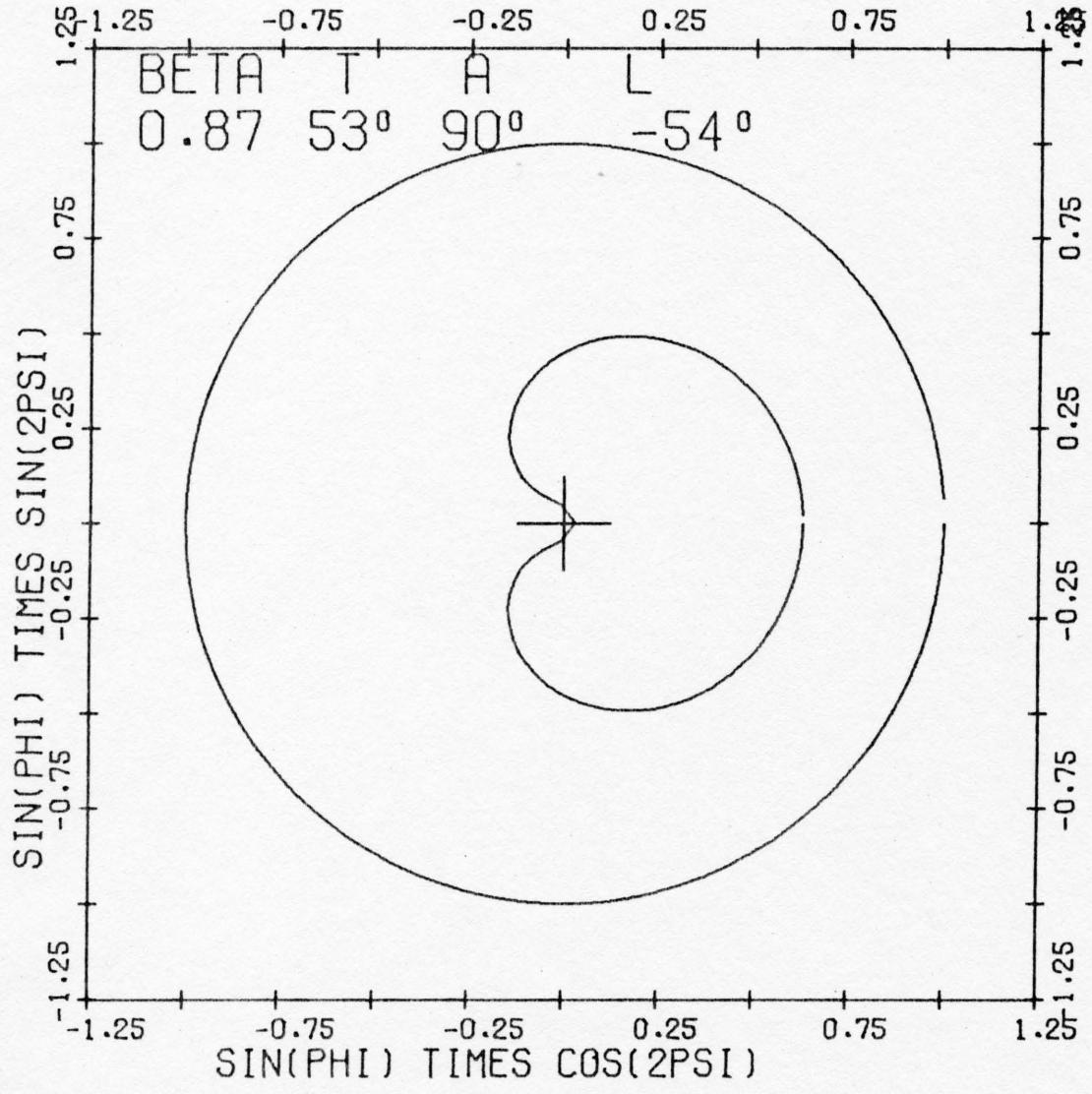

Figure 50. 2Ψ Versus sin ϕ for β=0.87, T=53°, P$\underset{\sim}{\rightarrow}$0

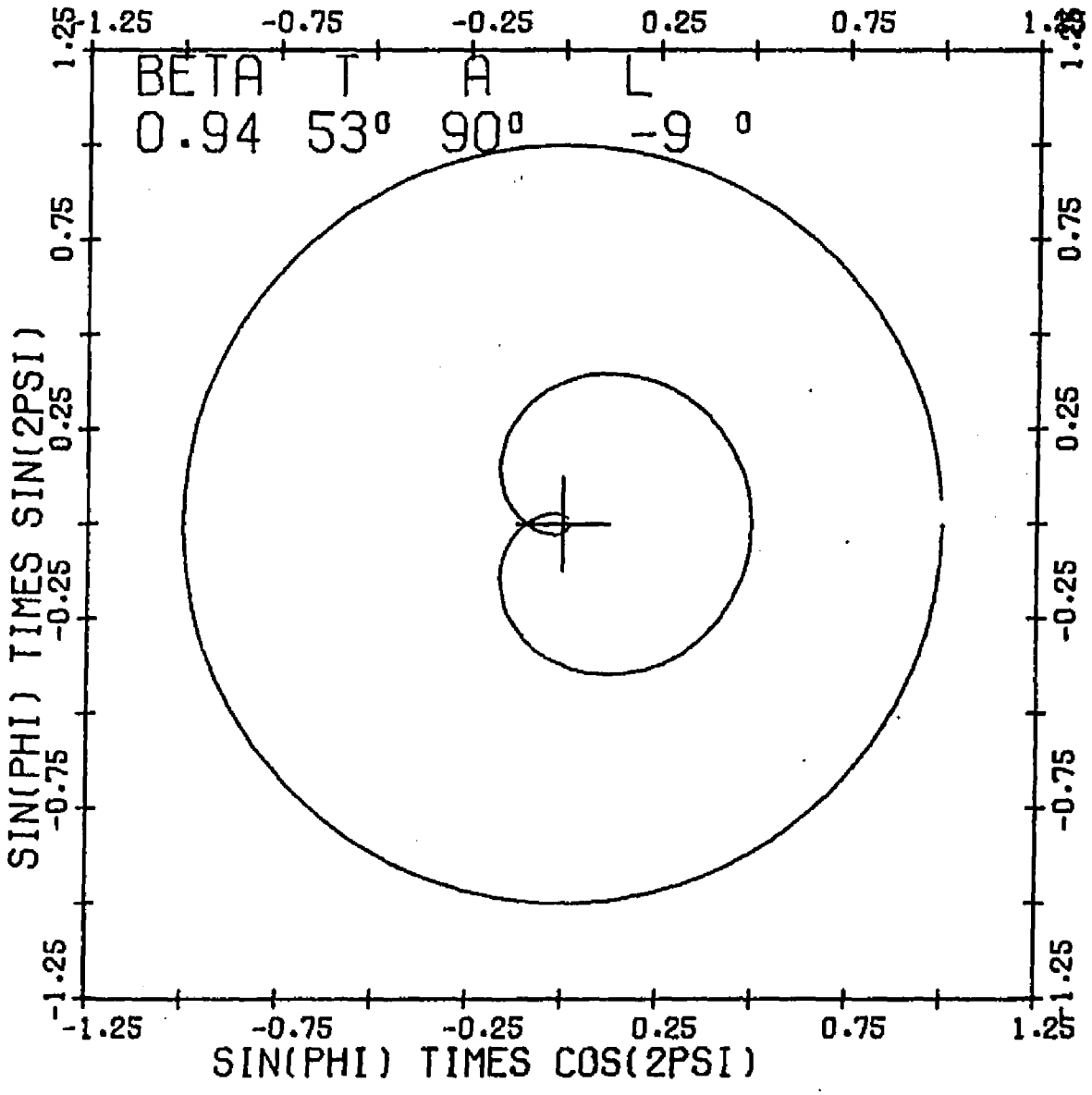

Figure 51. 2Ψ Versus sin ϕ for β=0.94, T=53°, P$\neq$0

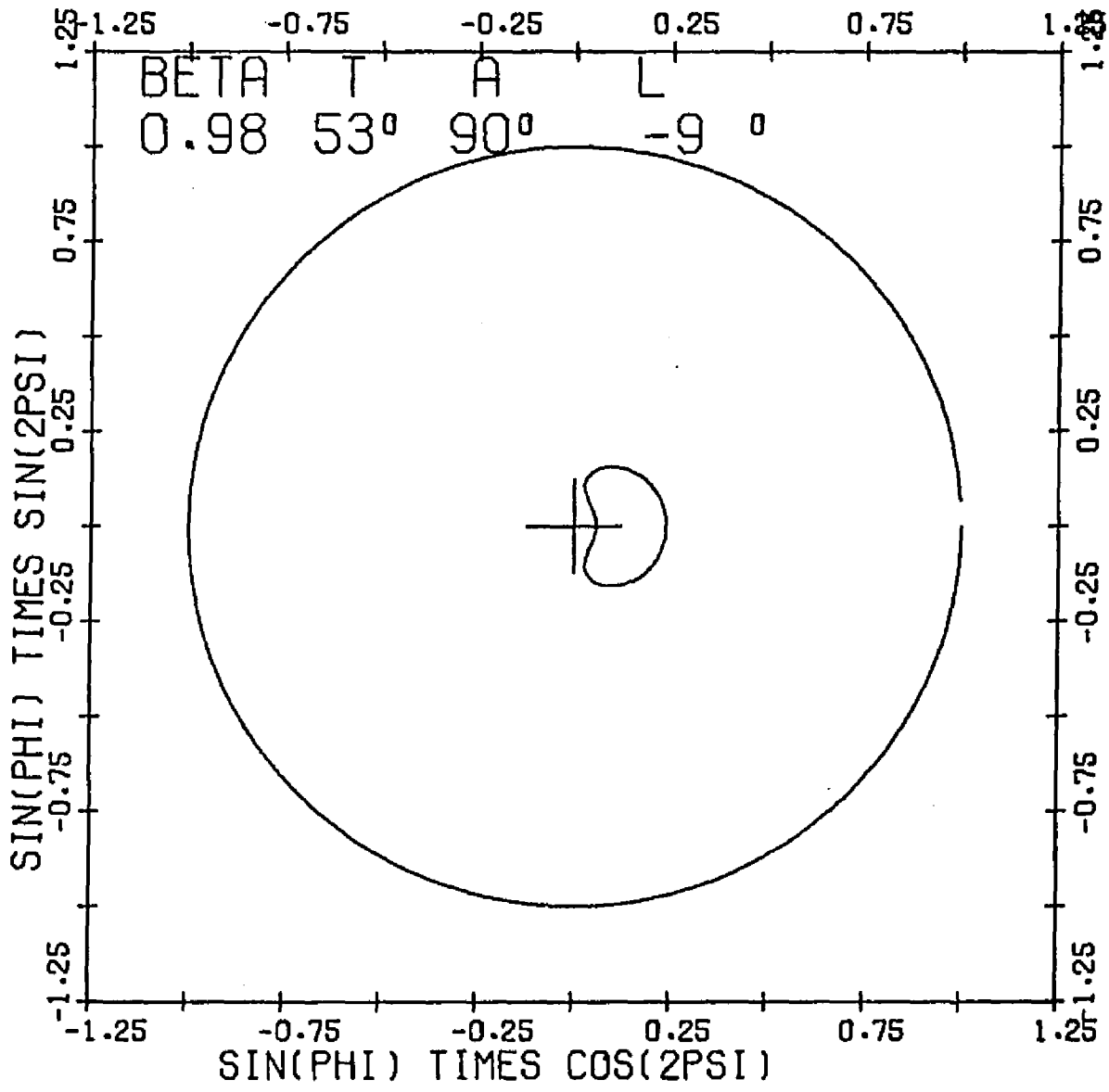

Figure 52. 2Ψ Versus sin ϕ for β=0.98, T=53°, P→0

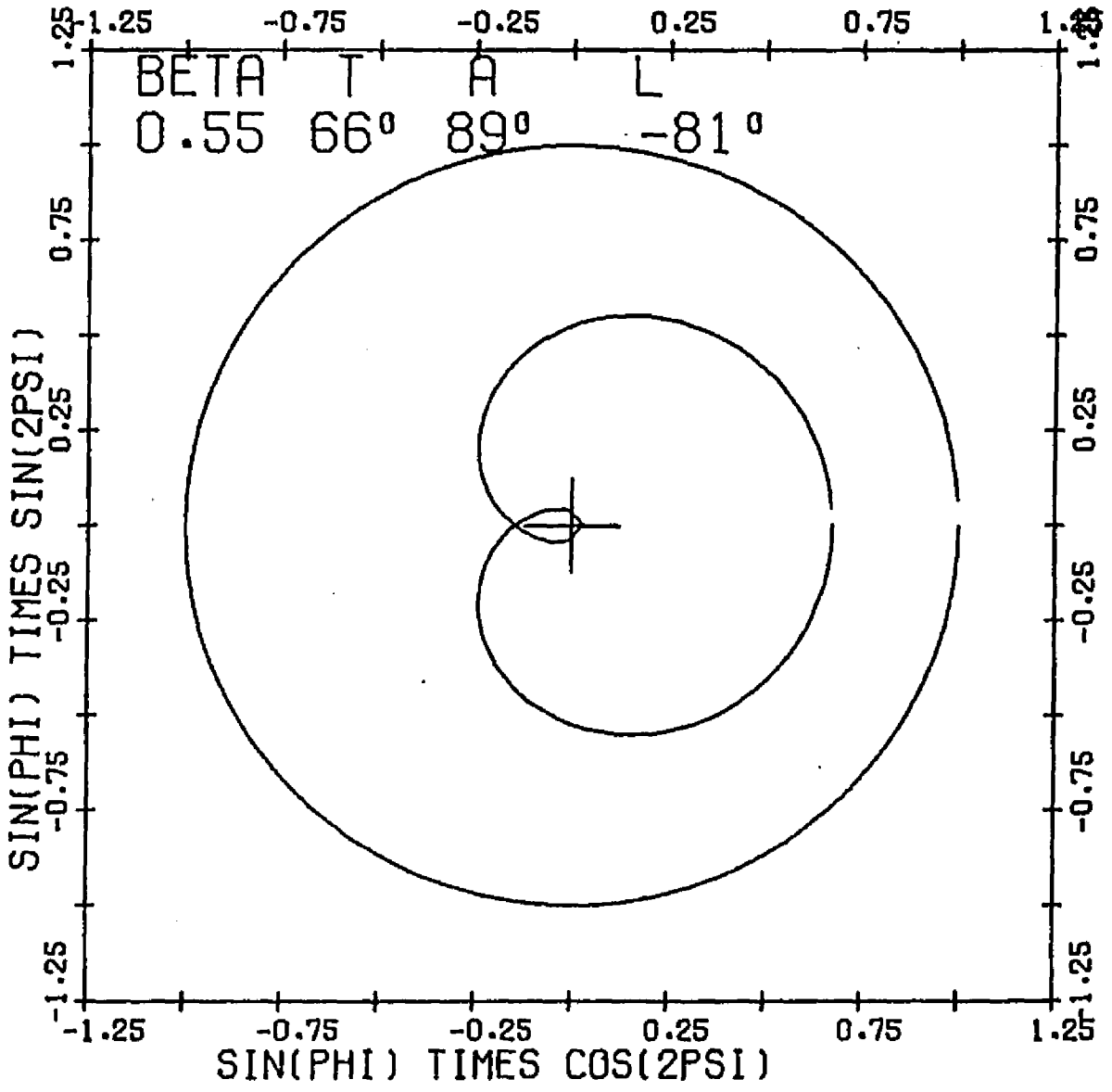

Figure 53. 2Ψ Versus sin ϕ for β=0.55, T=66°, P=0

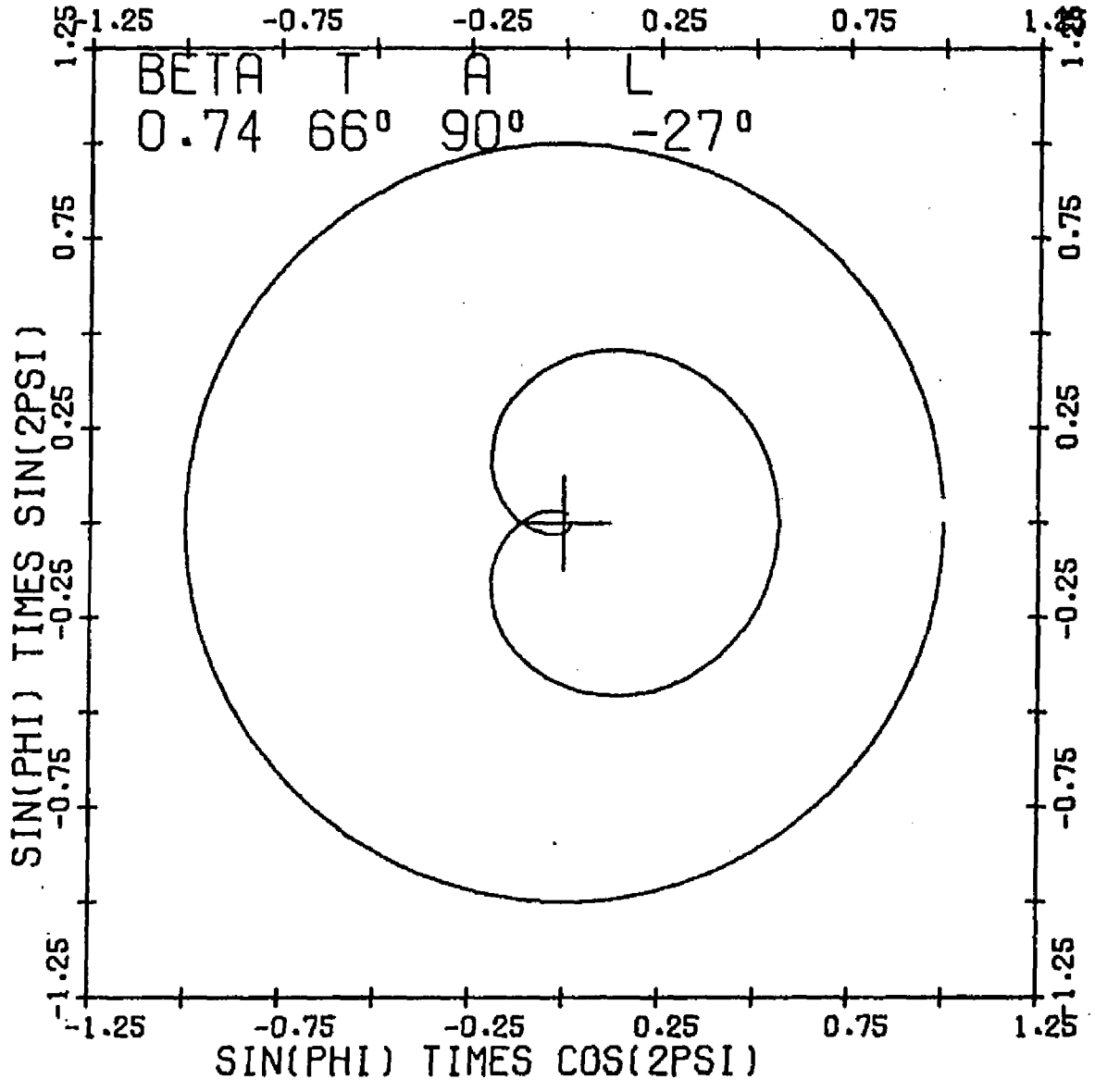

Figure 54. 2Ψ Versus sin ϕ for β=0.74, T=66°, P±0

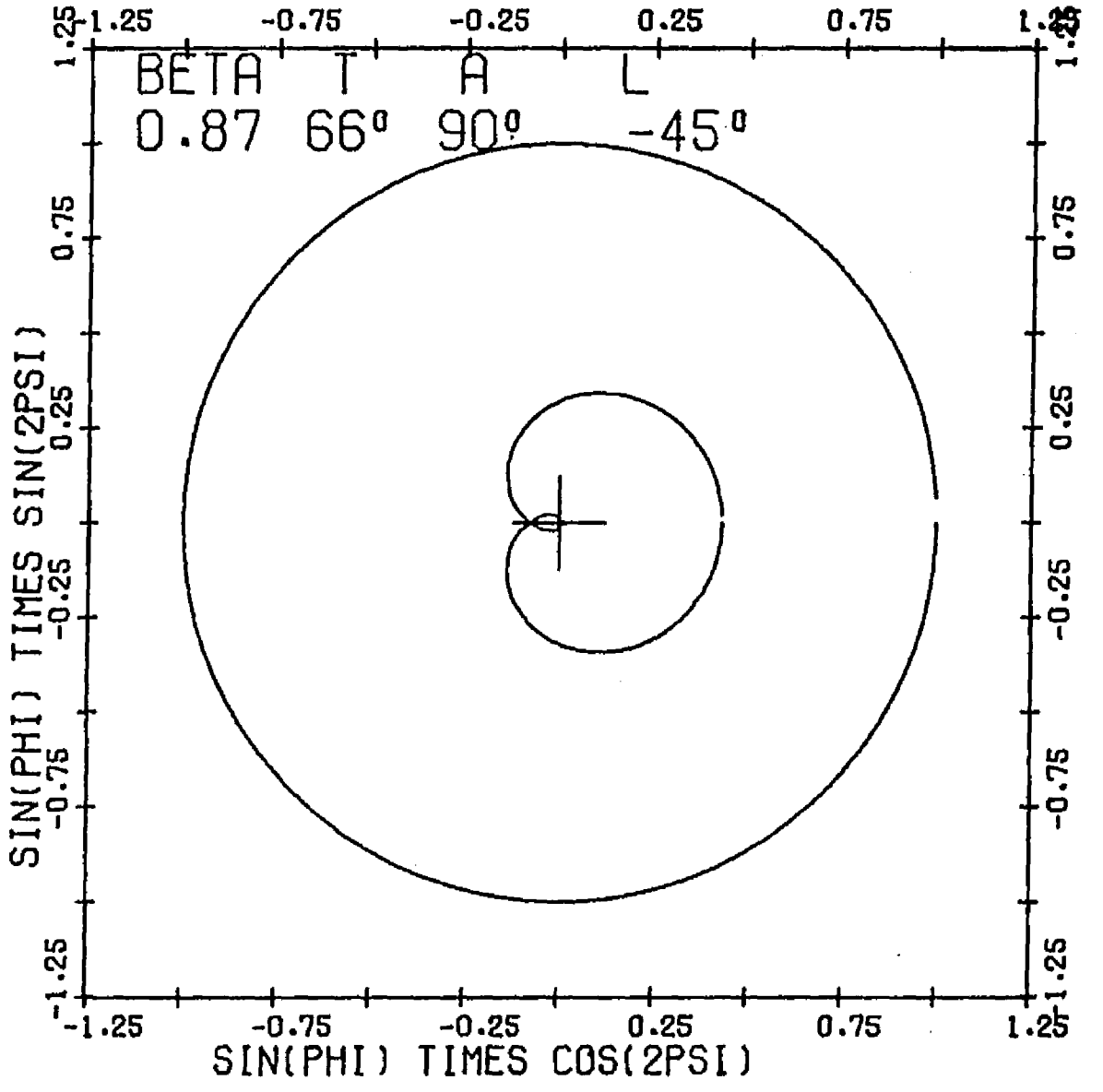

Figure 55. 2Ψ Versus sin ϕ for β=0.87, T=66°, P±0

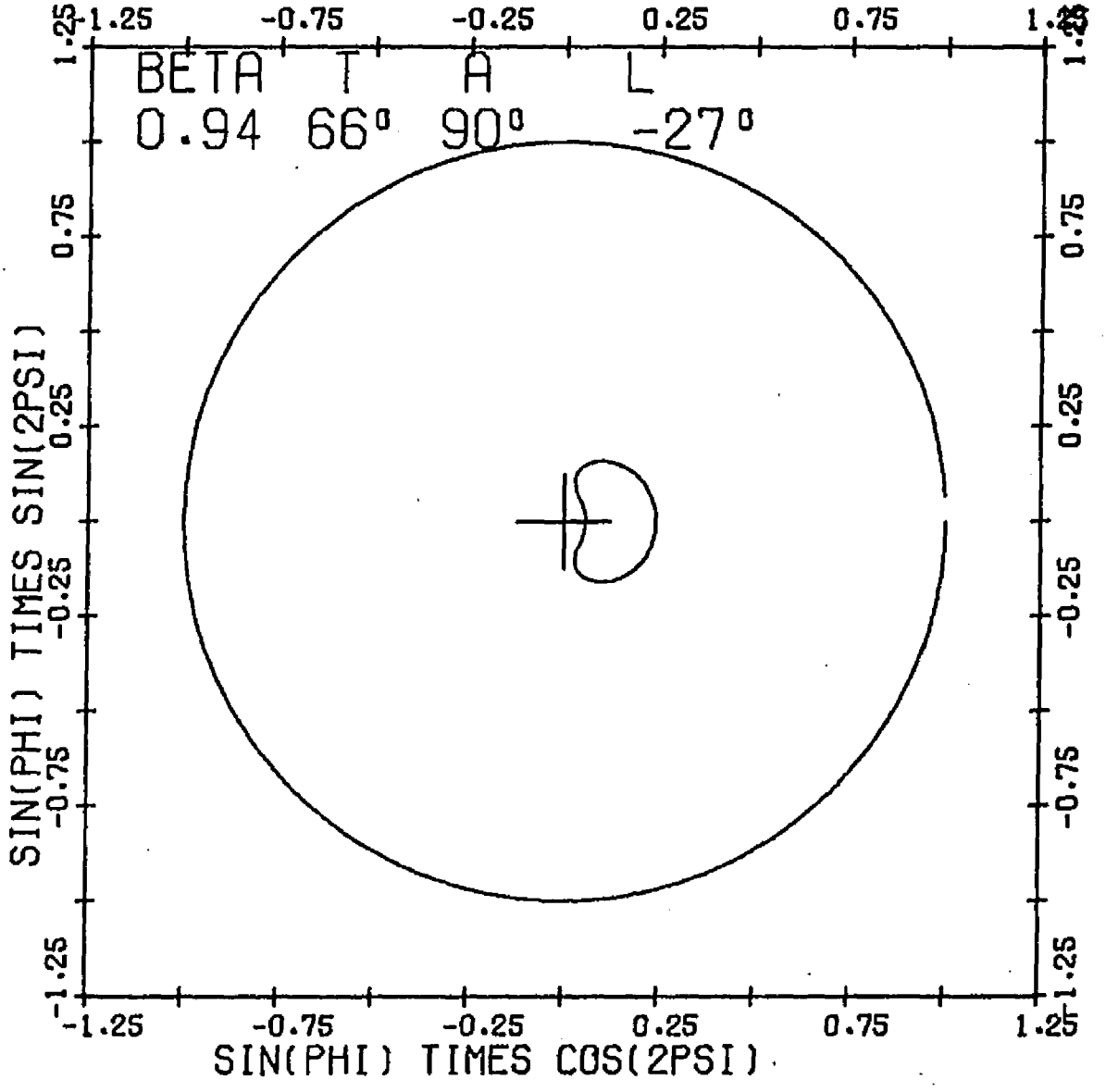

Figure 56. 2Ψ Versus sin ϕ for β=0.94, T=66°, P≠0

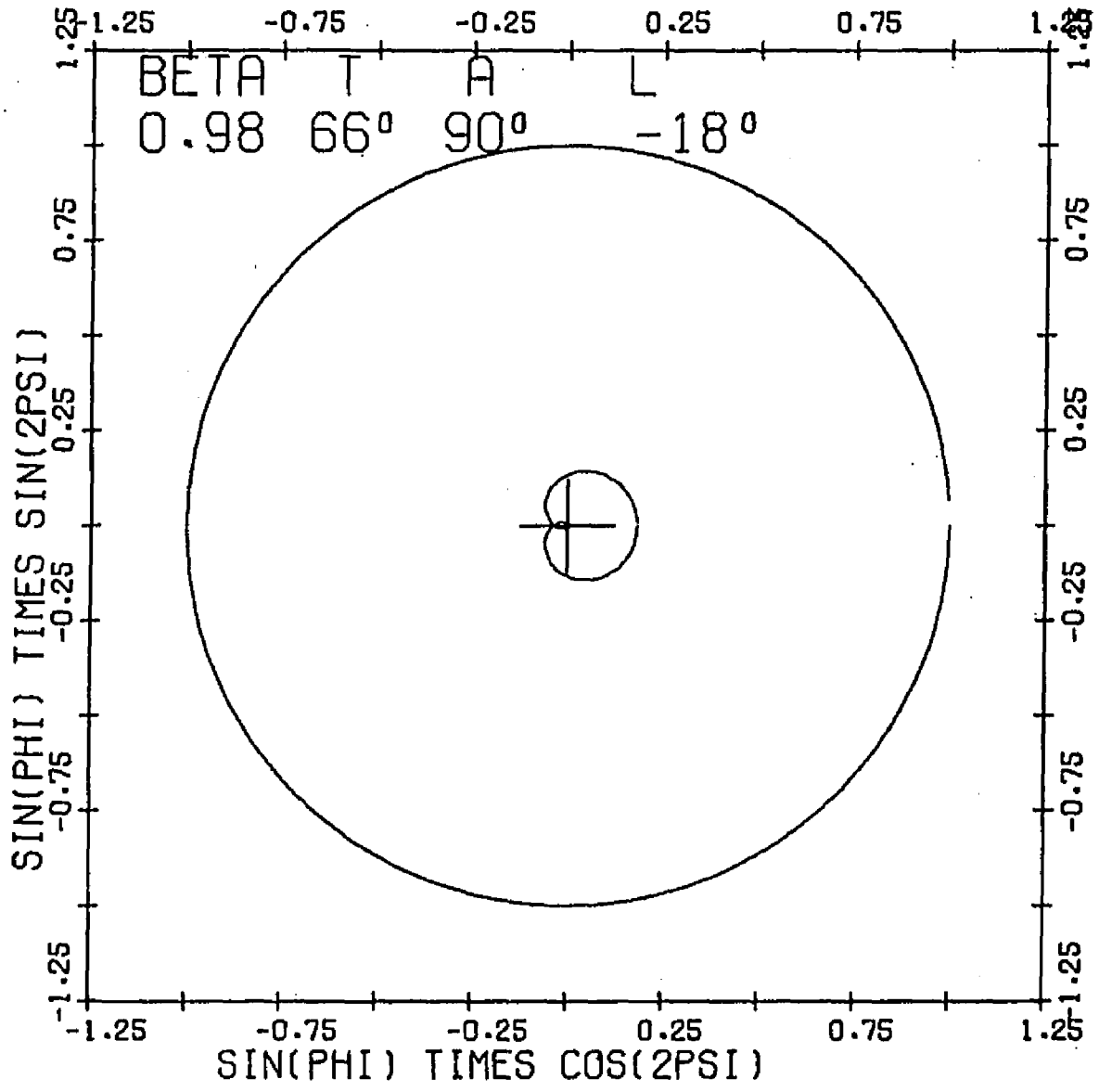

Figure 57. 2Ψ Versus sin ϕ for β=0.98, T=66°, P≒0

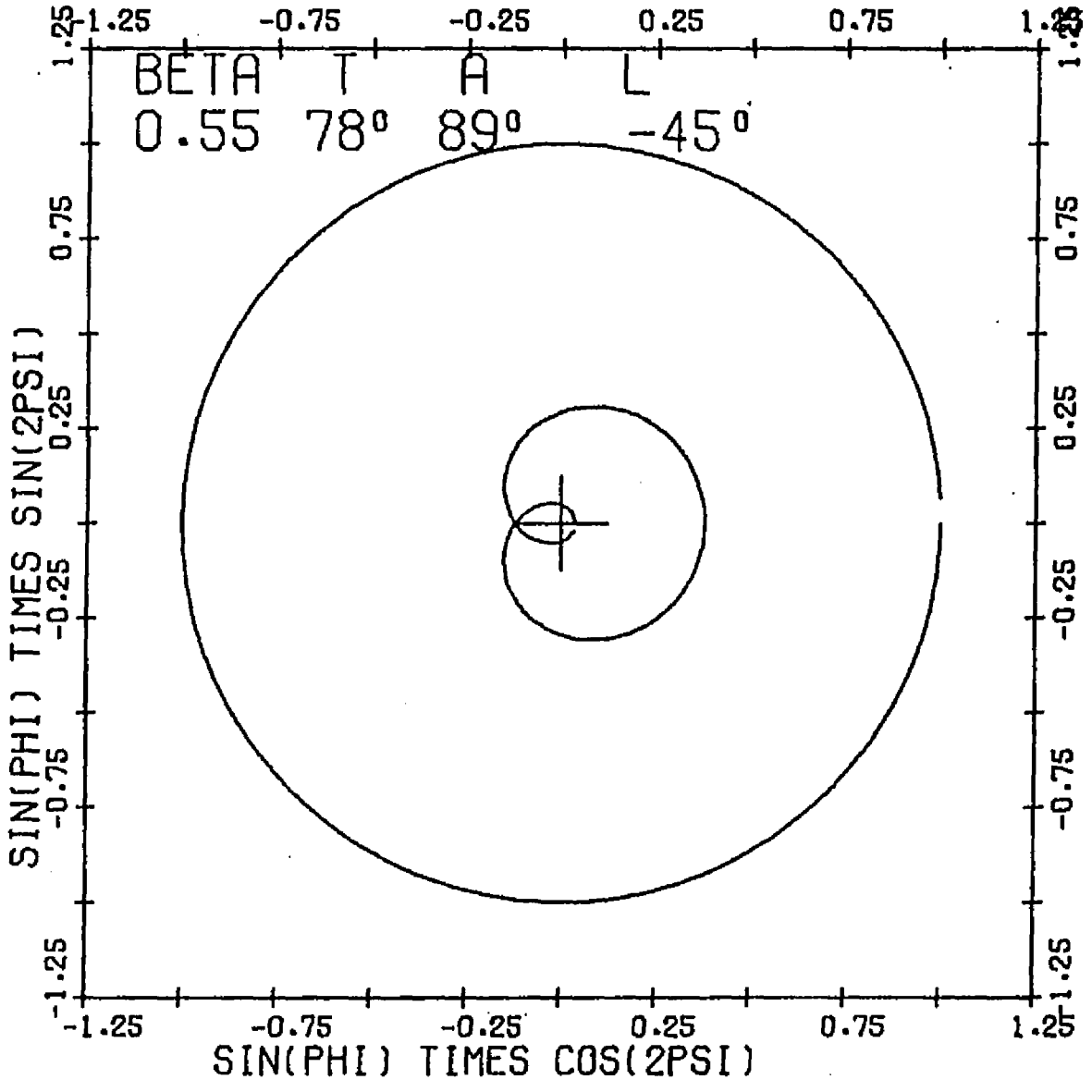

Figure 58. 2Ψ Versus sin ϕ for β=0.55, T=78°, P$\neq$0

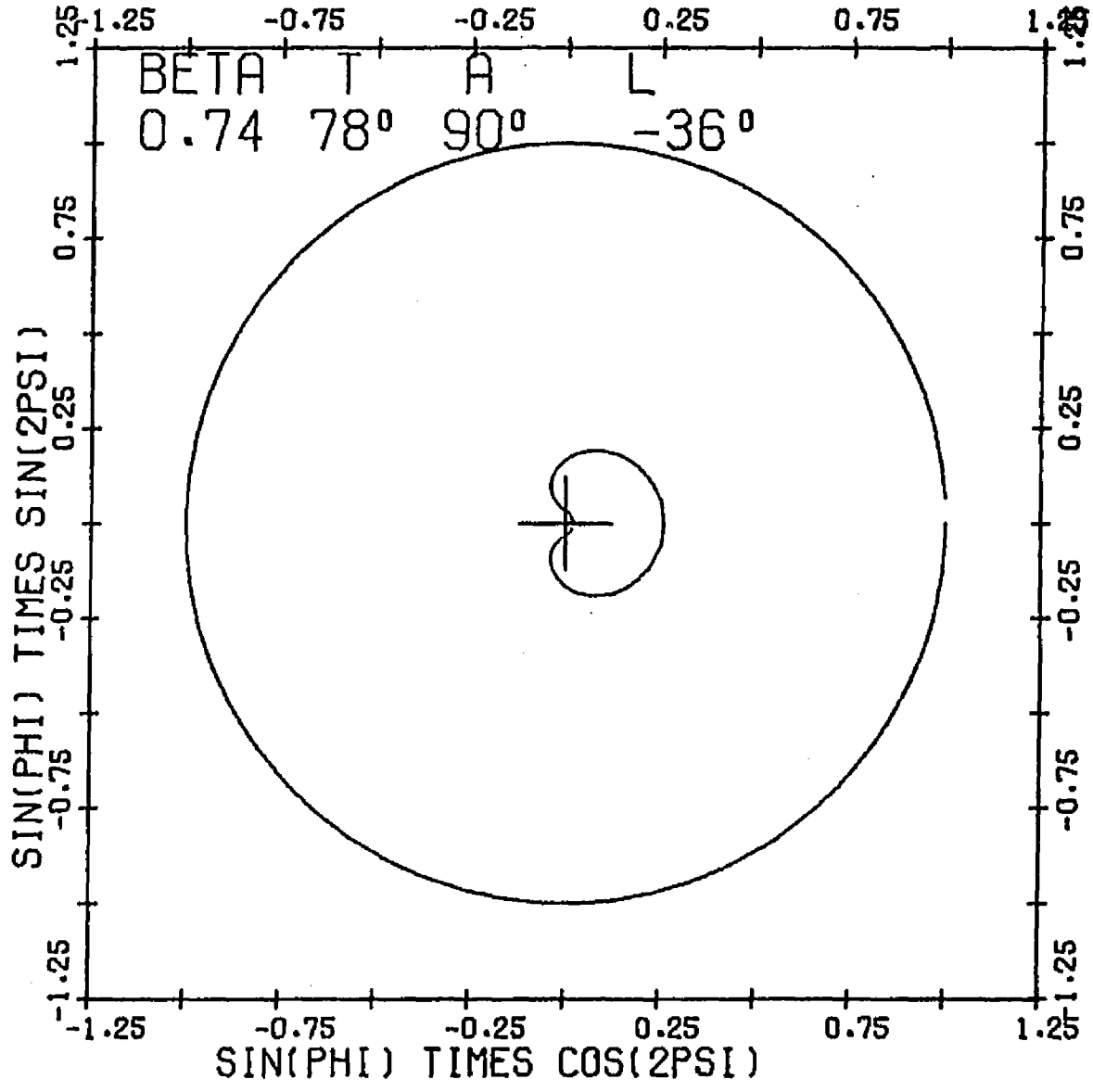

Figure 59. 2Ψ Versus sin ϕ for β=0.74, T=78°, P≒0

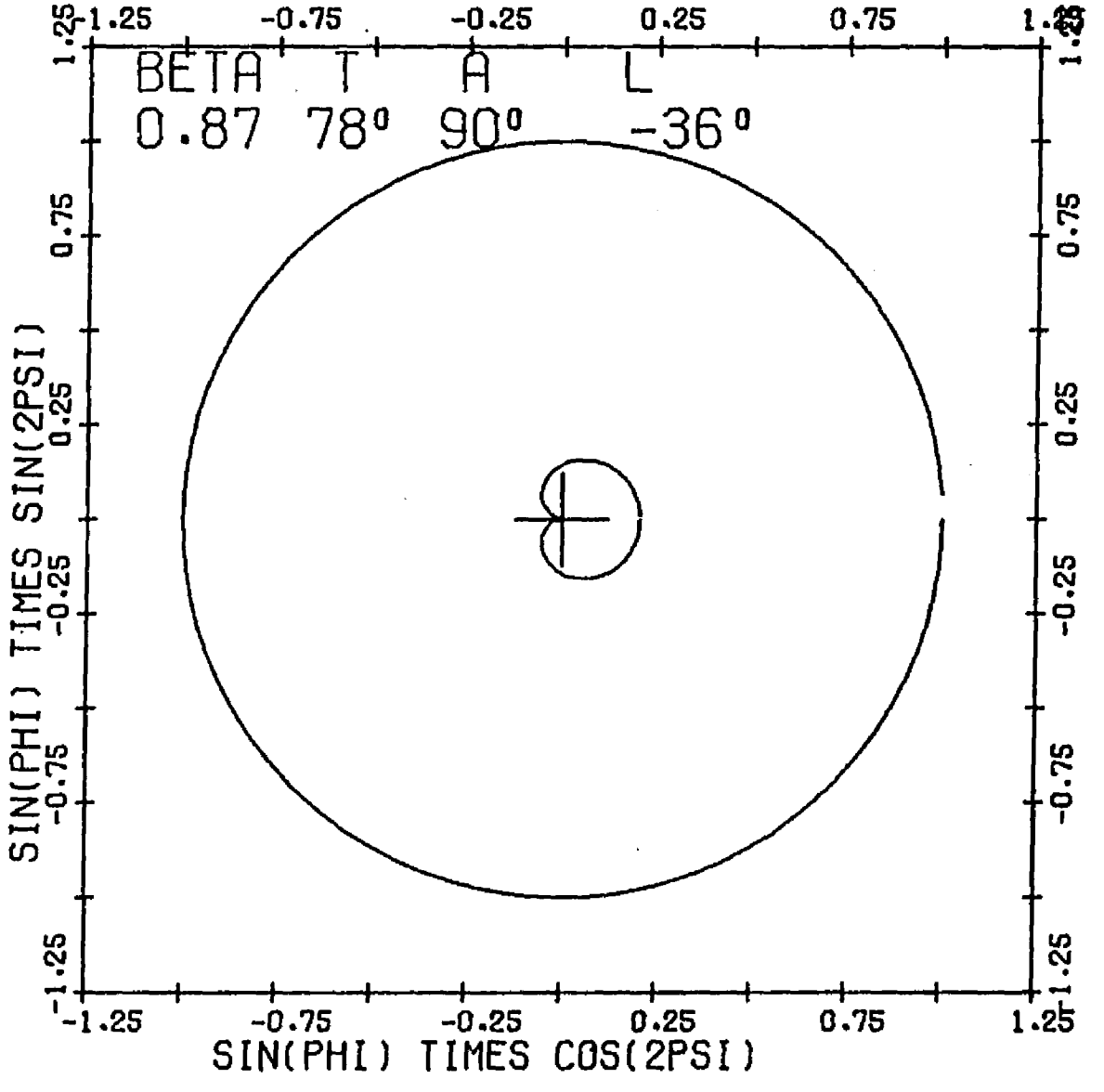

Figure 60. 2Ψ Versus sin ϕ for β=0.87, T=78°, P≠0

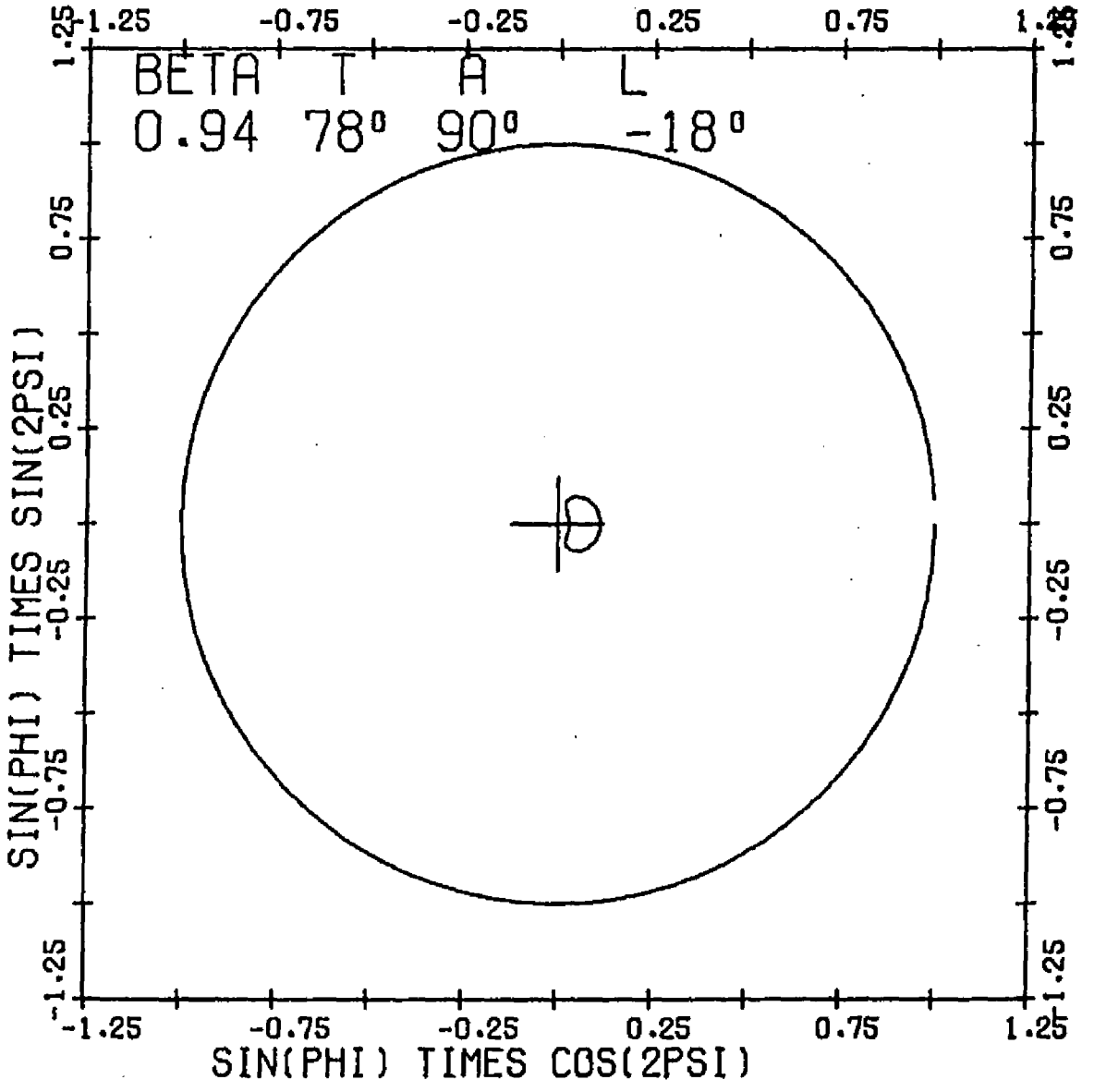

Figure 61. 2Ψ Versus sin ϕ for β=0.94, T=78°, P$\neq$0

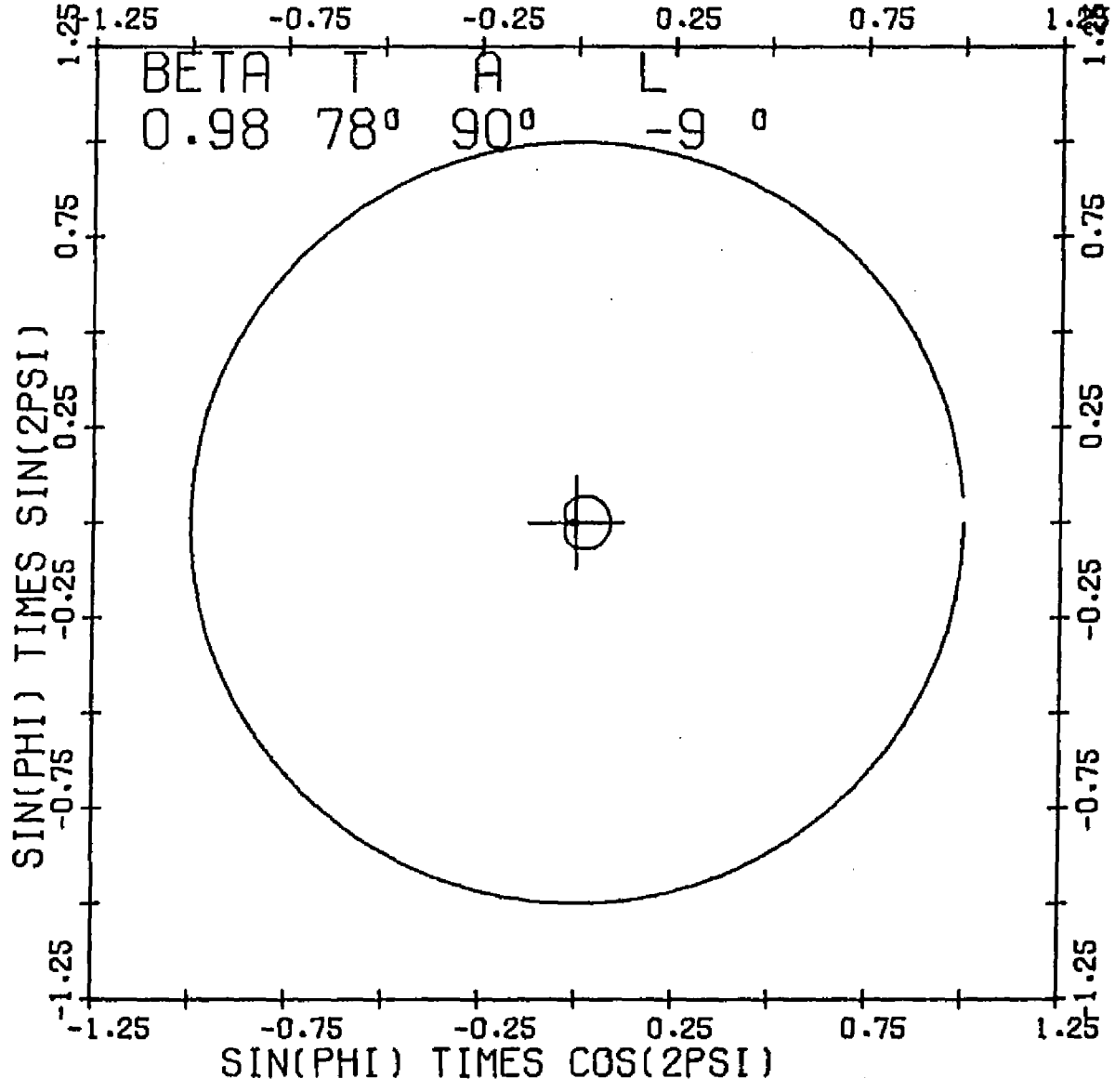

Figure 62. 2Ψ Versus sin ϕ for β=0.98, T=78°, P≠0

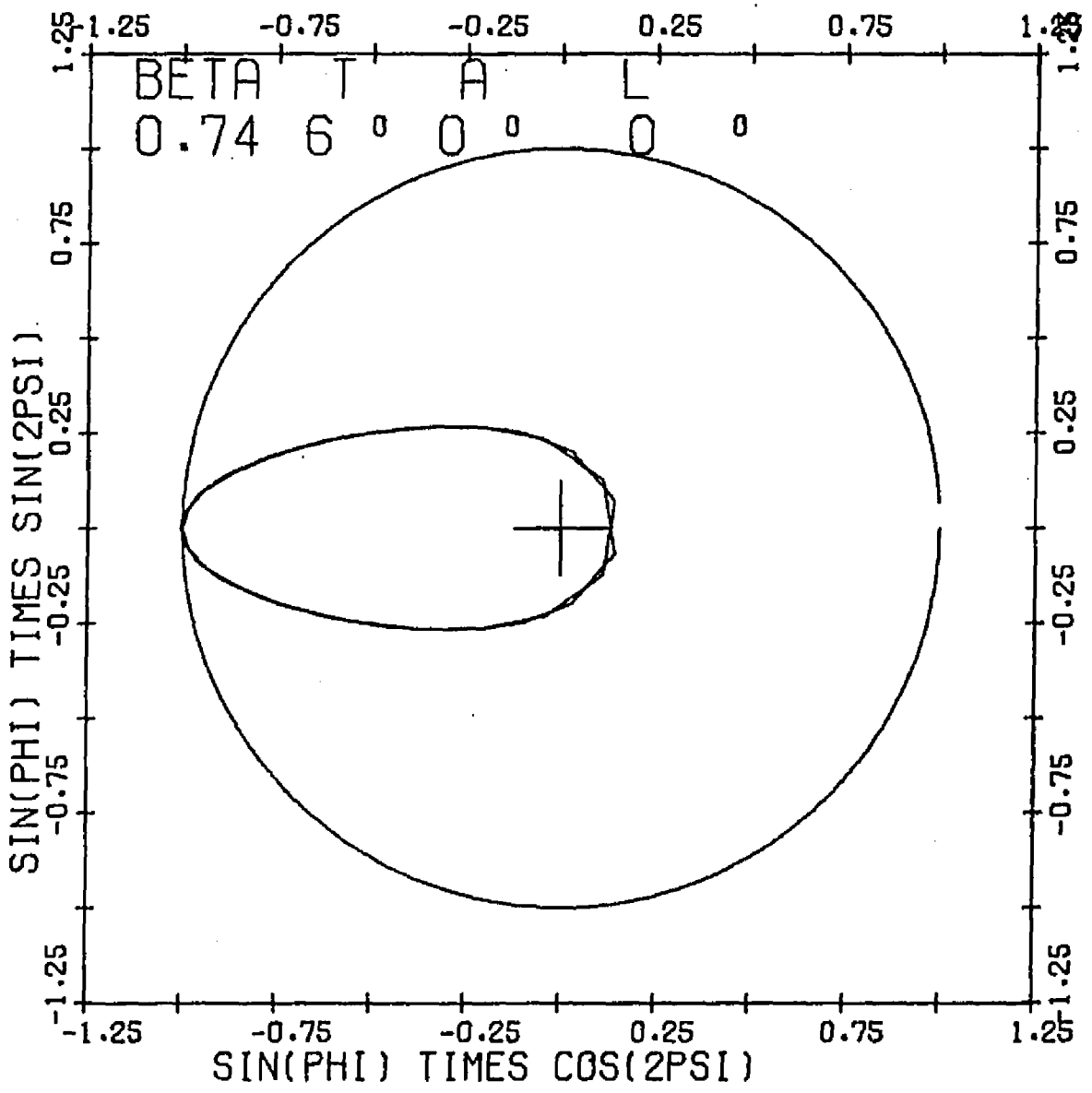

Figure 63. 2Ψ Versus sin ϕ for β=0.74, T=6°, A=0°, L=0°

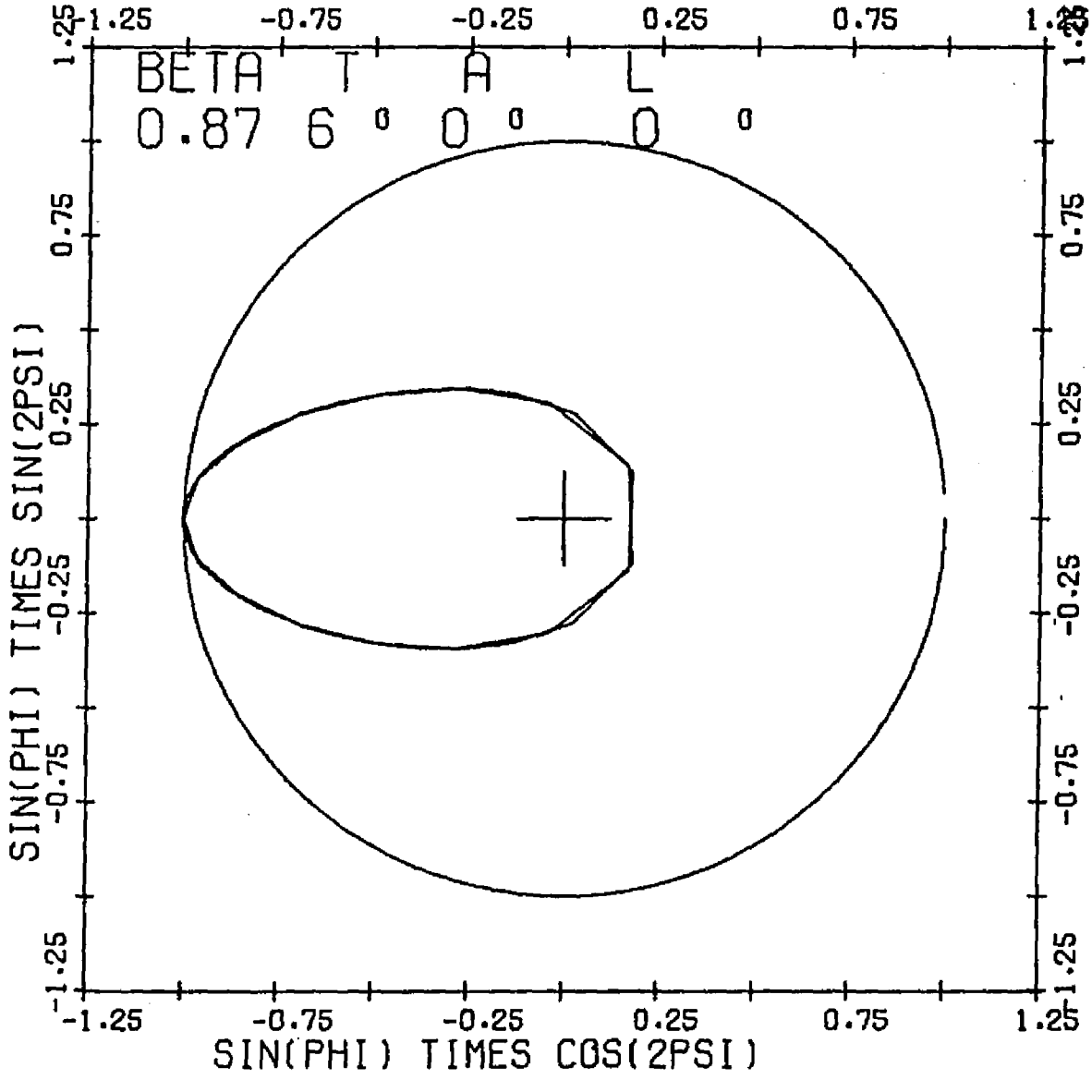

Figure 64. 2Ψ Versus sin ϕ for β=0.87, T=6°, A=0°, L=0°

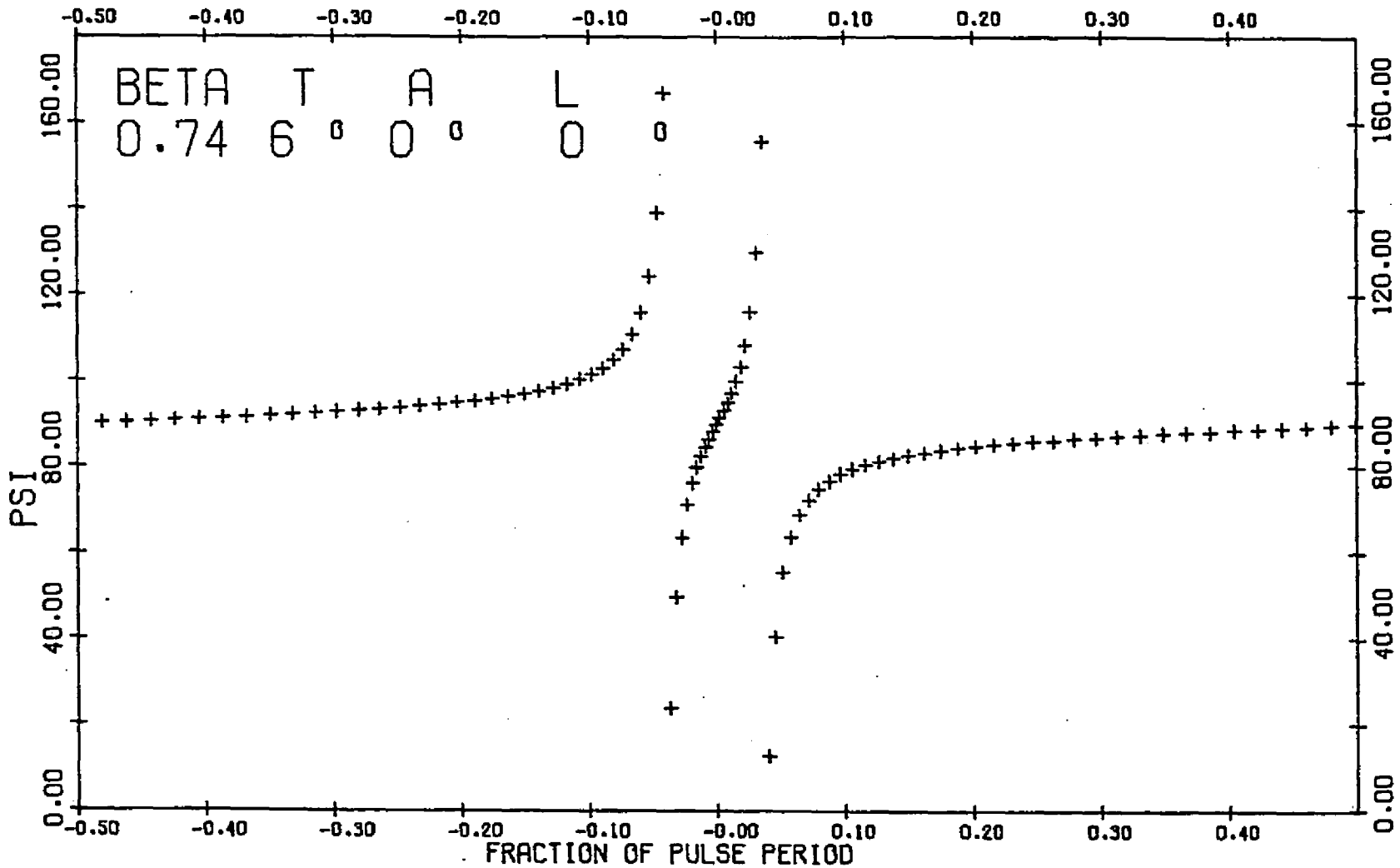

Figure 65. Ψ Versus Time for β=0.74, T=6°, A=0°, L=0°

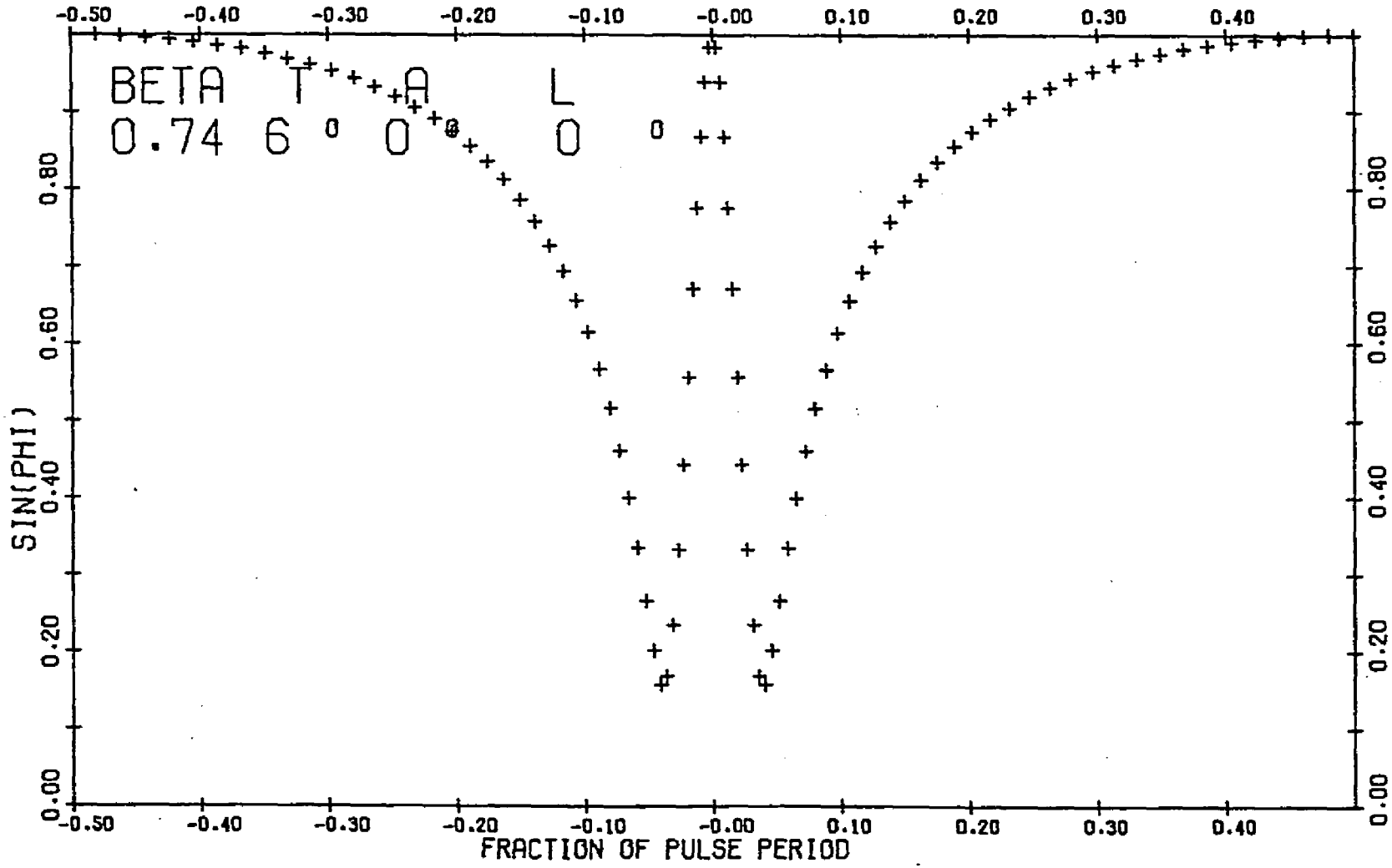

Figure 66. sin ϕ Versus Time for β=0.74, T=6°, A=0°, L=0°

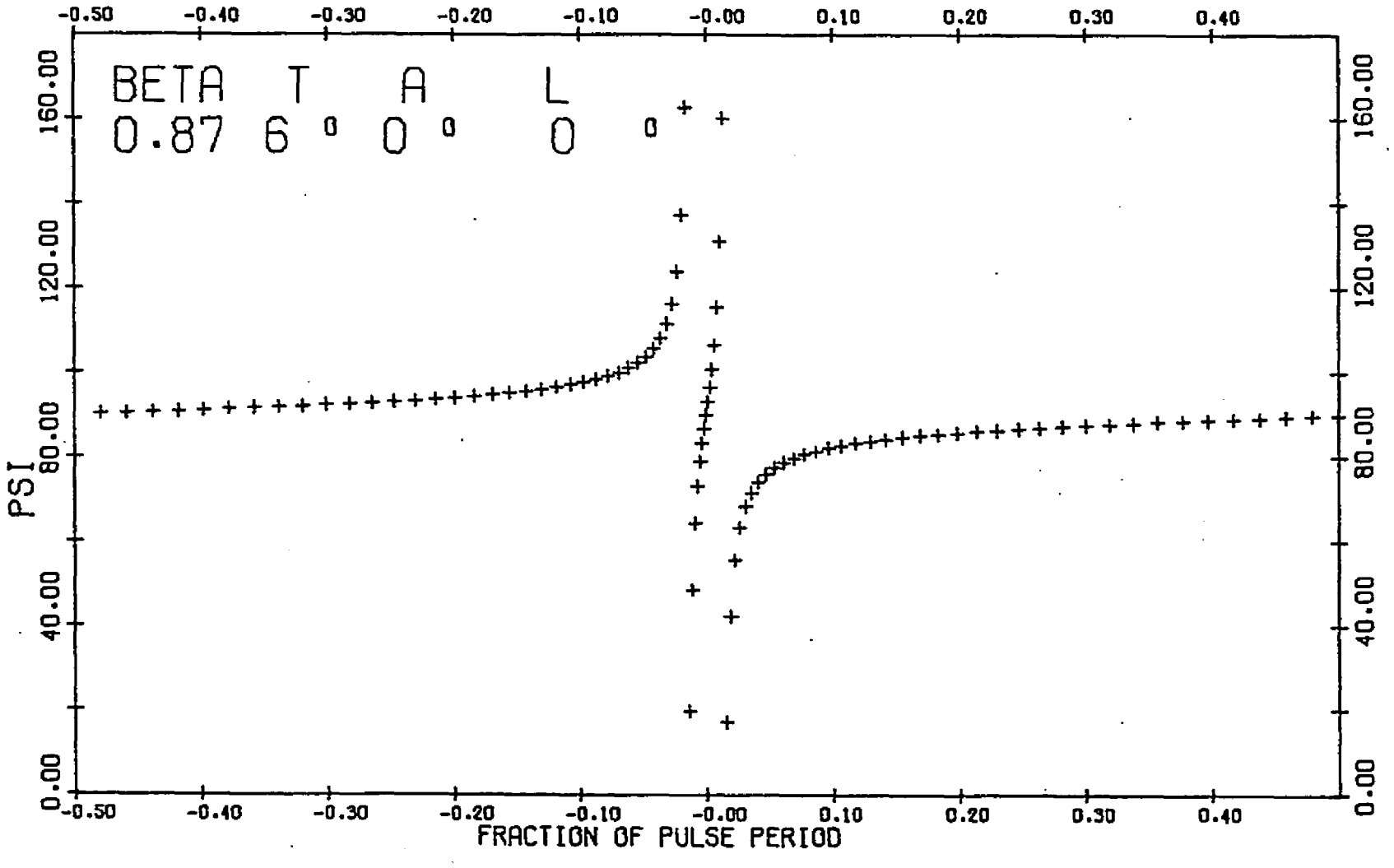

Figure 67. Ψ Versus Time for β=0.87, T=6°, A=0°, L=0°

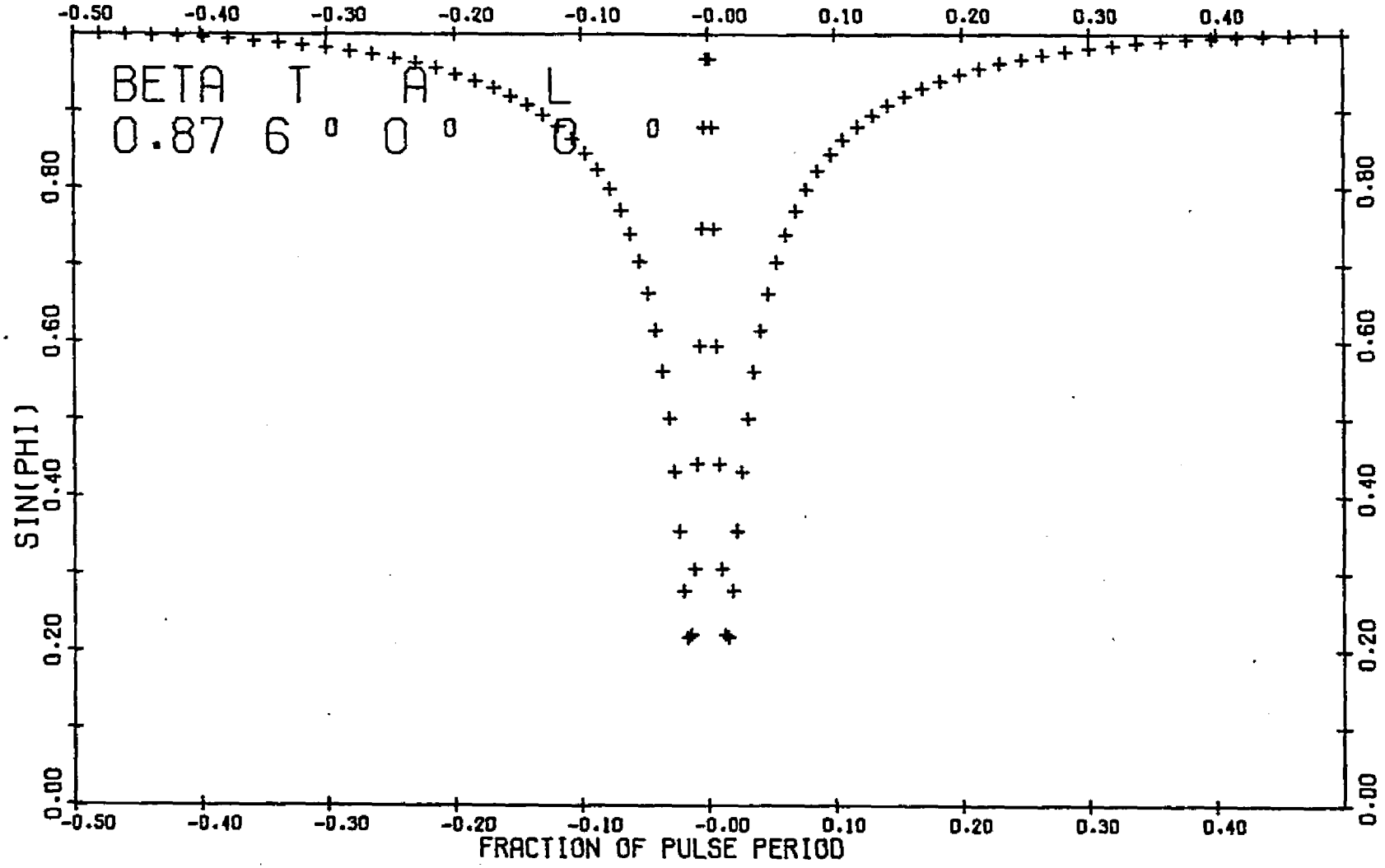

Figure 68. sin ϕ Versus Time for β=0.87, T=6°, A=0°, L=0°

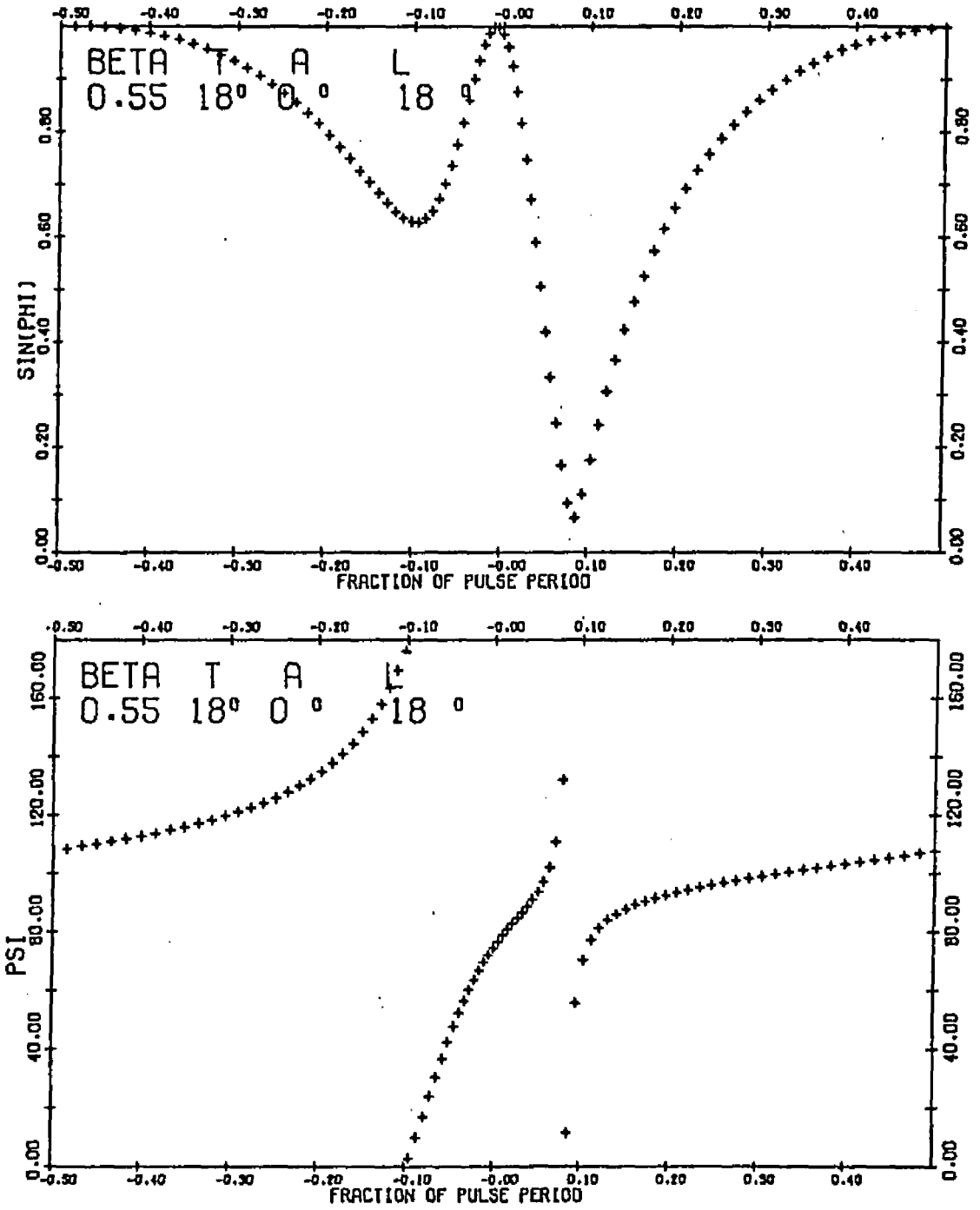

Figure 69. Polarization Time Behavior for β=0.55, T=18°, A=0°, L=18°

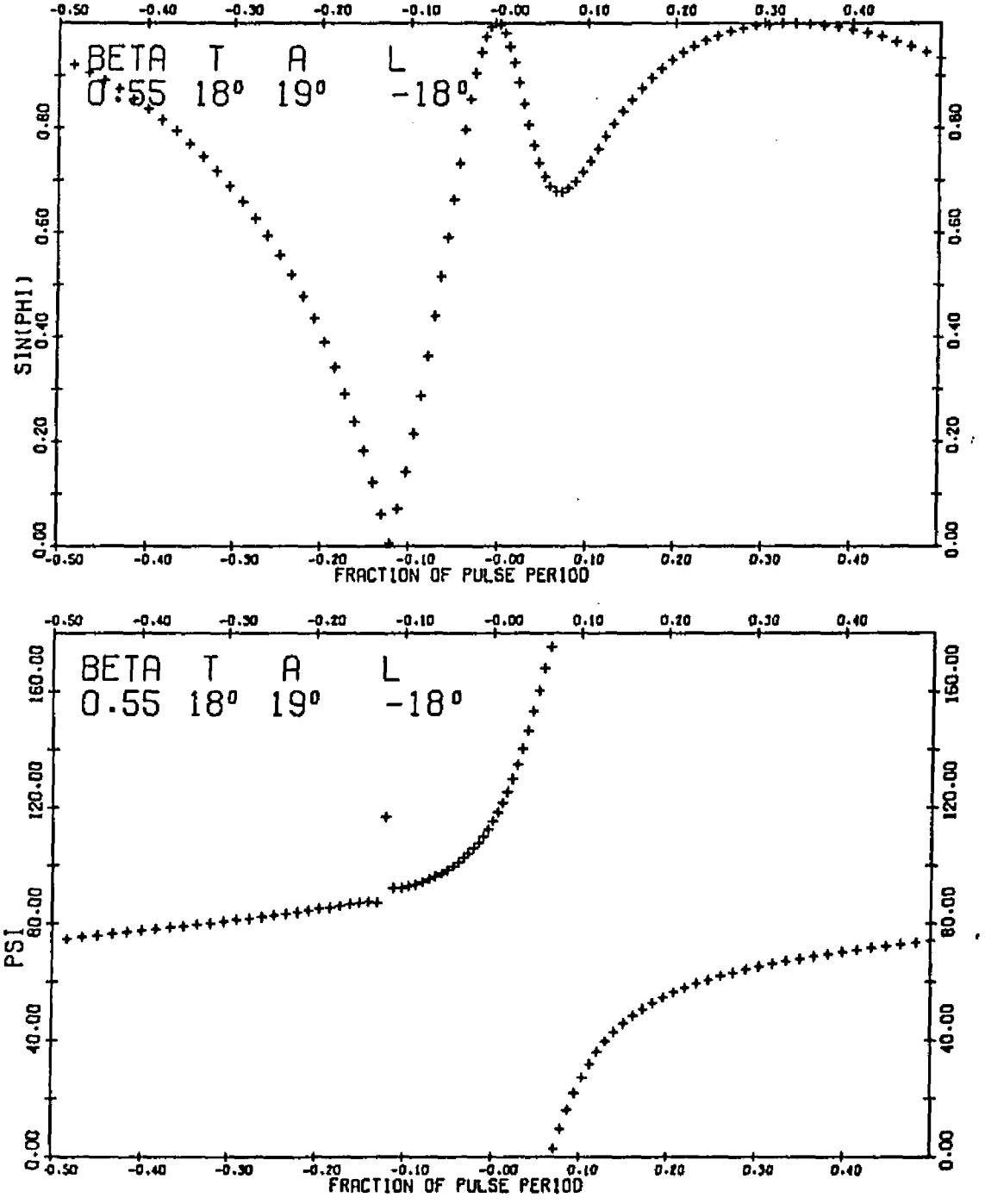

Figure 70. Polarization Time Behavior for β=0.55, T=18°, A=19°, L=-18°

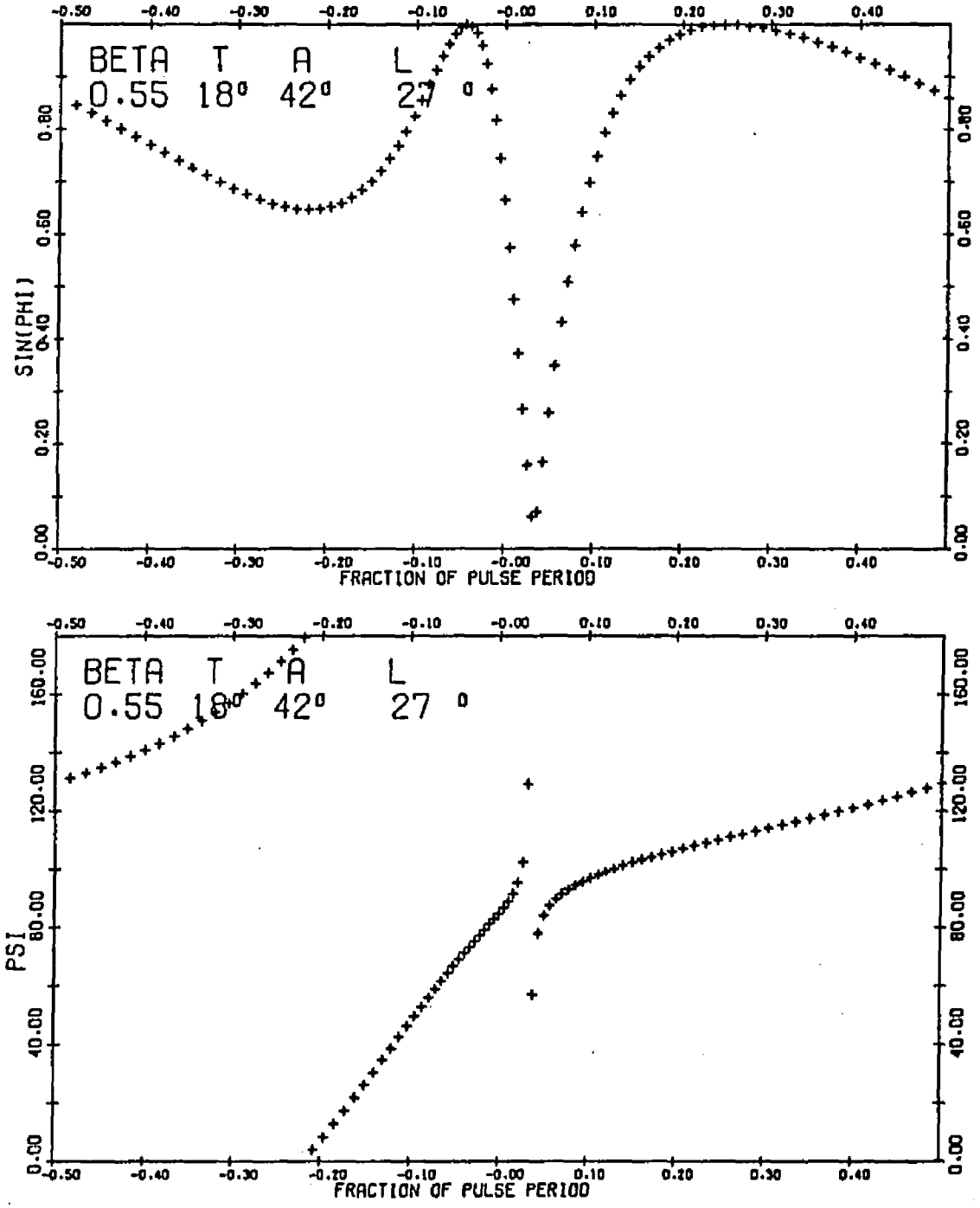

Figure 71. Polarization Time Behavior for β=0.55, T=18°, A=42°, L=27°

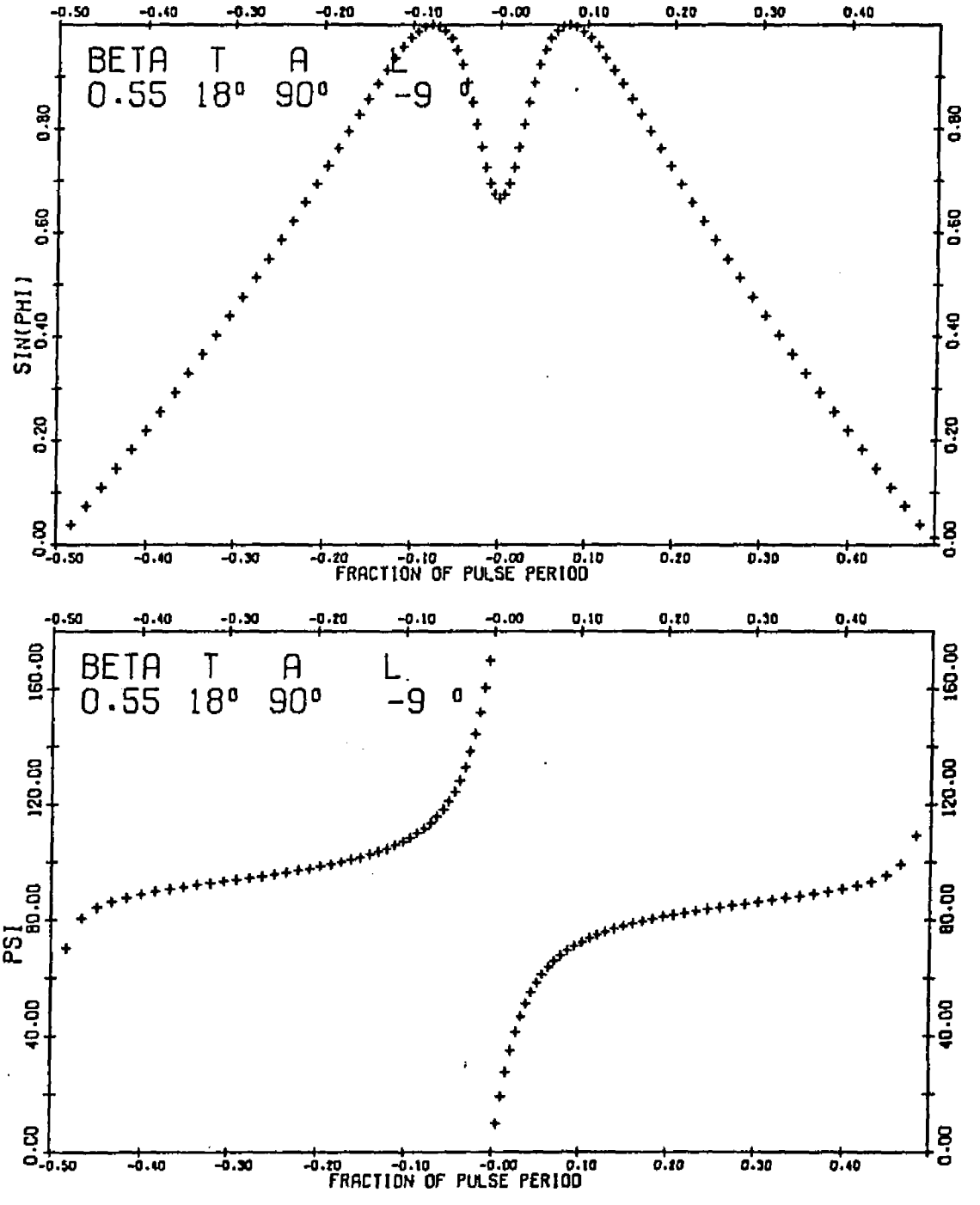

Figure 72. Polarization Time Behavior for β=0.55, T=18°, A=90°, L=-9°

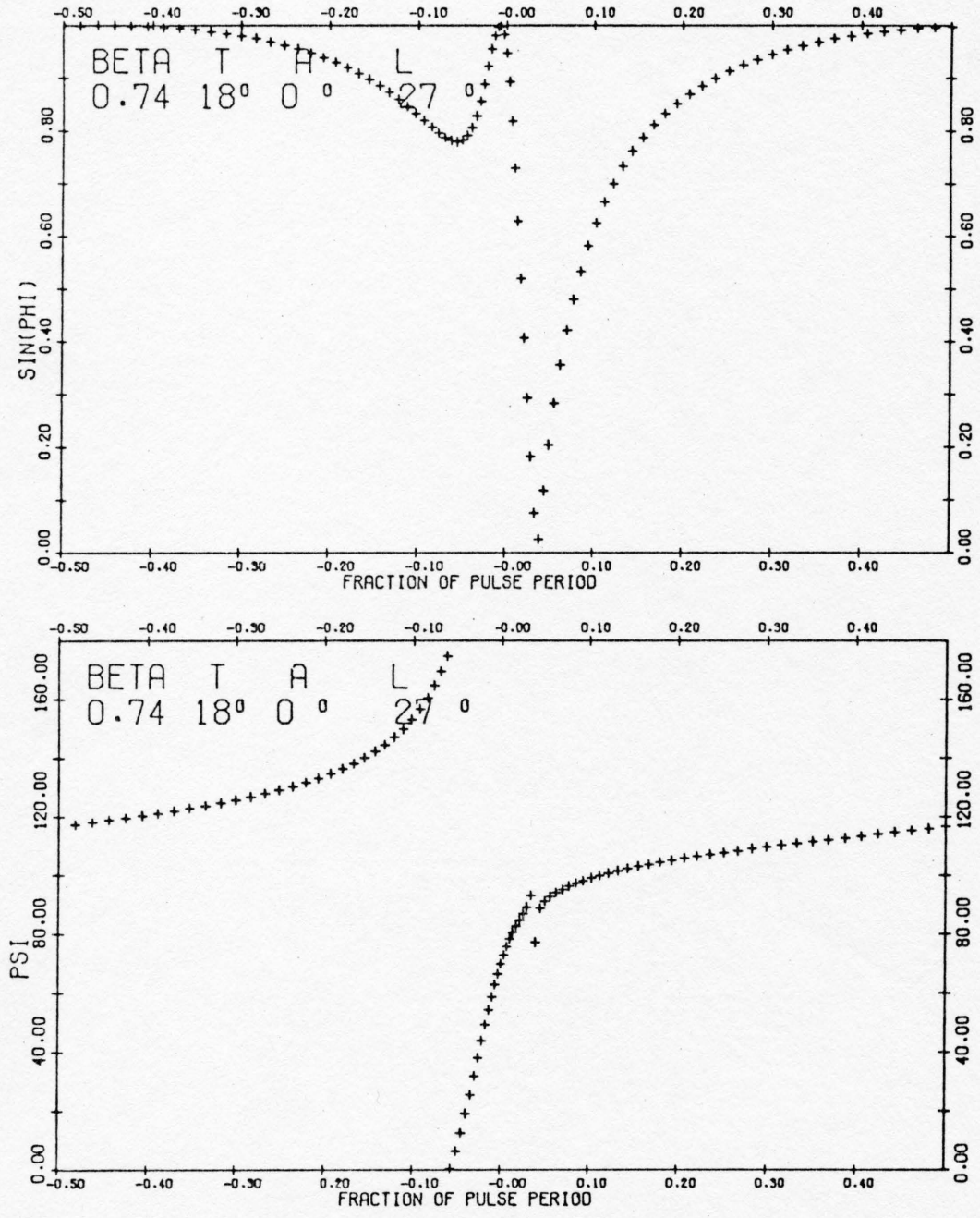

Figure 73. Polarization Time Behavior for β=0.74, T=18°, A=0°, L=27°

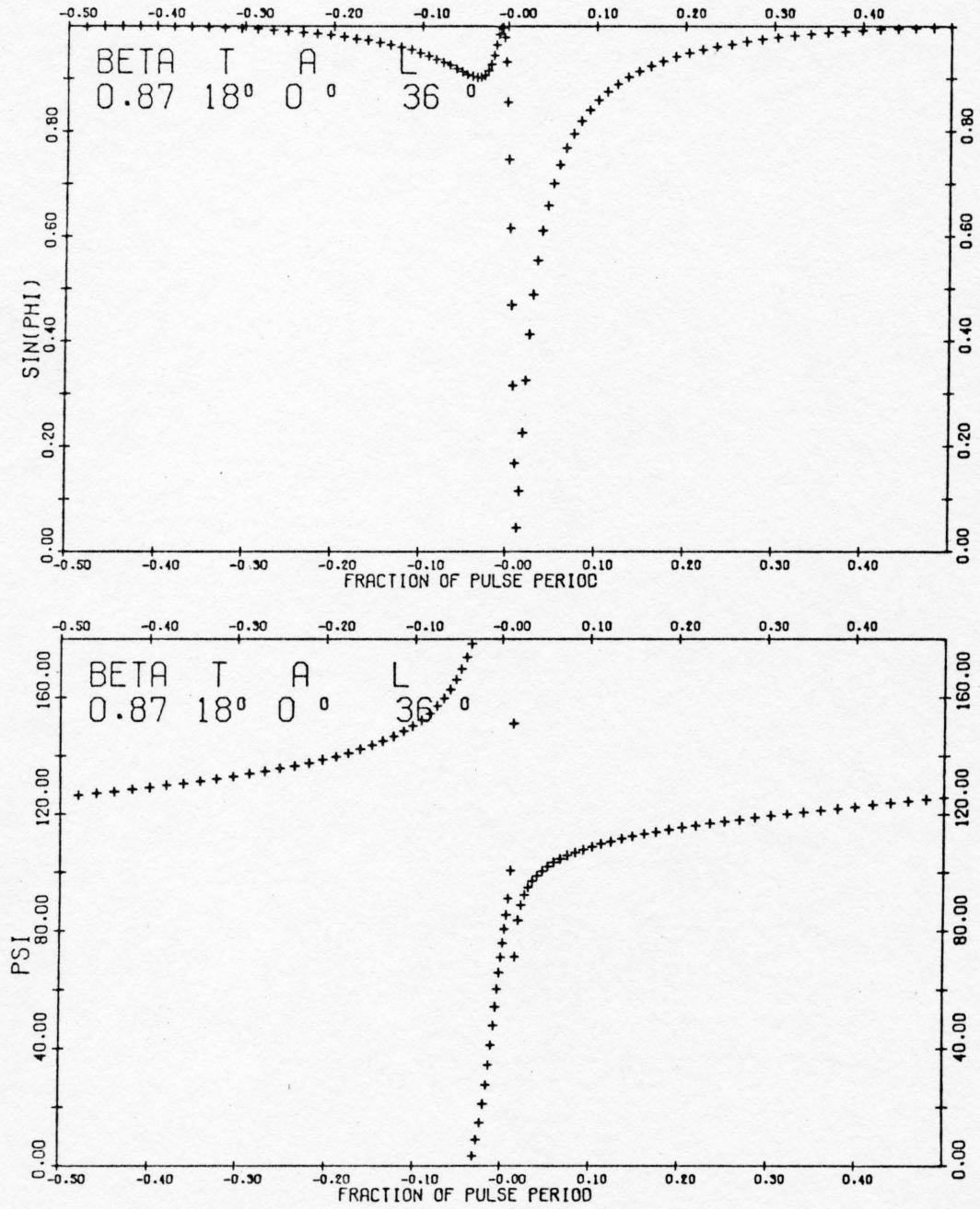

Figure 74. Polarization Time Behavior for β=0.87, T=18°, A=0°, L=36°

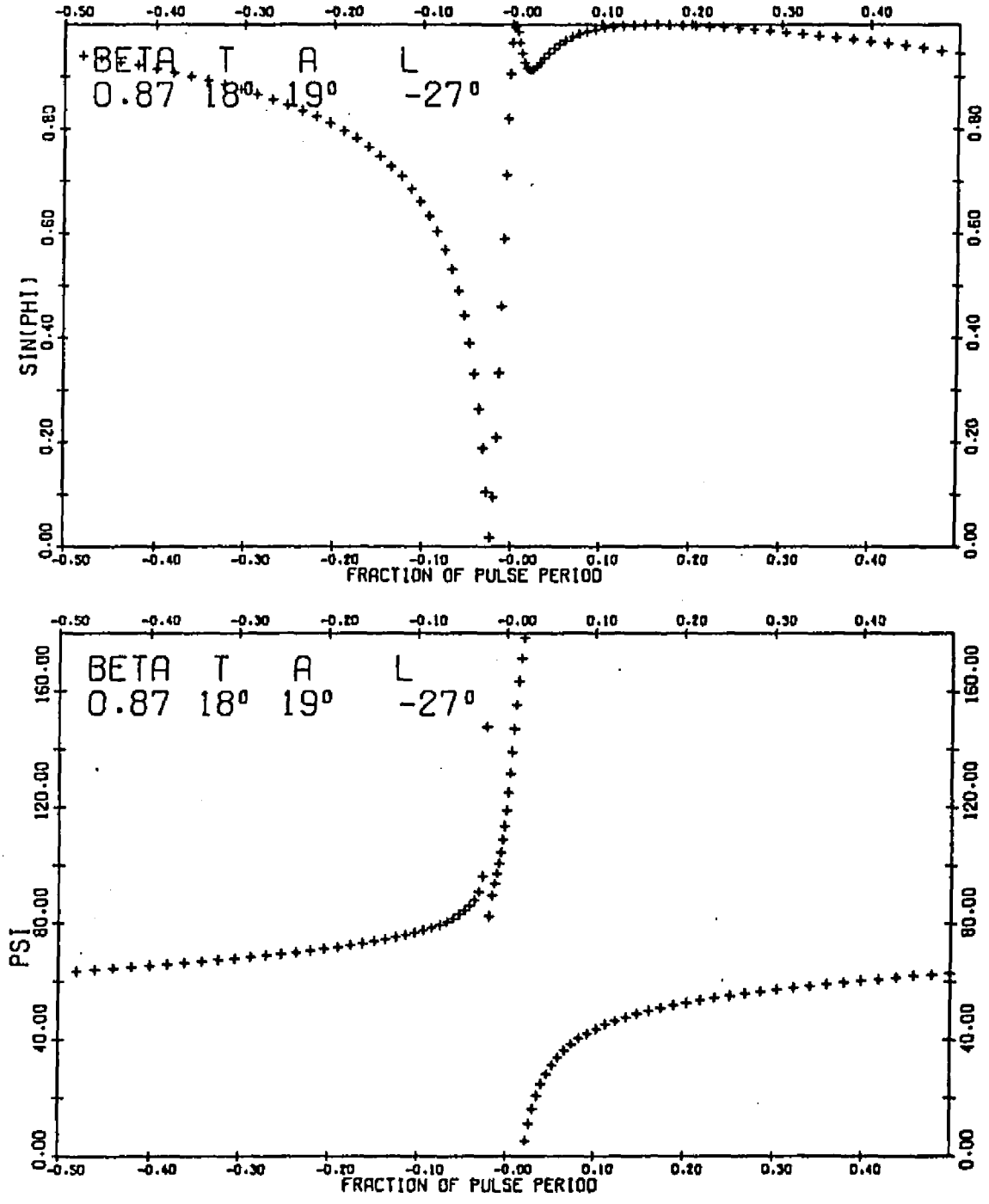

Figure 75. Polarization Time Behavior for β=0.87, T=18°, A=19°, L=-27°

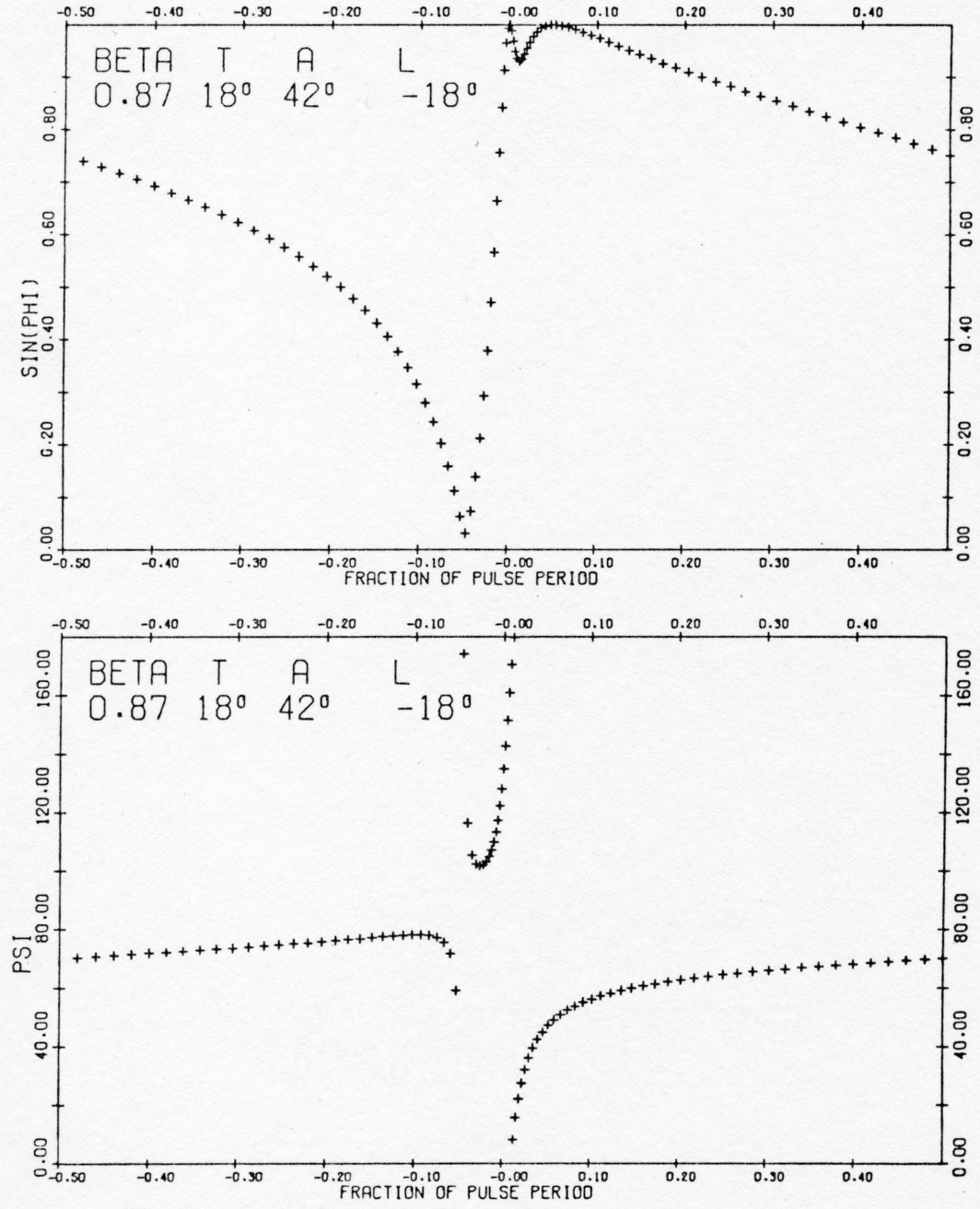

Figure 76. Polarization Time Behavior for β=0.87, T=18°, A=42°, L=-18°

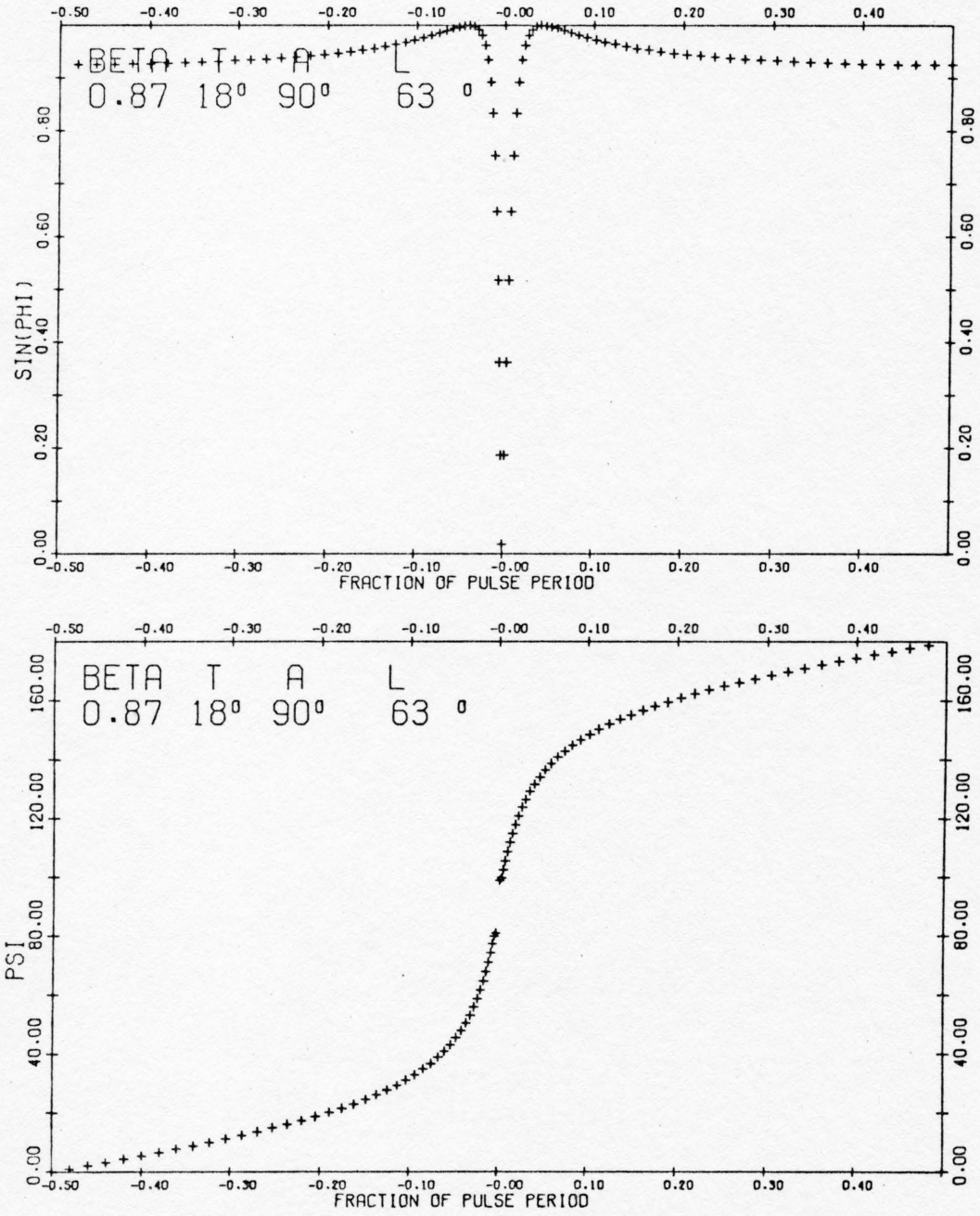

Figure 77. Polarization Time Behavior for β=0.87, T=18°, A=90°, L=63°

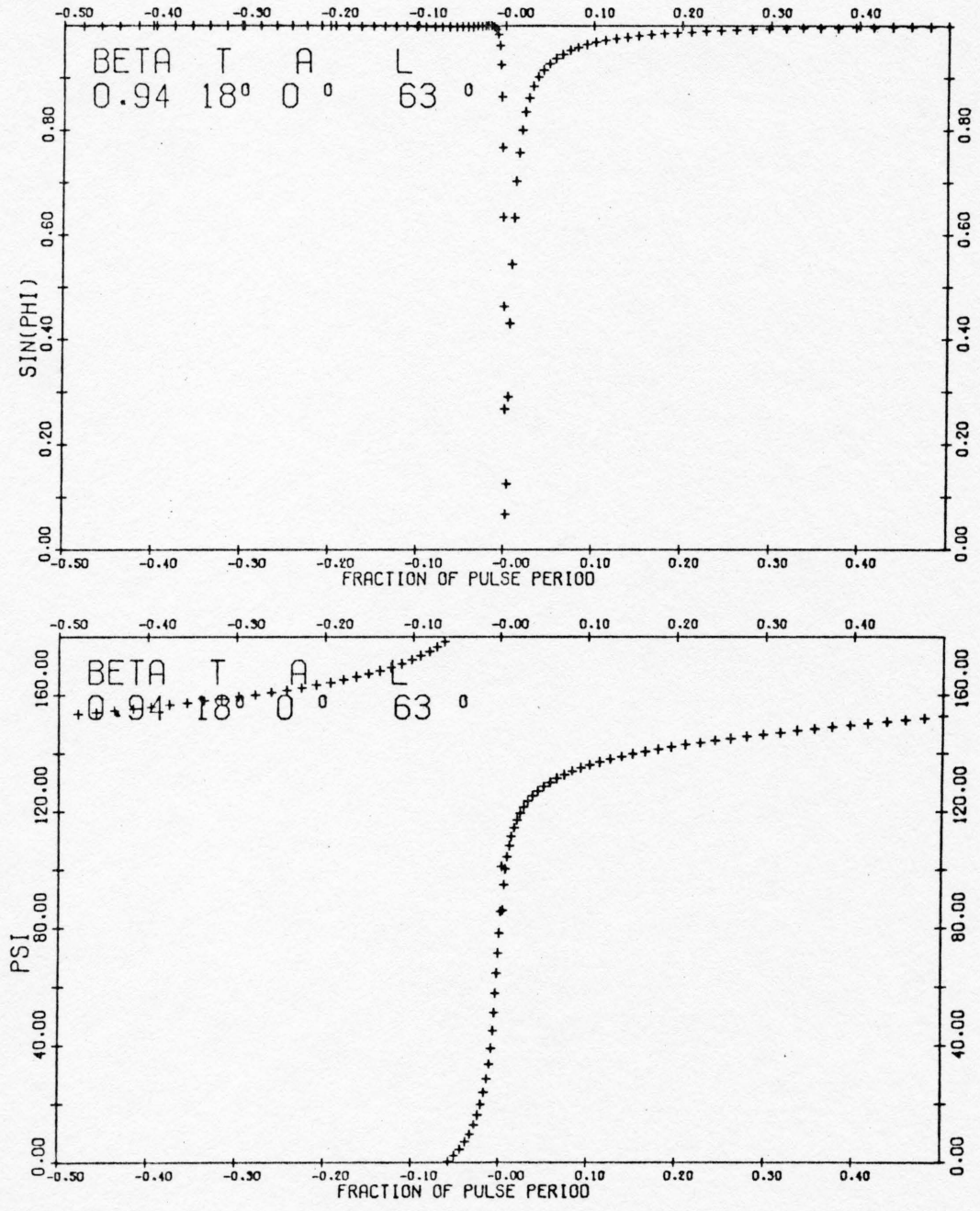

Figure 78. Polarization Time Behavior for β=0.94, T=18°, A=0°, L=63°

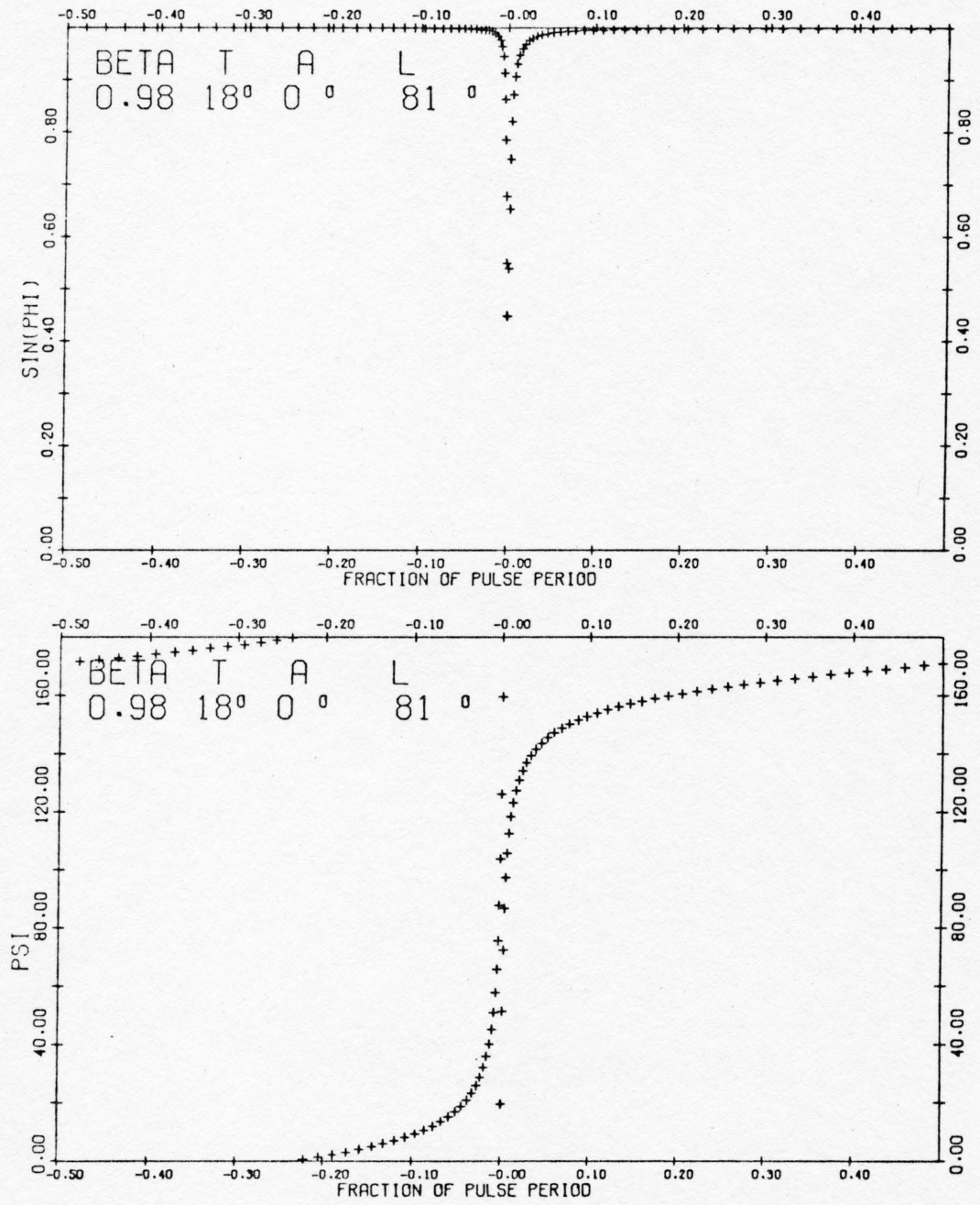

Figure 79. Polarization Time Behavior for β=0.98, T=18°, A=0°, L=81°

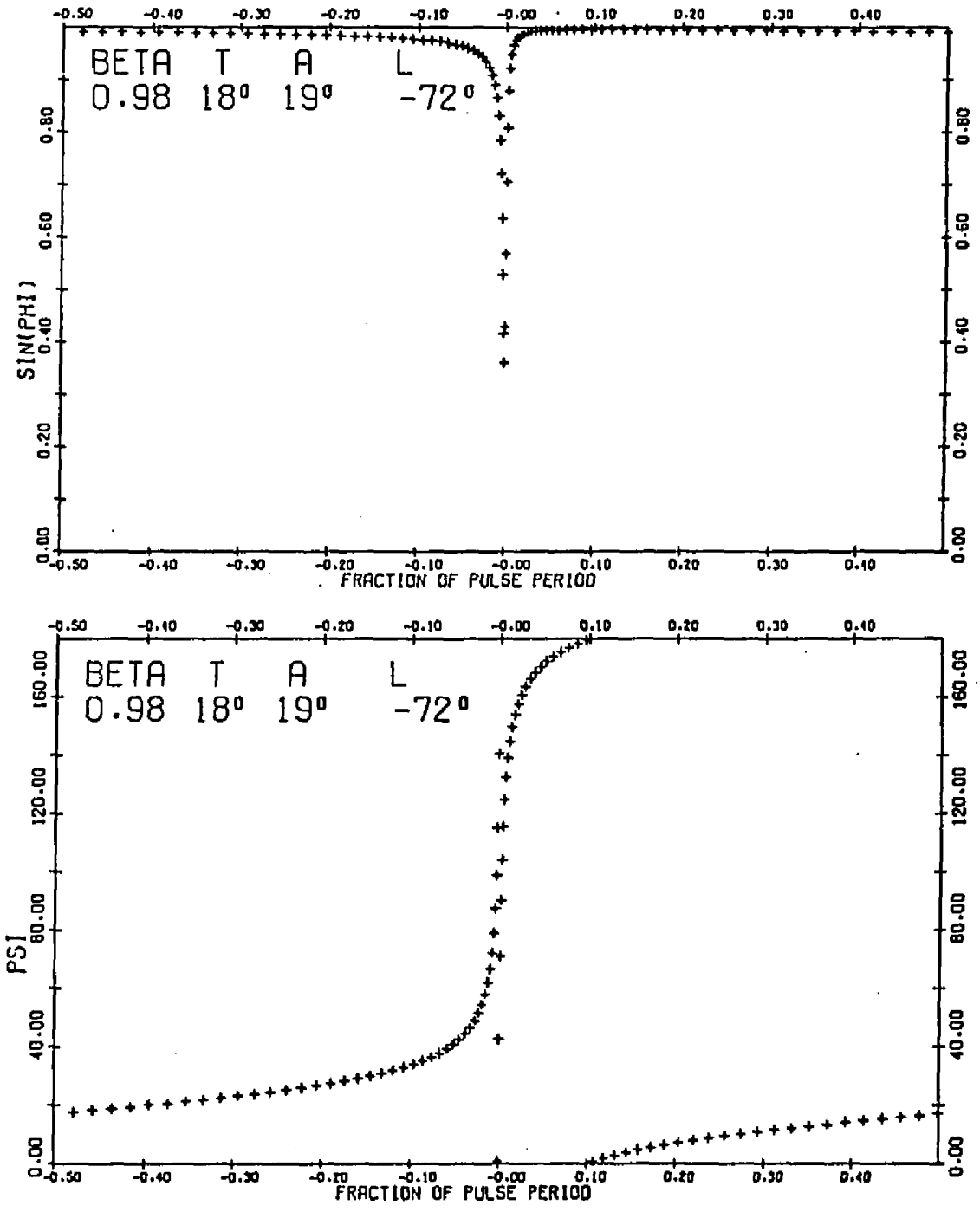

Figure 80. Polarization Time Behavior for β=0.98, T=18°, A=19°, L=-72°

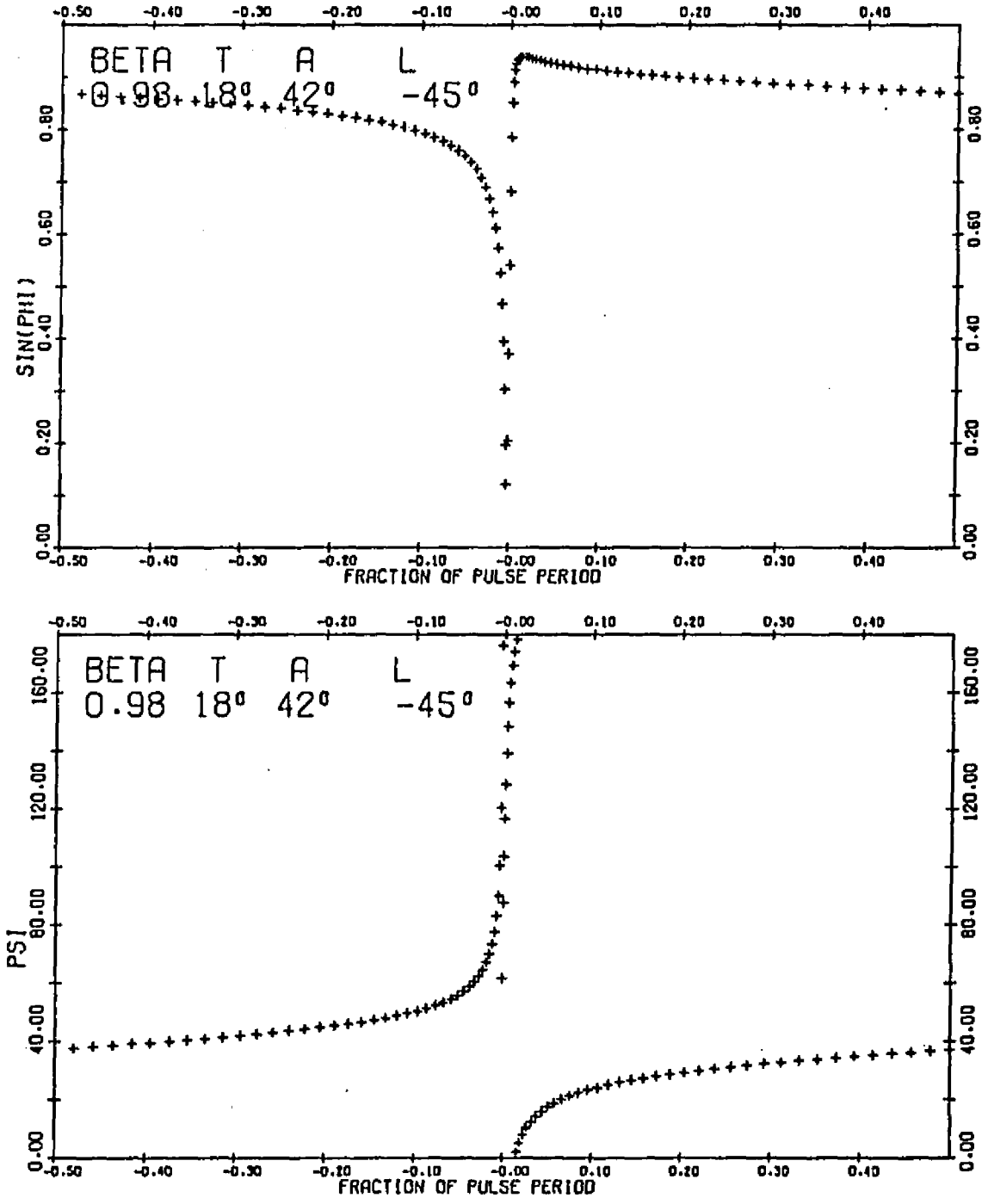

Figure 81. Polarization Time Behavior for β=0.98, T=18°, A=42°, L=-45°

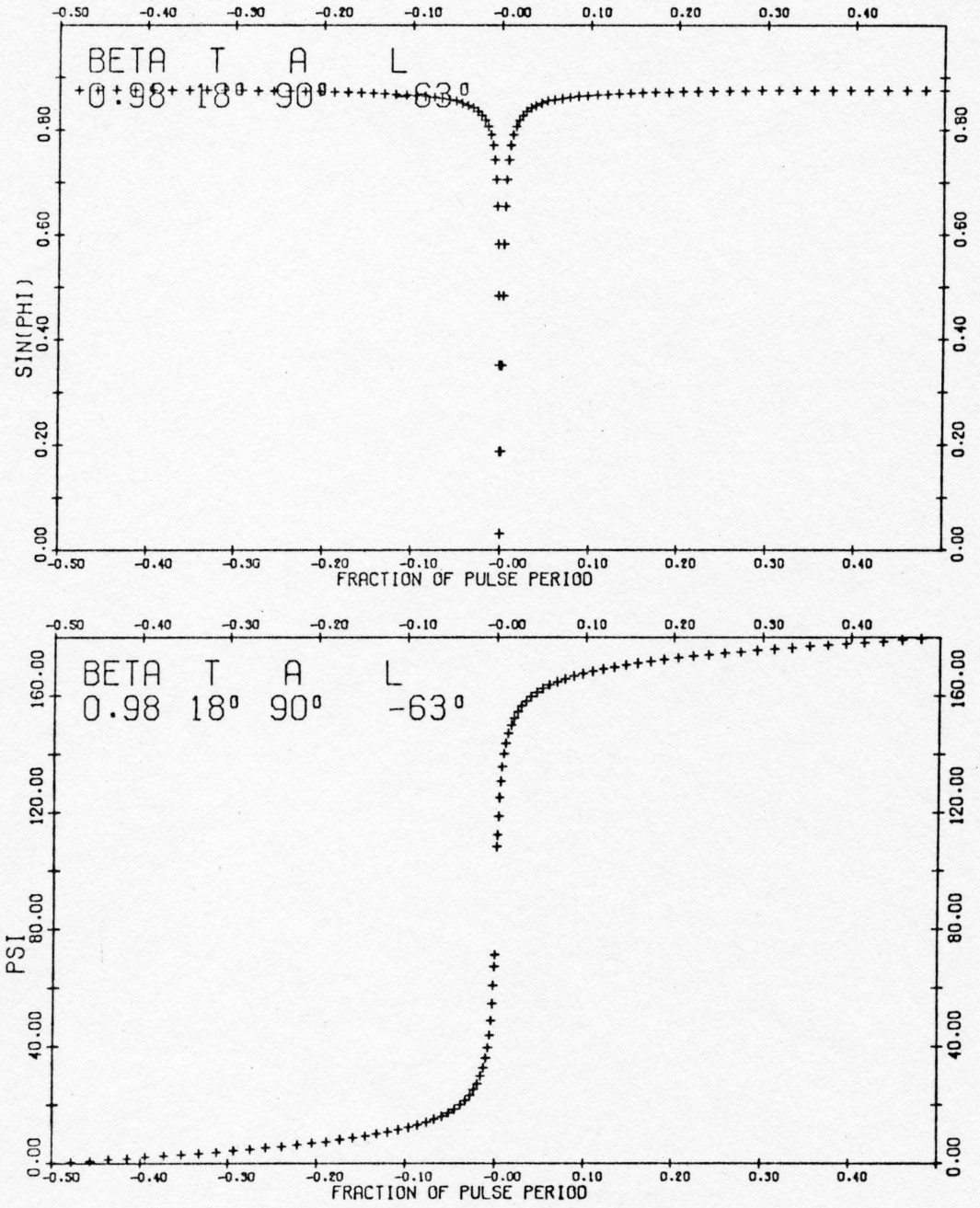

Figure 82. Polarization Time Behavior for β=0.98, T=18°, A=42°, L=-63°

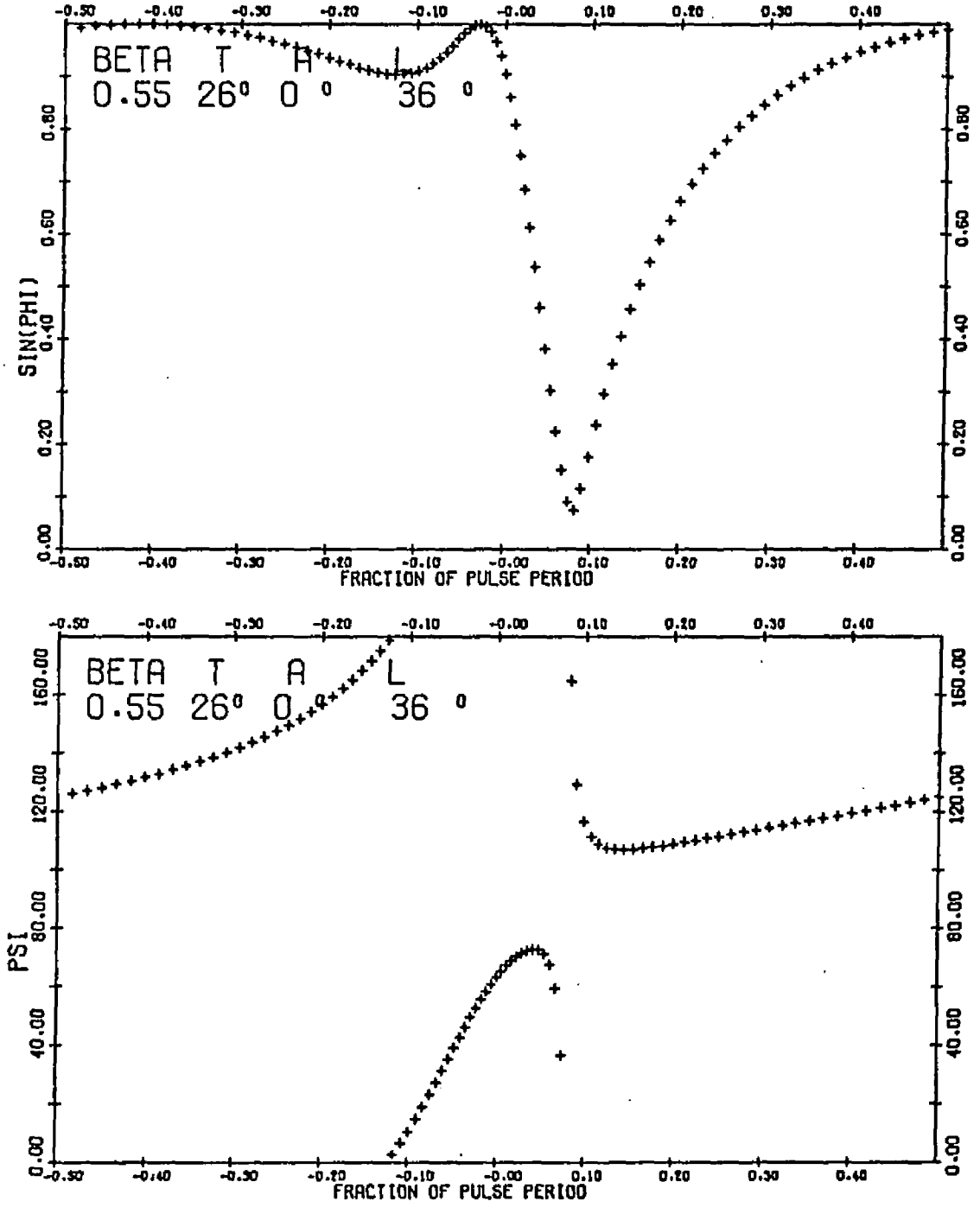

Figure 83. Polarization Time Behavior for β=0.55, T=26°, A=0°, L=36°

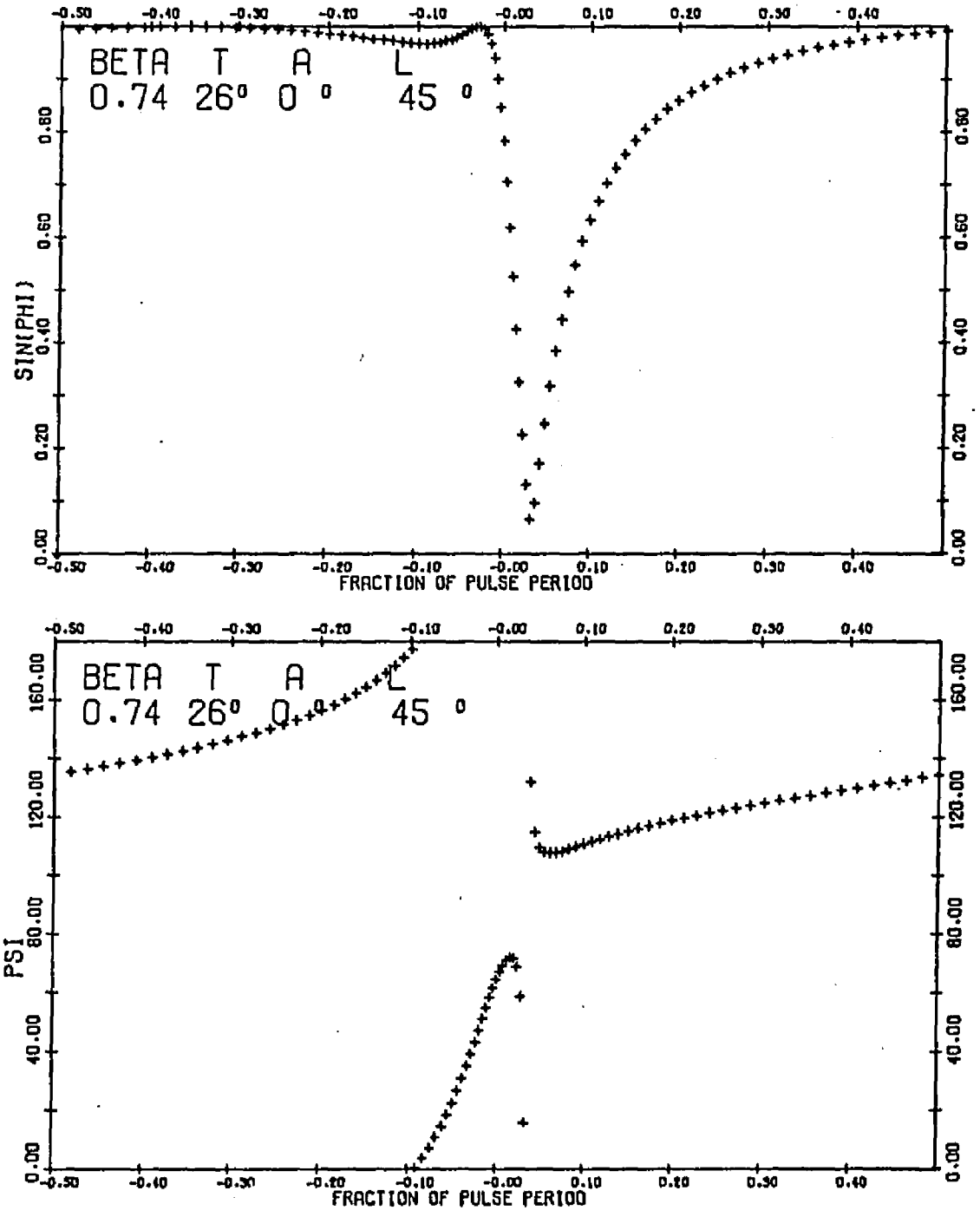

Figure 84. Polarization Time Behavior for β=0.74, T=26°, A=0°, L=45°

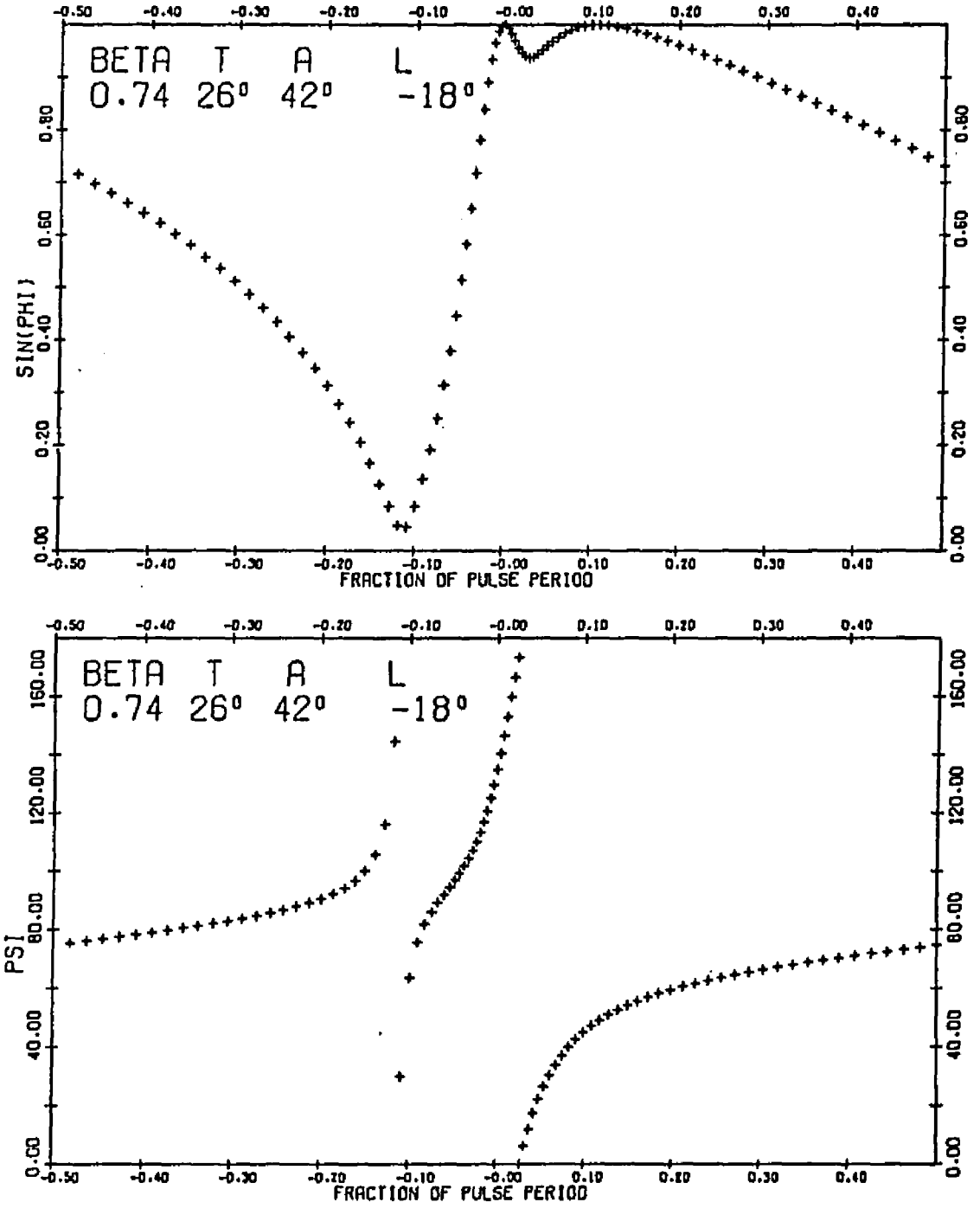

Figure 85. Polarization Time Behavior for β=0.74, T=26°, A=42°, L=-18°

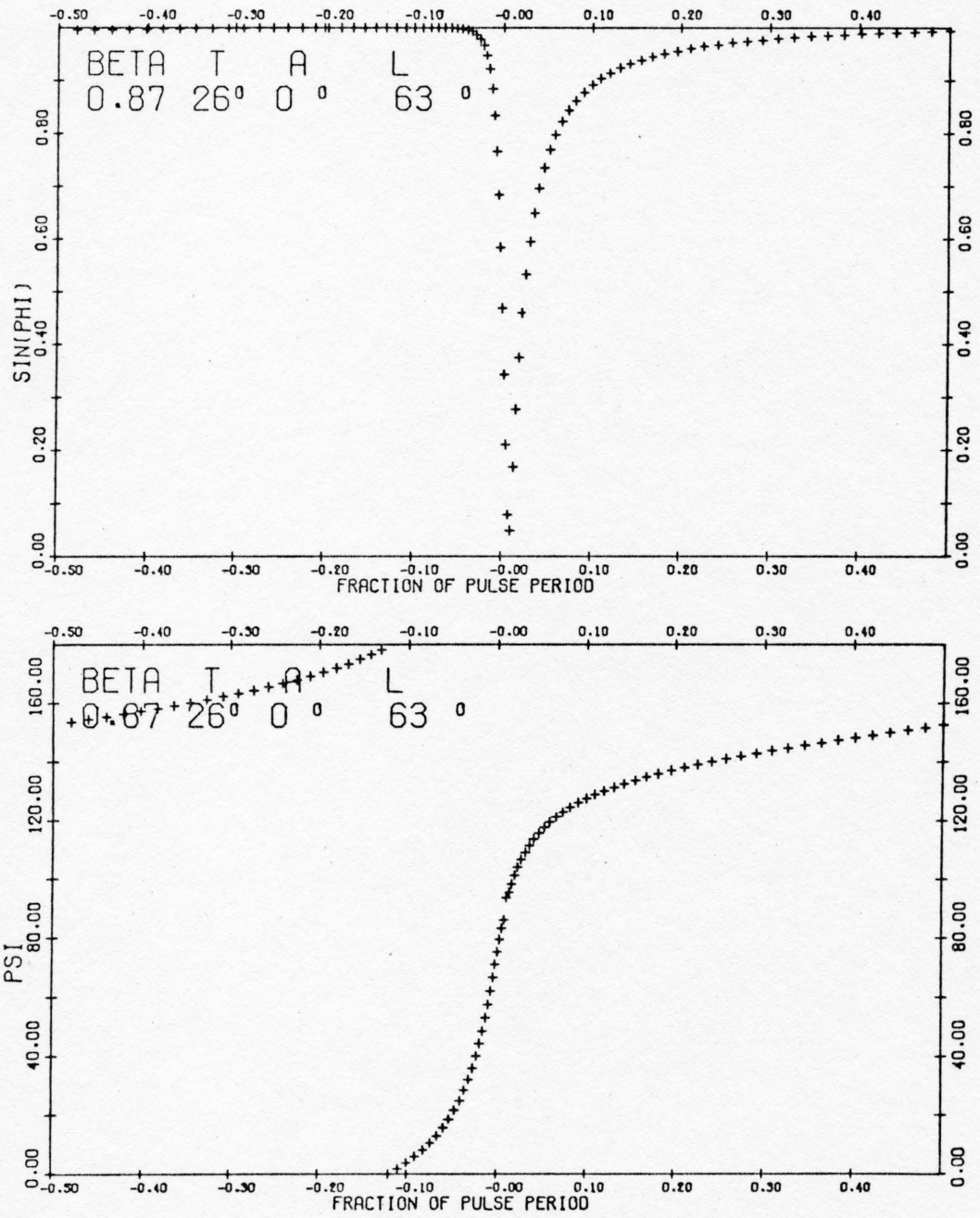

Figure 86. Polarization Time Behavior for β=0.87, T=26°, A=0°, L=63°

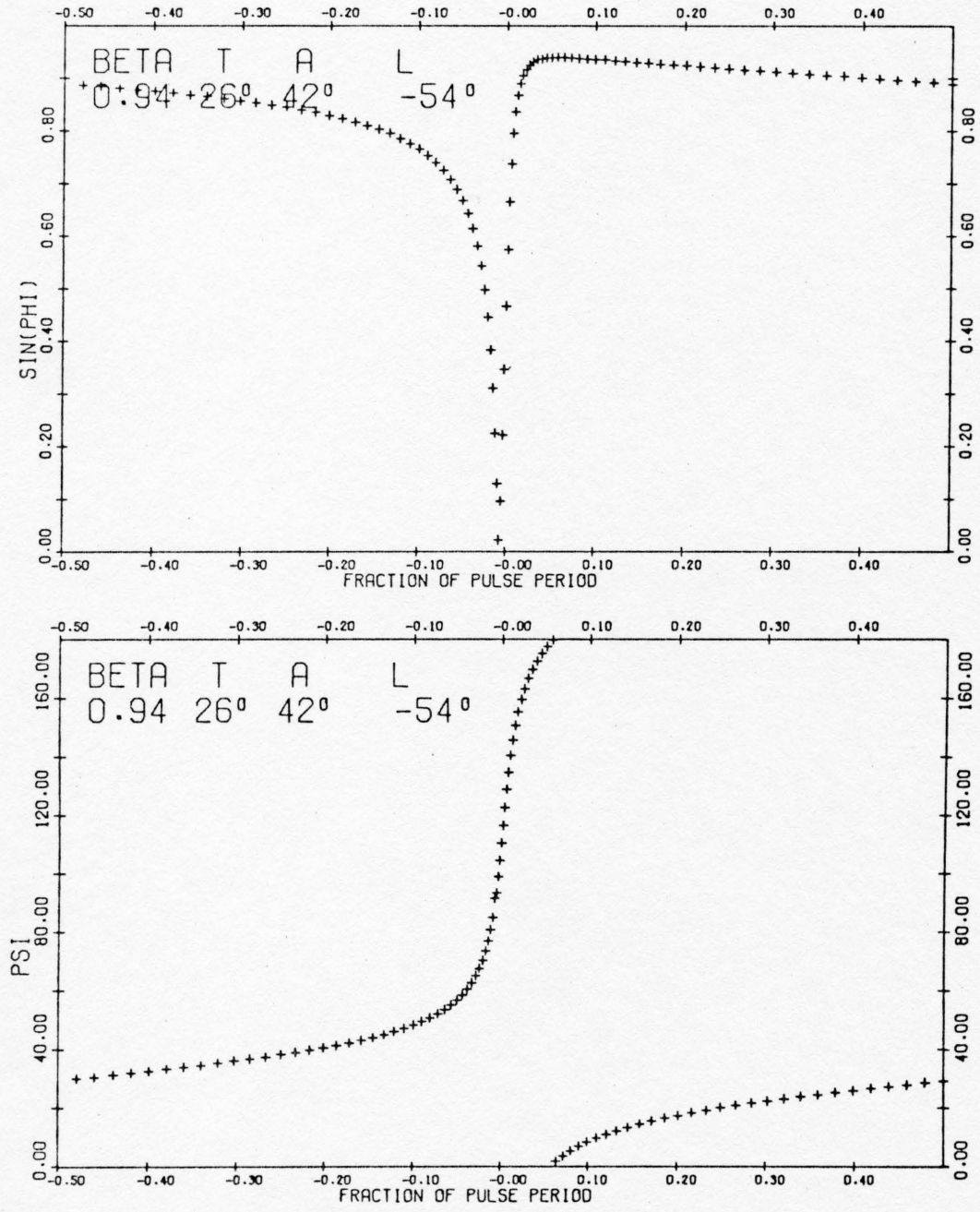

Figure 87. Polarization Time Behavior for β=0.94, T=26°, A=42°, L=-54°

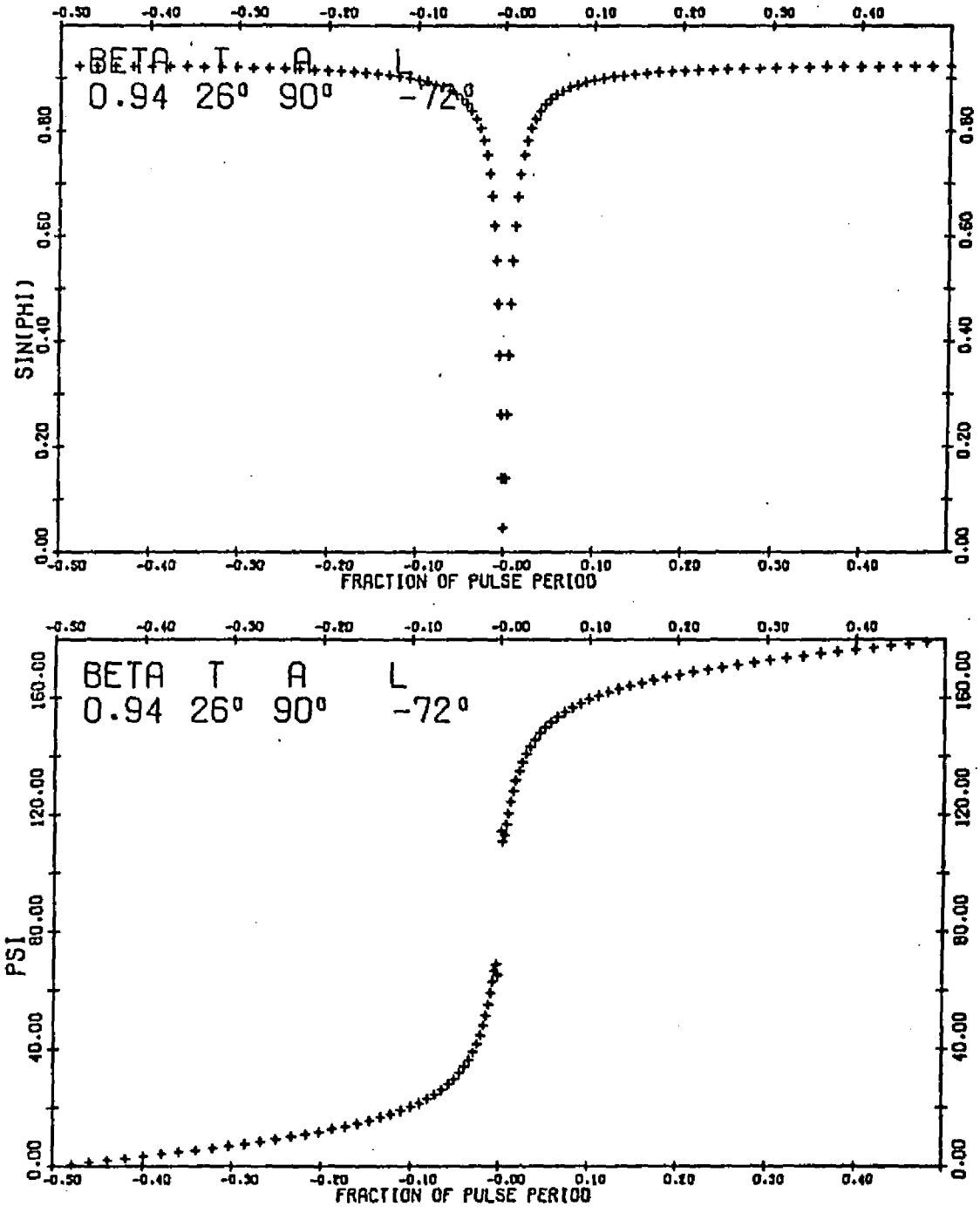

Figure 88. Polarization Time Behavior for β=0.94, T=26°, A=90°, L=-72°

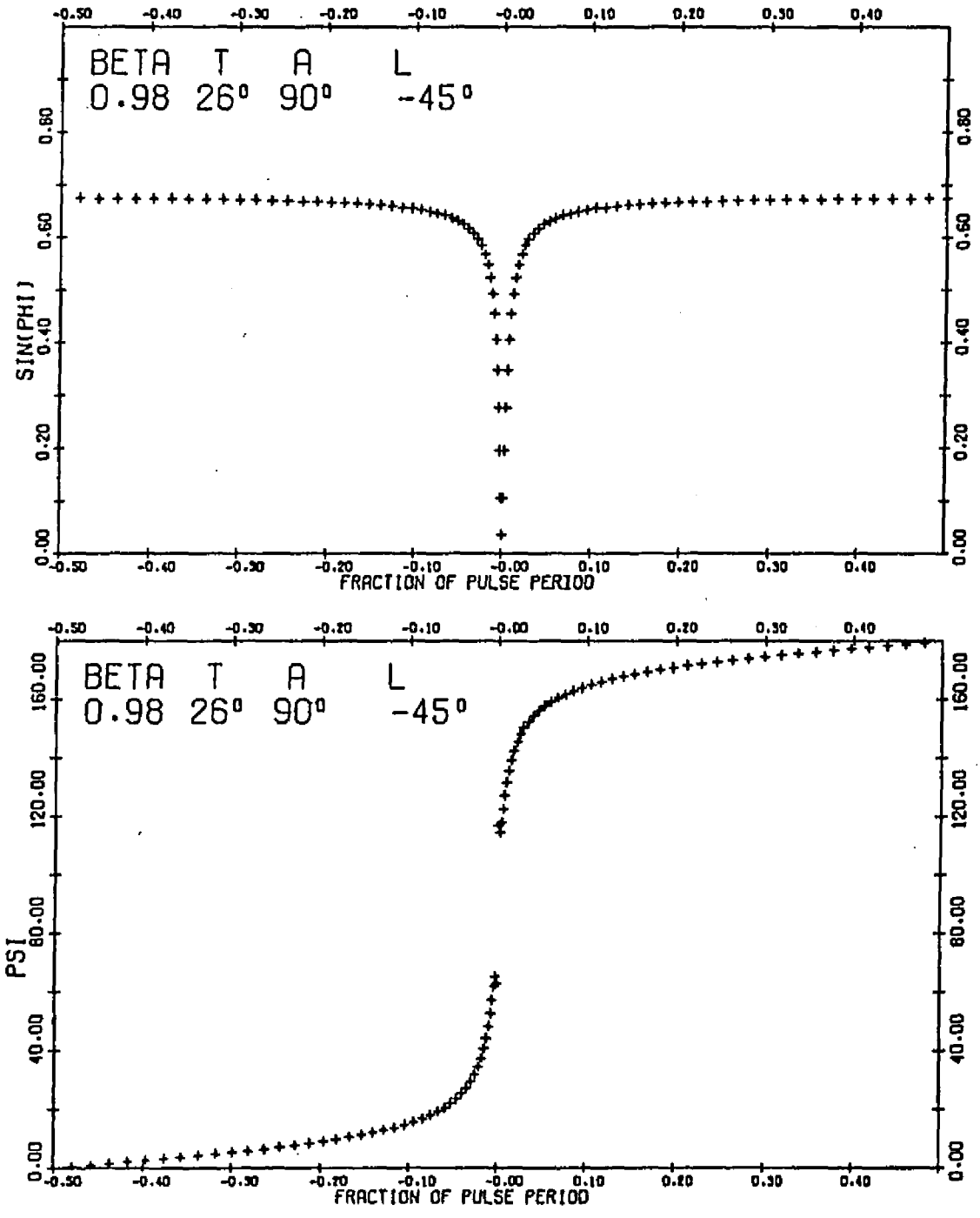

Figure 89. Polarization Time Behavior for β=0.98, T=26°, A=90°, L=-45°

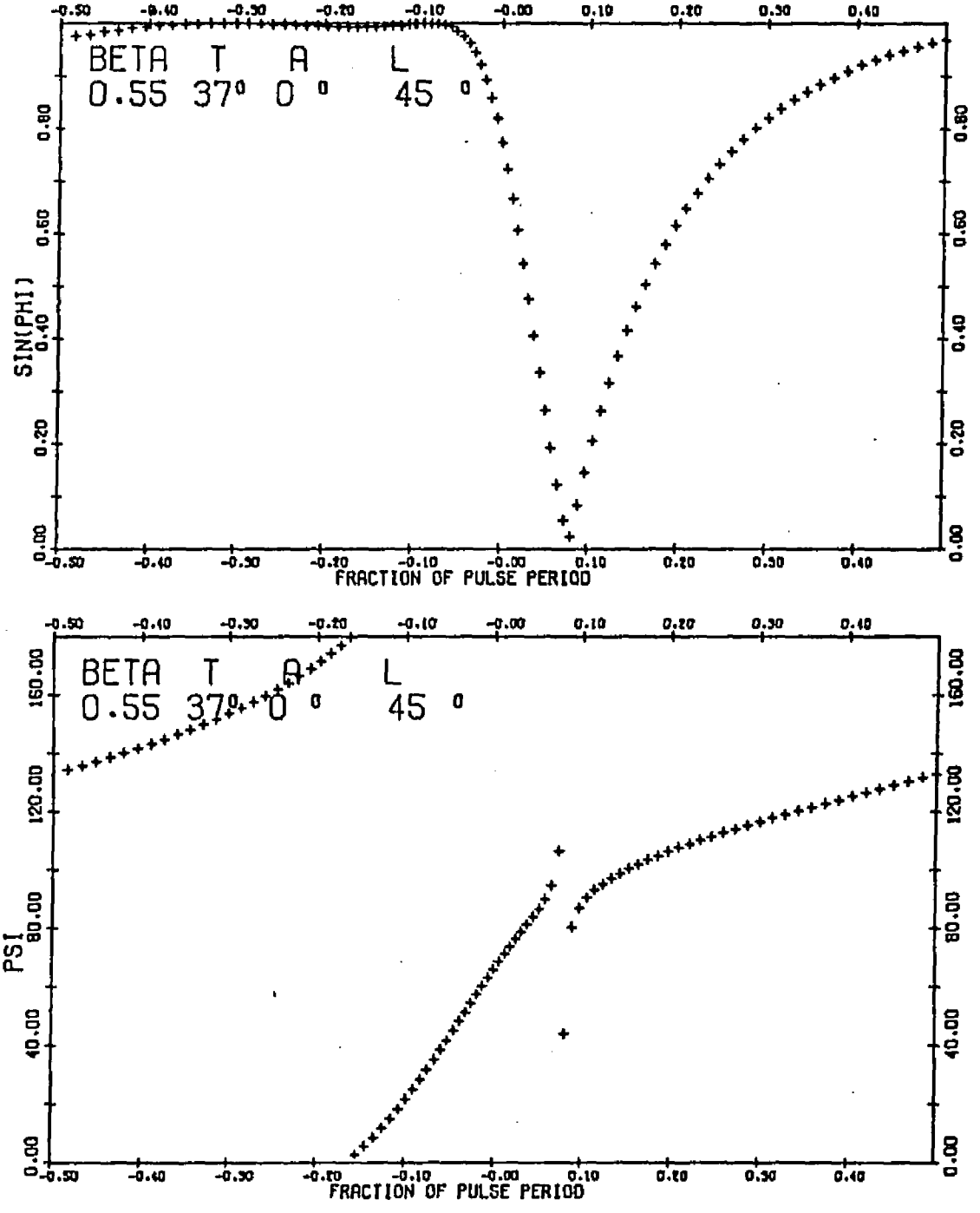

Figure 90. Polarization Time Behavior for β=0.55, T=37°, A=0°, L=45°

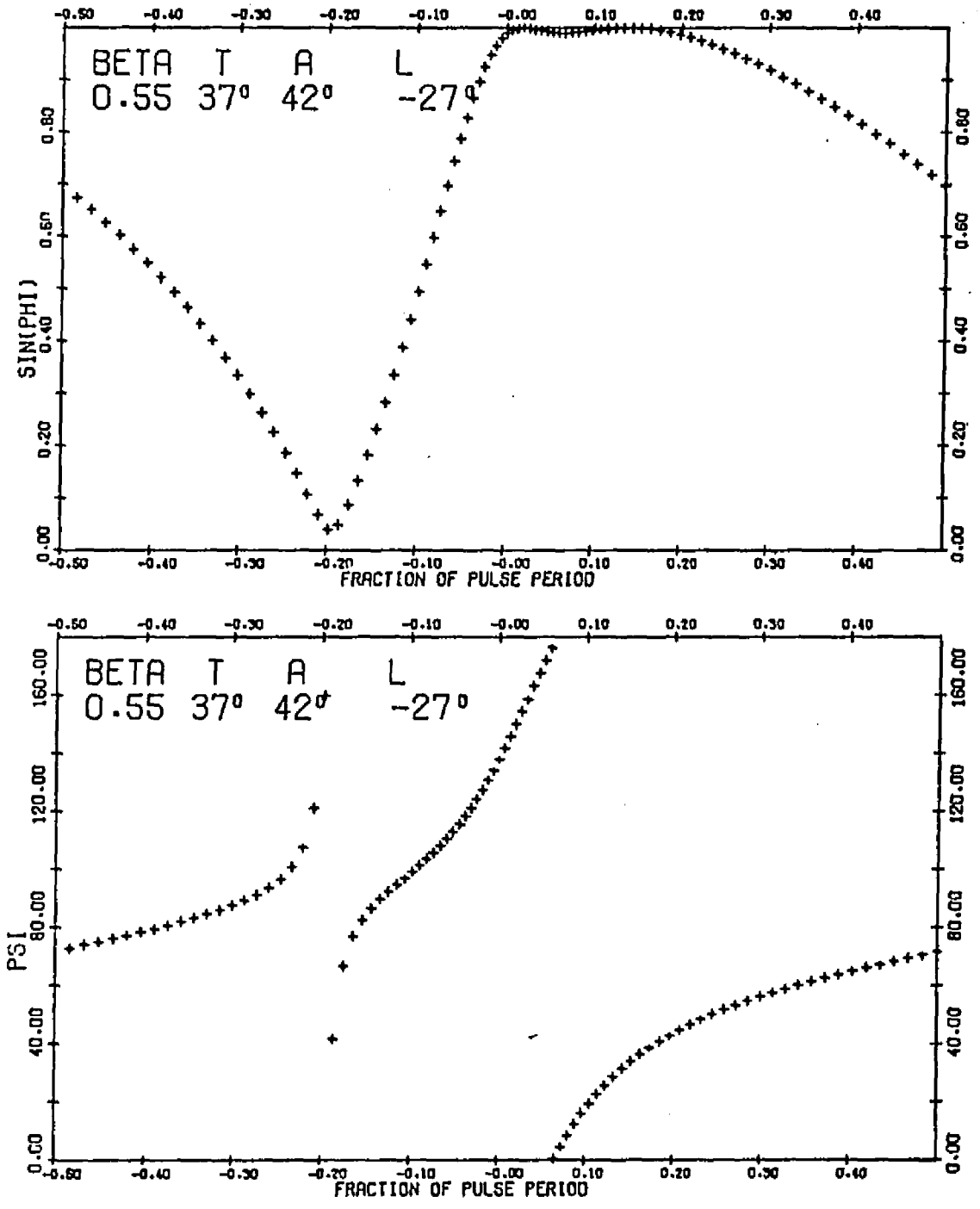

Figure 91. Polarization Time Behavior for β=0.55, T=37°, A=42°, L=-27°

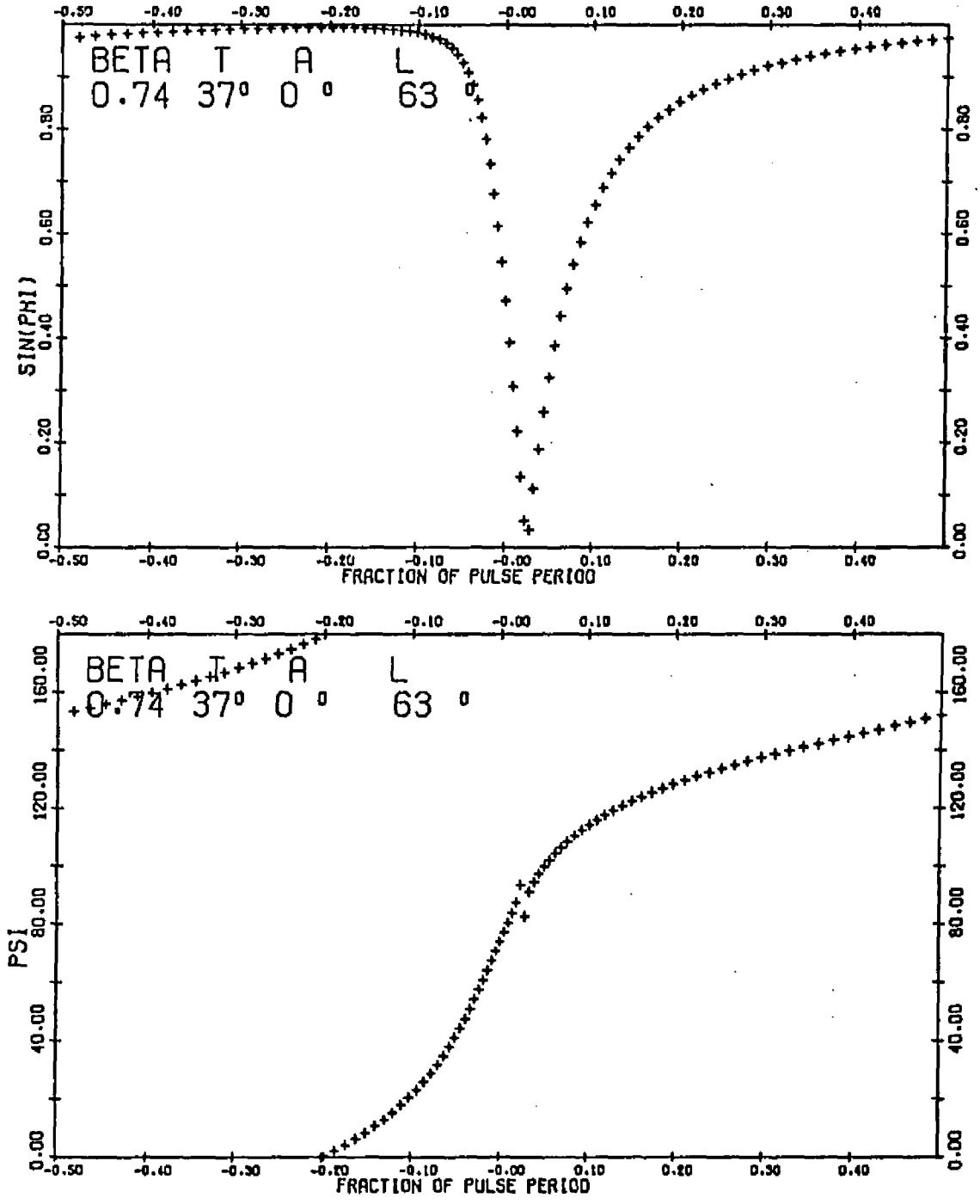

Figure 92. Polarization Time Behavior for β=0.74, T=37°, A=0°, L=63°

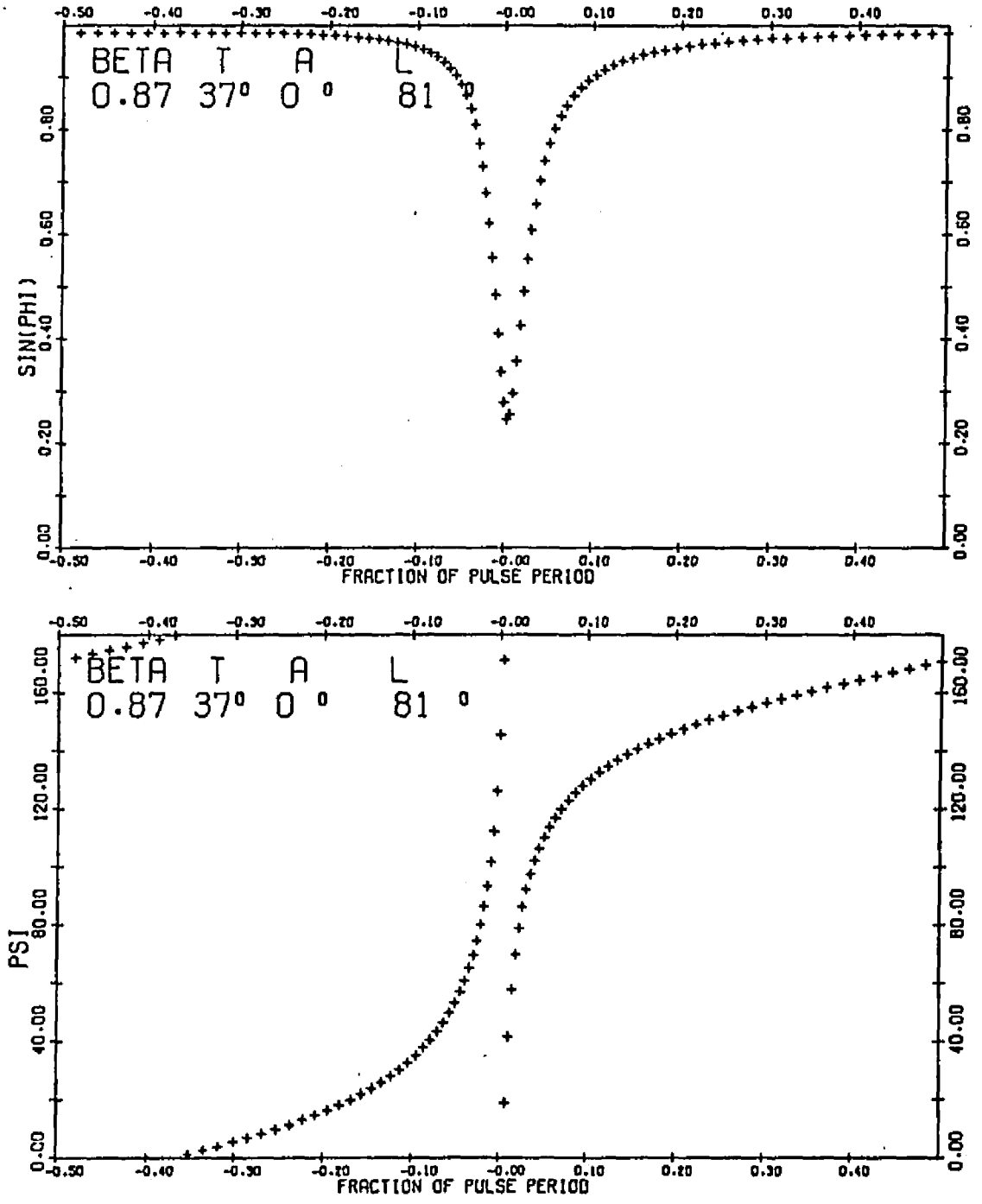

Figure 93. Polarization Time Behavior for β=0.87, T=37°, A=0°, L=81°

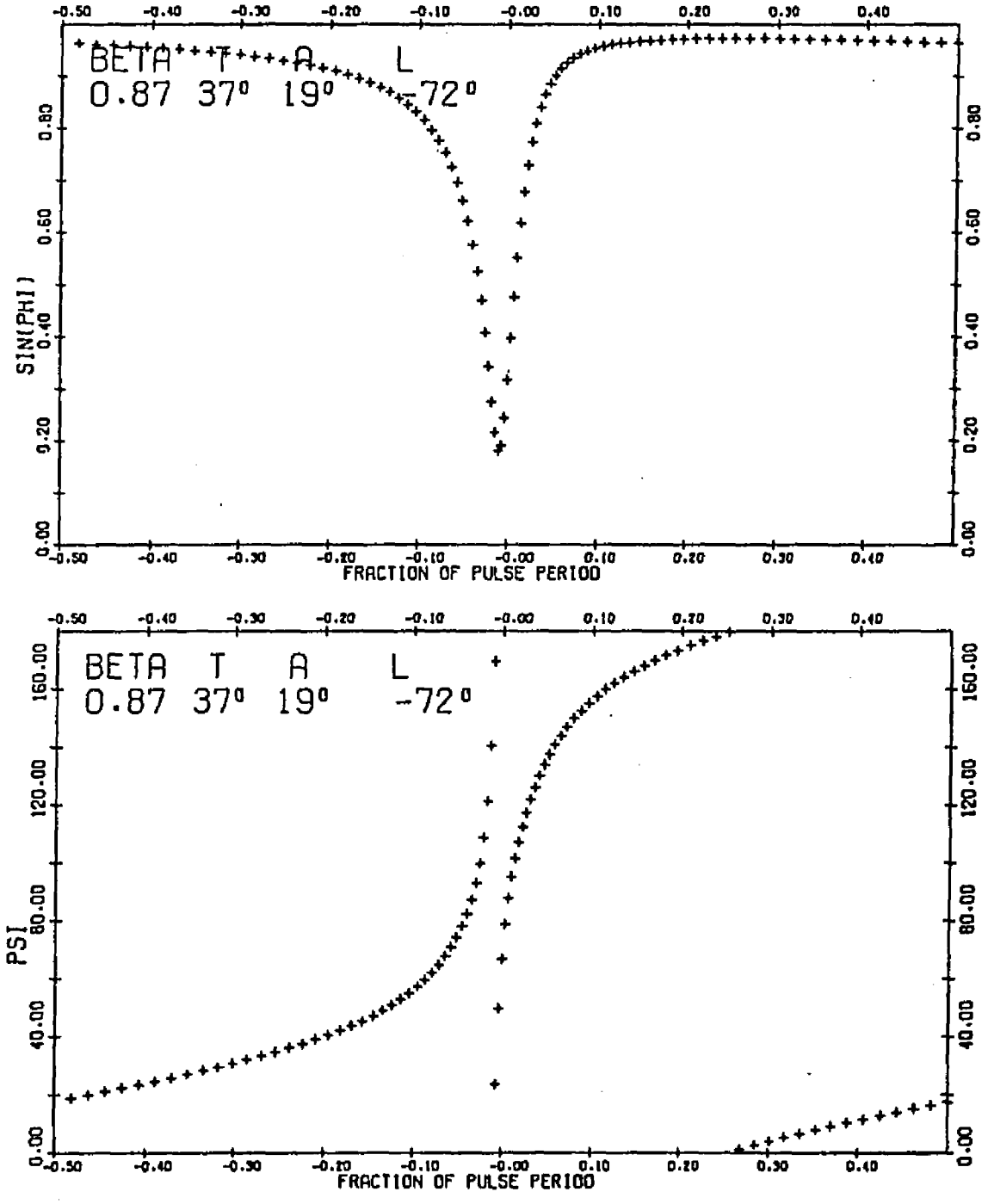

Figure 94. Polarization Time Behavior for β=0.87, T=37°, A=19°, L=-72°

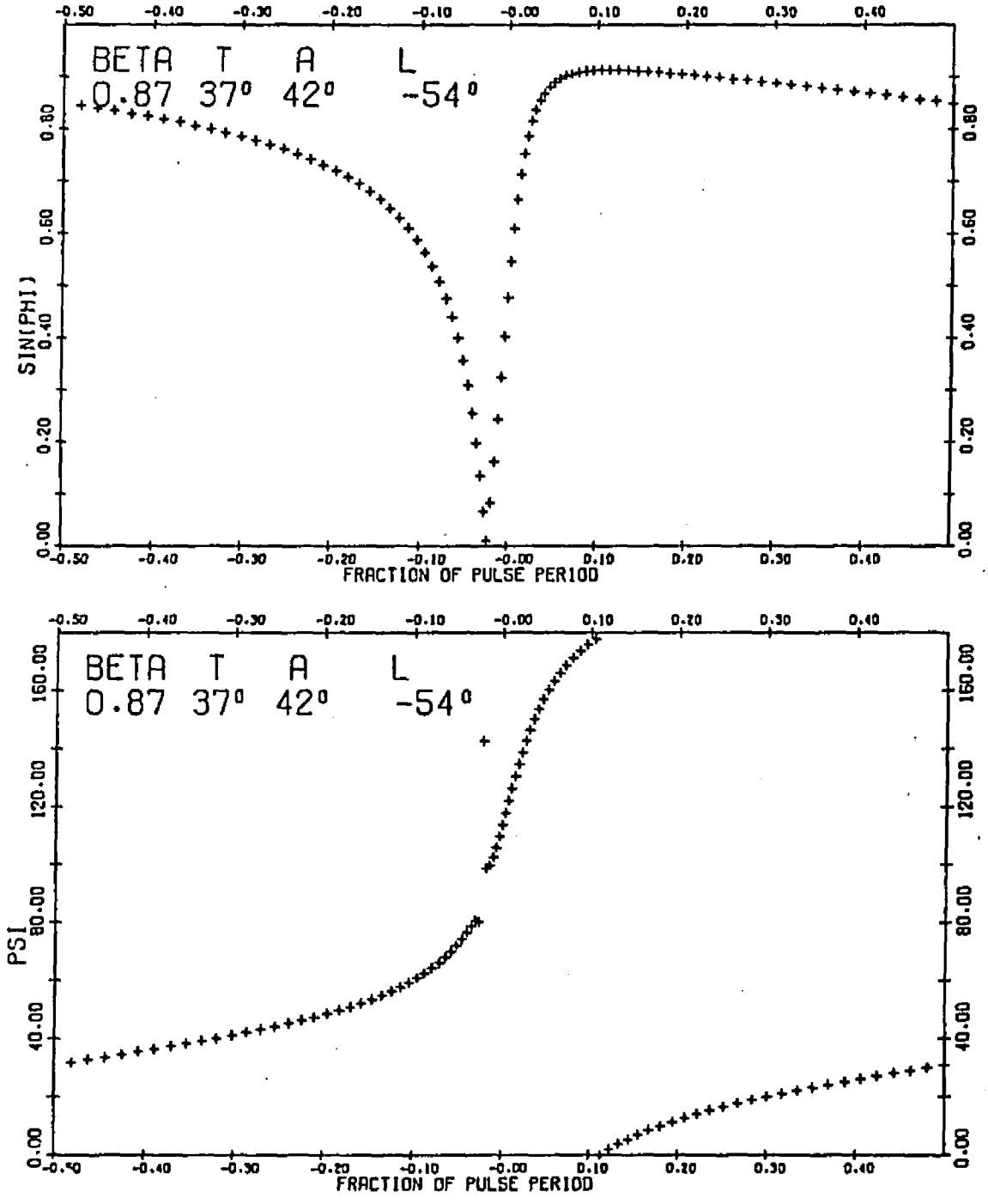

Figure 95. Polarization Time Behavior for β=0.87, T=37°, A=42°, L=-54°

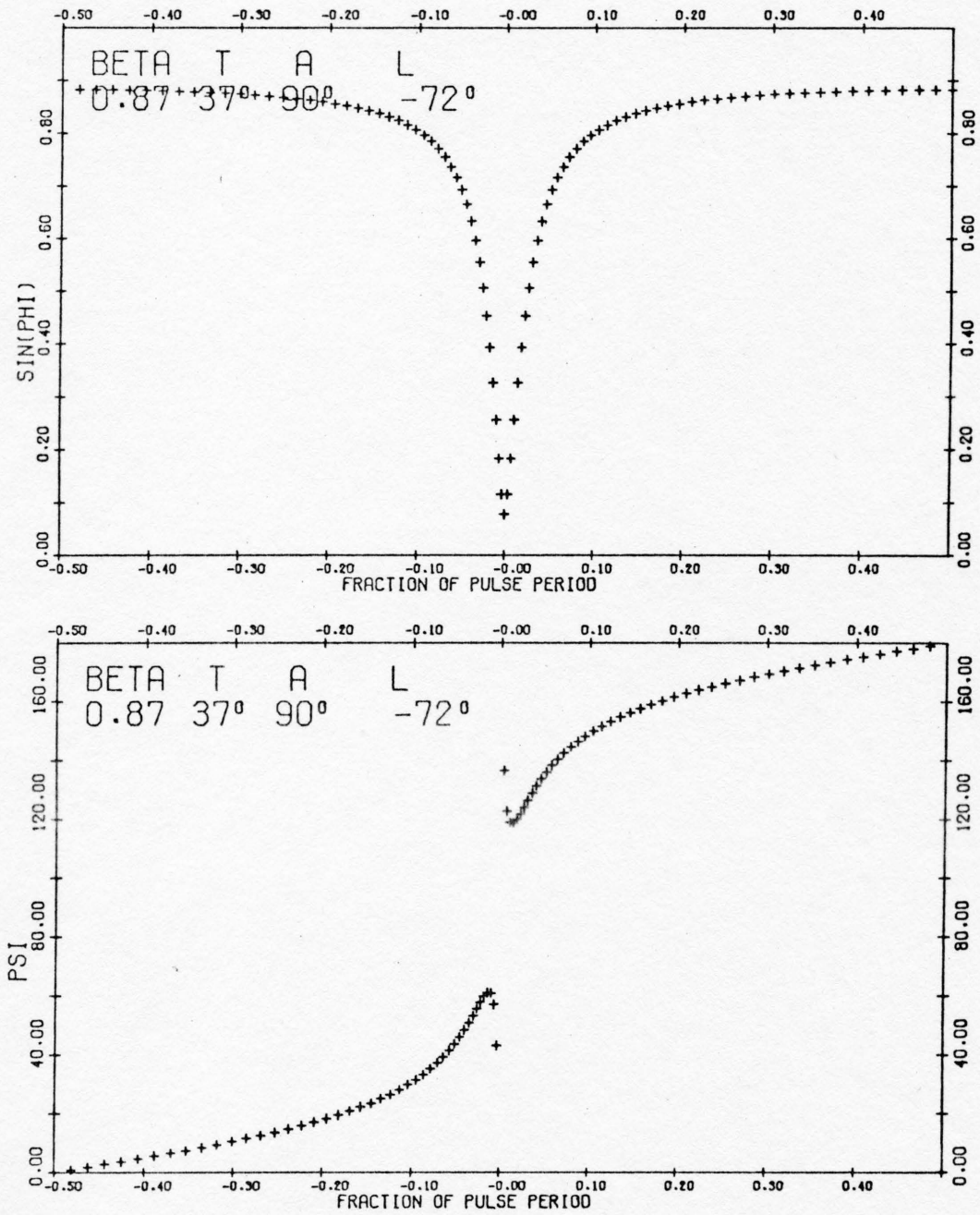

Figure 96. Polarization Time Behavior for β=0.87, T=37°, A=90°, L=-72°

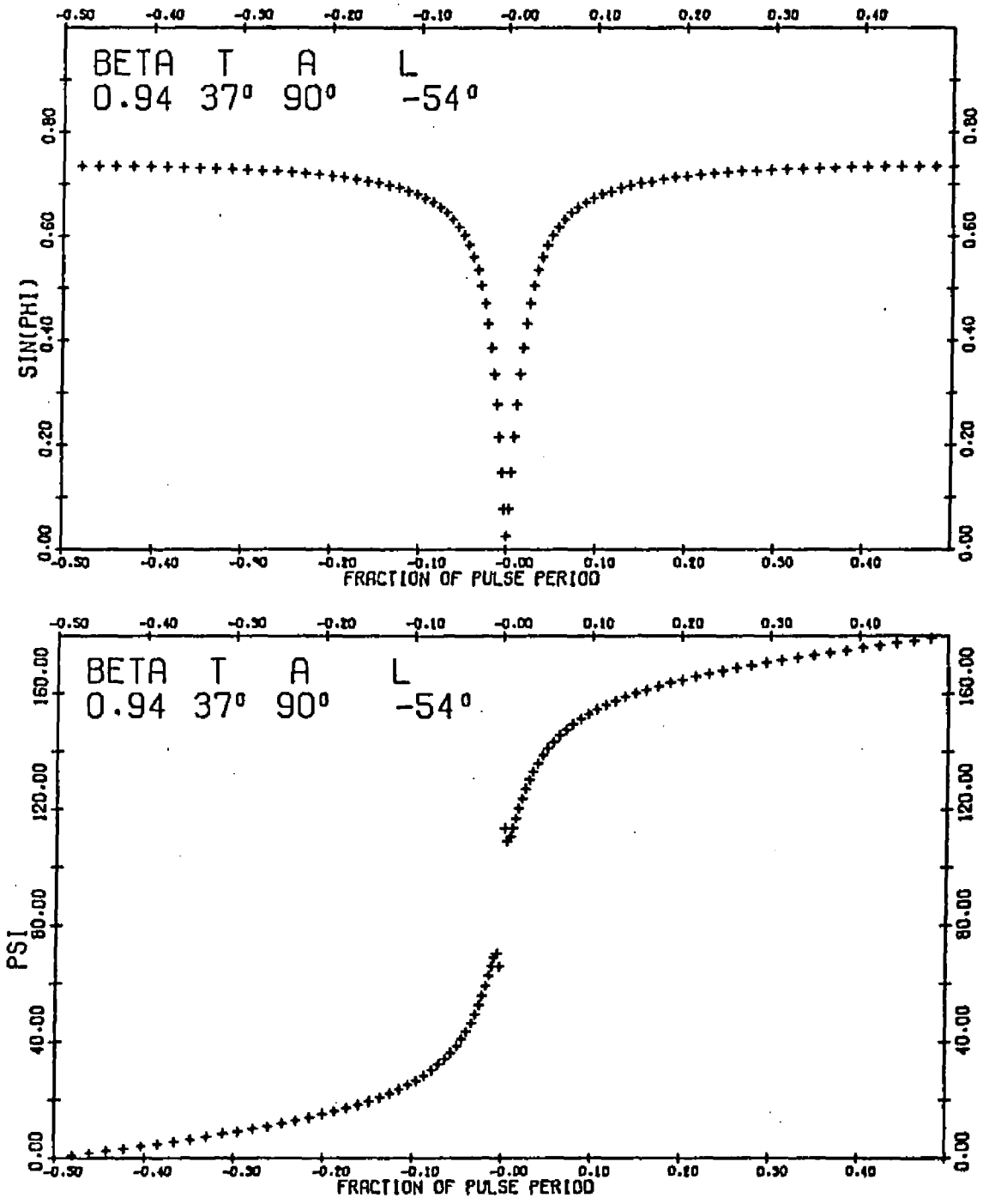

Figure 97. Polarization Time Behavior for β=0.94, T=37°, A=90°, L=-54°

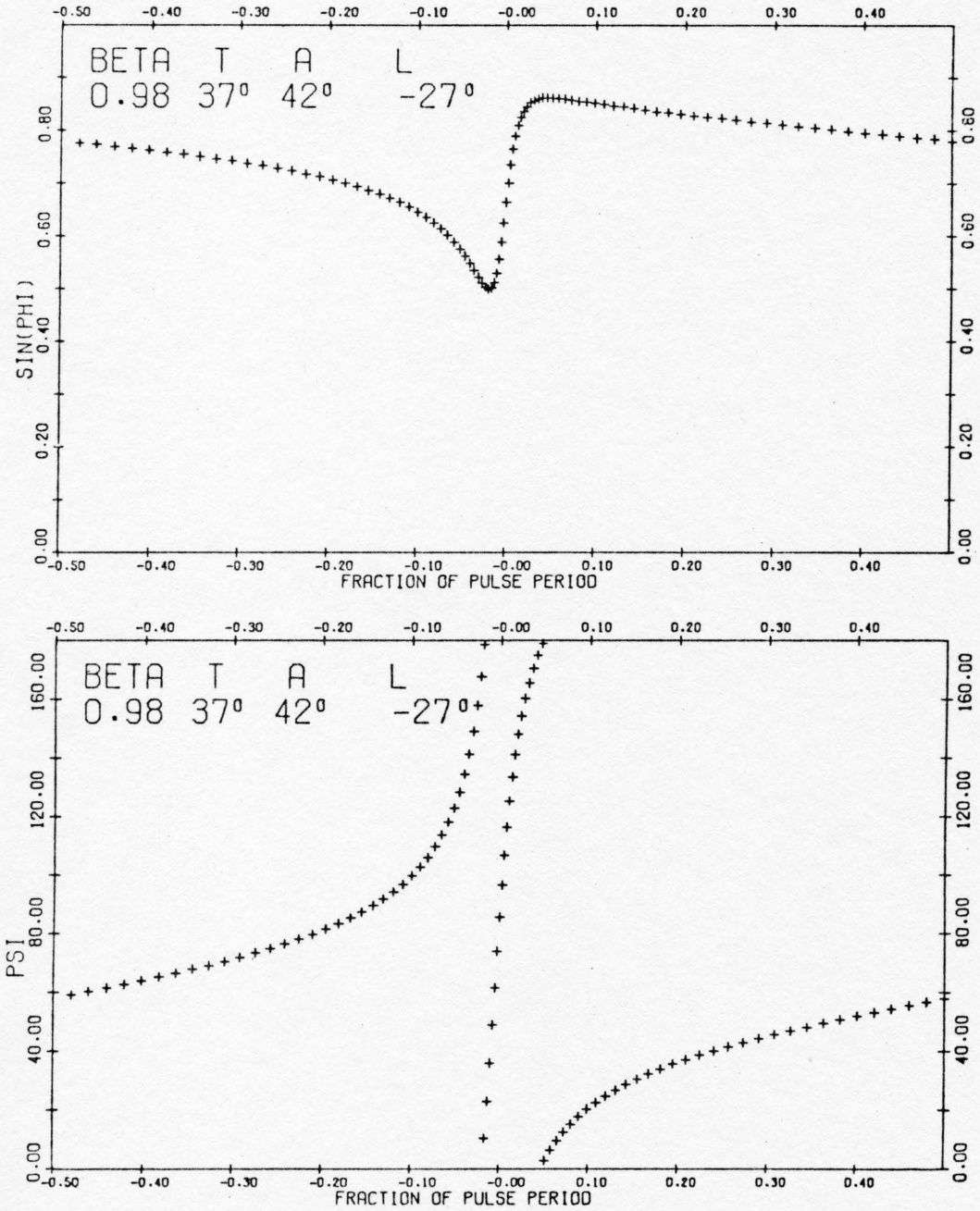

Figure 98. Polarization Time Behavior for β=0.98, T=37°, A=42°, L=-27°

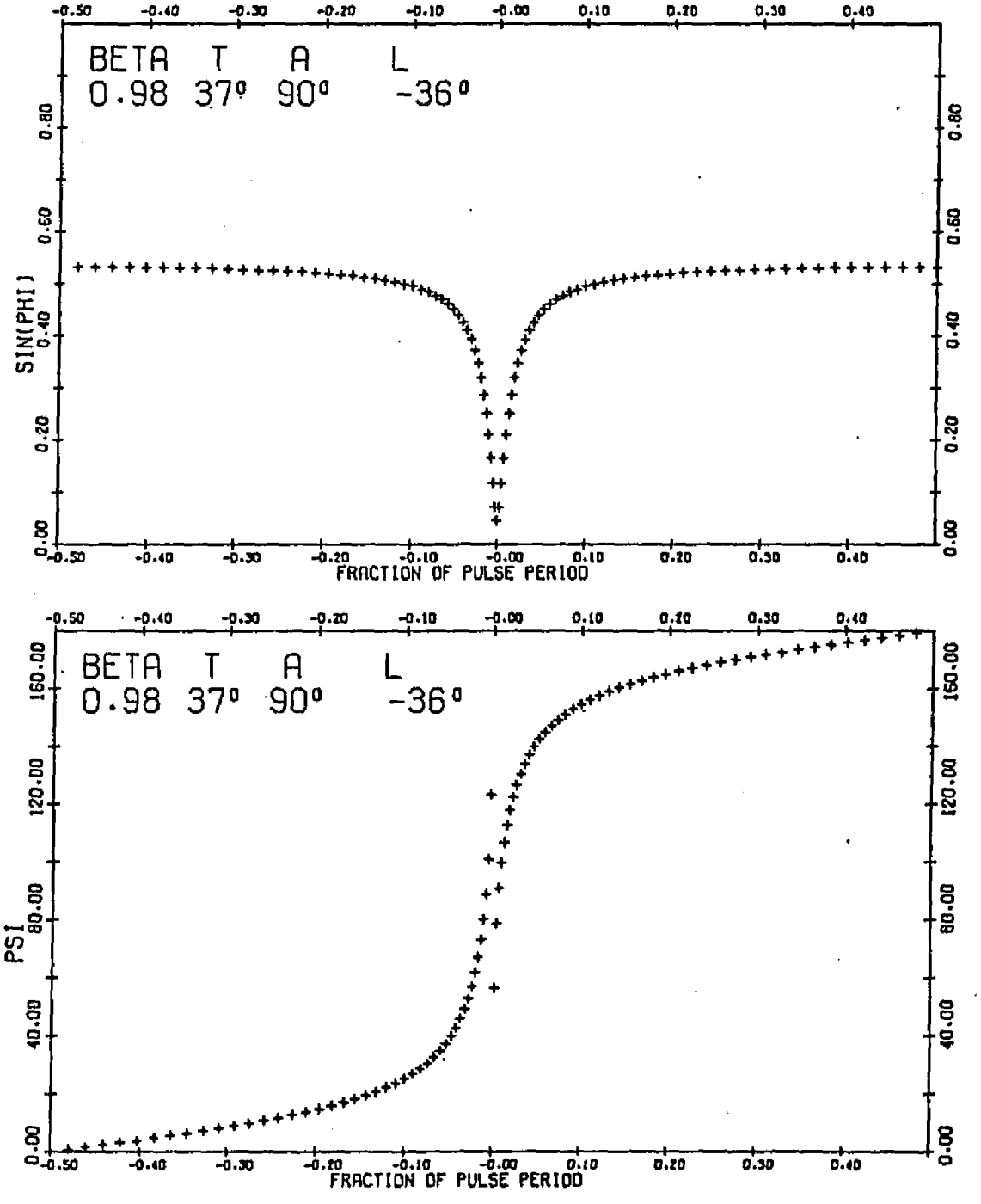

Figure 99. Polarization Time Behavior for β=0.98, T=37°, A=90°, L=-36°

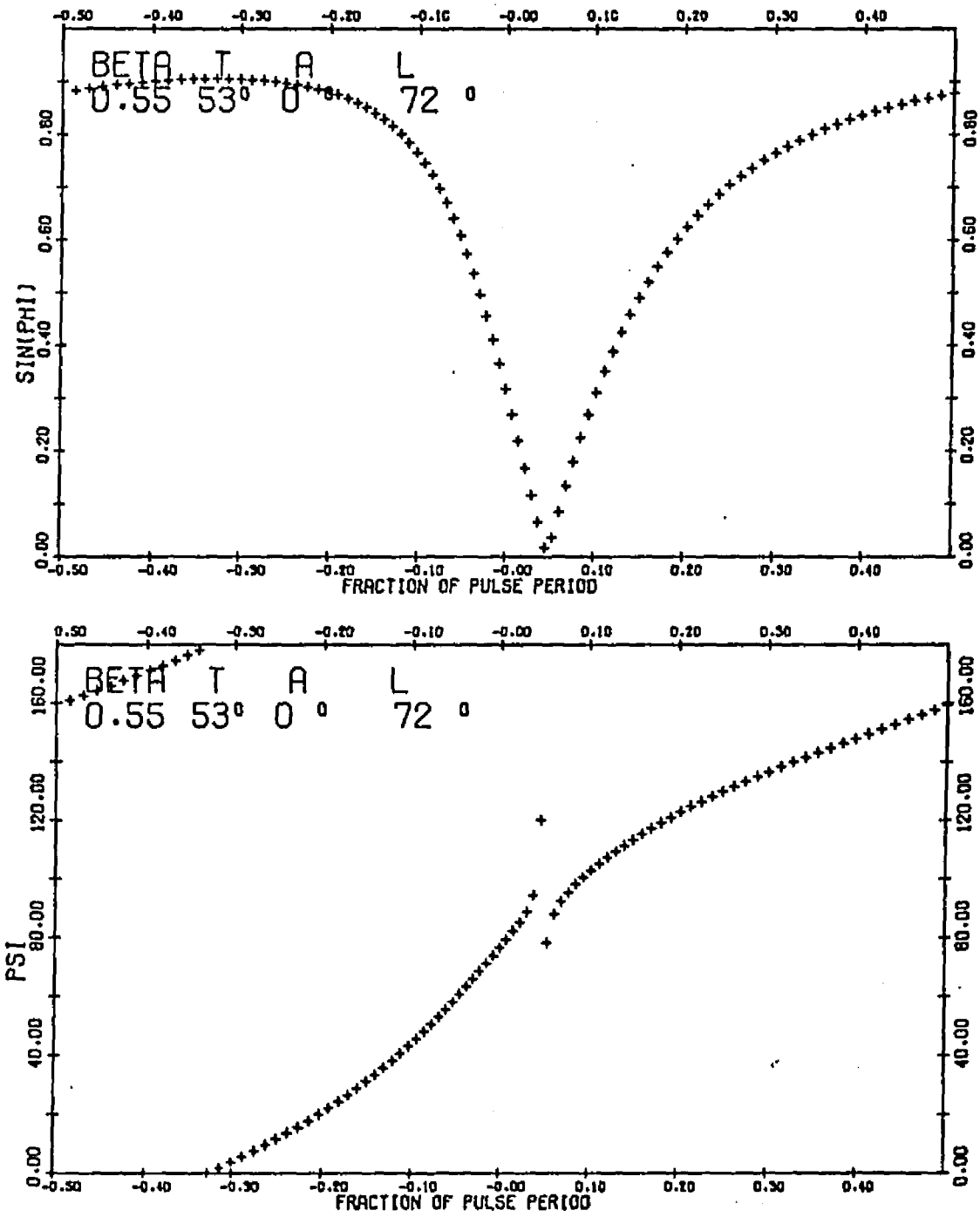

Figure 100. Polarization Time Behavior for β=0.55, T=53°, A=0°, L=72°

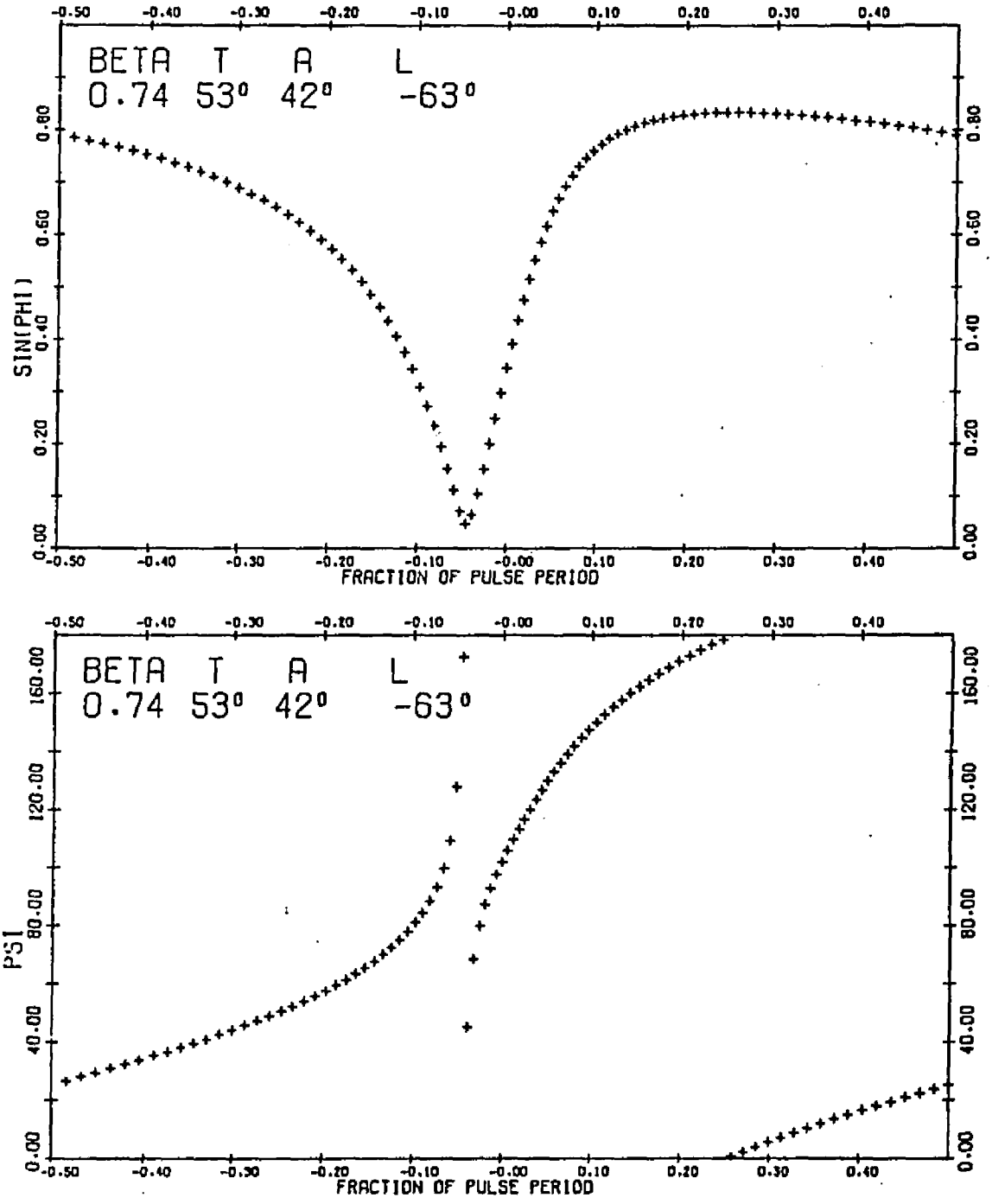

Figure 101. Polarization Time Behavior for β=0.74, T=53°, A=42°, L=-63°

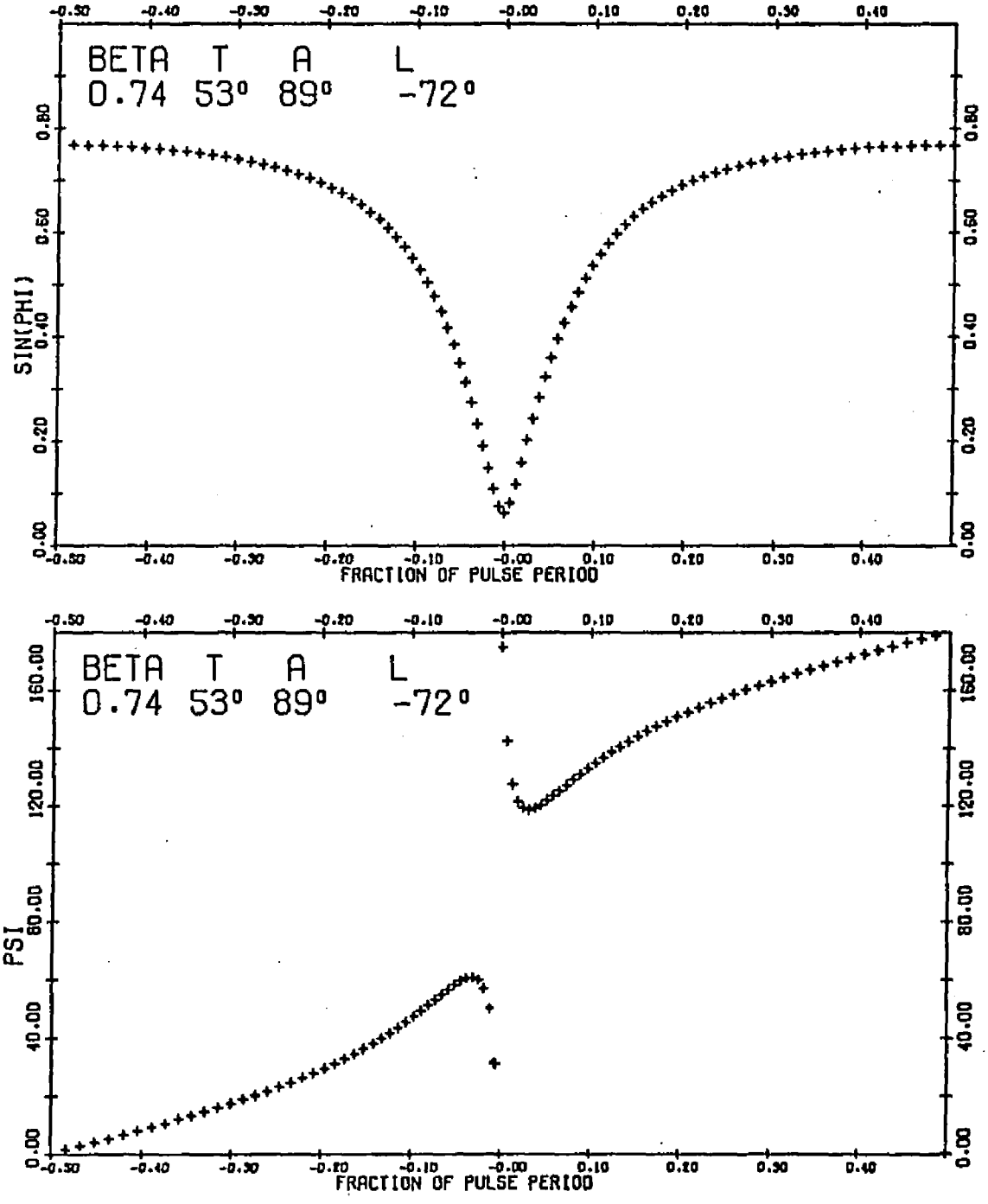

Figure 102. Polarization Time Behavior for β=0.74, T=53°, A=89°, L=-72°

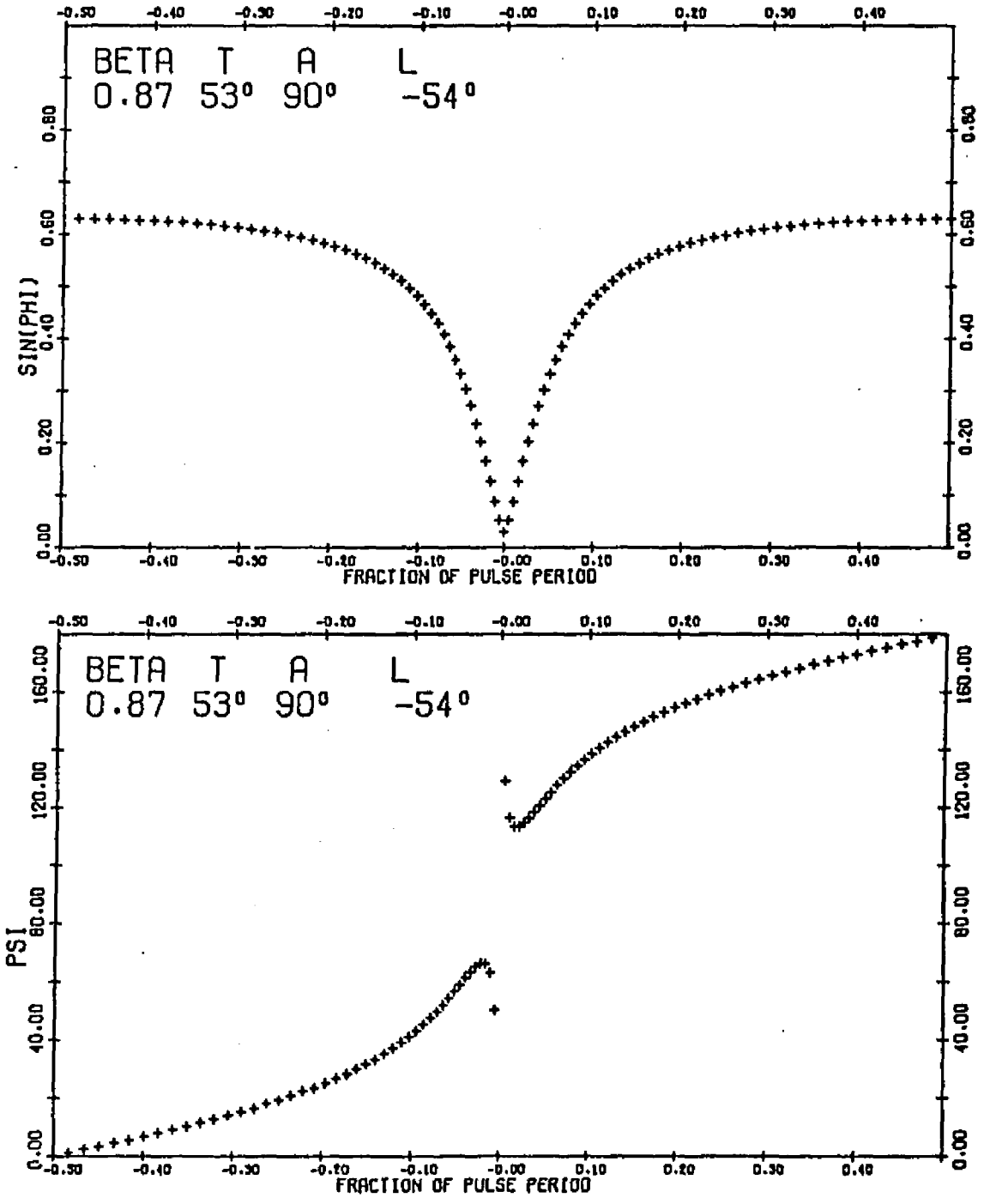

Figure 103. Polarization Time Behavior for β=0.87, T=53°, A=90°, L=-54°

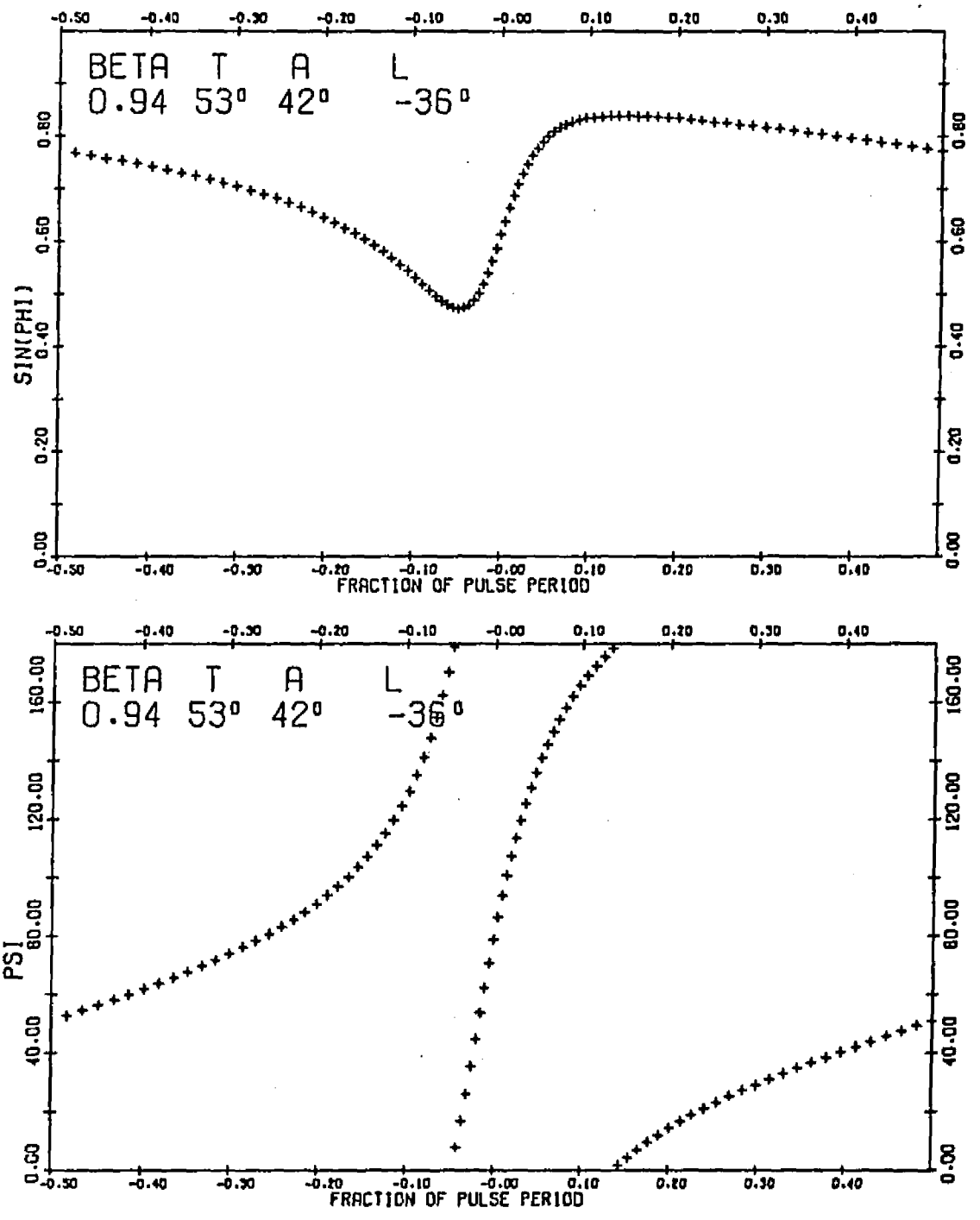

Figure 104. Polarization Time Behavior for β=0.94, T=53°, A=42°, L=-36°

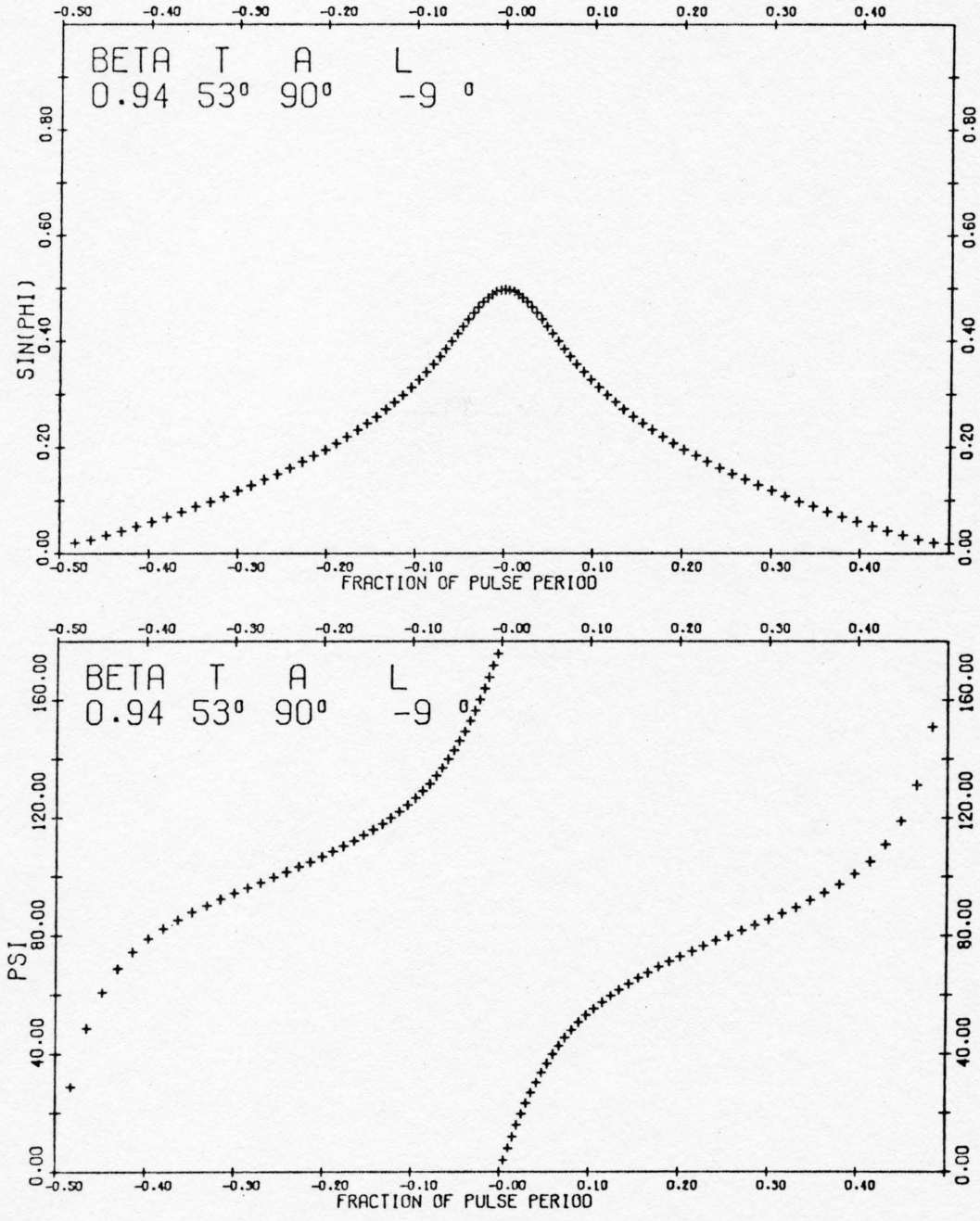

Figure 105. Polarization Time Behavior for β=0.94, T=53°, A=90°, L=-9°

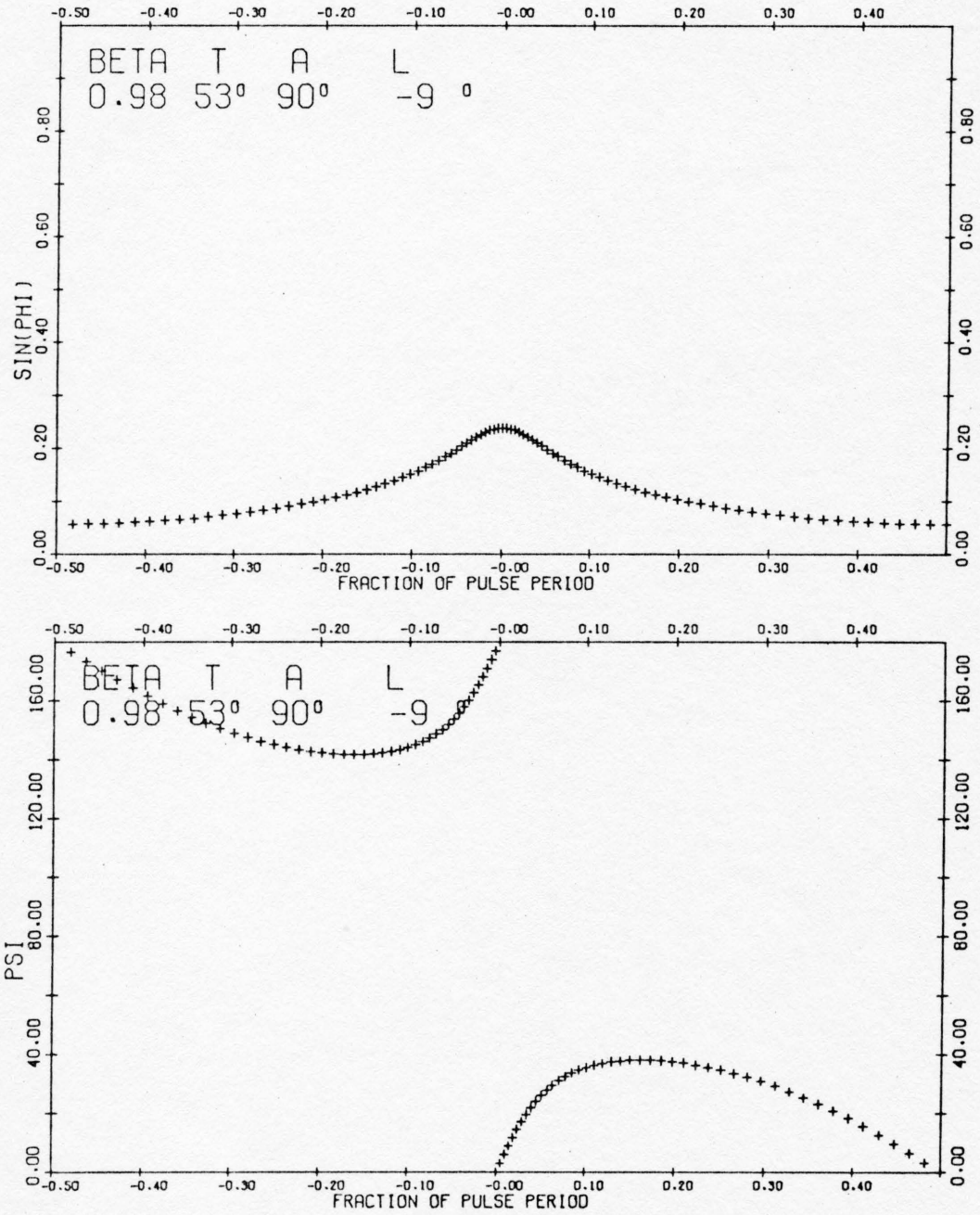

Figure 106. Polarization Time Behavior for β=0.98, T=53°, A=90°, L=-9°

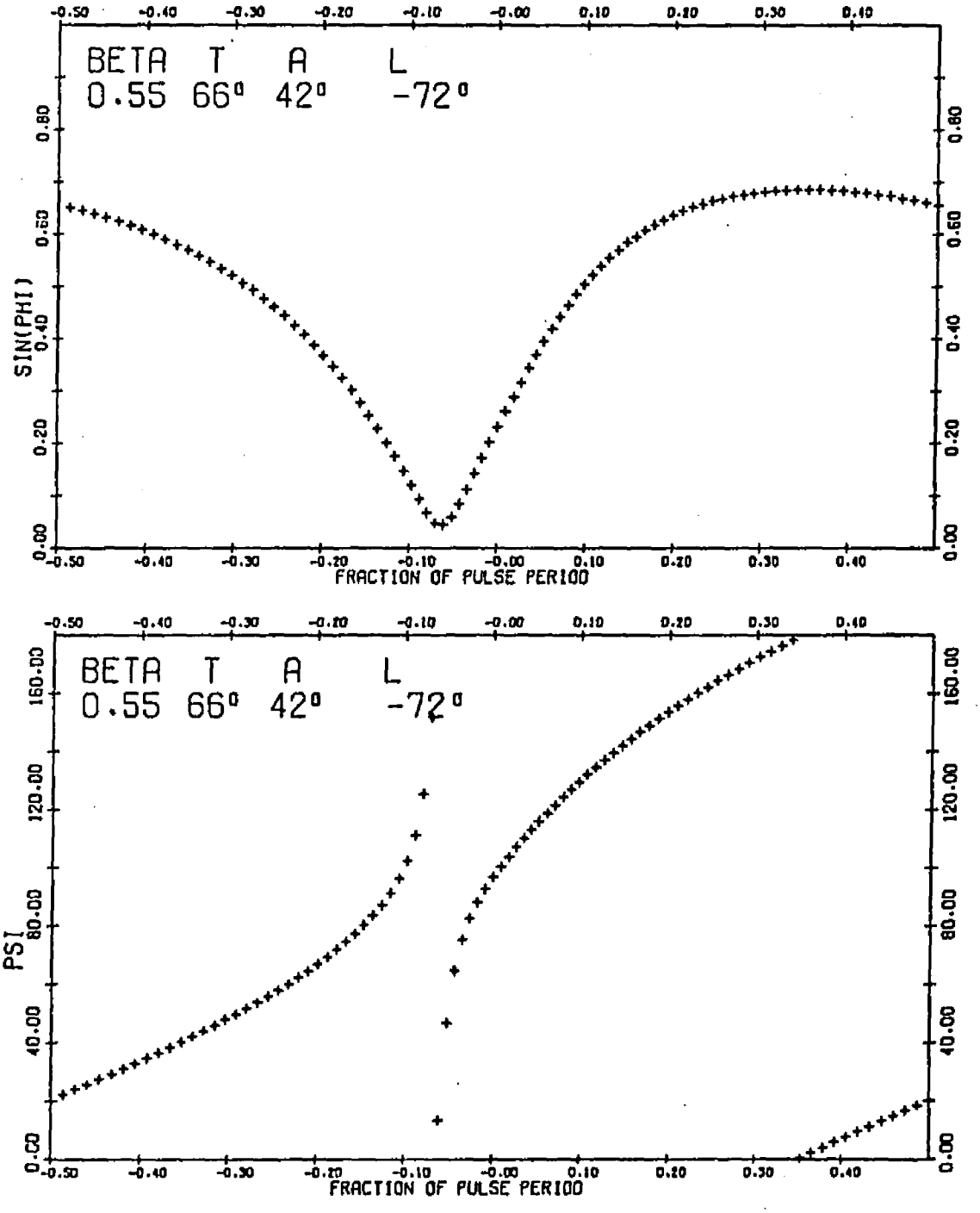

Figure 107. Polarization Time Behavior for β=0.55, T=66°, A=42°, L=-72°

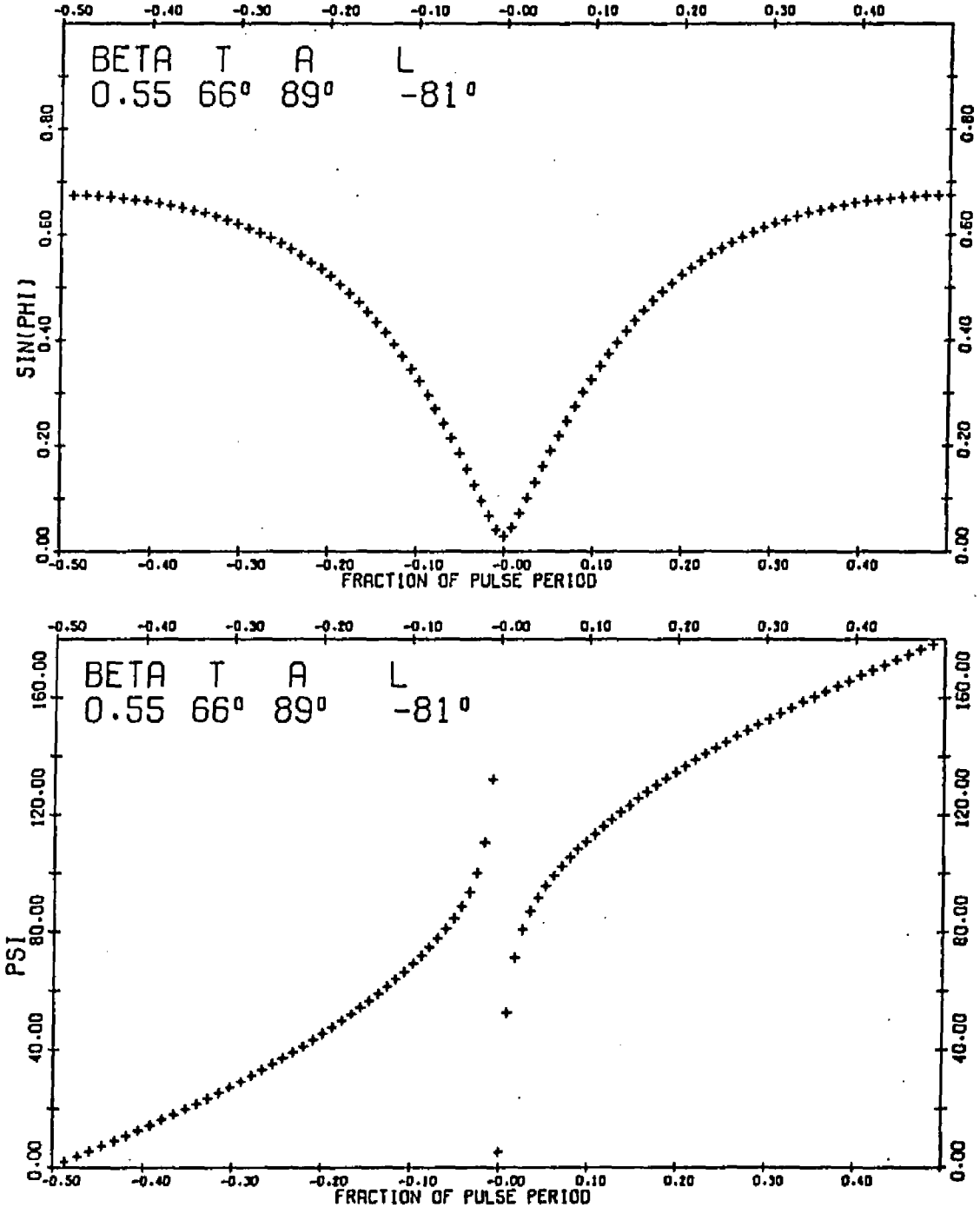

Figure 108. Polarization Time Behavior for β=0.55, T=66°, A=89°, L=-81°

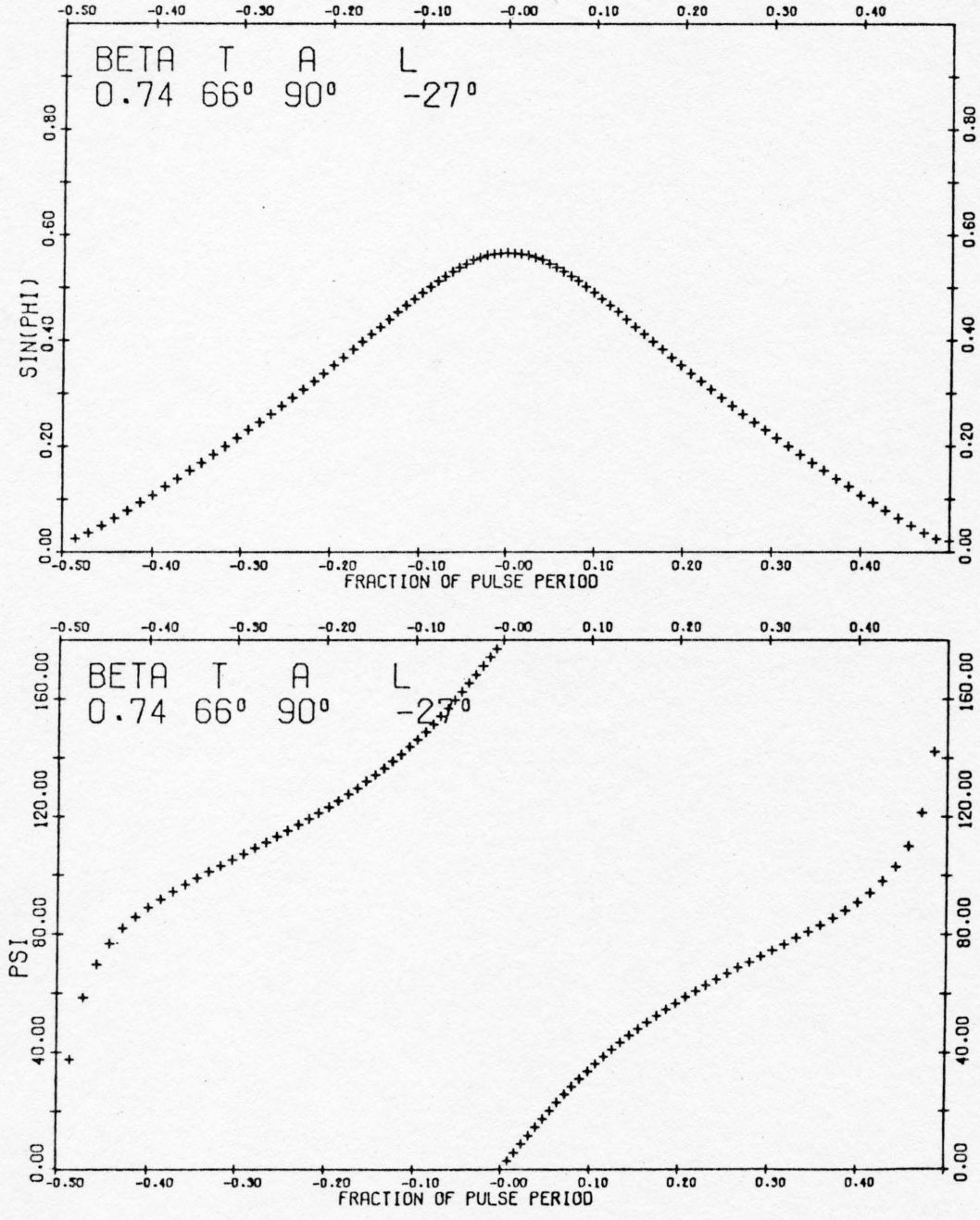

Figure 109. Polarization Time Behavior for β=0.74, T=66°, A=90°, L=-27°

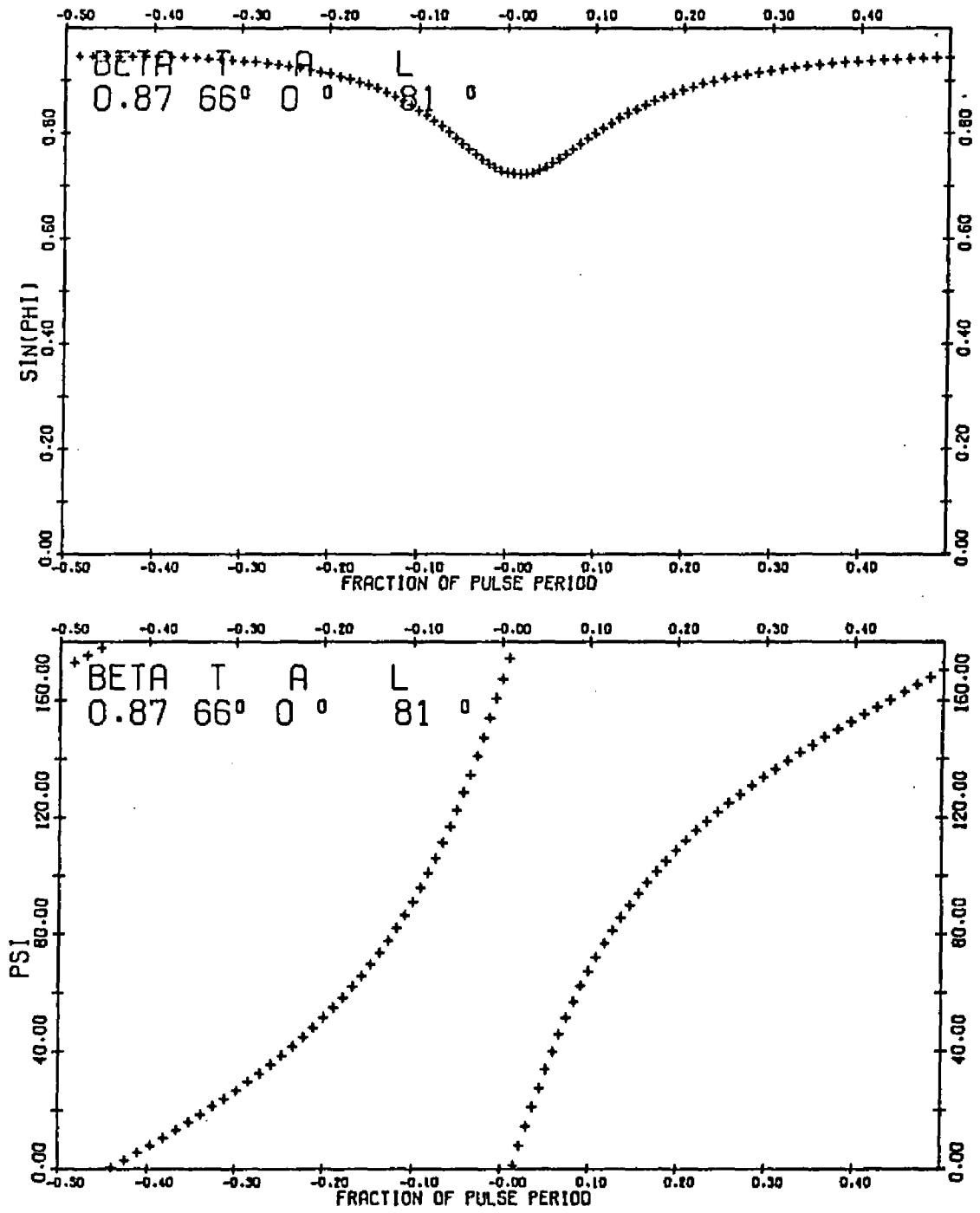

Figure 110. Polarization Time Behavior for β=0.87, T=66°, A=0°, L=81°

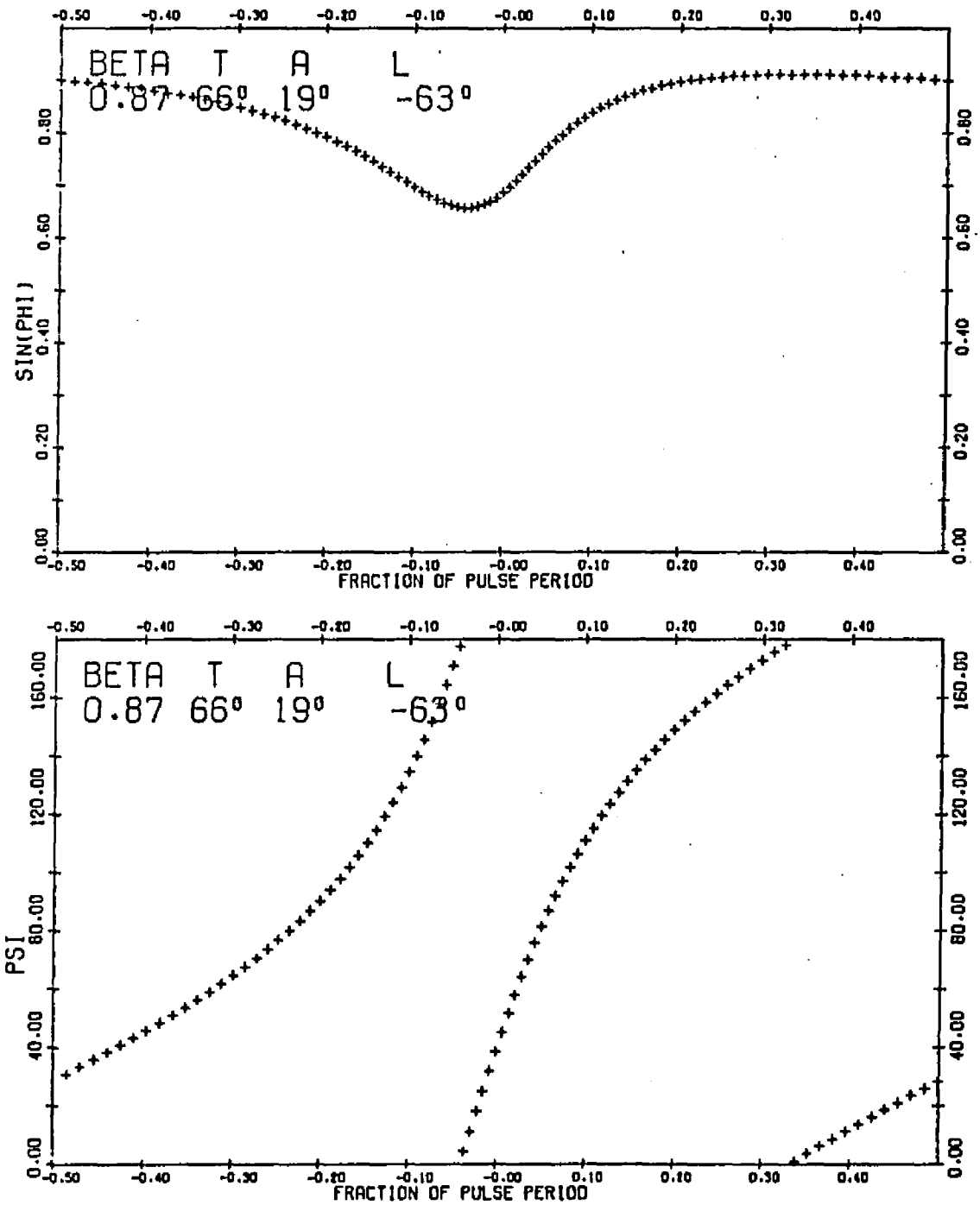

Figure 111. Polarization Time Behavior for β=0.87, T=66°, A=19°, L=-63°

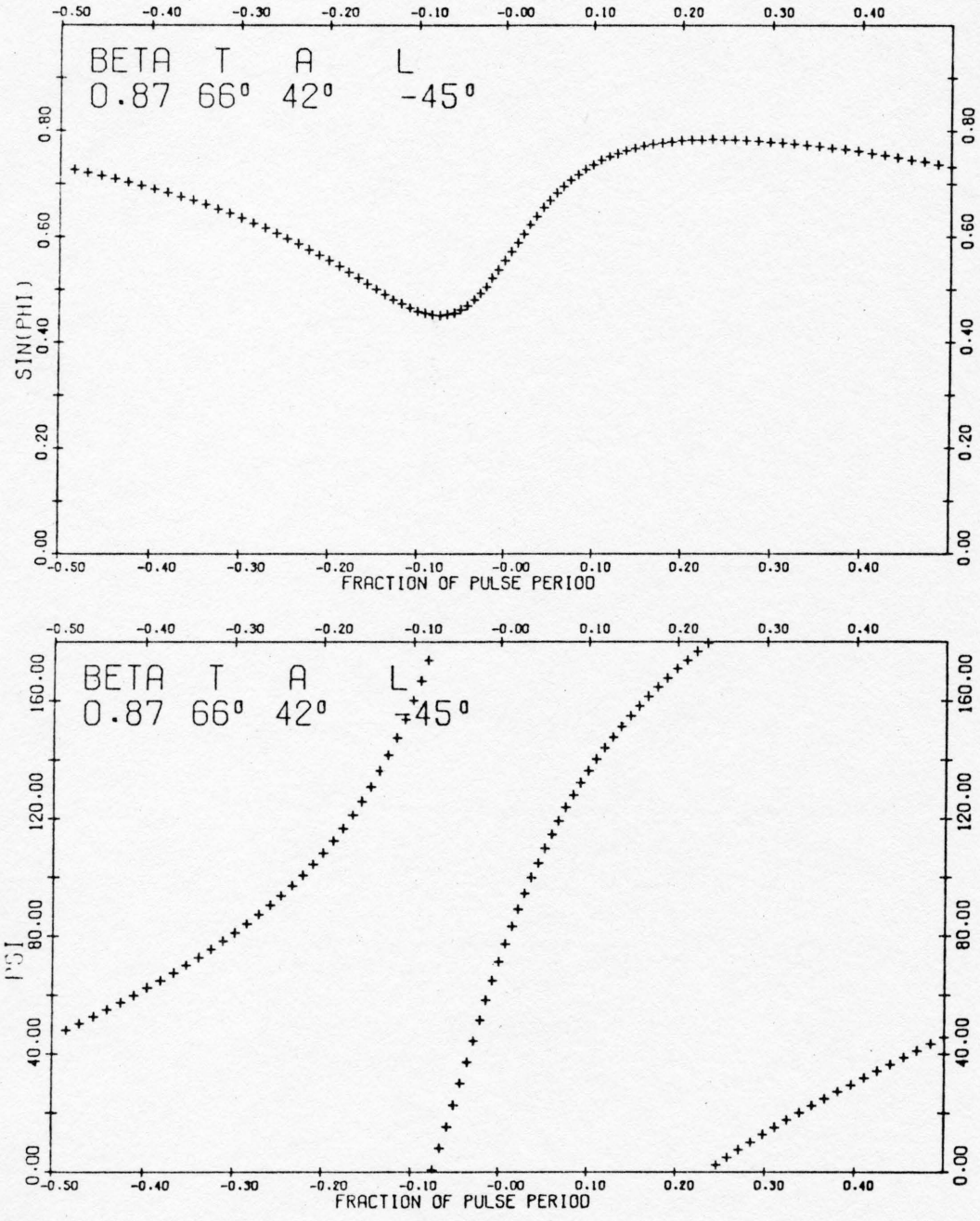

Figure 112. Polarization Time Behavior for β=0.87, T=66°, A=42°, L=-45°

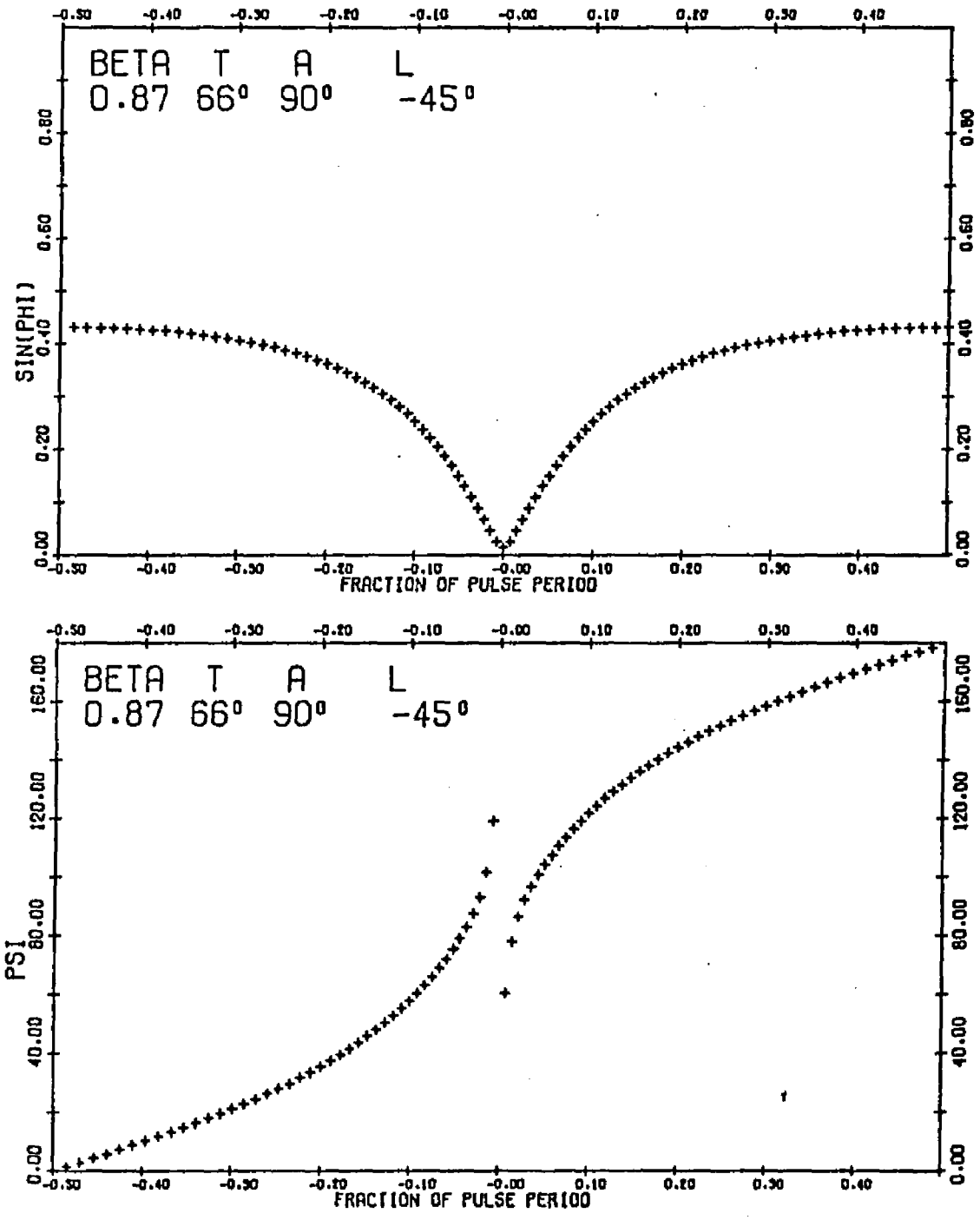

Figure 113. Polarization Time Behavior for β=0.87, T=66°, A=90°, L=-45°

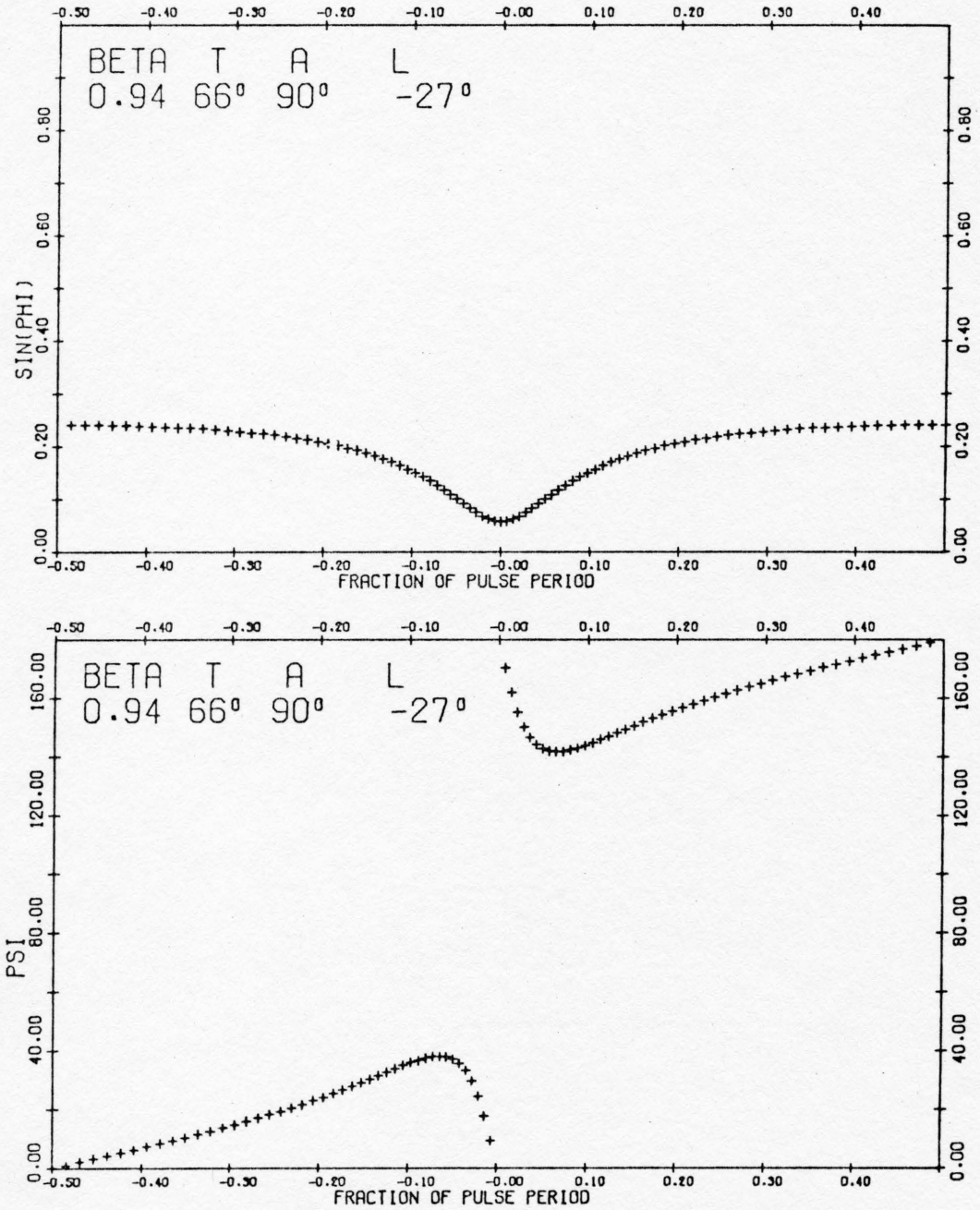

Figure 114. Polarization Time Behavior for β=0.94, T=66°, A=90°, L=-27°

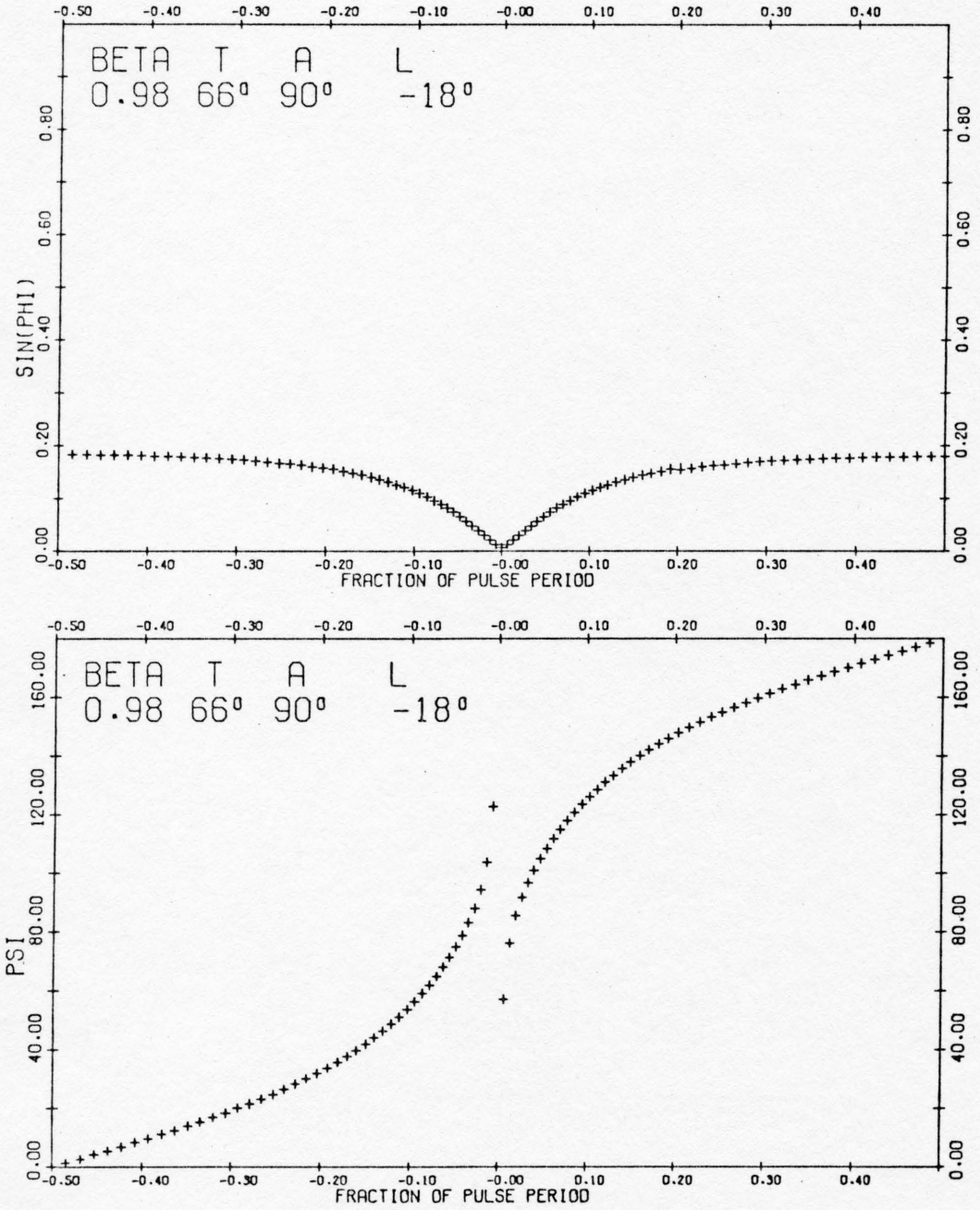

Figure 115. Polarization Time Behavior for β=0.98, T=66°, A=90°, L=-18°

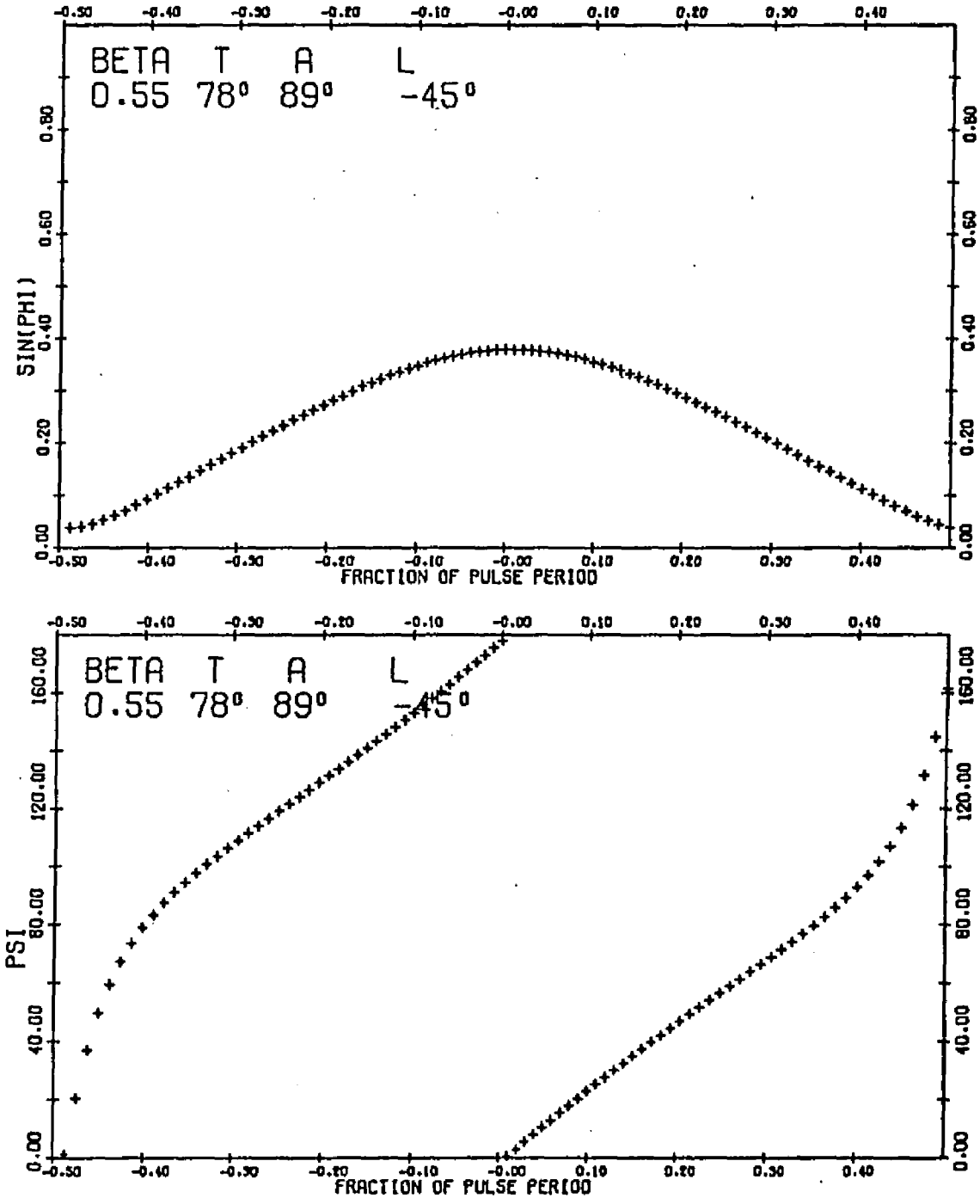

Figure 116. Polarization Time Behavior for β=0.55, T=78°, A=89°, L=-45°

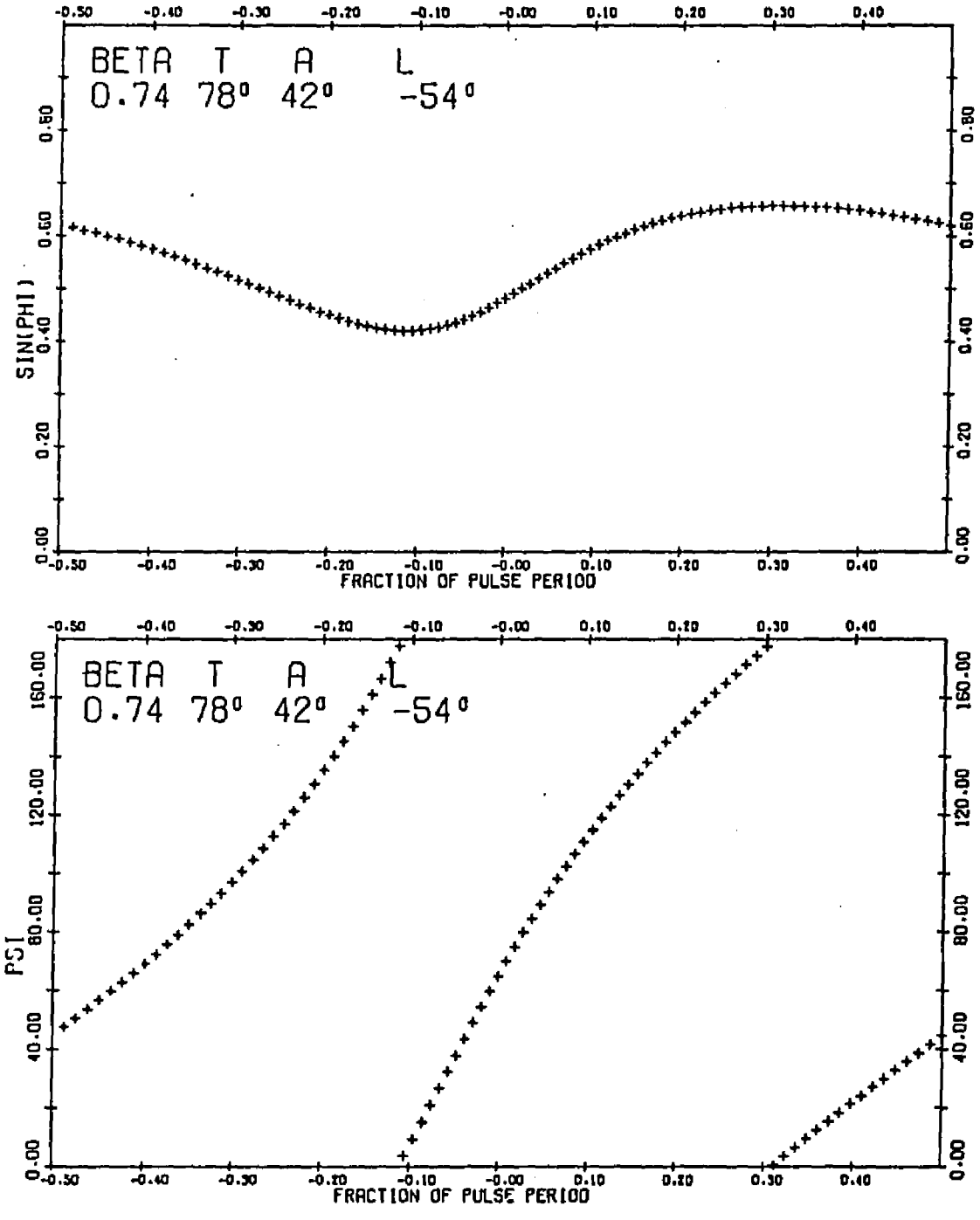

Figure 117. Polarization Time Behavior for β=0.74, T=78°, A=42°, L=-54°

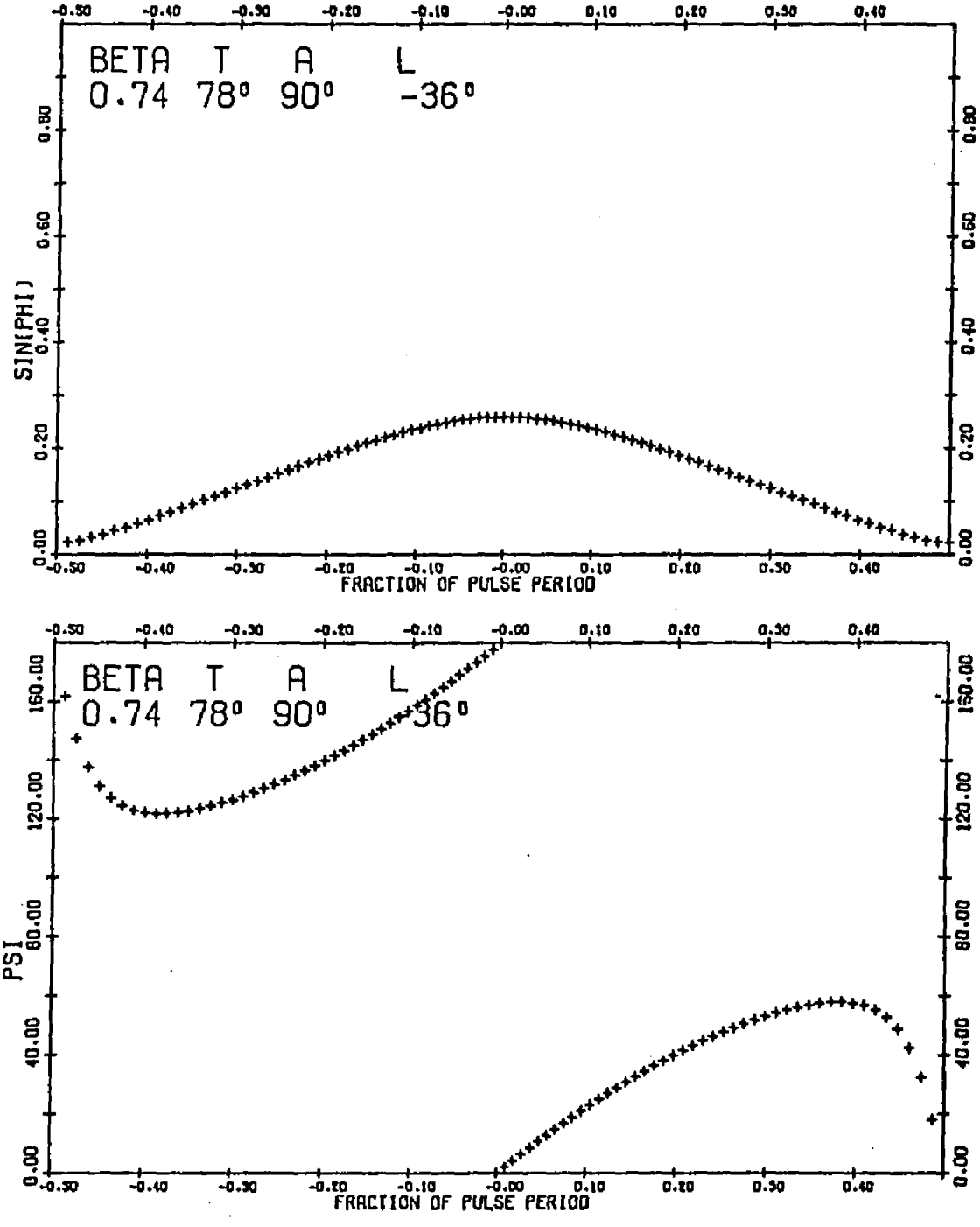

Figure 118. Polarization Time Behavior for β=0.74 T=78°, A=90°, L=-36°

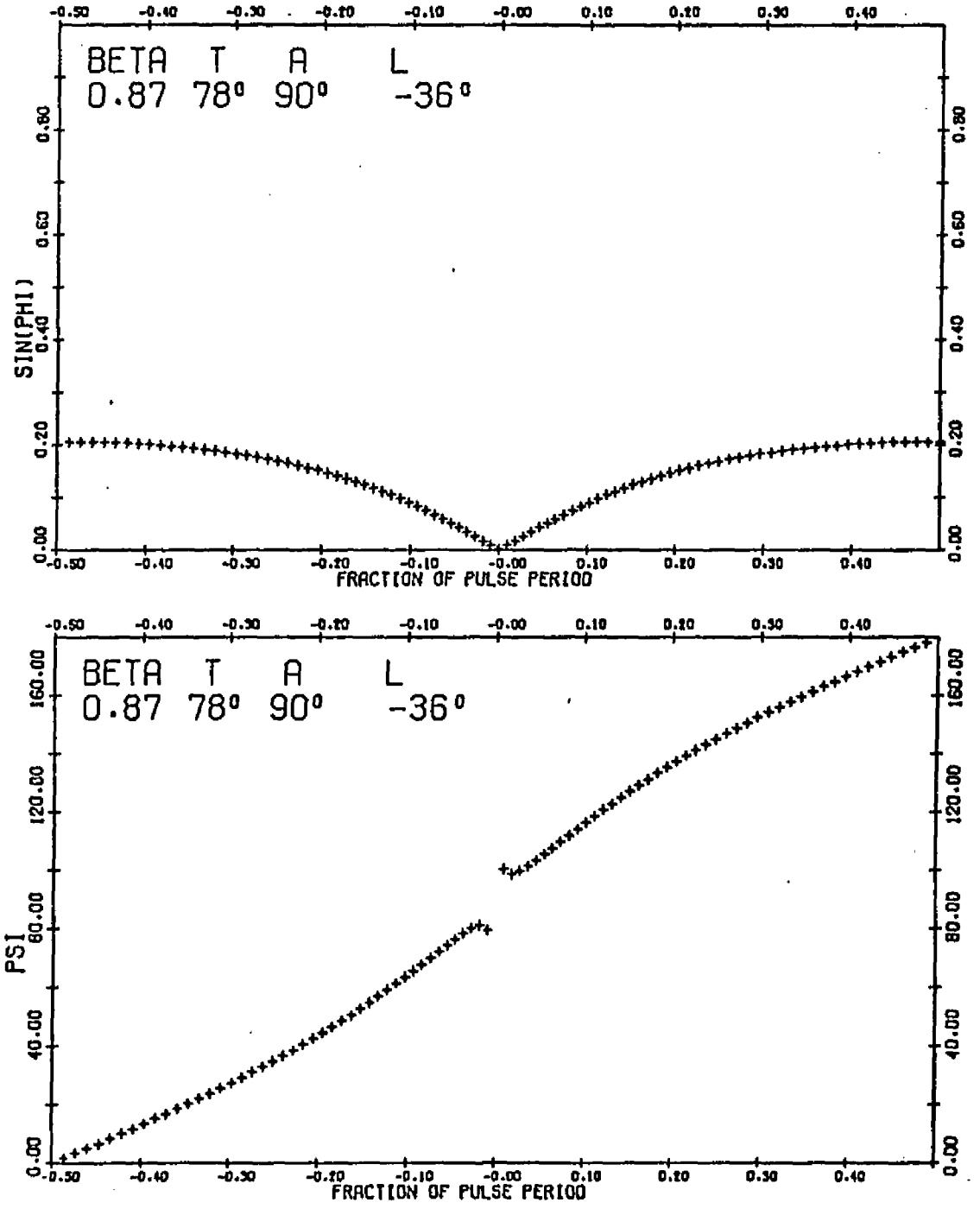

Figure 119. Polarization Time Behavior for β=0.87, T=78°, A=90°, L=-36°

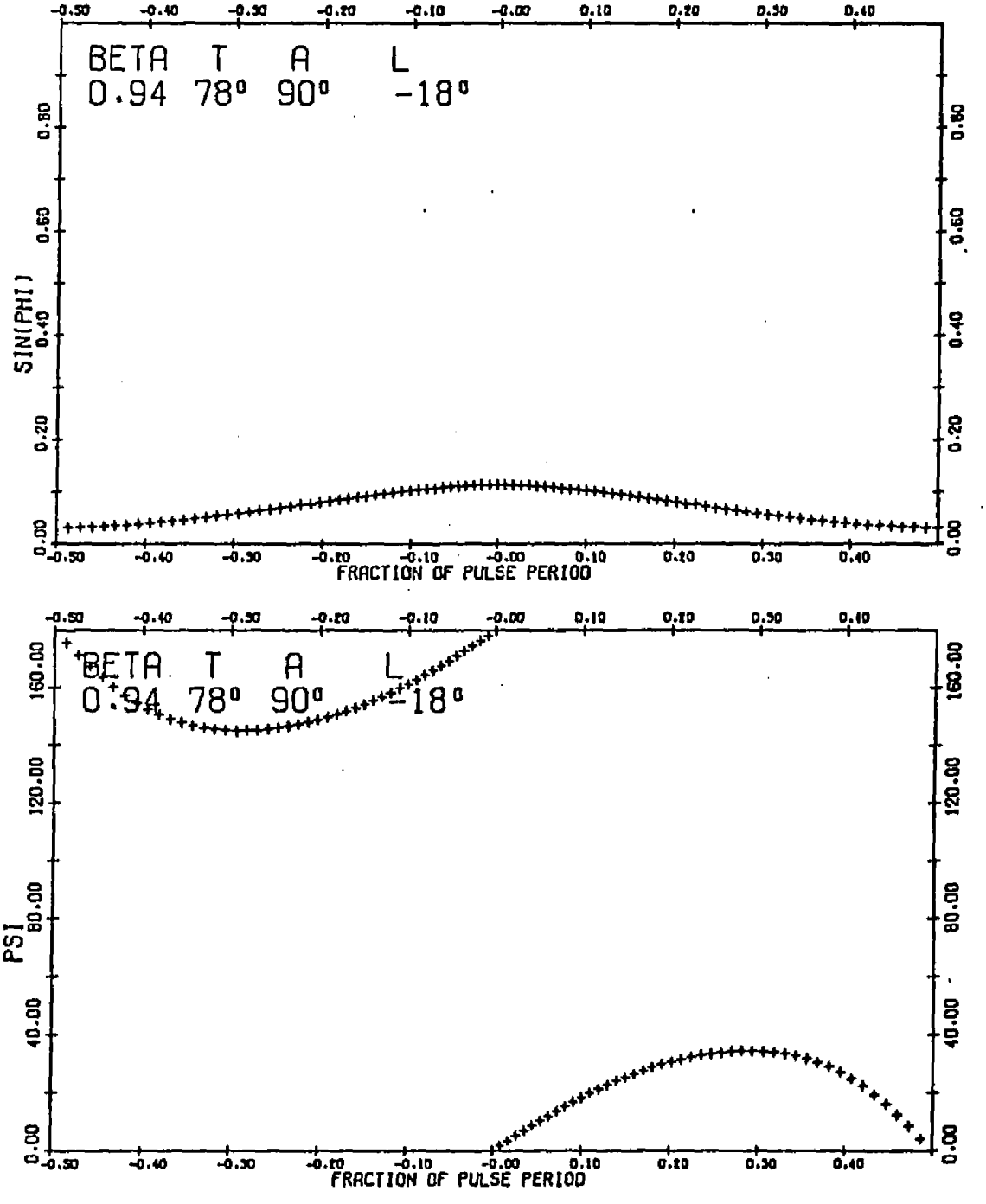

Figure 120. Polarization Time Behavior for β=0.94, T=78°, A=90°, L=-18°

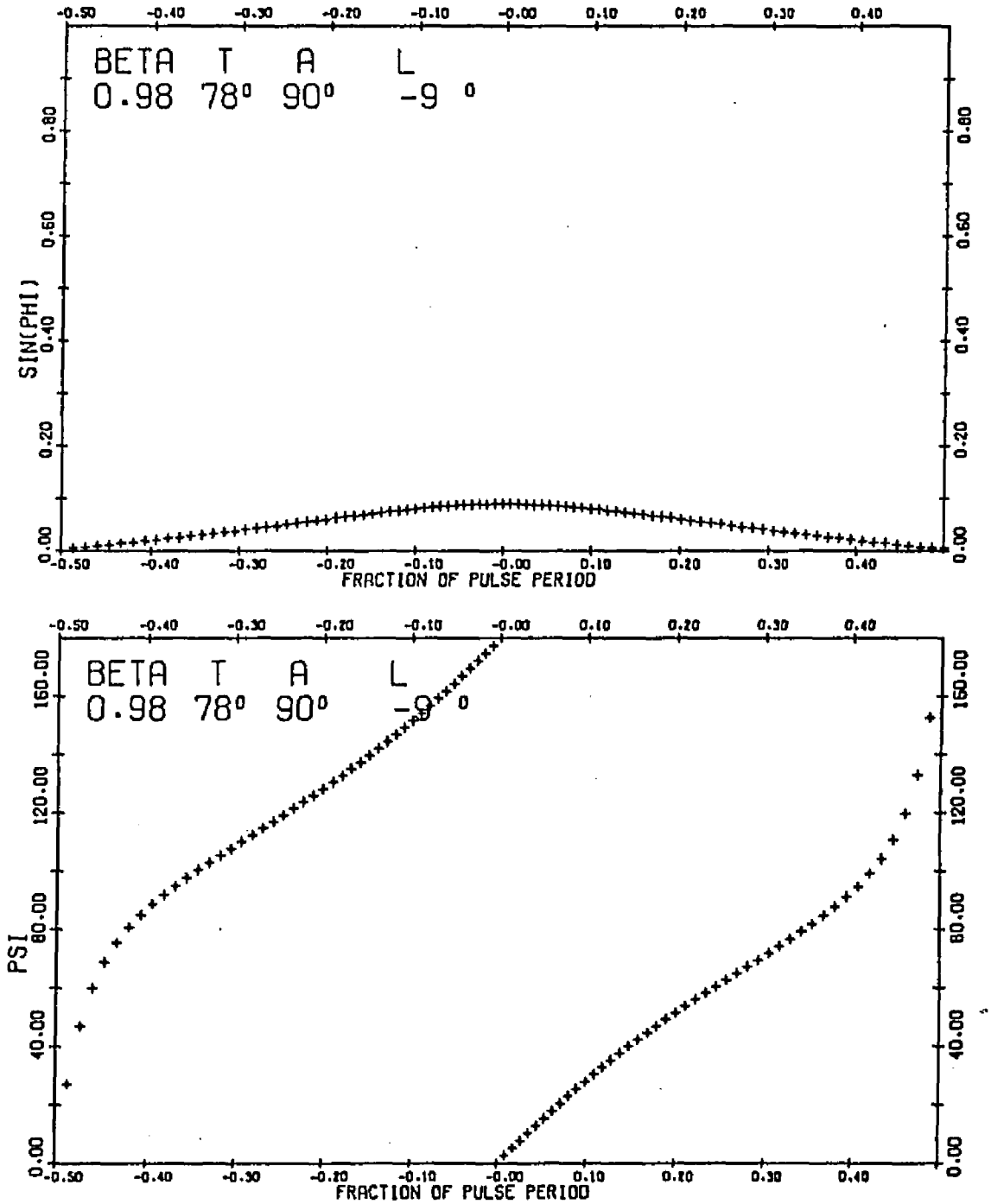

Figure 121. Polarization Time Behavior for β=0.98, T=78°, A=90°, L=-90°

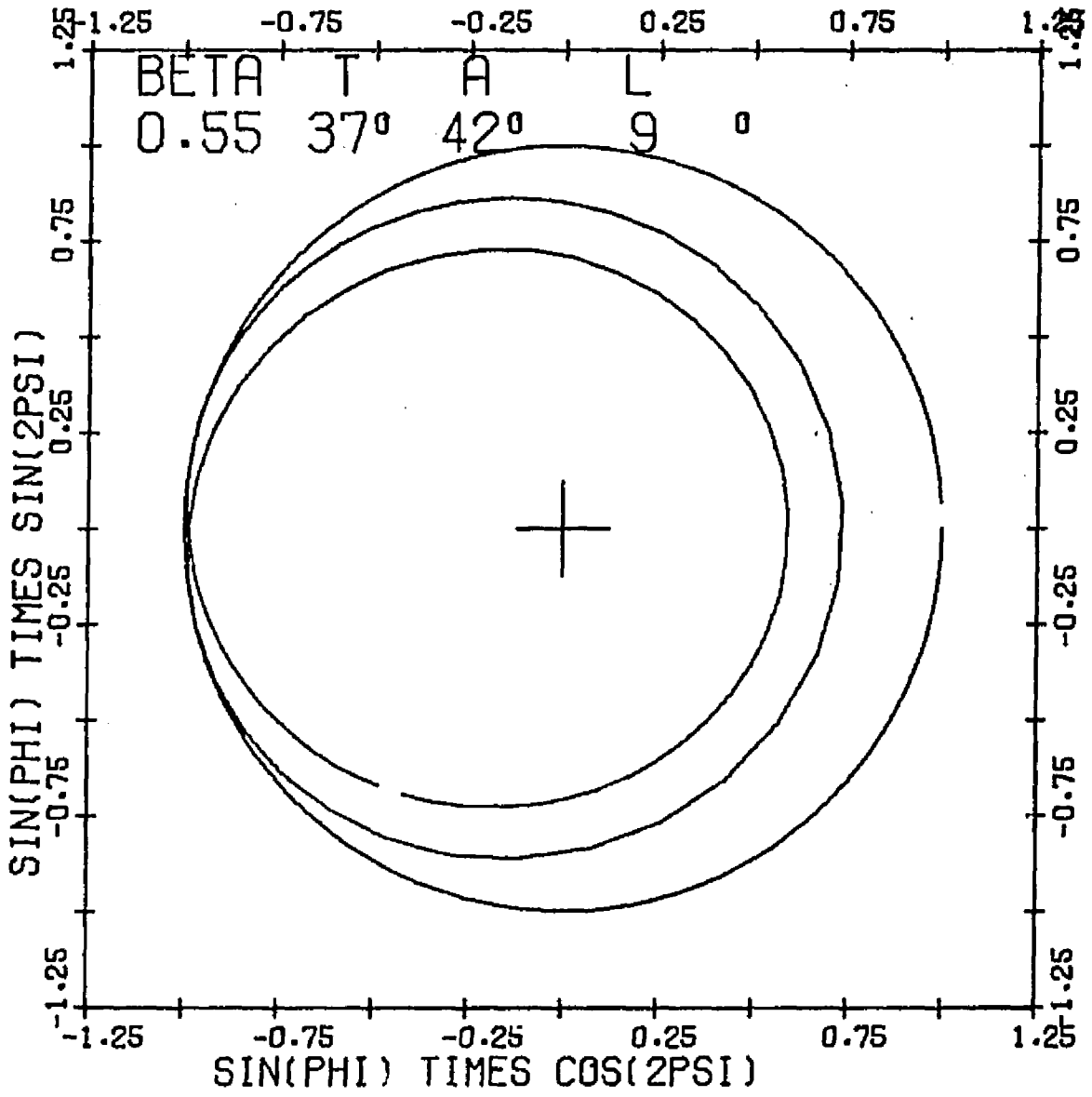

Figure 122. 2Ψ Versus sin ϕ for β=0.55, T=37°, A=42°, L=9°

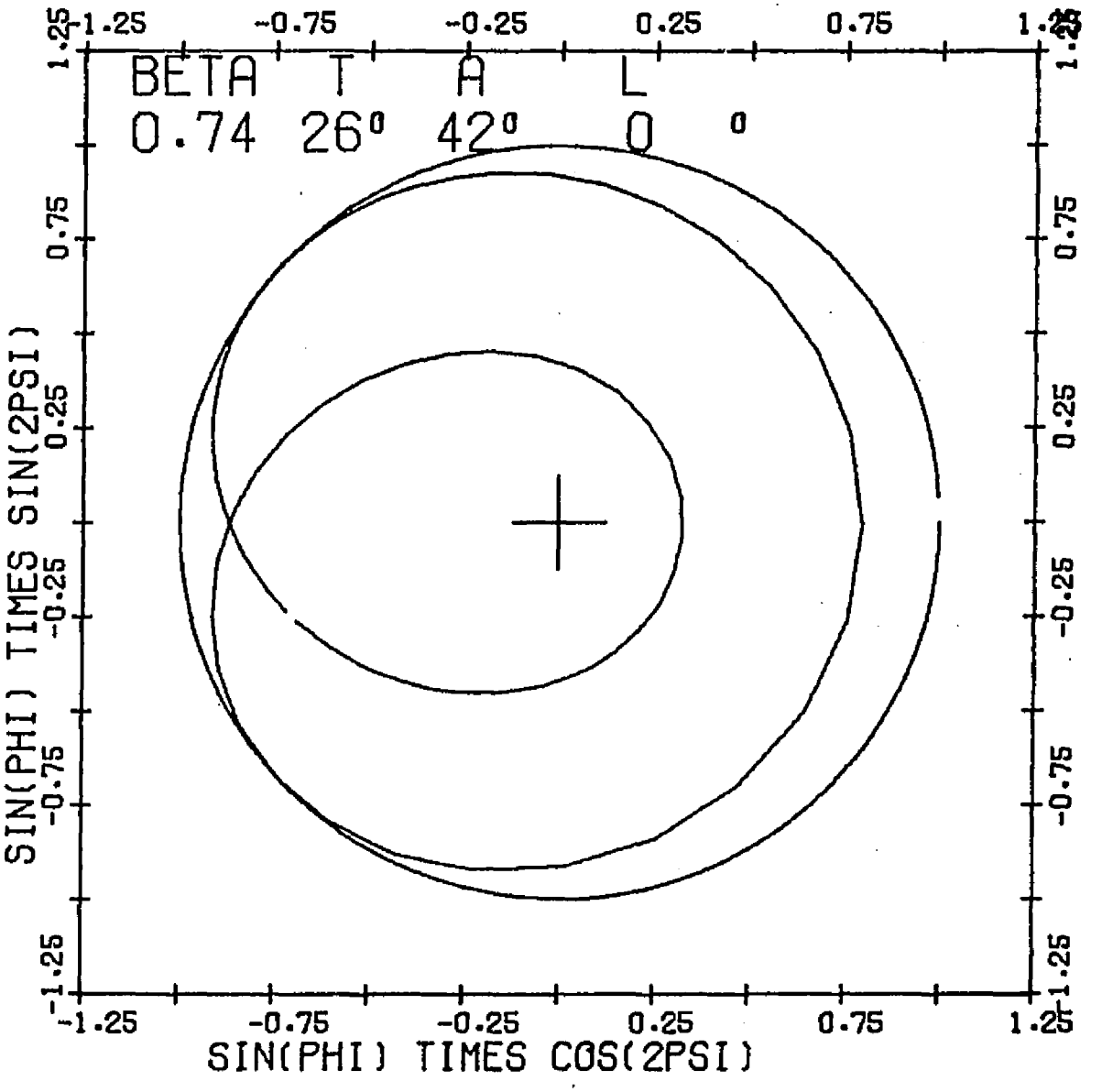

Figure 123. 2ψ Versus sin ϕ for β=0.74, T=26°, A=42°, L=0°

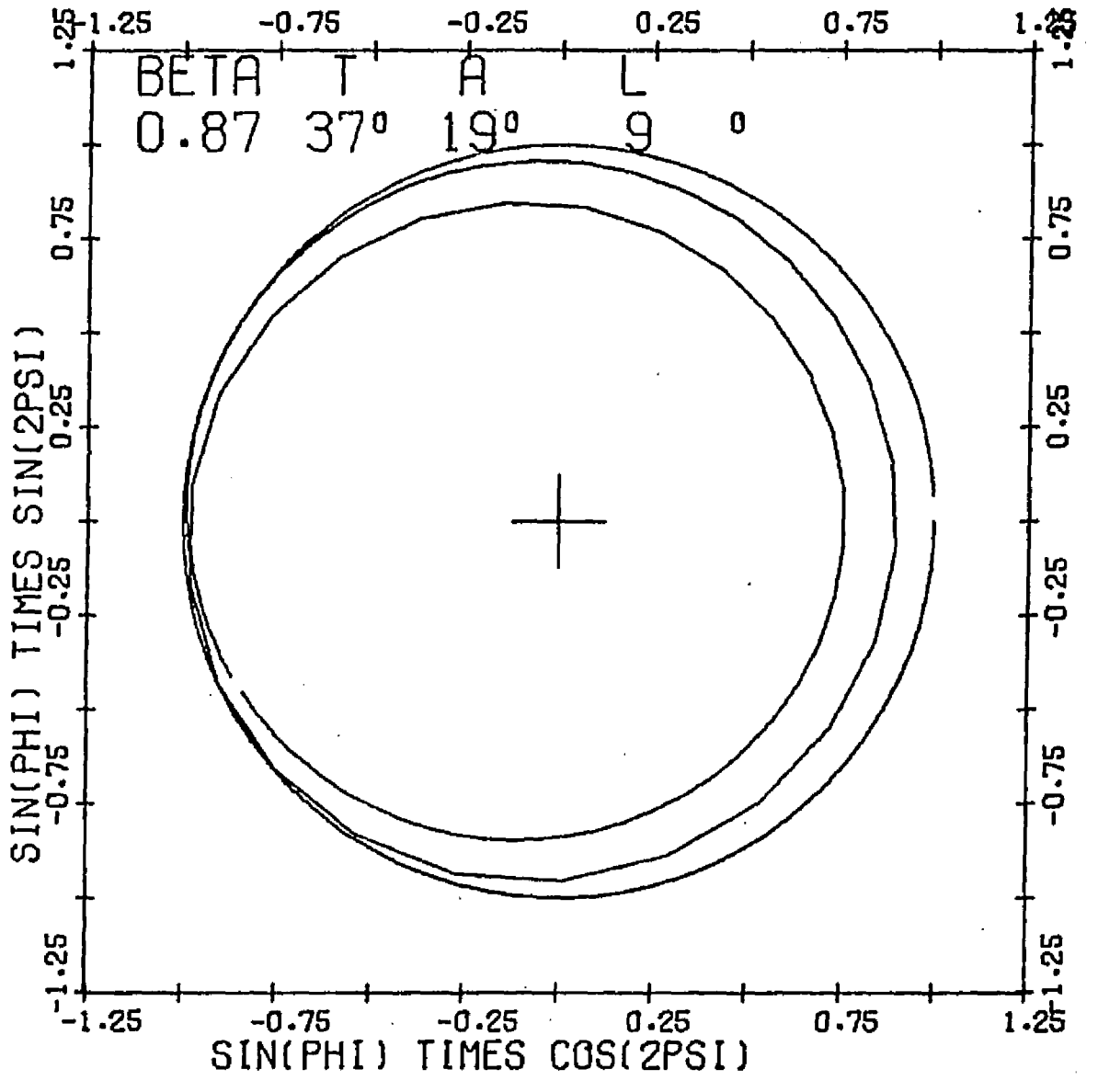

Figure 124. 2Ψ Versus sin ϕ for β=0.87, T=37°, A=19°, L=9°

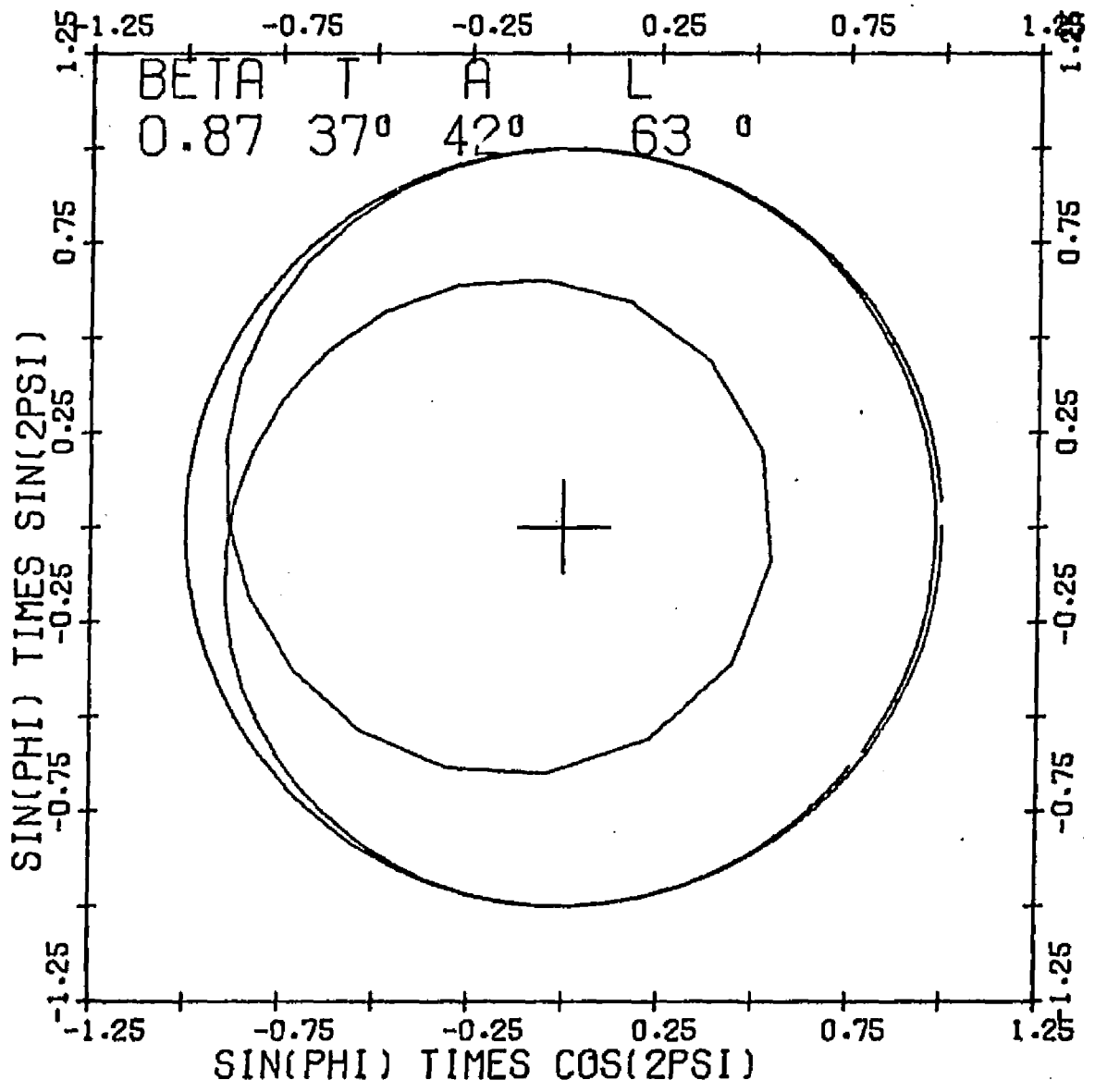

Figure 125. 2Ψ Versus sin ϕ for β=0.87, T=37°, A=42°, L=63°

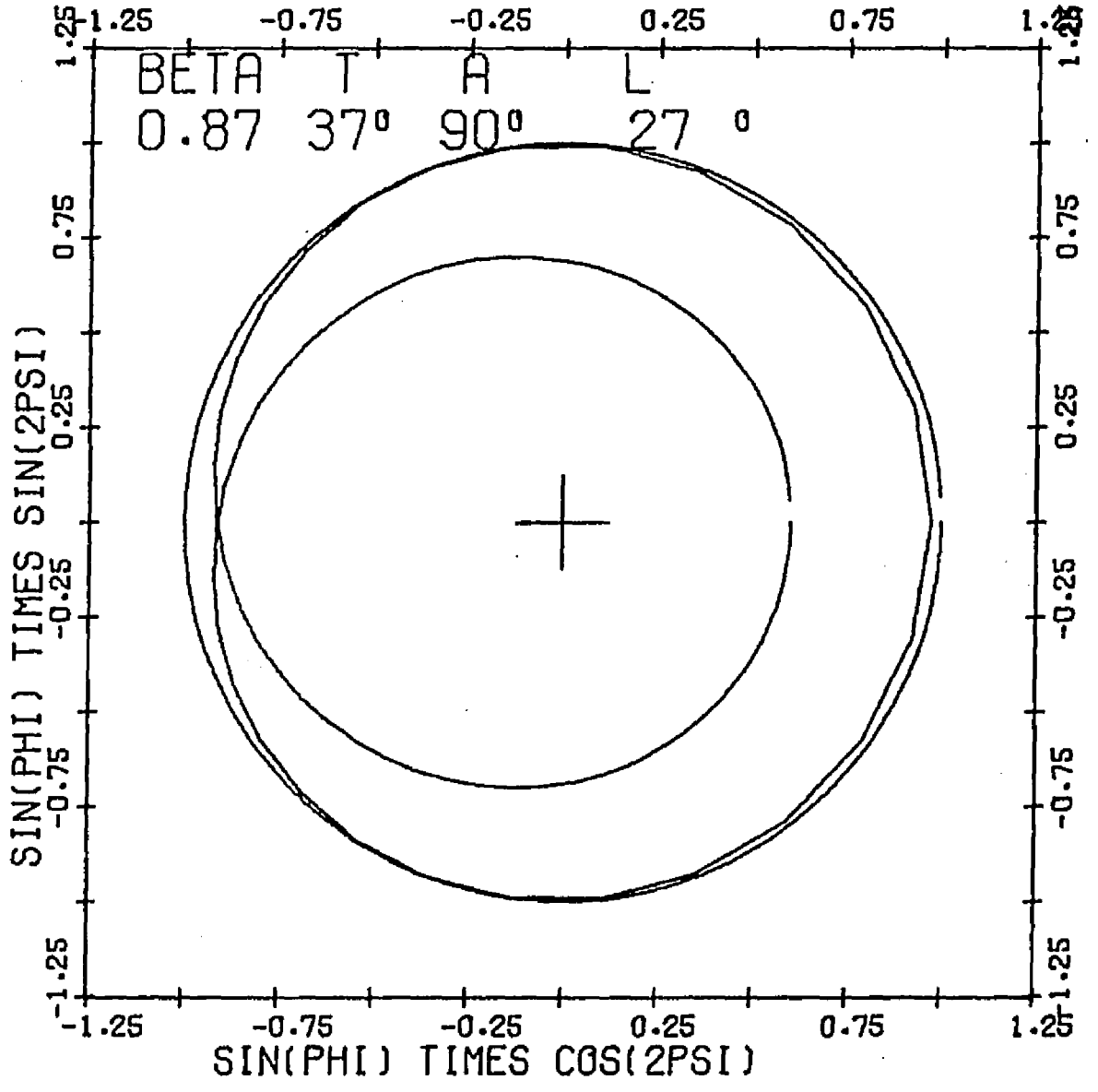

Figure 126. 2Ψ Versus sin ϕ for β=0.87, T=37°, A=90°, L=27°

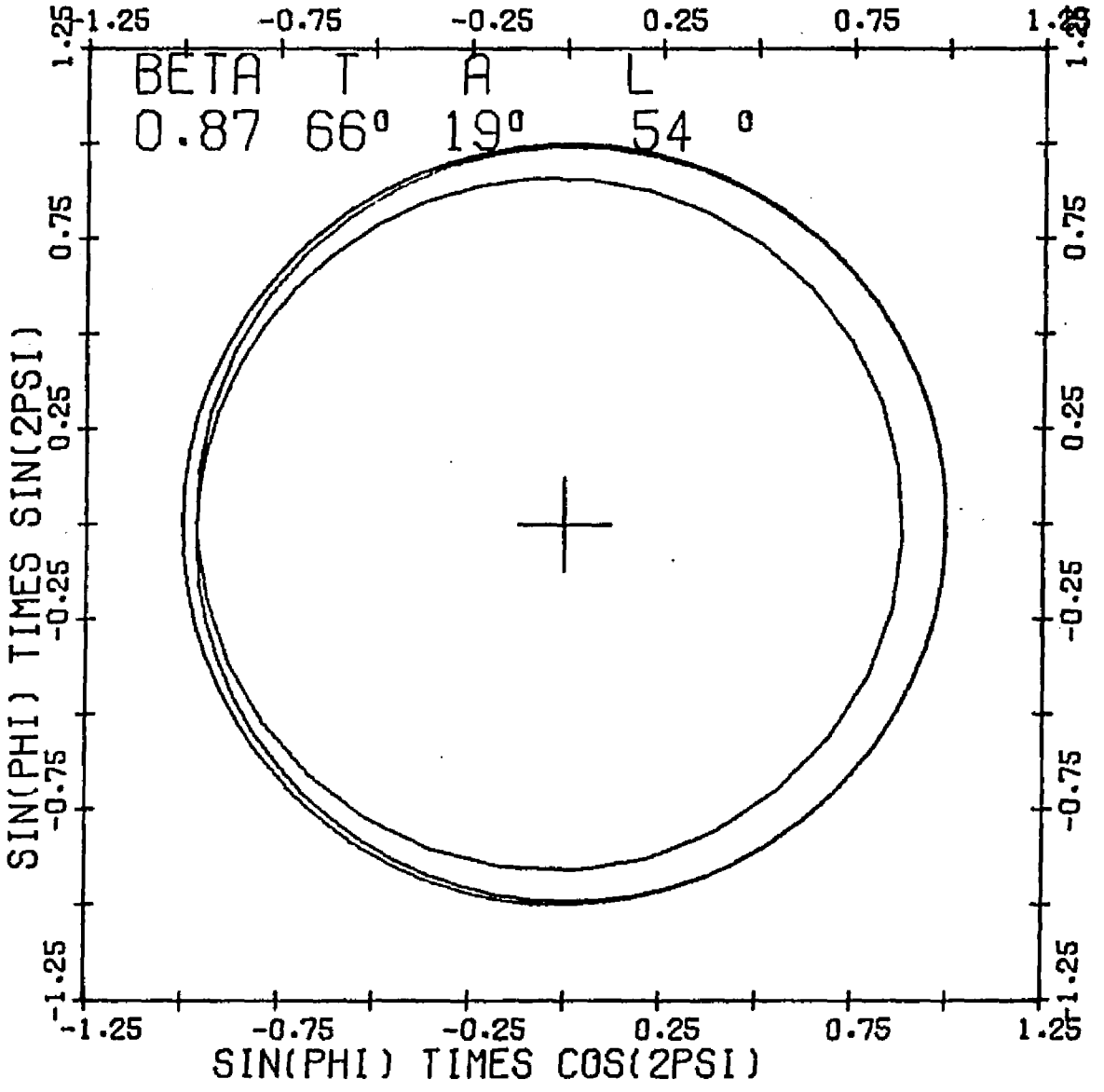

Figure 127. 2Ψ Versus sin ϕ for β=0.87, T=66°, A=19°, L=54°

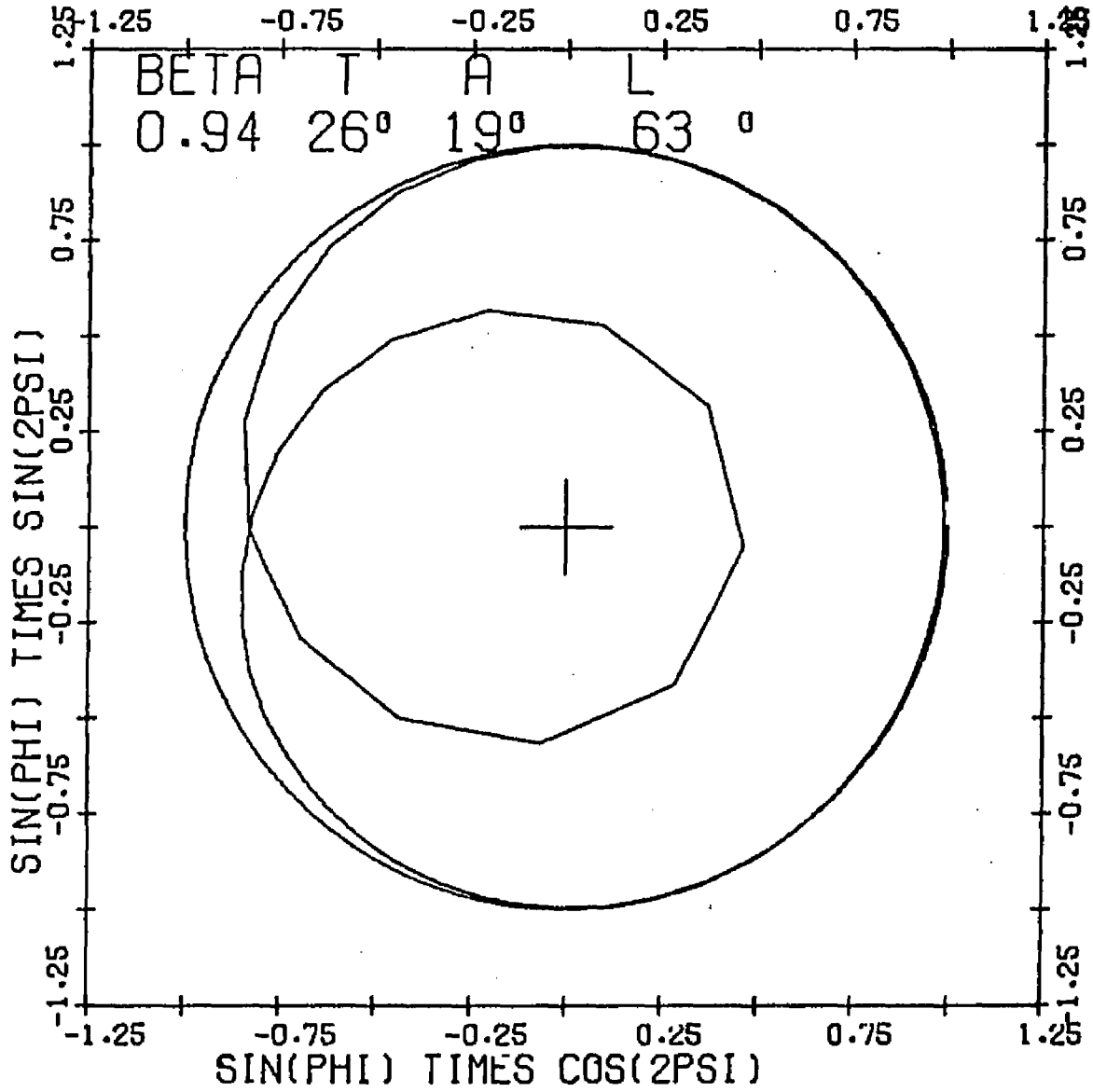

Figure 128. 2Ψ Versus sin ϕ for β=0.94, T=26°, A=19°, L=63°

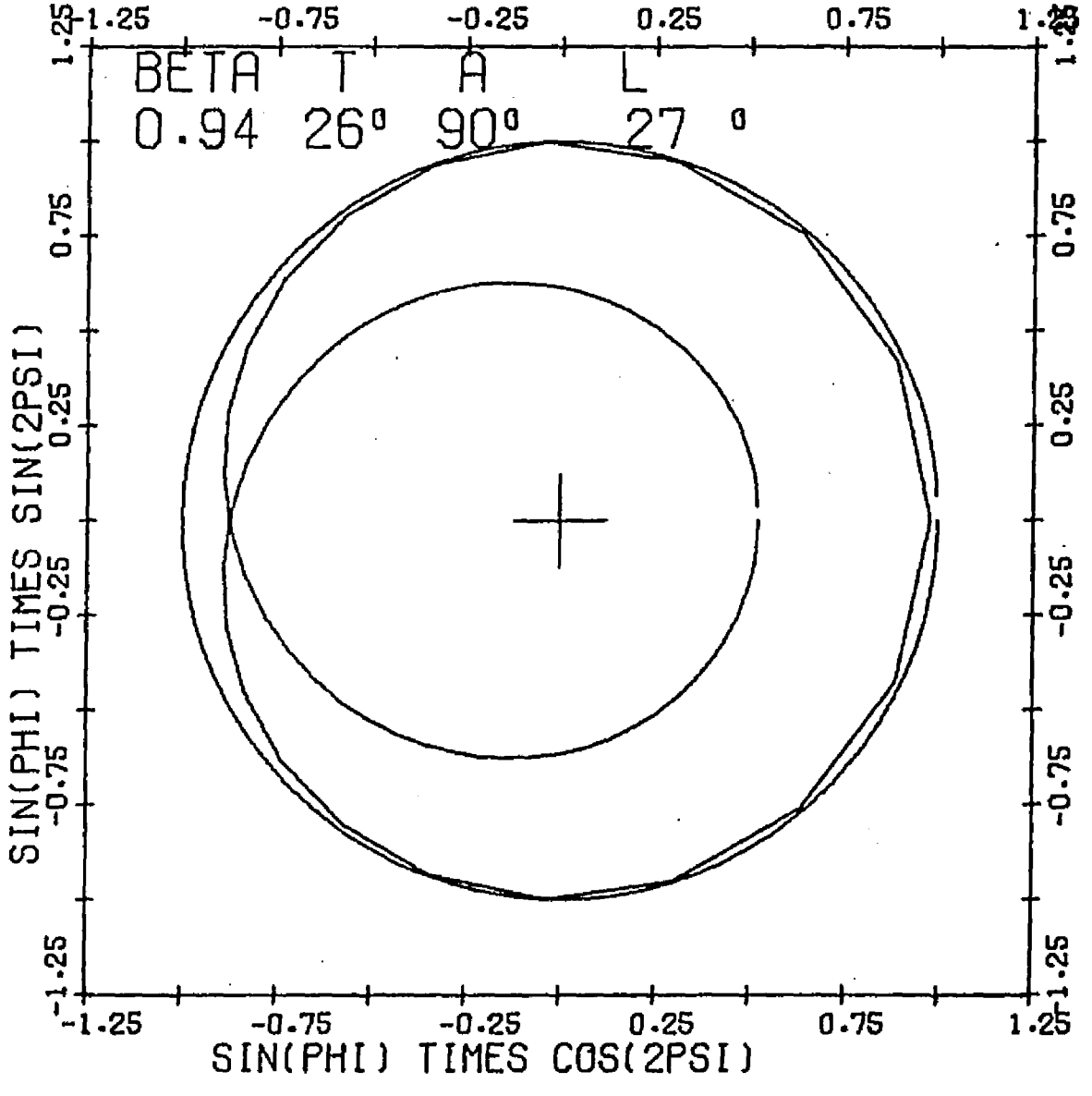

Figure 129. 2Ψ Versus sin ϕ for β=0.94, T=26°, A=90°, L=27°

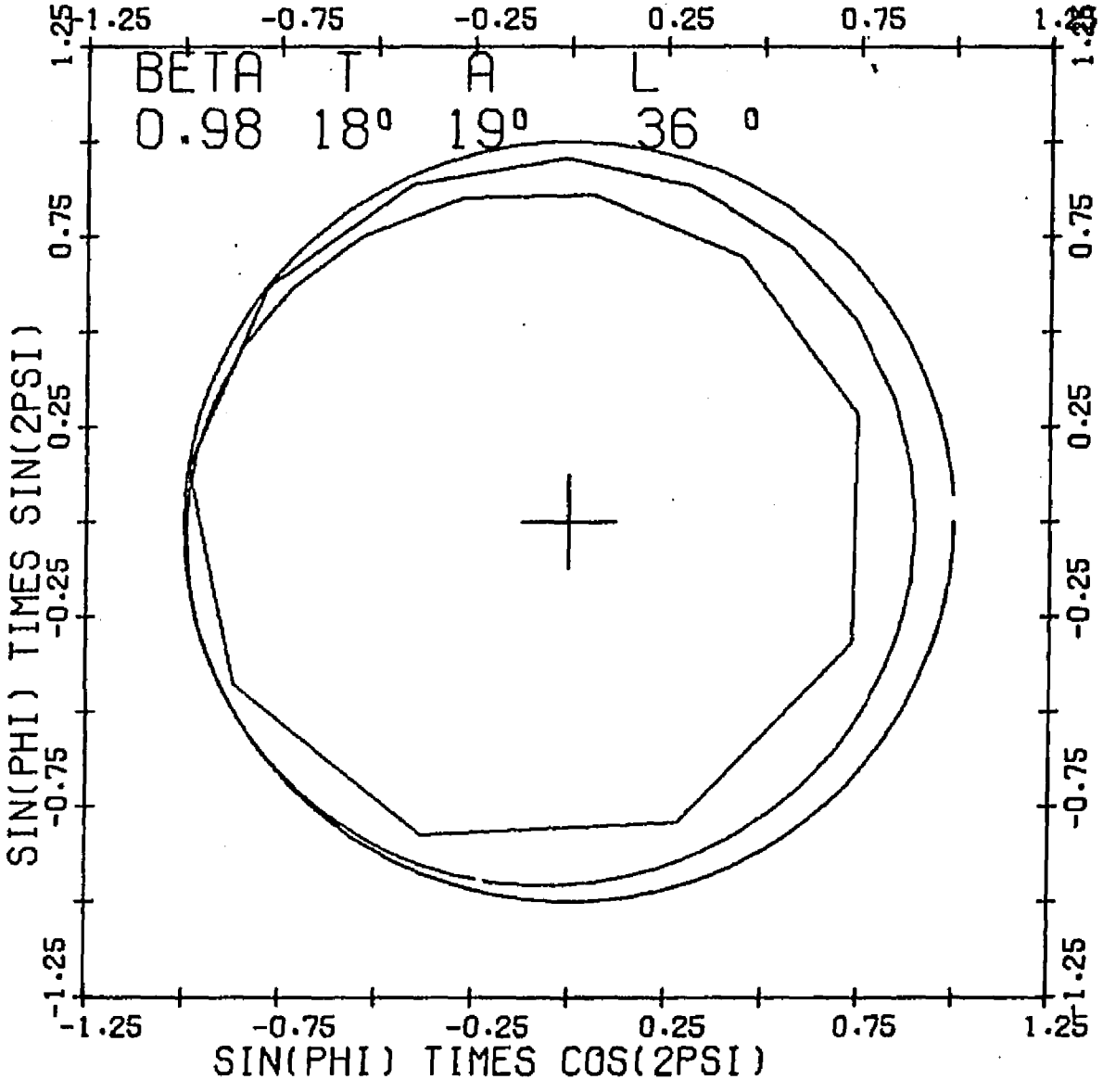

Figure 130. 2Ψ Versus sin ϕ for β=0.98, T=18°, A=19°, L=36°

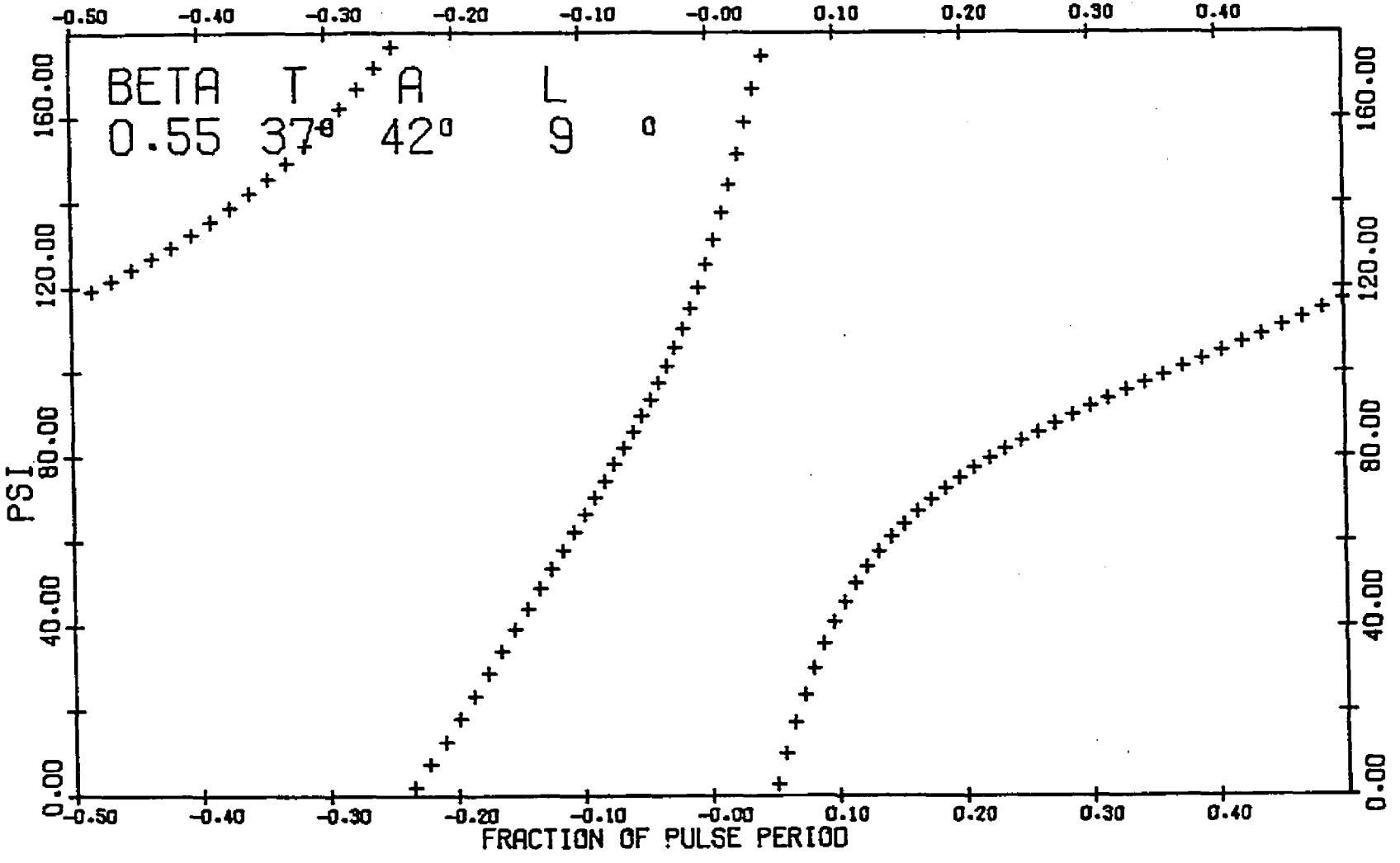

Figure 131. Ψ Versus Time for β=0.55, T=37°, A=42°, L=9°

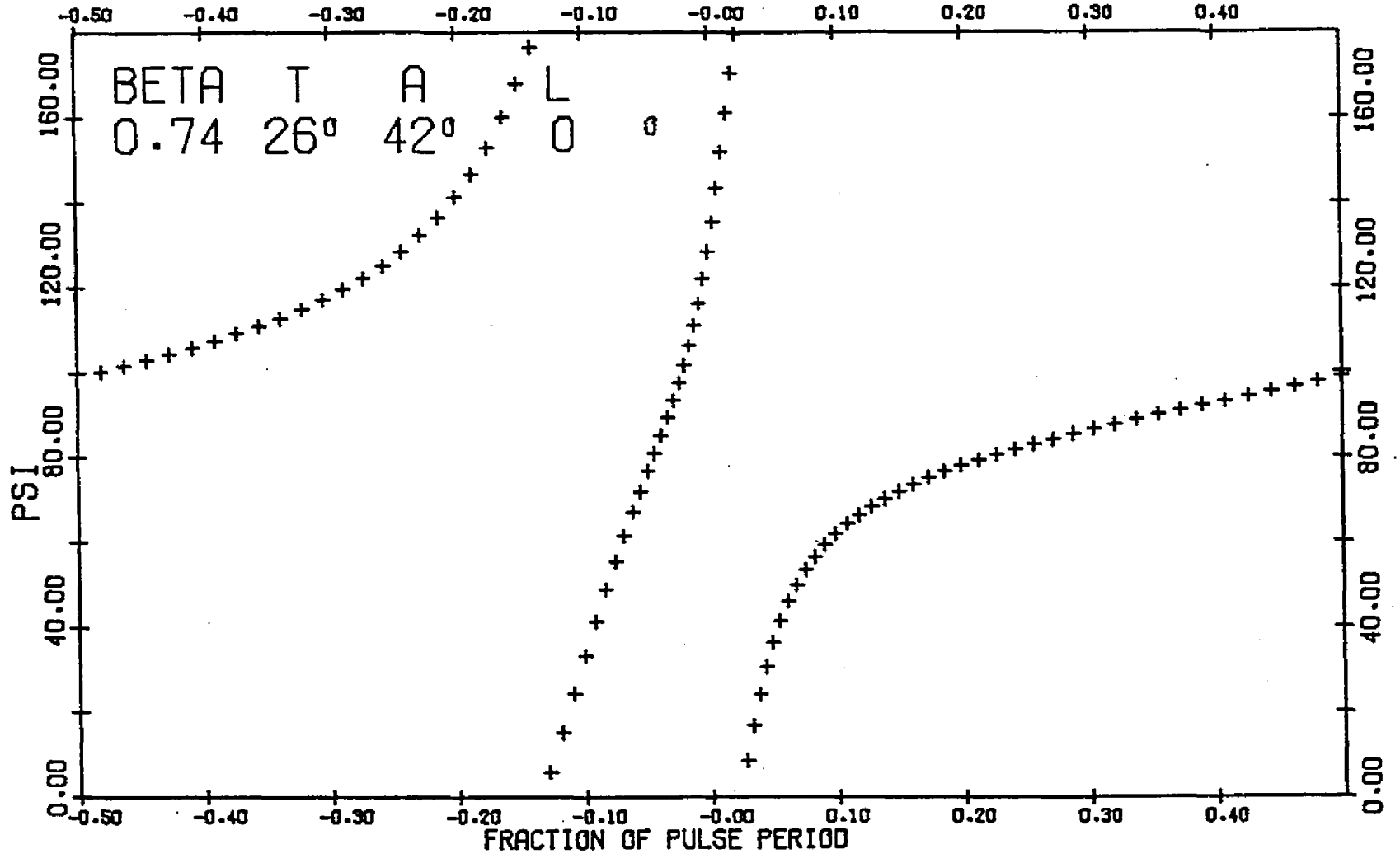

Figure 132. Ψ Versus Time for β=0.74, T=26°, A=42°, L=0°

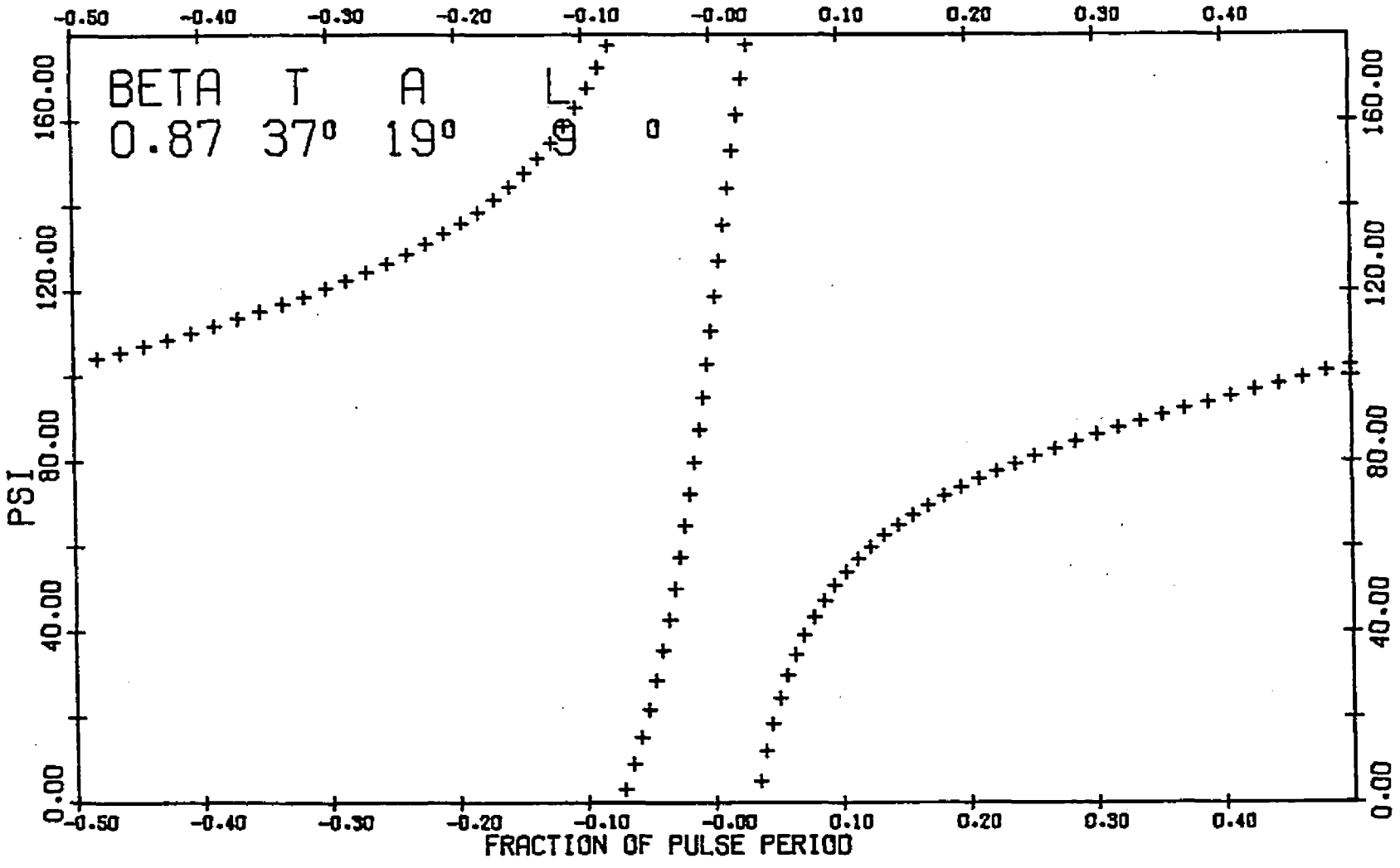

Figure 133. Ψ Versus Time for β=0.87, T=37°, A=19°, L=9°

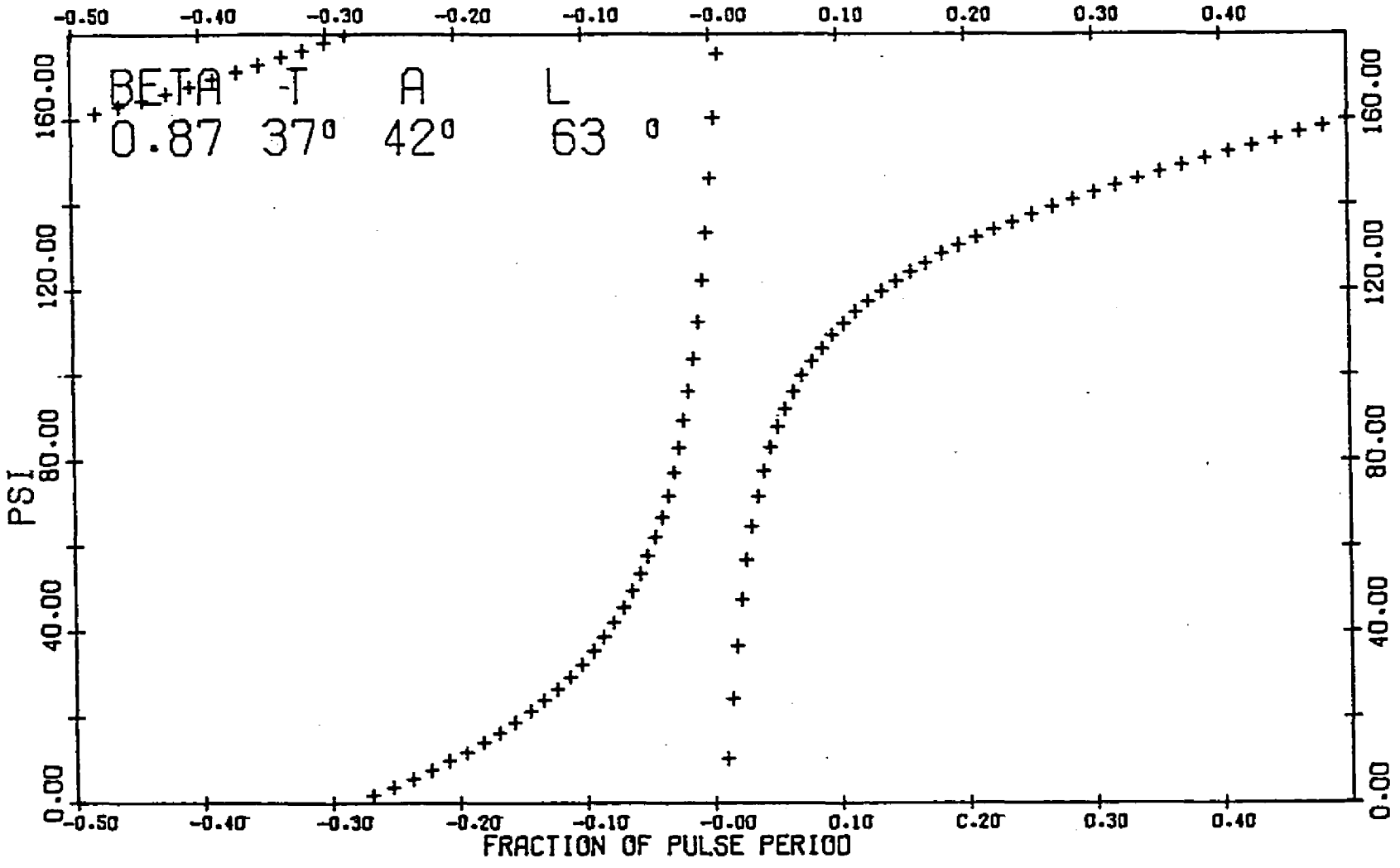

Figure 134. Ψ Versus Time for β=0.87, T=37°, A=42°, L=63°

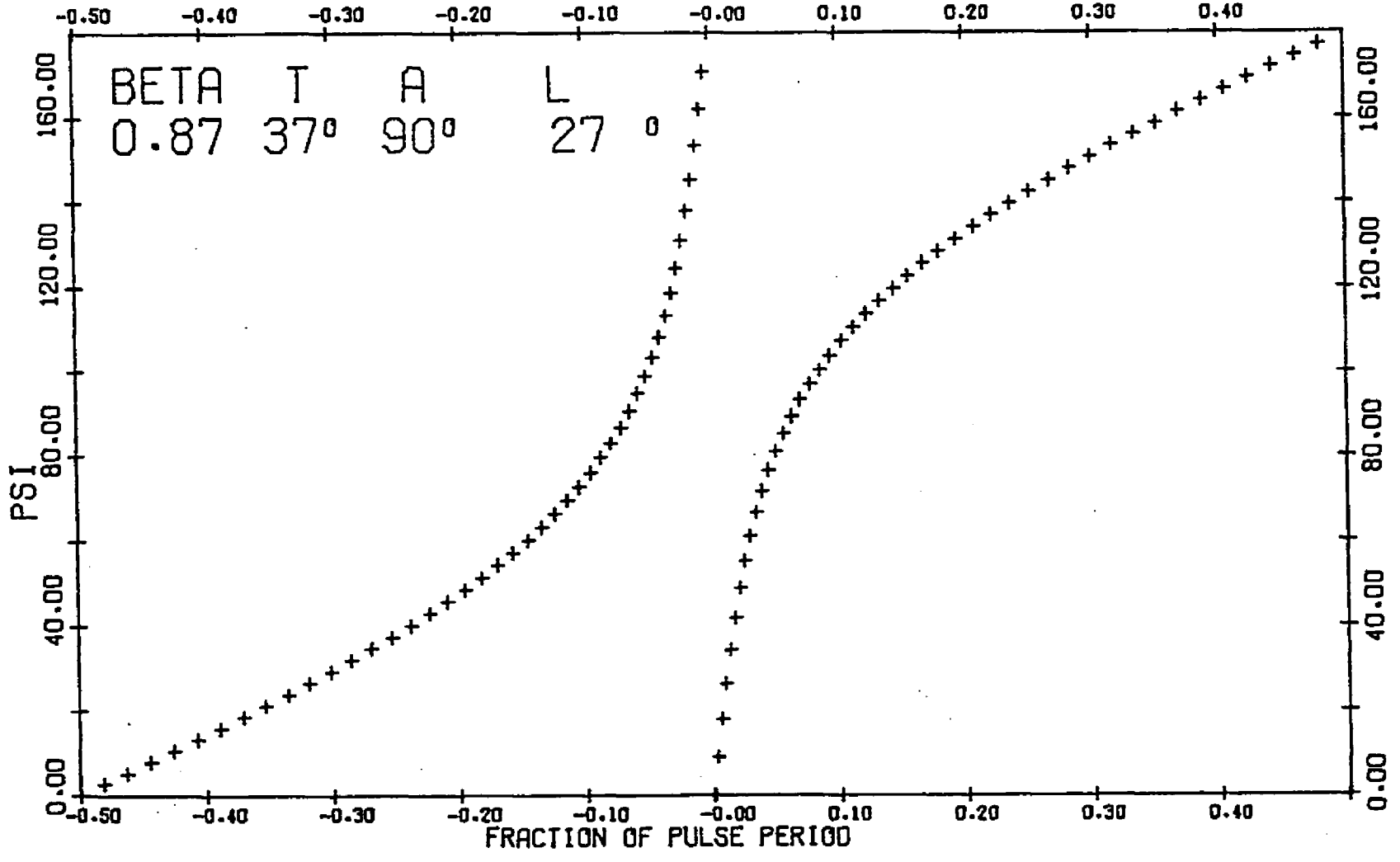

Figure 135. Ψ Versus Time for β=0.87, T=37°, A=90°, L=27°

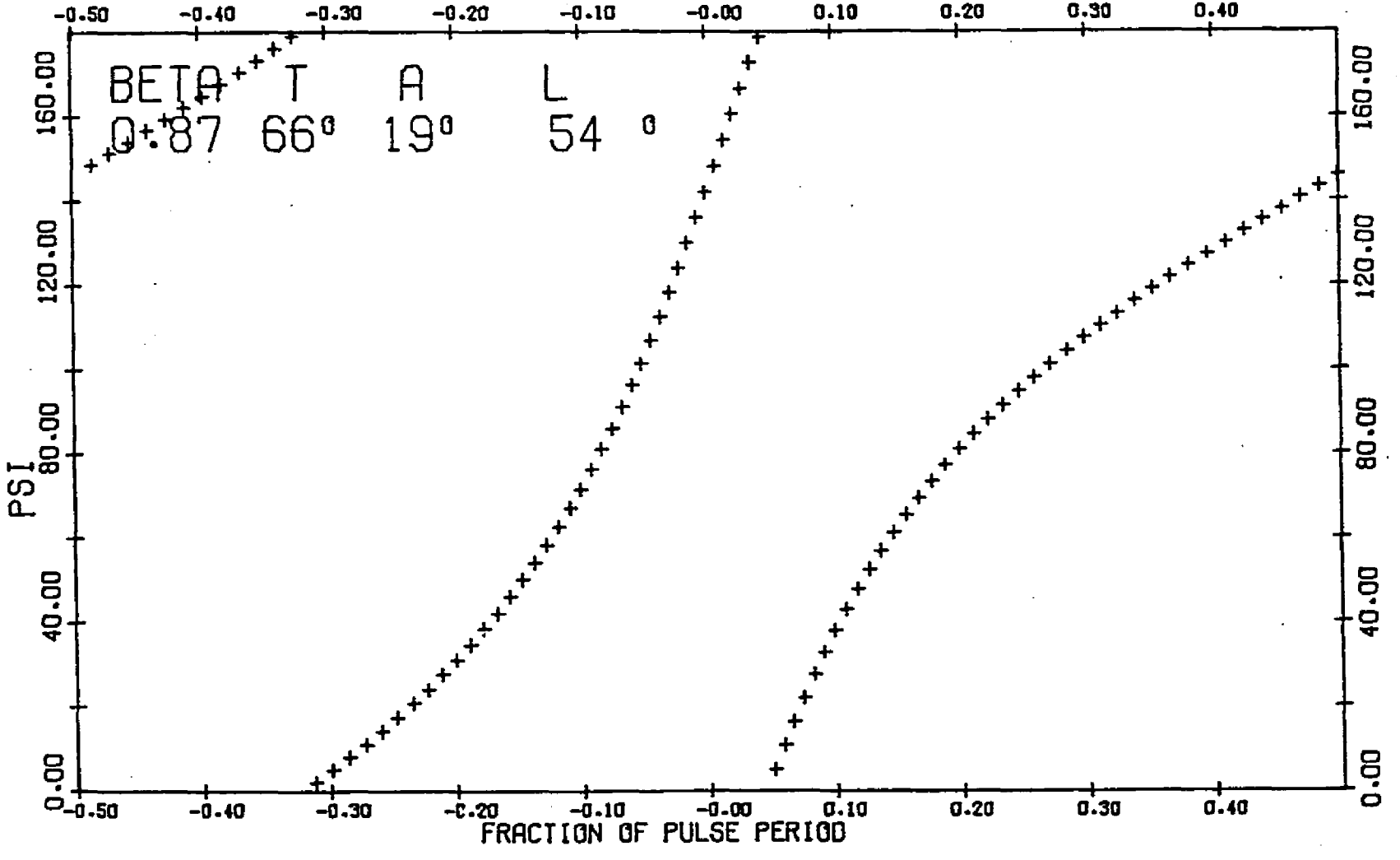

Figure 136. Ψ Versus Time for β=0.87, T=66°, A=19°, L=54°

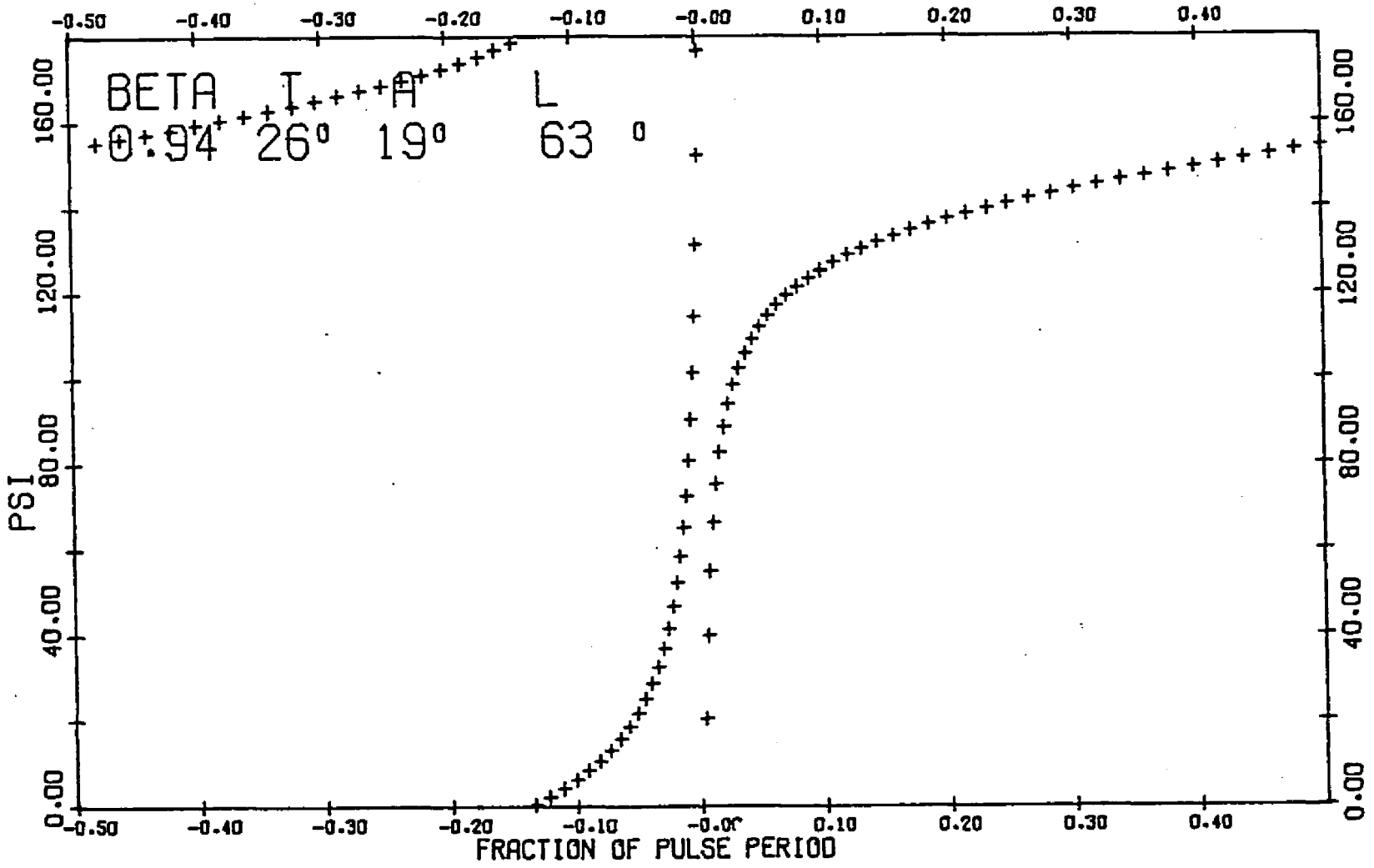

Figure 137. Ψ Versus Time for β=0.94, T=26°, A=19°, L=63°

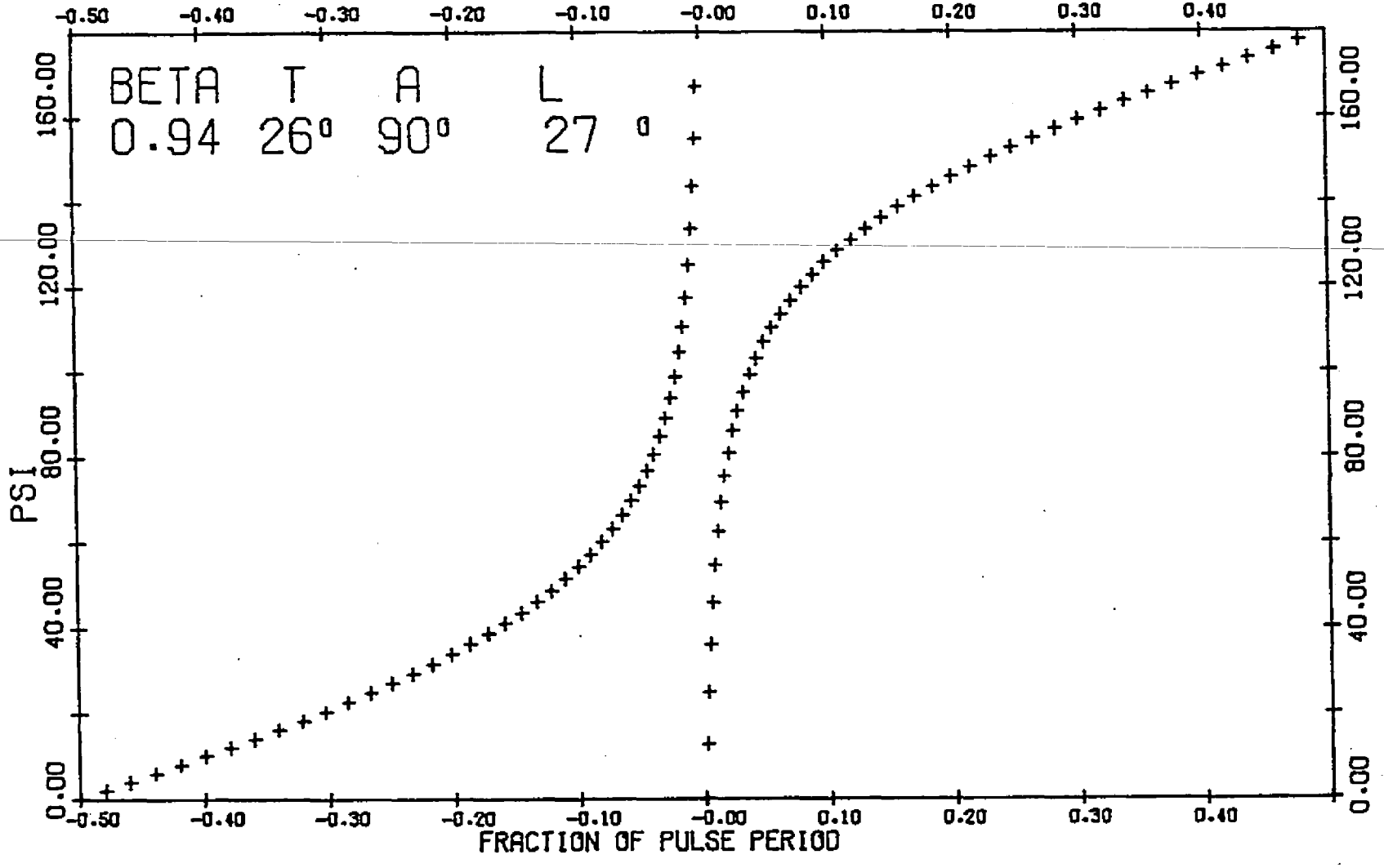

Figure 138. Ψ Versus Time for β=0.94, T=26°, A=90°, L=27°

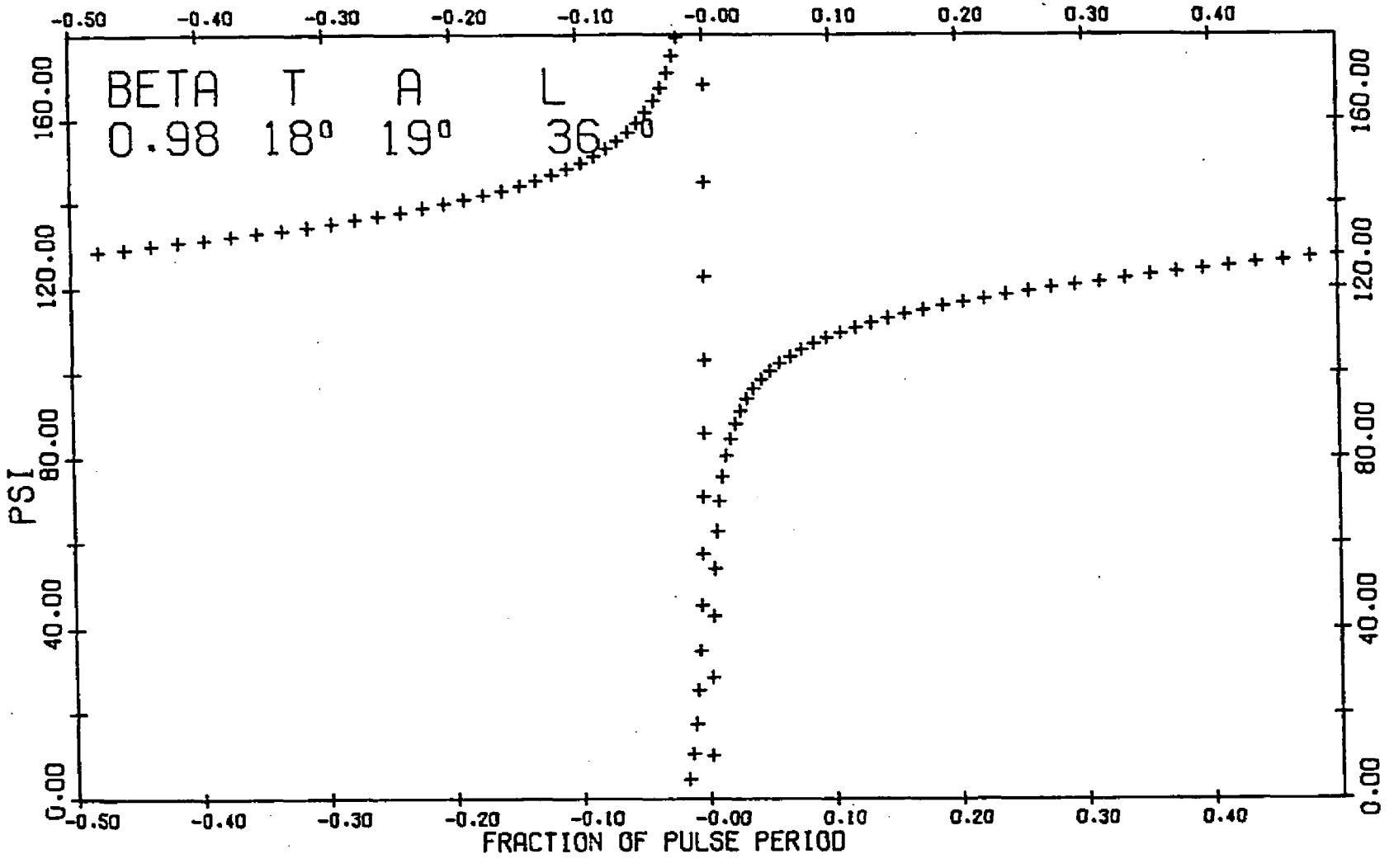

Figure 139. Ψ Versus Time for β=0.98, T=18°, A=19°, L=36°

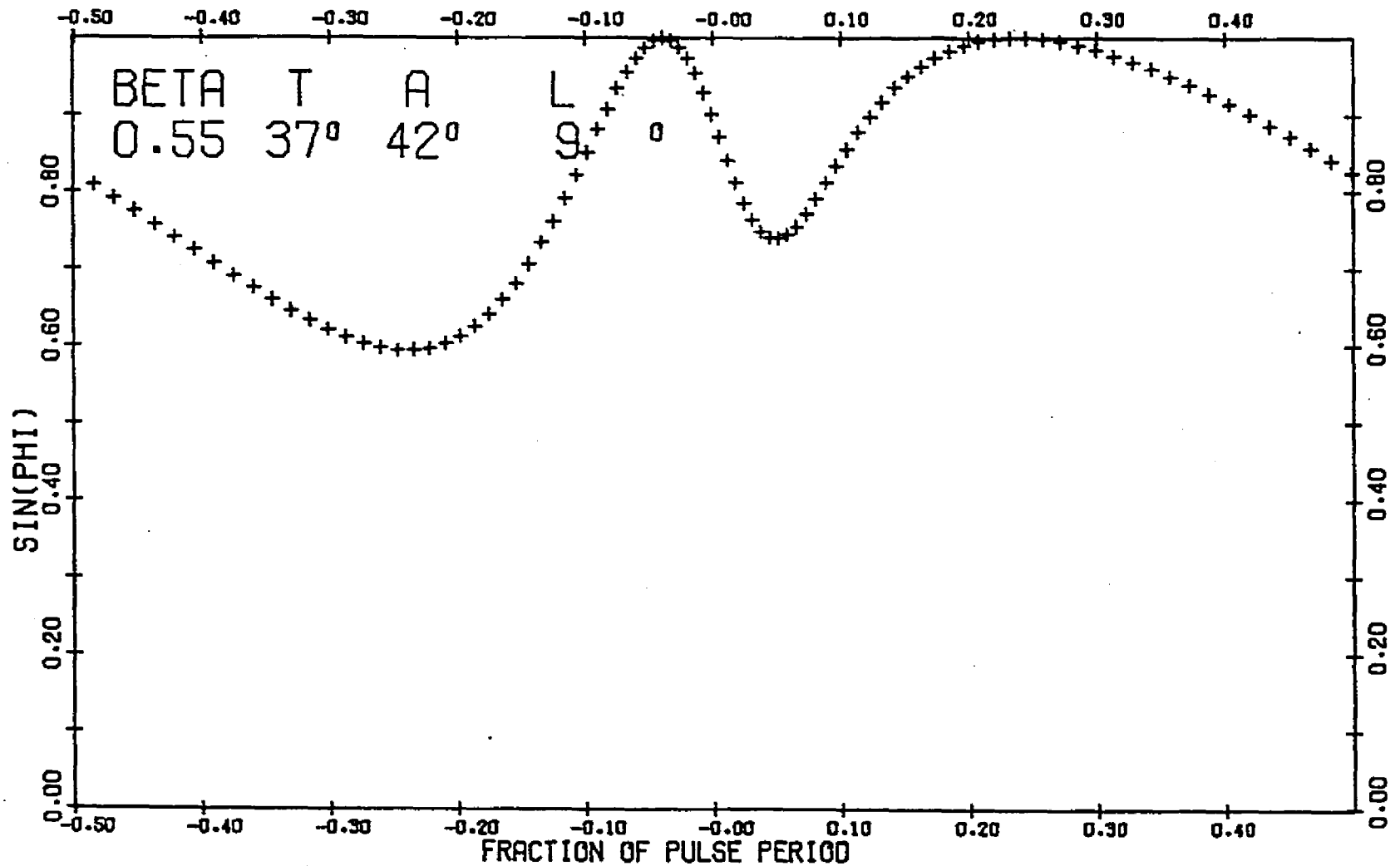

Figure 140. sin ϕ Versus Time for β=0.55, T=37°, A=42°, L=9°

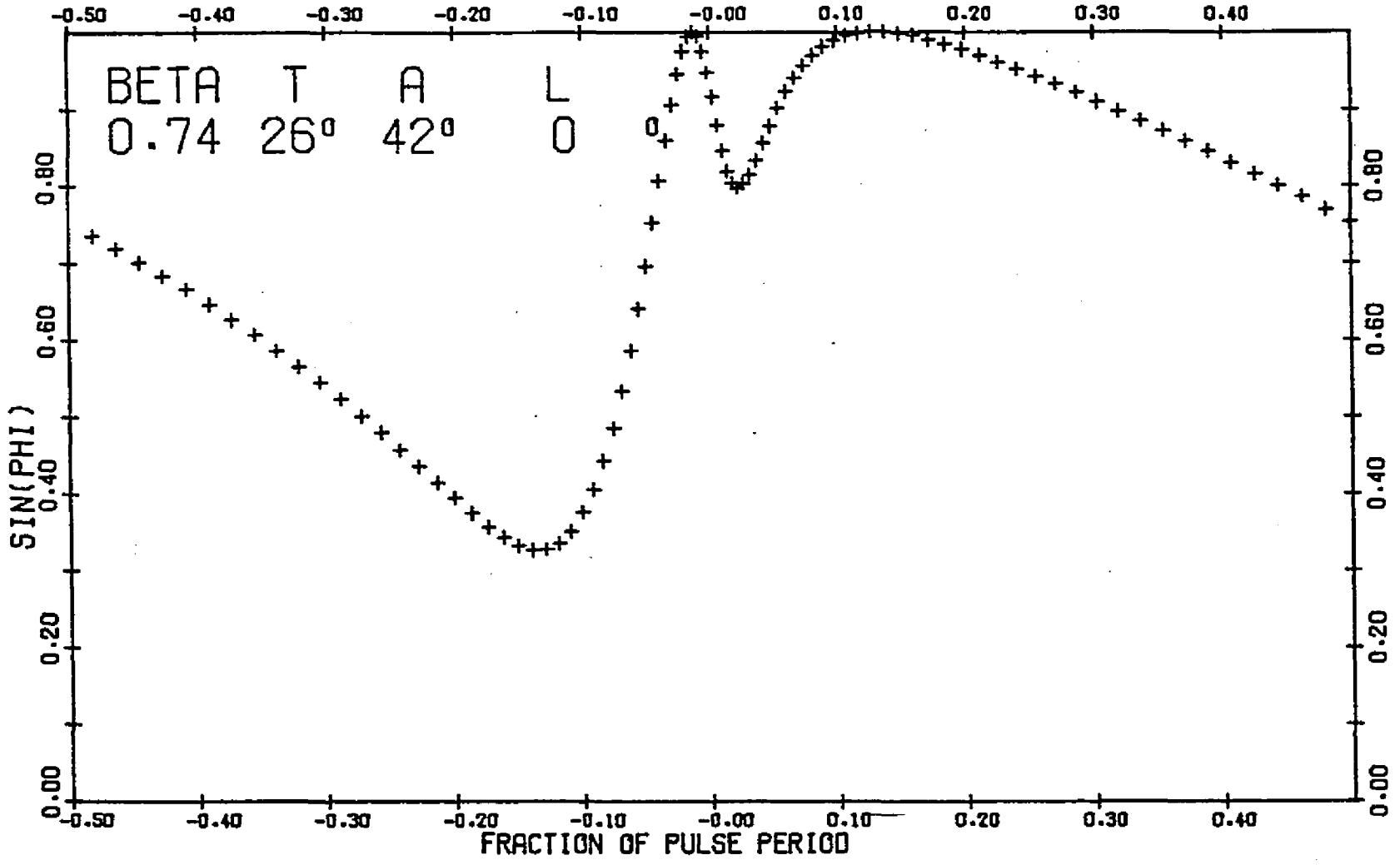

Figure 141. sin ϕ Versus Time for β=0.74, T=26°, A=42°, L=0°

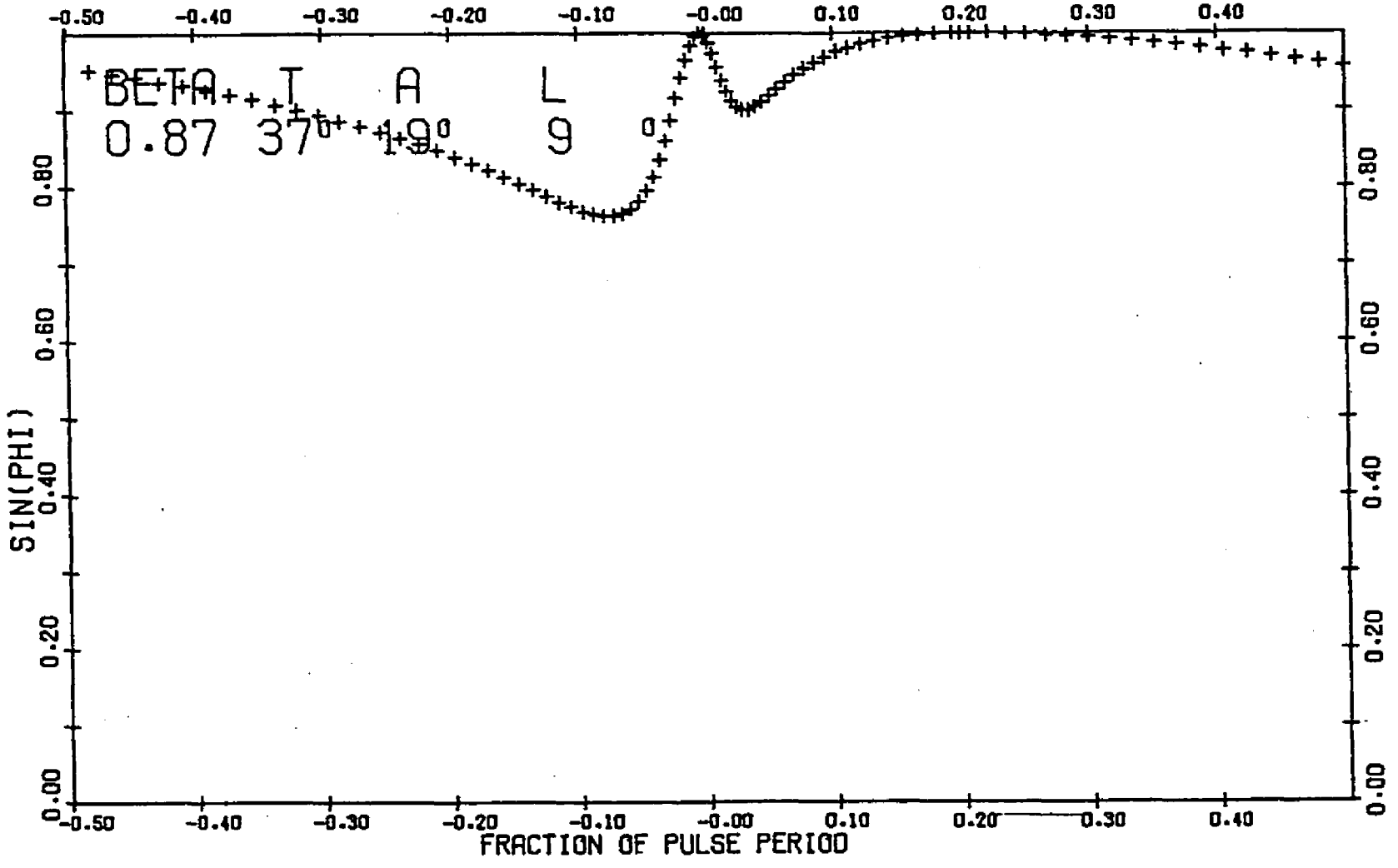

Figure 142. sin ϕ Versus Time for β=0.87, T=37°, A=19°, L=9°

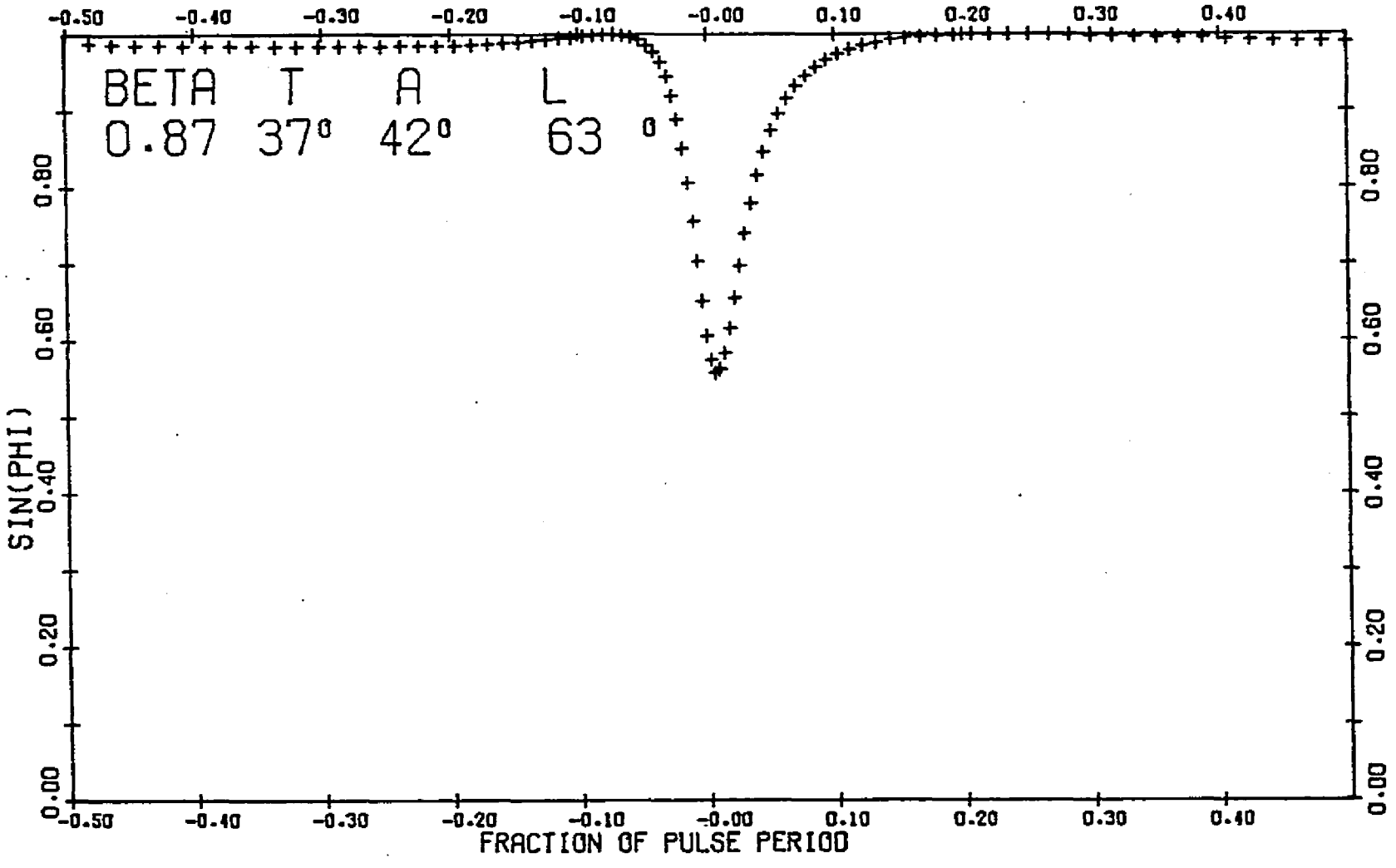

Figure 143. sin ϕ Versus Time for β=0.87, T=37°, A=42°, L=63°

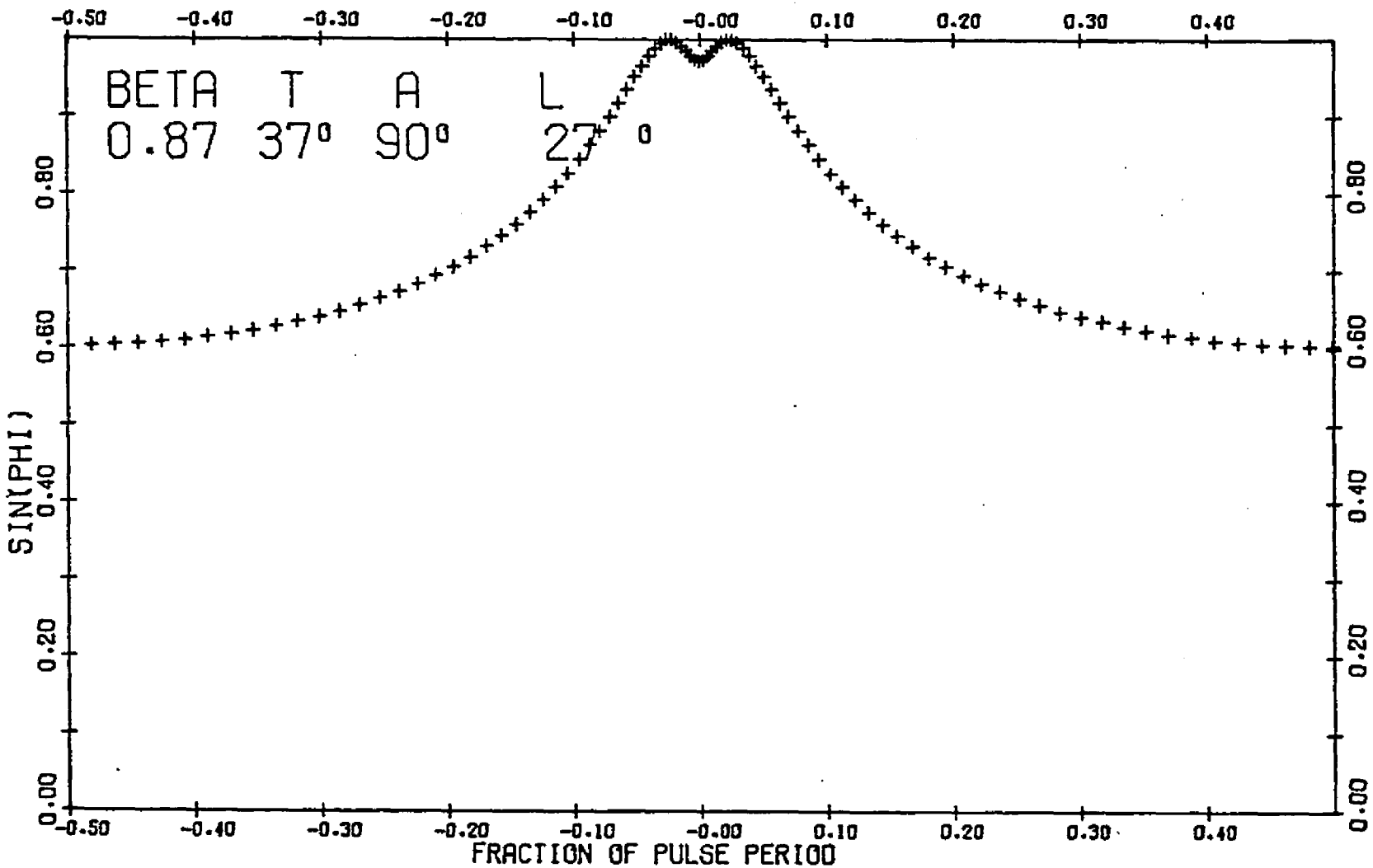

Figure 144. sin ϕ Versus Time for β=0.87, T=37°, A=90°, L=27°

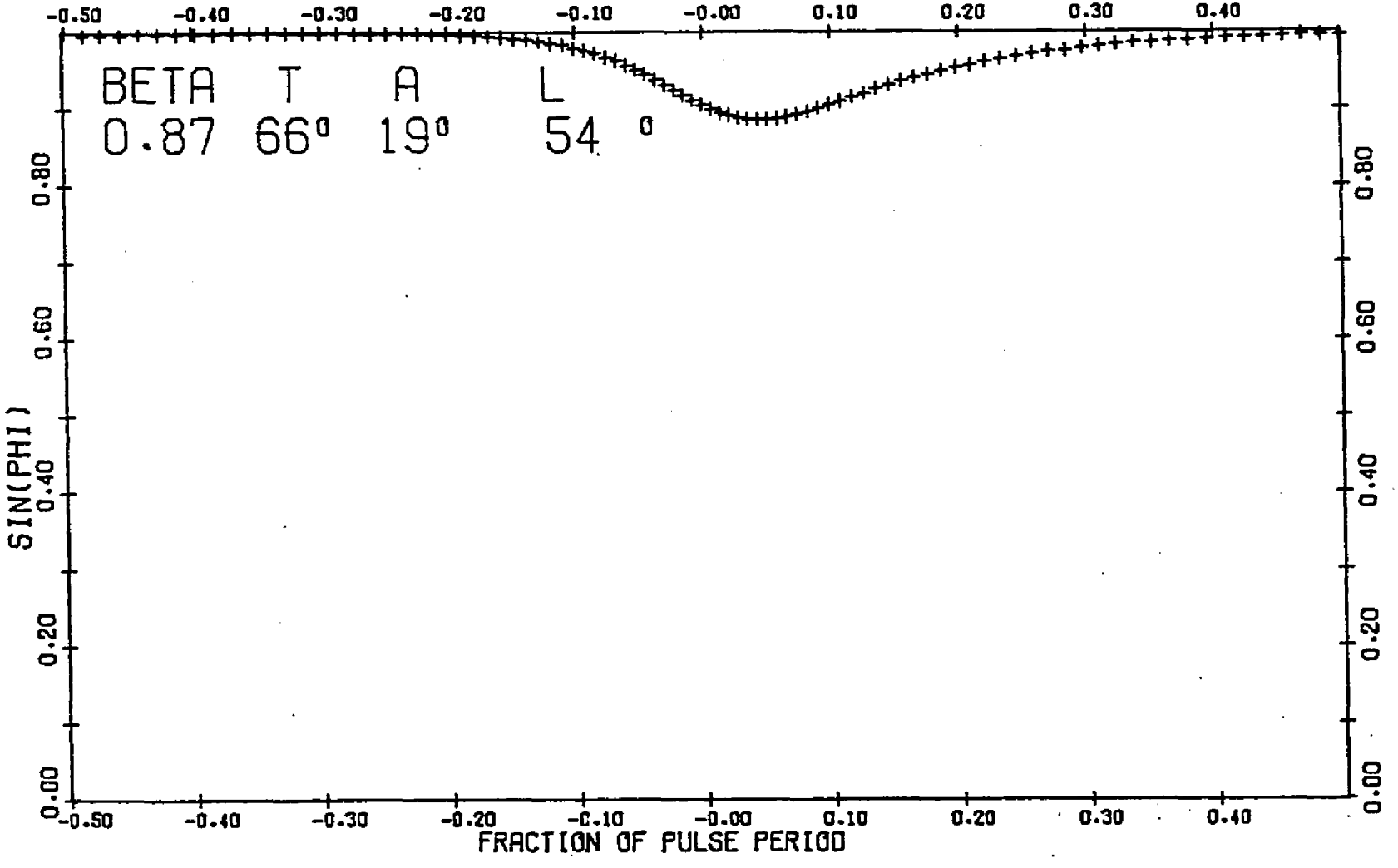

Figure 145. sin ϕ Versus Time for β=0.87, T=66°, A=19°, L=54°

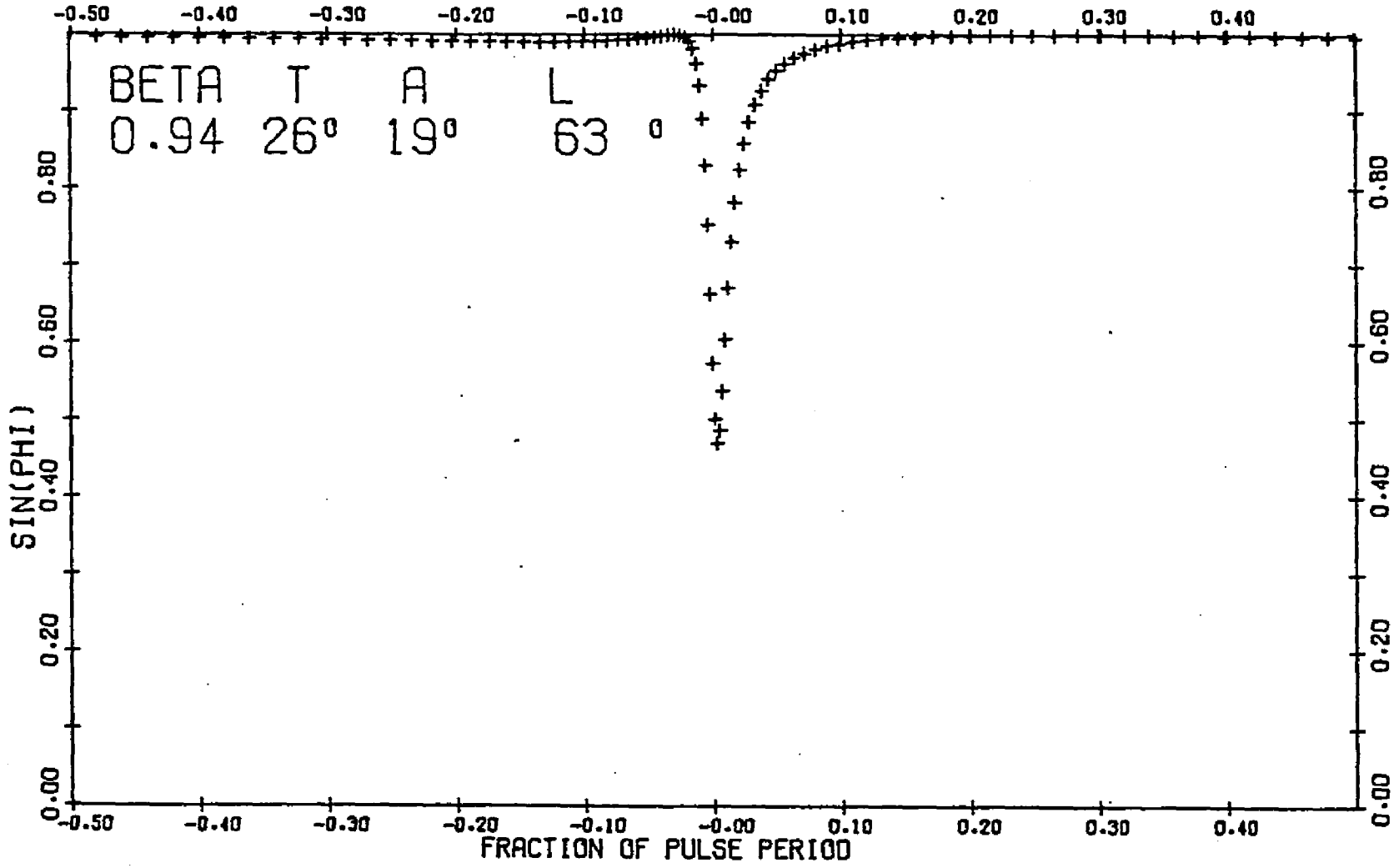

Figure 146. sin ϕ Versus Time for β=0.94, T=26°, A=19°, L=63°

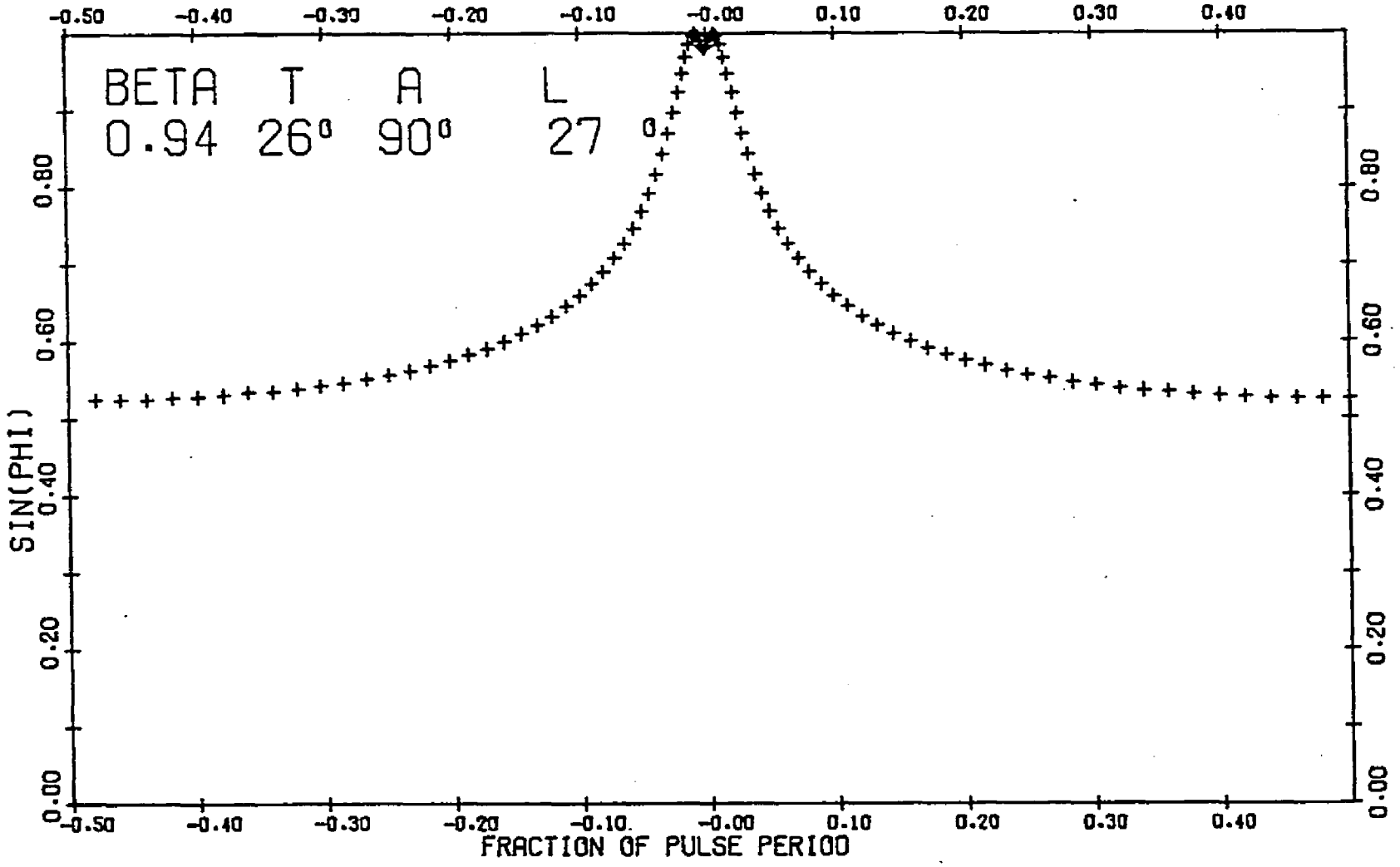

Figure 147. sin ϕ Versus Time for β=0.94, T=26°, A=90°, L=27°

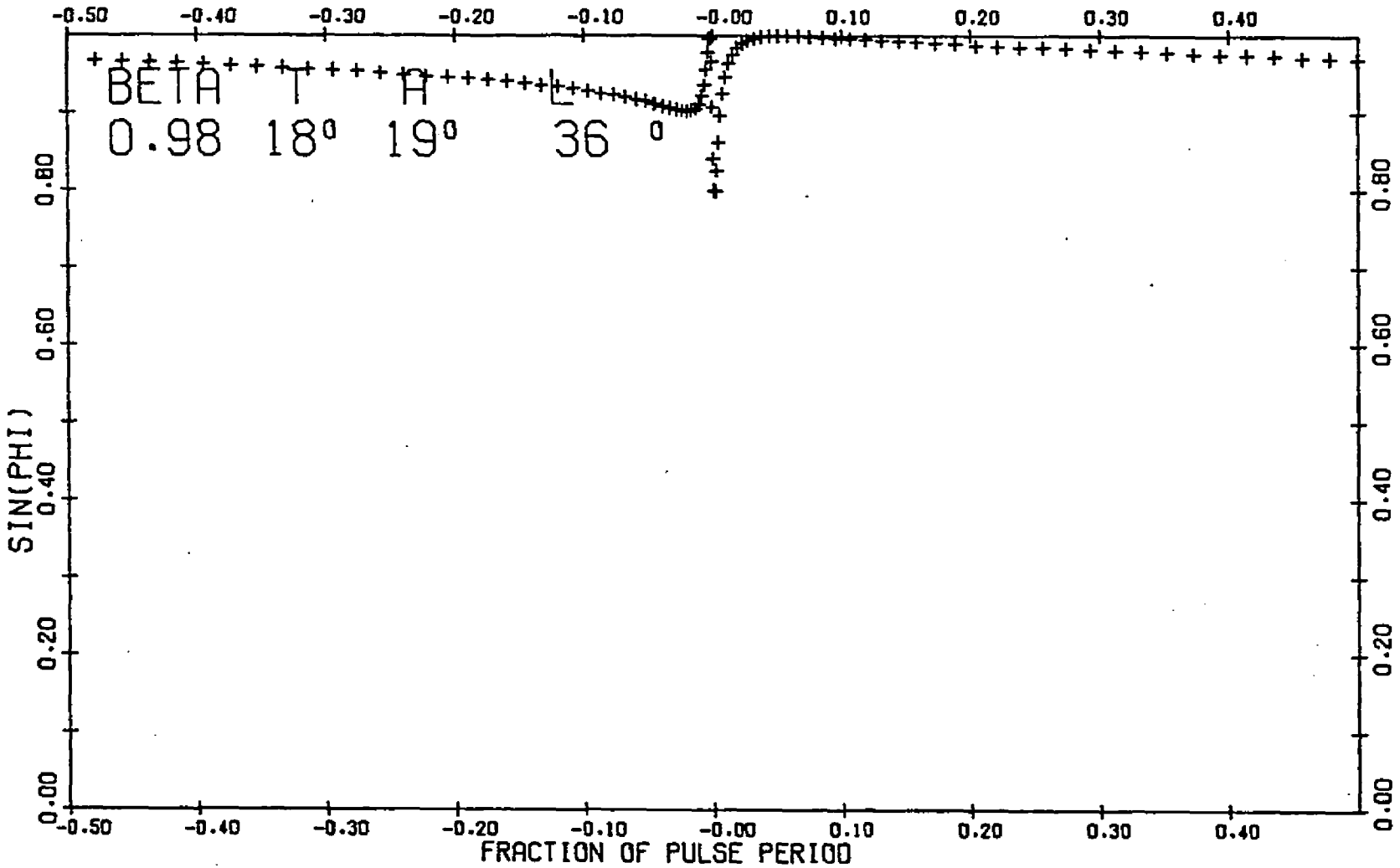

Figure 148. sin ϕ Versus Time for β=0.98, T=18°, A=19°, L=36°

A MODEL FOR THE SUB-PULSE AND INTEGRATED PULSE BEHAVIOR

In this section, I attempt to bring theory and observation together to come up with a physically reasonable model for the emission processes of pulsars. In order to do this, it is important to first give as complete a description of the phenomenon as possible.

A. The Observations and a Useful Classification Scheme

Pulsars are mainly radio objects. As their name implies, they emit pulses of radio waves at well defined intervals. The period of a pulsar is determined by counting pulses over a long time interval, and correcting for the motions of the earth in the interval. Periods range from 0.033 sec to 3.75 sec.

It is important to differentiate between the properties of individual pulses and the average, or integrated pulse of a pulsar. The integrated pulse is, in general, somewhat wider than the individual pulse, and may be thought of in some cases as an envelope within which the individual pulses come. The integrated pulse is usually quite stable (for integrations of a thousand pulses or so) in time, while individual pulses may have very different shapes from pulse to pulse.

Individual pulses are usually highly polarized at high frequencies, and many seem to be polarized 100%. There is usually some change of the Stokes parameters within an individual pulse, amounting to a rotation of the position angle and a change of the percentages of linear and circular polarization. Usually, the individual pulse shapes seem simple enough to be broken down into a few near Gaussian "sub-pulses", of approximately the same half-width.

The integrated pulse, then, is made up of many sub-pulses superimposed. It may have a very complex shape, or a very simple one, but many pulsars seem to have a double or multiple integrated pulse shape. The average width of the integrated pulse shape is close to 4% of the pulsar period, although there is a wide variation between different pulsars.

Some pulsars have an organized time behavior of sub-pulses within the integrated pulse. The sub-pulses seem to drift through the integrated pulse "window", coming usually (but not always) earlier and earlier in the "window" on succeeding pulses and fading away near the edges of the "window". In addition, the sub-pulses in a single individual pulse often follow each other in this behavior at a regular interval which is less than the "window" width. In one pulsar, at least, the sub-pulses also seem to fade and grow dimmer at some point in the

middle of the integrated pulse "window" and this point is called "Hankins' notch" after the discoverer (Hankins, 1973).

Many pulsars, while not showing sub-pulse behavior so organized as this, do seem to have individual pulse behavior which is somewhat modulated with a certain frequency, and could be thought of as having some form of "generalized" drifting behavior (see Backer, 1973).

There is often seen a polarization position angle sweep within the integrated pulse, and although the percentages of linear and especially circular polarization are often lower in the integrated pulse than in the individual pulses, they sometimes can be as much as 100% in the integrated pulse also.

The radio spectrum of individual pulses is difficult to measure and no consensus about it exists. However, the integrated pulse spectra of most pulsars seem to follow an approximate power law at moderate radio frequencies, and there may be spectral turnovers at low and high frequencies.

Some pulsars show very fine pulse structure within each sub-pulse and this is generally called microstructure. Its polarization, spectrum, pulse shape and other properties are unresolved. No adequate explanation for its existence has yet been offered.

An important datum is the flux of the radiation from pulsars combined with their great distances and the small size of the region in which emission takes place. The size of the emission region must be smaller than the distance light can travel in a pulse width. Distances can be estimated by assuming an electron density in interstellar space and measuring the differential delay of pulse arrival times at different frequencies (caused by the differing indices of refraction of the interstellar plasma at the two frequencies), or by dynamical methods if the 21 cm neutral hydrogen line shows up in absorption. By using the $1/r^2$ law for the flux, one finds that brightness temperature (i.e., the temperature of an equally bright black body of equal size) may be as high as 10^{26} °K and in the radio regime are never lower than 10^{20} °K. Since even non-coherent non-thermal radiation becomes absorbed when its brightness temperature becomes higher than the ambient electron temperature, this means that the radio radiation must be coherent. Coherence may come about either by spatial proximity of the emitting particles or by induced emission, but it must be present if electron temperatures as high as 10^{26} °K are to be avoided.

Finally, pulsars are extremely regular in their pulsations. Their periods may be measured to be constant to 7 decimal places or more on a short time scale, and to

be slowly increasing on a long time scale. Thus, a rotation "clock" gradually losing rotational energy is universally accepted as being responsible for their regularity.

Other properties of some pulsars, while extremely interesting, do not seem to be connected directly with their emission processes, and these will not be discussed. They include "spinups" or "glitches", proper motions, space velocities, precise positions, etc.

A useful classification scheme for pulsars has been invented by Taylor and Huguenin (1971). In this scheme, a pulsar is classified as type S if its average pulse shape is simple (dominated by a single component) and if it does not show appreciable systematic phase modulation of individual pulses (drifting). It will be of class D if its average pulse shape is determined to a large degree by a pronounced drifting or phase modulation of sub-pulses. It will be of class C if its average pulse shape is complex (has two or more clearly separated components of comparable intensity).

This classification scheme is useful because pulsars of different classes exhibit different behavior of other factors than average pulse shape. For instance, type S pulsars seem to be predominantly those of short period. Type D pulsars tend to have somewhat longer periods, and type C pulsars generally have the longest

periods. Also, type S pulsars have the smallest ratio of period to time derivative of period and type D pulsars the largest. Other remarkable differences between pulsar classes will be mentioned in one of the following sections, as each class is treated separately in an attempt to arrive at a satisfactory model.

B. Previous Models

Many widely different types of models have been put forth to describe pulsar emissions with varying degrees of success. I will discuss the features of two of the most prominent models.

Sturrock (1970, 1971) has put forth a model in which the emission comes from within a very few neutron star radii from the neutron star surface. In his model, the radio radiation is curvature radiation from cascades of electrons and positrons produced by pair production in the strong, open magnetic field lines near the magnetic polar caps. Pair production would take place, he says, in electron and proton polar zones for sufficiently high magnetic fields. His model does not fit the observed period vs. pulse width relation for pulsars unless he assumes that there are quantities of cold plasma in the magnetosphere which, by their inertia, drag the open field lines radially away from the star; this happens at a point much

nearer to the star than the speed-of-light cylinder. According to present theories of magnetic field decay with period in pulsars, his model predicts a long period cutoff in pulsar emissions, when the magnetic field becomes too weak for pair production to take place. Since it has been shown that pulsar radio radiation must be of a coherent nature, Sturrock postulates the emission will take place in thin charge sheets produced by a two stream plasma instability and thus the emitting particles would be spatially coherent and produce coherent radiation.

At different times, Sturrock has proposed different mechanisms for optical emission, and so his model can not be rightly said to make any testable predictions about it. X-ray emission would come from the proton polar zone and would only be found in pulsars with periods short enough (and thus magnetic fields high enough) for pair production from protons to take place.

Sturrock's model is attractive because it seems to explain a great deal. The period-pulse width distribution, the long period cutoff in observable pulsars, the presence of X-ray pulses in the Crab and Vela pulsars, and the approximate spectra of many pulsars can be readily interpreted on the basis of his model. There are difficulties, however. For instance, the difference between individual pulses and the integrated pulse from a pulsar is not

explained, except by saying that only a small part of a polar zone is undergoing pair production at a given time, and that the tightly beamed radiation from this single part is the individual pulse (Sturrock 1974). There is no explanation of why the individual sub-pulse widths from a given pulsar are nearly frequency invariant (Smith, 1970). Microstructure in the pulses is not explained.

There are polarization problems as well. Many pulsars show strong circular polarization in individual pulses. It is hard to see how curvature radiation could produce this unless the magnetic field lines were strongly twisted into spiral shapes near the neutron star surface. No account of how such an effect could be produced is given.

The optical radiation from the Crab pulsar has only an ad hoc explanation in Sturrock's model, and its polarization is not consistent with the non-relativistic single vector model (Cocke et al., 1973, and a later section of this dissertation), of which Sturrock's model is the leading example. In summary, Sturrock's model has its good and its bad points.

Let us turn now to another proposed model. This is the relativistic beaming model of F. G. Smith (1970, 1971a, 1971b, 1974). In this model, the sub-pulses are the result of the relativistic beaming of radiation from localized emission regions far out in the neutron star

magnetosphere (near the speed-of-light cylinder). The radiation, although nearly isotropic in the reference frame of the emission region, is tightly beamed in the observer's frame due to the variation of the relativistic beaming factor R with the angle between the line of relative velocity and the observed radiation.

The polarization (and indeed the radiation itself) is of the cyclotron pattern, which has a high degree of circular polarization if the observer looks along the magnetic field line and a high degree of linear polarization if he looks across the field line.

Microstructure in individual pulses is presumed due to variations in excitation within the sub-pulse emission region.

Since the individual pulse widths for pulsars are very small, the velocities of emission regions in Smith's model must be very great, typically about 0.9 of the speed of light. In consequence, in Smith's model, the individual pulses are only seen when their respective emission regions are coming most directly towards the observer (that is, at $\theta = 0$). The integrated pulse is essentially a probability distribution of emission region locations in longitude in the magnetic field. That is, the integrated pulse characteristics depend on the relative number of emission

regions, on the average, which happen to be at a given point in the magnetic field when that point passes through $\theta = 0$.

Since beaming is only produced by relativistic effects, we will only see pulsars which have a small value of the parameter T, the tilt of the rotation axis from the plane of the sky. In such cases, the integrated pulse will have the direction of sweep of polarization position angle opposite to the direction of sweep which a field line in the rotation equator would have. However, contrary to F. G. Smith's (1971b, 1974) contention, the direction of polarization position angle sweep in individual pulses could be either the same or opposite to this direction, depending upon whether the local magnetic field line passes above or below our line of sight.

Smith's model is attractive because of the things it explains well. The behavior of the sub-pulses in polarization and the way that they add up to the integrated pulse are very well described. The near frequency independence of the sub-pulse widths and polarization are treated with care and seem to be well explained for cases where the spectral index of the pulsar is frequency independent.

The model explains the observed period-sub-pulse width distribution quite well by stating that the radius

at which the emission takes place is about the same for all pulsars.

There are no problems with coherence of the radiation from a sub-pulse emission region, presumably because of bunching of the emitting particles. Contrary to the assertions of Manchester et al. (1973), it is questionable that the smallest time scale structures observed in the pulsars PSR 1133+16 and PSR 0950+08 constrict the size of a sub-pulse emission region sufficiently to make the radiation energy density (and thus the particle energy density) greater than the magnetic field energy density. The field therefore may remain relatively stable and can direct the motion of the particles to produce significant amounts of polarization.

Problems with the theory are many. Cyclotron radiation is narrow-band, but the sub-pulses are observed to be of a broad-band nature. Indeed, the beaming mechanism itself requires broad-band emission, since at different values of θ for an emission region the observed frequency will be Doppler shifted from the emitted frequency by different amounts.

No explanation of why the emission takes place where it does is forthcoming from Smith. Whether the emission takes place on open or closed field lines is not

discussed. There is no discussion of how the emitting particles got to where they are with non-relativistic velocities, etc.

There may be problems, also, with the sub-pulse widths being too frequency independent. Manchester et al. (1973) show that between 100 and 1400 MHz, where the integrated spectrum of the pulsar 0329+54 suffers a turnover, the sub-pulse widths do not change. If the sub-pulse spectra also suffer a turnover in this region, they should change width according to Smith's model, since $R(\theta) = f(\varepsilon)$. However, the spectrum of a single sub-pulse has not been adequately measured.

In general then, the model of Smith, while strong on detailed agreement with observation, is weak on physics. The model of Sturrock is strong on physics but weak on detailed agreement with observation. Any model should be strong in both categories in order to be acceptable. This is the goal of the second part of this dissertation. Physical arguments and calculations are presented in Section II.C. and detailed observational fits of the model proposed are undertaken in Section II.D.

C. Toward a Physical and Geometrical Model

It must first of all be stated that the polarization properties of the individual sub-pulses is of the

highest importance in coming up with a model. This is because the sub-pulses seem to be basic to the emission process, i.e., because all integrated pulses in all pulsars are built up of sub-pulses, and because the polarization properties seem to vary smoothly and continuously (for the most part) within a single sub-pulse.

Since the ratio of the circularly polarized flux to the linearly polarized flux is Lorentz invariant (Cocke and Holm, 1972) we can rely on it to tell us something about the emission process, regardless of the velocities or orbital circumstances of the emitting particles. In Figure 149 are shown a few of the individual pulses from PSR 0329+54, a simple pulsar with weak outriders to the integrated pulse shape. These data are taken from Smith (1972) and show the ratios of the Stokes parameters I, V/I and $\sqrt{Q^2+U^2}/I$, or the circular and linear amounts of polarization at 408 MHz. The three pulses shown are taken from a sequential series of 10, and were selected because of their high intensities and the degree of variation of linearly polarized flux through the pulse. Here, they are numbered according to their position in the sequence from the top of Smith's Figure 11, and the error bars are an estimate of the inaccuracy in measuring Smith's published plots, and do not reflect on the quality of his data.

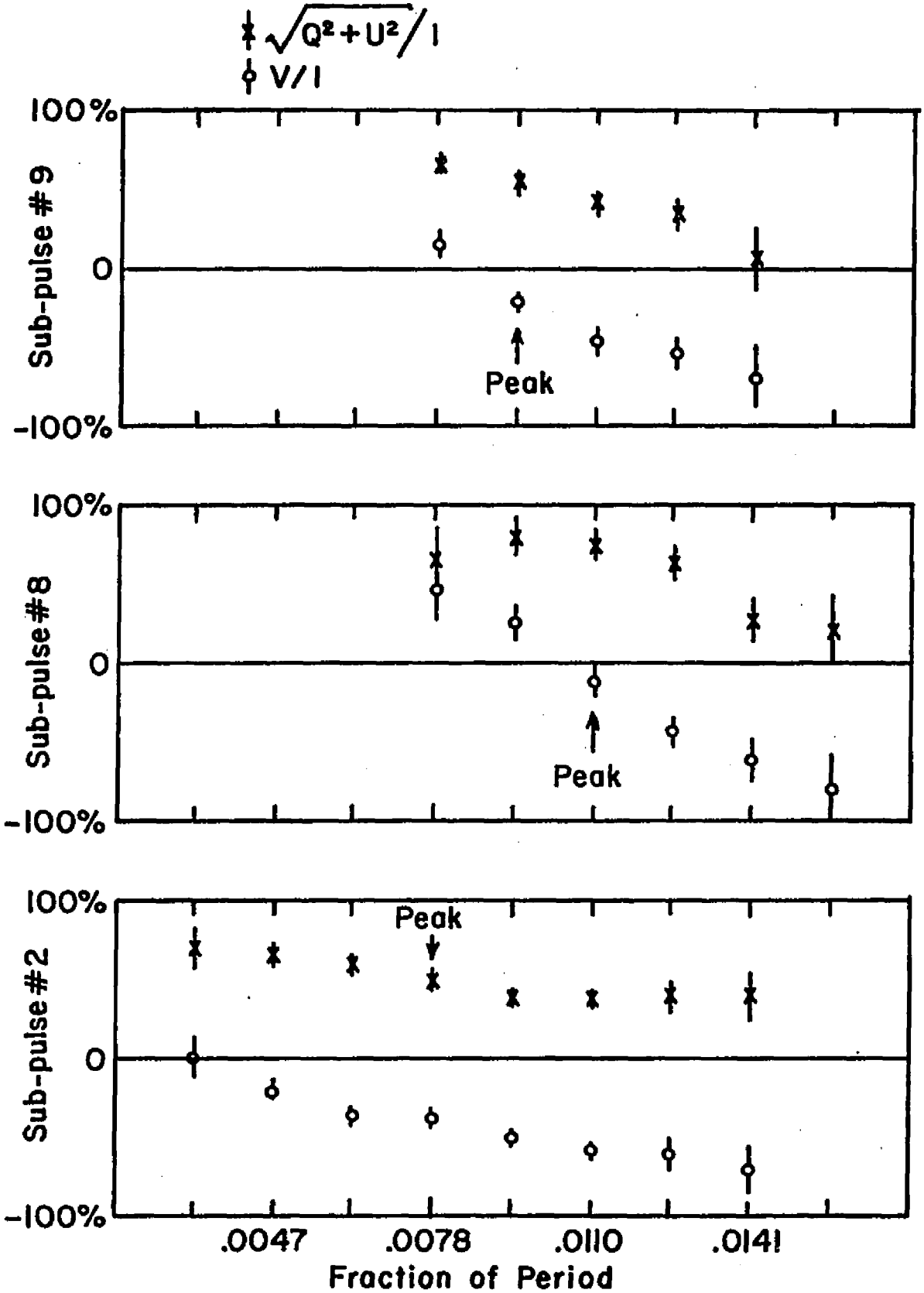

Figure 149. Individual Pulses From PSR 0329+54

It can be seen from this figure that in the individual sub-pulses, the percentage linear polarization is highest when the percentage circular polarization changes sign, and the percentage circular polarization is highest when the linear polarization is lowest. This in itself does not tell us much, as many emission processes produce this result. The interesting feature is that the maximum percentage of circular polarization is the same as the maximum percentage of linear polarization, the total polarization remaining approximately constant throughout the sub-space. Such a situation is highly unlikely for emission processes such as Cerenkov, curvature, and stimulated linear acceleration radiation, as in these processes the percentage linear polarization and the percentage circular polarization depend on peculiarities of the particle energies and of the magnetic or velocity fields, with the percentage circular polarization often remaining small in comparison with the linear polarization.

That the circular polarization often goes to 100%, and behaves in the way described here, in pulsar sub-pulses is borne out by the work of Rankin et al. (1974) who studied individual pulses from PSR 0823+26, a type S pulsar of 0.53 second period, PSR 0834+06, a type C pulsar of 1.27 second period, and PSR 2303+30, a type D pulsar of 1.58 second period.

Two radiation processes which produce polarizations similar to those seen in Figure 149 are the cyclotron process and synchrotron radiation from a single electron (Eastlund, 1970). In both processes the linear and circular polarizations are about the same in maximum, and the total percentage polarization throughout the polar diagram is constant.

In cyclotron radiation, the maximum in I is found to be in the direction of the magnetic field, and thus should be coincident with a maximum of the percentage circular polarization in the emission frame. We see from Figure 149 that this is not true for the sub-pulses we observe in PSR 0329+54. Contrariwise, for synchrotron radiation from a single ultrarelativistic electron, the maximum in I should come when the percentage linear polarization is at a maximum in the emission frame. The sub-pulses from PSR 0329+54 do not show this behavior either. Thus, we conclude that if cyclotron radiation or synchrotron radiation from a single electron pattern produces the sub-pulses, we, the observers, must not be in the emission frame, but that the emission frame and our frame are in relative motion, so as to produce a shift in the position of the intensity peak.

Putting this argument into quantitative terms, the Lorentz transformation properties of the Stokes

parameters are as follows (Cocke and Holm, 1972, McCrea, 1972):

$$I' = I[\gamma(1-\beta \cos \delta)]^{-3}$$

$$Q' = Q[\gamma(1-\beta \cos \delta)]^{-3}$$

$$U' = U[\gamma(1-\beta \cos \delta)]^{-3}$$

$$V' = V[\gamma(1-\beta \cos \delta)]^{-3}$$

where γ, β and δ are as previously defined in this dissertation. We can see that

$$\frac{Q'}{I'} = \frac{Q}{I} \quad \text{and} \quad \frac{U'}{I'} = \frac{U}{I}$$

so that

$$\frac{\sqrt{Q'^2+U'^2}}{I'} = \frac{\sqrt{Q^2+U^2}}{I}$$

and

$$\frac{V'}{I'} = \frac{V}{I} \ ,$$

justifying the statement that the ratios of the percentages of polarization are Lorentz invariant. However, any one Stokes parameter is not Lorentz invariant, but is multiplied in transformation by a factor containing the relative velocity of the reference frames and the angle between the relative velocity and the emission direction. Thus, in undergoing the Lorentz transformation, the maximum in I is changed by this factor.

This makes possible the statement that the emission in sub-pulses from PSR 0329+54 may be either cyclotron radiation or coherent synchrotron radiation from identically orbiting electrons, but that the position in time of the peak intensity has been shifted by a Lorentz transformation.

If one is to explain the sub-pulses from PSR 0329+54 by such an emission mechanism, then the reference frame of the emission must be moving relativistically with respect to the observer, and thus must not be on or corotating near to the neutron star surface. If the radiation is to be explained by some other process of production, then it must explain both the relative times of intensity maximum and circular polarization maximum and the fact that the maximum circular and linear percentage polarizations are about the same.

The full-width at half maximum of sub-pulses #8 and #9 is about 5 ms, or about 0.7% of the period of PSR 0329+54. If the pulse width is formed predominantly by the beam pattern of a single electron, it would imply that the beam-width $1/\gamma$ of the electron equalled approximately 0.045 radian, so that γ would be about 22 for the electron. If the pulse width were formed predominantly by relativistic beaming of the cyclotron pattern by a relativistically orbiting emission region it would correspond to a γ of about 3 for the emission region. We will refer to these figures later on to decide on physical conditions within the emission region.

In Figure 150 is shown the variation of linear polarization position angle for the same three sub-pulses as in Figure 149. Here we see that although there is a swing of position angle within each pulse the swing seems to come at a phase fixed with respect to the sub-pulse peak in sub-pulses #8 and #9, while the sub-pulse #2 shows a time behavior of position angle different from the other two.

That this type of behavior is also exhibited in other pulsars is borne out by the work of Rankin et al. (1974) and of Taylor et al. (1971), who found that in general, polarization properties are fixed to phase in the sub-pulse, not to rotational phase.

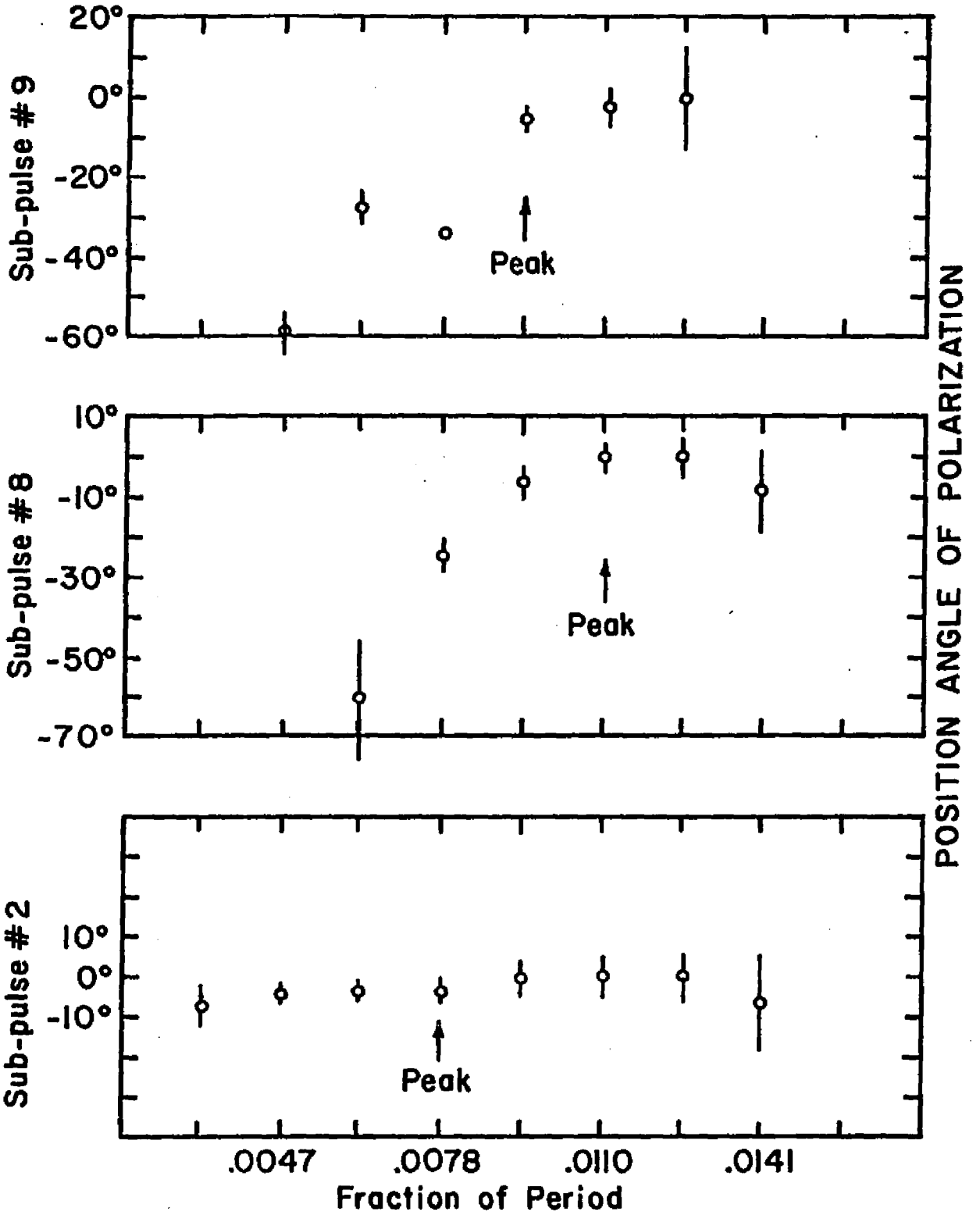

Figure 150. Variation of Linear Polarization Position Angle for Individual Pulses From PSR 0329+54

I interpret these observations in the following way. The run of position angle and polarization amount is about the same in the sub-pulses, implying that the magnetic field in the emission regions has about the same orientation. This implies that the emission regions which produce the sub-pulses are close together. Sub-pulse #9, the exception to the above, I suspect to be a blend of two sub-pulses at closely similar phases. This suspicion is borne out by the full width at half maximum of I for sub-pulse #9, which is about 50% greater than that for the other two sub-pulses.

However, while the emission regions are close together since they have similar polarization behaviors, they must be somewhat separated since the position angle changes come at different times in the integrated pulse. That is, the sub-pulses cannot be formed by a single emission region which somehow beams its radiation in several different directions, corresponding (for example) to different electron pitch angles, for in that case the polarization changes of the sub-pulses would take place at the same phase relative to the pulsar's rotation, and not relative to sub-pulse intensity variations.

In PSR 0329+54 the central part of the integrated pulse, which sub-pulses #2, 8, and 9 were taken from, is only about 5 ms wide, which indicates that the sub-pulses

(of about the same width) must be concentrated around the mean time of maximum. What, on the other hand, about the sub-pulses which make up the outriders to the main integrated pulse shape?

Pulse #7 of Smith's (1972) Figure 11 is a good example of an outrider sub-pulse. Its polarization vs. time is shown in Figure 151. Note that this pulse shows a little contamination in the trailing edge by a small central sub-pulse, but this should not be significant for times earlier than about .005 period. As can be seen, this pulse exhibits very little circular polarization, and linear polarization ~100%. Here there is very little if any change of position angle through the sub-pulse, also. So it appears that the sub-pulse of the outrider is very different from that of the central pulse. Thus, it must originate in a different place than the central pulse; both its polarization properties and arrival time being different, and this implies that its magnetic field line orientation and physical location differ from those of the central pulse.

In all of the following physical discussion, the system of units followed will be the cgs or Gaussian system of units. Whenever a physical quantity is given as a number times a physical quantity with different units, one

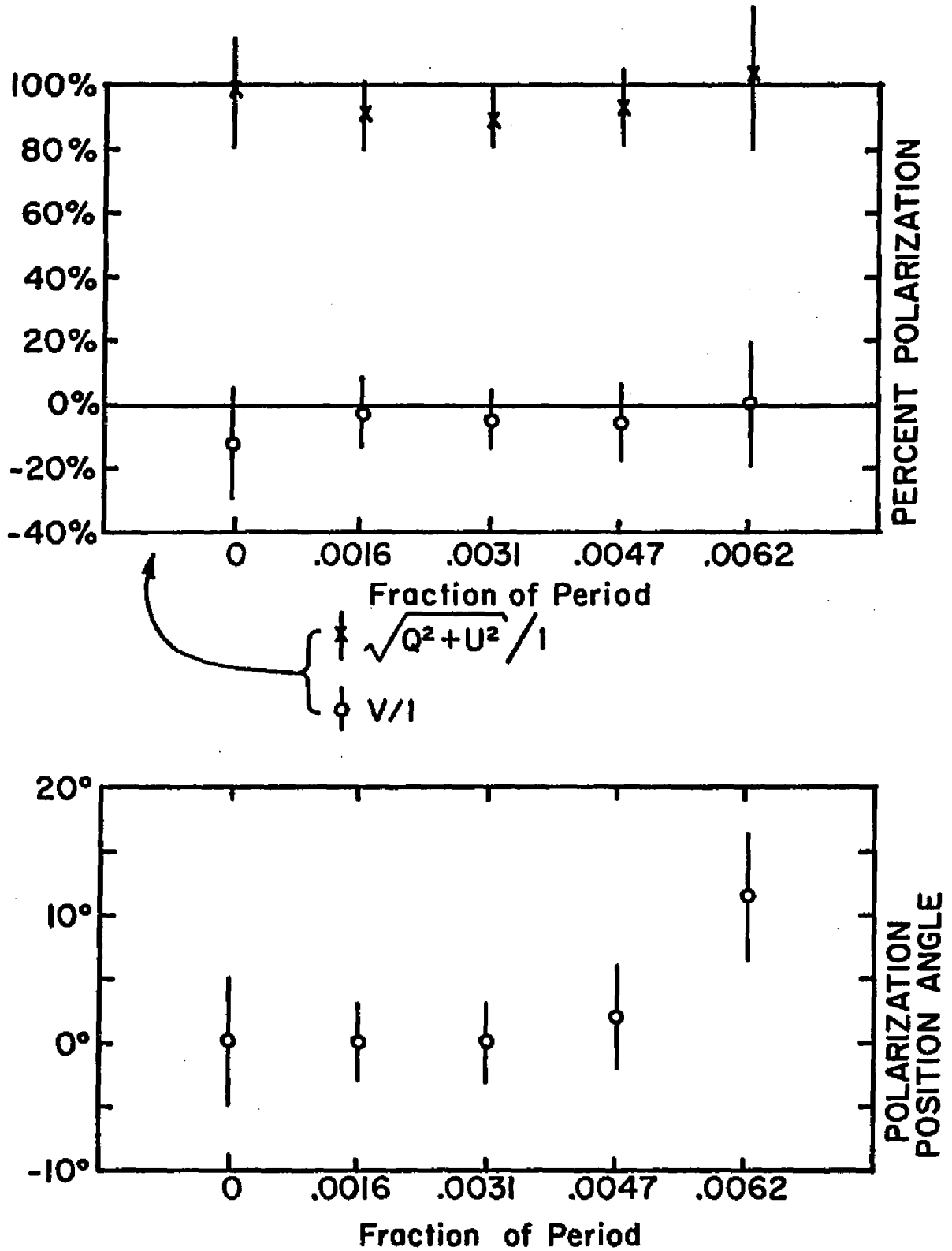

Figure 151. An Outrider Pulse From PSR 0329+54

may assume that the number has the proper cgs units to make the equivalence meaningful.

Also, in the discussion, it will always be assumed that n = 1 for the plasma of the pulsar magnetosphere (n being the index of refraction) or equivalently, that the emitted frequencies are very much greater than the plasma cutoff frequency. This assumption is necessary for two reasons:

(1) Without the assumption, the propagation of the emission through the plasma becomes very complicated, especially near the speed-of-light cylinder where one expects the plasma to be breaking away from certain field lines (see Lerche, 1974).

(2) If $n \neq 1$, the equation used in the generalized single vector model must be modified to account for the difference. In particular, in that case

$$\tan \delta' = \frac{\sin\delta}{\gamma(\cos \delta - \beta/n)}$$

and

$$\nu' = \gamma\nu(1-\beta n \cos \delta)$$

and

$$\frac{I(\nu)}{I'(\nu')} = [\gamma(1-\beta n \cos \delta)]^{-3}$$ (see Elitzur, 1974).

Let us see if we can infer the physical properties of the emission regions on the assumption that the radiation is either cyclotron or single electron synchrotron. First we will make the cyclotron assumption. If the radiation is of a cyclotron nature, then the beaming must be relativistic beaming from an orbiting source of $\gamma \simeq 3$, or $\beta \simeq 0.94$. Taking the magnetic field strength to be approximately that of a dipole,

$$\frac{B}{B_s} = \left(\frac{r_s}{r} \right)^3$$

where B is the field strength, r is the distance from the neutron star, and subscripted quantities refer to the surface of the neutron star. Taking $B_s \simeq 10^{12}$ gauss and $r_s \simeq 10^6$ cm, we find that at $\beta = 0.94$

$$r \geq \frac{0.94c}{\Omega}$$

where c is the speed of light and Ω is the rotational frequency. For PSR 0329+54, Ω is 8.79, so that

$$r \geq 3.2 \times 10^9 \text{ cm}$$

$$\left(\frac{r}{r_s} \right)^3 = 3.3 \times 10^{10}$$

so that

$$B \leq \frac{10^{12}}{3.3 \times 10^{10}} \simeq 3 \times 10^{+1} \quad \text{or} \quad 30 \text{ gauss.}$$

Then ω_G, the cyclotron angular frequency, which is given by $\omega_G \simeq 1.8 \times 10^7$ B for electrons, is

$$\omega_G \leq 5.4 \times 10^8$$

or

$$\nu_G \leq 8.6 \times 10^7 \text{ Hz}$$

where ν_G is the natural cyclotron frequency. Since the observing frequency is 4.1×10^8 Hz, the radiation might be observed if it is cyclotron. For $\nu_G = 8.6 \times 10^7$ Hz, we would expect to see radiation in our frame at

$$\nu = \frac{\nu_G}{\gamma(1-\beta \cos \delta)}$$

which becomes

$$\nu = \frac{\nu_G}{3(.06)} \qquad \text{for} \quad \cos \delta = 1$$

or

$$\nu = 5.56 \, \nu_G = 4.8 \times 10^8 \text{ Hz} \quad .$$

Since the radiation we are considering is at 4.1×10^8 Hz, our order of magnitude estimates seem internally consistent so far.

Taking the synchrotron assumption, we know that the electron $\gamma \lesssim 22$, because of the width of the sub-pulse. Modification of the width by extra relativistic beaming due to orbiting would not be very great unless the field configuration were such that the beam emitted at $\theta = 0°$ should strike us. For synchrotron radiation from a single electron, the radiation is strong between the fundamental frequency ω_F, where

$$\omega_F = \omega_G/(\gamma \sin^2 \theta_o) \ , \tag{28}$$

and 0.3 times ω_c, the critical frequency, where

$$0.3\ \omega_c \simeq \frac{1}{2}\ \omega_G\ \gamma^2 \sin \theta_o \ . \tag{29}$$

Here θ_o is the pitch angle of the electron. From (28) we see that an observing frequency of $\nu = 4.1 \times 10^8$, or $\omega = 2.6 \times 10^9$ implies that

$$\omega_G < \omega\gamma \sin^2 \theta_o$$

or

$$\omega_G < \gamma(\sin^2 \theta_o)\ (2.6\text{x}10^9)$$

and taking

$$\gamma = 22 \quad , \quad \omega_G \lesssim 5.7 \times 10^{10} \sin^2 \theta_o \quad .$$

From (29) we see that

$$\omega_G \gtrsim \frac{2\omega}{\gamma^2 \sin \theta_o}$$

and substituting $\gamma = 22$ and $\omega = 2.6\text{x}10^9$, we have

$$\omega_G \gtrsim \frac{1.1\text{x}10^7}{\sin \theta_o}$$

and, combining our two expressions for ω_G, we get

$$5.7 \times 10^9 \sin^2 \theta_o \gtrsim \frac{1.1\text{x}10^7}{\sin \theta_o}$$

or

$$\sin^3 \theta_o \gtrsim \frac{1.1\text{x}10^7}{5.7\text{x}10^9}$$

or

$$\sin^3 \theta_o \gtrsim .0019$$

$$\sin \theta_o \gtrsim .124$$

or

$$\theta_o \gtrsim 7^\circ \quad .$$

This result is not changed if the radiation is proton synchrotron.

What does the amount of polarization tell us about the emission region? Well, for synchrotron radiation from a single electron, the polarization is a function of frequency, given by

$$\pi = \frac{K_{2/3}\ (\nu/\nu_c)}{\int_{\nu/\nu_c}^{\infty} K_{5/3}\ (n)\,dn}$$

where

$$\nu_c = \frac{3}{4\pi}\,\omega_G\,\gamma^2\,\sin\theta_o \quad ,$$

and $K_{2/3}$ and $K_{5/3}$ are modified Bessel functions (Ginzburg and Syrovatskii, 1965). In order for the radiation in all directions to be 70% polarized, ν/ν_c must be about 0.6. For it to be ~100% polarized, ν/ν_c must be greater than 10. Thus, for the central sub-pulses,

$$\nu \gtrsim (0.6)\,\frac{3}{4\pi}\,\omega_G\,\gamma^2\,\sin\theta_o$$

and putting in $\gamma = 22$, $\nu = 4.1 \times 10^8$, and $\omega_G = 1.8 \times 10^7$ B, we find that

$$4.1 \times 10^8 \geq (0.6)(0.24)(1.8 \times 10^7)(484)\ B \sin \theta_o$$

$$\frac{4.1 \times 10^8}{1.25 \times 10^9} \geq B \sin \theta_o$$

or

$$B \sin \theta_o \leq 3.3 \times 10^{-1} \quad .$$

Taking as an example $\sin \theta_o = .124$, the minimum from previous considerations, we find

$$B \lesssim 2.7 \text{ gauss}$$

which corresponds to a dipole field distance of

$$r \gtrsim r_s \sqrt[3]{B_s/B}$$

or

$$r \geq 7.18 \times 10^9 \text{ cm} \quad .$$

This is about 2.3 times the radius of the speed-of-light cylinder. For all other allowed values of $\sin \theta_o$, r is greater.

If the surface magnetic field were as low as 10^{11} gauss, the radius at which synchrotron emission could be producing the sub-pulses would be reduced by a factor of $3\sqrt{10} = 2.15$. This would make the emission possible from about the radius of the speed-of-light cylinder. From the observed spin-down rate of PSR 0329+54, it does not, however, seem likely that the magnetic field is this low.

For the polarization to be ~100%, these distances are even greater. I conclude that if the magnetic field strength is approximately dipolar, and if the radiation is of a synchrotron nature, either the magnetic field at the surface of PSR 0329+54 is $<10^{12}$ gauss, or the radiation comes from great distances above the rotational pole of the pulsar, at distances several times the radius of the speed-of-light cylinder from the surface.

From the first adiabatic invariant of charged particle motion in a magnetic field,

$$\frac{B}{\sin^2 \theta_o} = \text{constant} \quad .$$

If the particles producing the radiation from PSR 0329+54 come from the surface, no matter what their initial pitch angle may be, the pitch angle will decrease along the trajectory outward until it is less than 7°, or any

arbitrary limit. It is instructive to see at what radius this takes place for a pulsar. Then

$$\frac{\sin^2 \theta_o}{\sin^2 \theta_{os}} = \frac{B_o}{B_s} = \left(\frac{r_s}{r} \right)^3$$

Taking $\sin^2 \theta_{os} = 1$ and $\sin^2 \theta_o = \sin^2 (7°) = .015$ we find that

$$\left(\frac{r_s}{r} \right)^3 = .015$$

or

$$\left(\frac{r_s}{r} \right) = \sqrt[3]{.015}$$

or

$$r \approx 4.0\, r_s$$

Thus, at any distance from the neutron star greater than about 4 radii, none of the electrons or protons leaving the star will have pitch angles greater than 7° and none could (according to our criteria above) produce the radiation from PSR 0329+54. However, as we have seen before, the fact that the maximum intensity is displaced from the minimum circular polarization ensures that the emission

must come from a reference frame much farther out, where relativistic beaming can modify the pulse shape.

It is a simple matter to show that the sub-pulse emission region is localized in the magnetic field. In order for there to be significant light variations from a source of emission, the size ΔX must be smaller than the distance light can travel in the time of variation Δt. Or,

$$\frac{\Delta X}{\Delta t} < c$$

and for PSR 0392+54, taking $\Delta t = .005s$, we have

$$\Delta X < (.005)(3 \times 10^{10})$$

or

$$\Delta X < 1.5 \times 10^{8} \text{ cm} \quad .$$

Since the radius of the speed-of-light cylinder is about 3.1×10^{9} cm, we see that the size of the emission region in our frame must be less than 4.5% of the radius of the speed-of-light cylinder. Of course, if the emission comes from the speed-of-light cylinder, the size of the emission region in the emission frame may be γ times larger, due to the Lorentz contraction.

A minimum size of the emission region may be set in other ways. The most stringent condition for emission near the light cylinder is that used by Manchester et al. (1973) which states that for the radiation to be highly polarized in an orderly fashion, the emitting particles must be well guided by the magnetic field, and thus the particle energy density, which is greater than the emitted radiation energy density, must be less than the magnetic energy density.

Using the relation $F = \rho_{rad}\, c$, we can calculate the radiation energy density at the source in the following way. The peak radiation flux density for PSR 0329+54 at the earth is 2×10^{-21} ergs/(cm^{2}sec Hz) over a bandwidth of 10^5 Hz at a frequency of 430 MHz (Manchester, 1971a). Thus, the peak flux here at earth is

$$2 \times 10^{-16} \text{ ergs/(cm}^2 \text{ sec)}.$$

By the inverse square law, F_{here} (the flux here) is given by

$$F_{here} = \frac{F_{er}}{\gamma^4 (1-\beta \cos \delta)^4} \left(\frac{\gamma^2 X^2}{d^2} \right)$$

(See McCrea 1972), where F_{er} is the flux in the emission frame, X is the size of the emission region in our frame

(it may be γ higher in the emission frame) and d is the distance of the pulsar. Using the observed dispersion measure of PSR 0329+54, DM = 26.8, and the approximate relation,

$$d \simeq 1.24 \times 10^{20} \text{ DM}$$

(Smith, 1972), we have

$$d \simeq 3.3 \times 10^{21} \text{ cm}$$

with an estimated error of about the same magnitude.

For an assumed γ of 3 and cos δ = 1, and an emission region spherical in the corotating frame, we have

$$F_{here} = \frac{10^4 \, F_{er} \, X^2}{1.1 \times 10^{43}}$$

or

$$F_{er} = \frac{2.2 \times 10^{23}}{X^2}$$

or

$$\rho_{rad} = \frac{2.2 \times 10^{23}}{3 \times 10^{10}} \frac{1}{X^2}$$

$$\rho_{rad} = \frac{7.3 \times 10^{12}}{X^2} \text{ ergs/cm}^3 \quad .$$

Now, assuming a dipole field strength and $B_s = 10^{12}$ gauss, we have for $\gamma = 3$, $B \leq 30$ gauss, and so the magnetic energy density, $B^2/8\pi$, is

$$< 36 \text{ ergs/cm}^3 \quad .$$

Setting $\rho_{rad} < B^2/8\pi$, we have

$$\frac{7.3 \times 10^{12}}{X^2} < 36$$

or

$$X^2 > 2.0 \times 10^{11} \text{ cm}^2$$

or

$$X > 4.5 \times 10^5 \text{ cm}$$

very approximately. This corresponds to a size in the emission frame γ times larger. This shows that if the radiation is cyclotron, its coherence cannot be produced by a single bunch of particles since $X >> \lambda$, where λ is the observed wavelength of the radiation.

Of course, if the radiating region is essentially two dimensional, this conclusion does not hold. For then the maximum size of the emission region which we calculated is the dimension along the line of sight. The other dimensions could be infinite (if the region were flat) without affecting the coherence of the radiation due to the bunch. A calculation of the radiation density at the emission region would then have X to be transverse dimension of the emission region. Thus, in order for a single bunch to produce the coherency, we would have an emission region some 20 cm thick and 10^6 cm wide, a flatness of better than 2 parts in 10^5 over ten kilometers. This may be possible, but seems unlikely.

Finally, we must contend with the broad band character of pulsar sub-pulse emission. One way to produce quasibroadband cyclotron radiation is with semi-relativistic particles. In such a case, where γ is of the order of a few for the electrons, the spectrum will consist of lines at the harmonics of the cyclotron frequency. In turn, if the magnetic field of the emission region varied across its dimensions by an amount sufficiently great as to make the cyclotron frequency on one side double that on the other side, the resulting radiation would appear to be broad band at any frequency greater than the smallest cyclotron frequency. This would mean that the magnetic

field strength on one side of the region would be twice that on the other. Such variation in a radial direction is not feasible for cyclotron emission at or about $\gamma = 3$ and with dimensions < 4.5% of the light cylinder radius in the emission frame. This would correspond to only a 4.5% change in β from one side of the emission region to the other, and since $B \propto \beta^{-3}$,

$$dB \propto -3\beta^{-4}\, d\beta$$

or at $\beta \simeq 1$

$$\Delta B \propto -3\Delta\beta \quad ,$$

a 4.5% change in β would yield only a 15% change in B. Thus, the spectrum would be made of gaps and bands of radiation at widely separated frequencies. However, if the radiation we see is in the higher harmonics to begin with, the gaps might appear only at very low frequencies and account for spectral turnover there, such as is observed in some pulsars.

Another possible way to get broadband cyclotron emission is by a varying corotational speed across the emission region. In this case also we specify semi-relativistic particles to get harmonics of the cyclotron

frequency, and now let the corotational γ of the emission region be such as to make the relativistic Doppler shift on one side of the region higher than on the other. Since

$$\nu = \nu'/(\gamma(1-\beta \cos \delta))$$

the factor we must worry about is $1/\gamma(1-\beta \cos \delta)$, which we will call D.

$$D = \frac{1}{\gamma(1-\beta \cos \delta)}$$

$$\frac{dD}{d\beta} = \frac{-\frac{d\gamma}{d\beta}(1-\beta \cos \delta) + \gamma \cos \delta}{\gamma^2(1-\beta \cos \delta)^2}$$

Since $\frac{d\gamma}{d\beta} = \beta\gamma^3$, we have

$$\frac{dD}{d\beta} = -\frac{\beta\gamma}{(1-\beta \cos \delta)} + \frac{\cos \delta}{\gamma(1-\beta \cos \delta)^2}$$

Near $\gamma = 3$, the maximum $\frac{dD}{d\beta} \simeq 46$, and the minimum $\frac{dD}{d\beta} \simeq -7$. $\frac{dD}{d\beta} = 0$ near $\cos \delta = \beta$. If the size of the emission region is 4.5% of the speed-of-light cylinder radius, this means that near $\delta = 0$,

$$\Delta D \simeq 46\ \Delta\beta$$

$$\Delta D \simeq 46(.045) = 2.07 \quad .$$

At the point where $\frac{dD}{d\beta} = -7$,

$$\Delta D \simeq -7(.045) = -0.32 \quad .$$

The observation time of the interval where $\frac{dD}{d\beta} \simeq 0$ is very short, and so might be unobservable. At any rate, if the continuum of radiation is being produced in such a way, we must again be observing the higher harmonics, where a Doppler shift of ~0.3 would more than overlap the cyclotron harmonic lines.

A combination of these two effects, the change of magnetic field across the emission region and the change in the Doppler shift, might serve, however, to produce the continuum (or perhaps semi-continuum) seemingly present in the spectra of individual sub-pulses (Taylor, et al. 1974).

Recent observations by Manchester et al. (1974) give strong evidence that the emission from a single pulsar may come from two different processes. They observe that many pulsars exhibit some sub-pulses which are polarized orthogonally to other sub-pulses at the same rotational phase in the period, and that the combination of two orthogonally polarized sub-pulses within the same individual pulse sometimes leads to a resultant very low

linear polarization. The circular polarization at that point does not seem to change much. Although Manchester et al. interpret these observations in terms of different emission regions of orthogonal field direction, or in terms of the operation of a mode switching maser, I feel it much more probable that there are two different radiation processes acting at or near the same point.

One of these processes would be polarized perpendicularly to the magnetic field projection, such as synchrotron or cyclotron radiation, while the other would be polarized parallel to the field projection, such as curvature radiation or stimulated linear acceleration radiation. They could only be polarized orthogonally if the magnetic field direction were the same for both sub-pulses, placing them close together in the magnetosphere. There is some evidence from Figure 14b of Manchester et al. (1974) that the sub-pulses of the polarization orthogonal to the more common polarization have little circular polarization, and if this is the case, one would be tempted to attribute them to curvature or stimulated linear acceleration radiation.

It would be good to say a word about the micro-structure observed in some pulsars at this stage. A good example of such structure is seen in PSR 0950+08 which exhibits fluctuations on a time scale of 10 μs or less

(Hankins, 1971). Immediately this demands that the bandwidth of such fluctuations must be greater than 10^5 Hz. In addition, it suggests that the size of the sub-pulse emission region is

$$\Delta X < c\Delta t$$

or

$$\Delta X < (3\times10^{10})(10^{-5})$$

or

$$\Delta X < 3 \times 10^5 \text{ cm}$$

in our reference frame.

Finally, we will say a word about the drifting subpulses. Previous explanations include slowly changing excitation near the neutron star surface due to plasma waves, and the drift of particle bunches through the magnetic field due to field curvature and gradient. While these explanations may be true, for all I know, I would like to propose yet another possible mechanism. If the emission comes from somewhere in the corotating magnetosphere and is beamed along the field line even in the emission frame, we will see the radiation as strongest close to the time when the field line is pointing along

our line of sight. Relativistic beaming will change the pulse shape somewhat, and shift the peak slightly in time, but will not alter the previous statement significantly. Further, if the sub-pulse emission region is moving systematically along the field line, the time of observed intensity and polarization behavior will also change systematically with time.

As an example, we will take the case where A = 0° and T = 0°. Here we will call θ_1 and t_1 the orbital phase and observation time of sin ϕ = 0, when the field line is pointing along our line of sight. In this case

$$\left(\frac{dt_1}{dt} \right) = \frac{d}{dt} \left(\theta_1 - \beta \sin \theta_1 \right) / \Omega$$

but for A = 0°, cos θ_1 = β/cos T, and for T = 0°, we have cos θ_1 = β. Thus,

$$\left(\frac{dt_1}{dt} \right) = \left(\frac{d\theta_1}{dt} - \beta \cos \theta_1 \frac{d\theta_1}{dt} - \sin \theta_1 \frac{d\beta}{dt} \right) / \Omega$$

$$= \left[\frac{d\theta_1}{dt} \left(1 - \cos \theta_1 \right) - \sin \theta_1 \frac{d\beta}{dt} \right] / \Omega$$

$$= \left[\frac{1}{\gamma^2} \frac{d\theta_1}{dt} - \sin \theta_1 \frac{d\beta}{dt} \right] / \Omega \quad .$$

But $\theta_1 = \arccos \beta$ so

$$\frac{d\theta_1}{dt} = - \frac{1}{\sqrt{1-\beta^2}} \frac{d\beta}{dt} = -\gamma \frac{d\beta}{dt}$$

and

$$\left(\frac{dt_1}{dt} \right) = \frac{d\beta}{dt} \left(- \frac{1}{\gamma} - \sin \theta_1 \right) / \Omega$$

$$= \frac{d\beta}{dt} \left(- \frac{2}{\gamma} \right) / \Omega$$

For a typical pulsar with drifting sub-pulses, PSR 0809+74 of 1.29 second period,

$$\frac{dt_1}{dt} \simeq - .0048$$

(taken from the data of Taylor et al., 1971), so that

$$\left(- \frac{2}{\gamma} \right) \frac{d\beta}{dt}/\Omega = - .0048$$

$$\left(- \frac{2}{\gamma} \right) \frac{d\beta}{dt} = - \frac{.0048\ p}{2\pi}$$

$$\frac{d\beta}{dt} = \frac{\gamma(.0048)(1.29)}{4\pi}$$

$$\frac{d\beta}{dt} = \gamma(.00049) \quad .$$

For $\gamma = 1$, or emission from the surface, this would imply that

$$\frac{dr}{dt} = \frac{c}{\Omega}\frac{d\beta}{dt} = \frac{.00049\ c}{\Omega}$$

or

$$\frac{dr}{dt} = \frac{(.00049)(3\times10^{10})}{(4.87)} = 3 \times 10^{6} \text{ cm/sec}$$

or

$$\frac{dr}{dt} = 30 \text{ km/sec outward} \quad ,$$

a not unreasonable velocity of an emission region. For $\gamma = 2$,

$$\frac{dr}{dt} = 60 \text{ km/sec} \quad ,$$

also reasonable. Carrying this idea further, the total change in t_1 is only about -100 ms, or -.08 p, and since

$$\frac{dt_1}{dt} = \left(-\frac{2}{\gamma}\right)\frac{d\beta}{dt} \,/\, \Omega$$

$$\Delta t_1 \simeq \left(-\frac{2}{\gamma}\right)\Delta\beta \,/\, \Omega$$

so that

$$\frac{\Delta t_1}{P} = - \frac{2}{\gamma} \frac{\Delta\beta}{2\pi} = - \frac{\Delta\beta}{\pi\gamma} \quad ,$$

and

$$\Delta\beta = - \frac{\pi\gamma\Delta t_1}{P} = - .25\ \gamma \quad .$$

For $\gamma \simeq 1$, this implies that β need change by a total of .25, not enough for relativistic effects to become of great importance, but enough for the change in γ to produce some curvature in the drift bands, as Backer (1973), has found for some pulsars. For $\gamma > 1$, β needs to change a great deal for the total observed effect to be produced. In this case, the mechanism may not be as attractive, unless definite changes in polarization properties and pulse shapes are observed between very early and very late sub-pulses.

A corollary to this proposition for the marching sub-pulses may help explain the double peaked structure of some pulsars' integrated pulses, as well as the change in component half-width with frequency observed by Taylor et al. (1974). This would also be a product of emission beamed along the magnetic field lines. For small values of T, double linear polarization minima are possible, as was

discussed in Part I of this dissertation. These minima of sin ϕ, and corresponding pulse peaks, would be separated approximately by

$$2t = 2(\theta_1 - \beta \sin \theta_1 \cos T) / \Omega$$

for very small values of T, and thus, taking T = 0° and A = 0° we have cos $\theta_1 = \beta$, and

$$2t = 2(\theta_1 - 1/\gamma) / \Omega$$

and

$$2t = 2(\arccos (\beta) - 1/\gamma) / \Omega$$

$$2t = 2(\arcsin (\tfrac{1}{\gamma}) - \tfrac{1}{\gamma}) / \Omega .$$

One of these peaks would correspond to the outward flow of particles along the field line, and the other to an inward flow (if there is one). As one can see, as γ increases, 2t decreases. Also, as γ increases, relativistic effects become more important, and the pulse peaks become more asymmetrical, being inclined by relativistic beaming effects more toward the center of the profile, where the factor R is greatest. In some cases, R may be great

enough to make a third, centrally located component in the integrated profile.

In Figure 152 is shown a plot containing both the time between the minima of linear polarization for A = 0° and the maximum allowed value of T for which double minima are possible, according to Table 4 of this dissertation. If the integrated profile double peaks are due to the mechanism suggested here, both an approximate value of β and a maximum value for T for the emission region may be picked off this plot, if A ≃ 0°. F. G. Smith (1971b) claims that there is evidence that A > 0° for the emission of sub-pulses, but does not state what that evidence is. At any rate, for values of A different from 0°, the time between double linear polarization minima is greater than for A = 0°, all other parameters being equal.

Since integrated pulse components get closer together in time for pulsars of double pulse structure as frequency goes up (Smith, 1972), this might indicate that higher frequency radiation is emitted from regions of higher γ than that at lower frequencies.

Observational tests of this hypothesis which seem to be easily made are tests of individual pulse polarizations. The behavior predicted by the model is that there should be rapid polarization angle sweeps of near 180° near to the peaks of the individual pulses, that linear

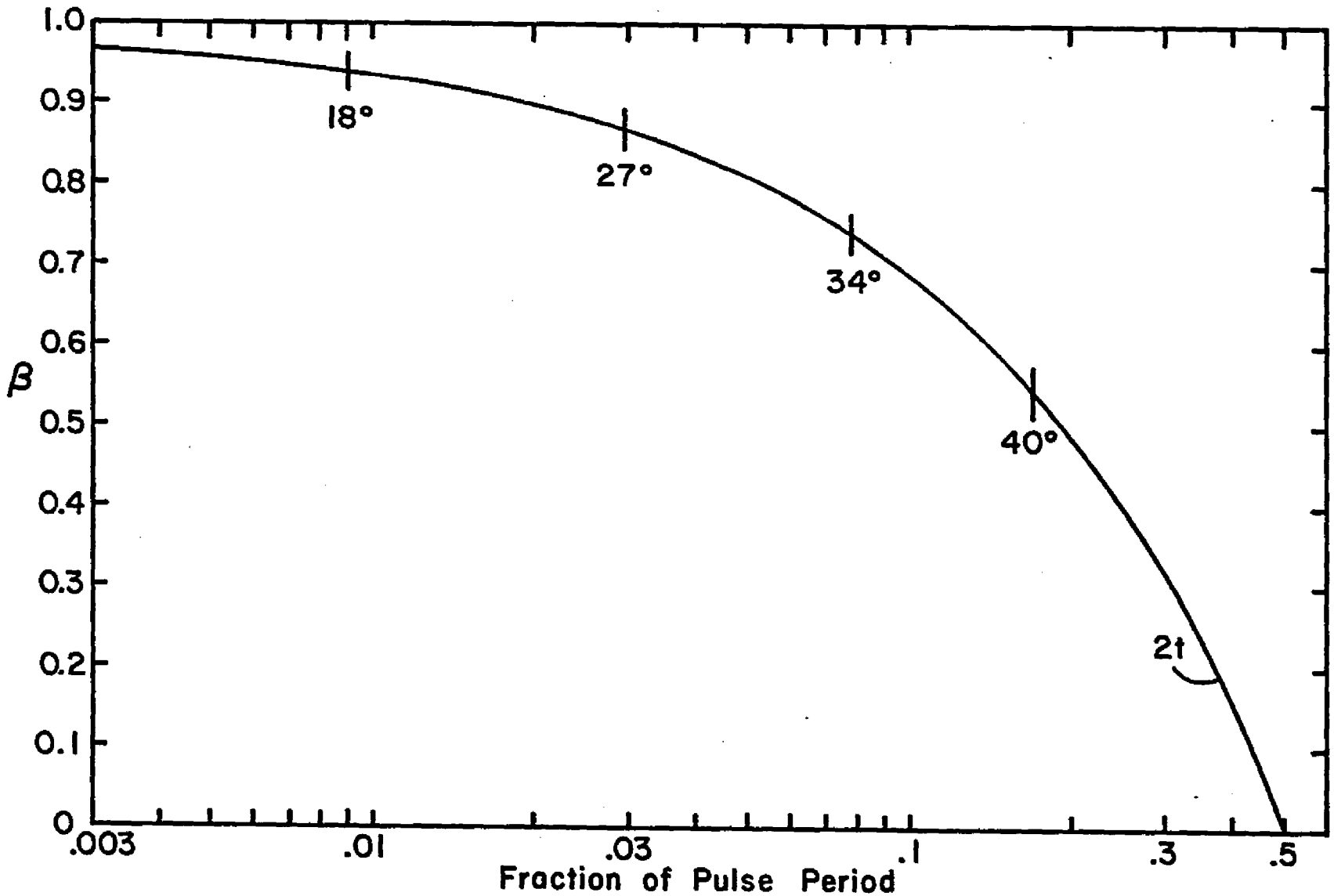

Figure 152. Time Between Polarization Minima, and Maximum T of Double Minima

polarization minima should come at these times, and that the individual pulse peaks should be somewhat nearer the center of the profile than these rapid polarization changes. Figure 6b of Manchester et al. (1974) shows some pulses which seem to bear out these predictions, and others in which the case is not clear cut. Further work with other pulsars is necessary to clarify this point.

I would like to conclude these remarks on physical models by reiterating that:

(1) There may be two or more orthogonally polarized emission processes going on in the same region of the magnetosphere.

(2) The variation of sub-pulse intensity peaks from the times of extrema in polarization may indicate that the emission regions are corotating at a distance from the neutron star.

(3) Some interesting properties of pulsar radiation, such as marching sub-pulses and the variation of integrated profiles with frequency, may be tentatively explained by assuming that the radiation is beamed in the emission frame, and that emission may come from varying points along the same magnetic field line.

In the next section, the assumption that the generalized relativistic vector model holds for emission from sub-pulses will be tested against observations of a

few representative pulsars and further conclusions about pulsar emission and evolution will be derived.

D. Fits by the Relativistic Vector Model

In this section we will assume that the generalized single vector model is a valid description of the polarization changes within a single sub-pulse in a pulsar. Fits of the model to various "representative" pulsars will be presented, and the correlation between various model parameters and other observed properties will be discussed. In the final section, a possible interpretation of the period-pulse-width distribution in pulsars will be presented, based on these correlations, and finally, an attempt will be made to incorporate all we have learned into a model for pulsar sub-pulse emission.

1. A Fit to the Crab Nebula Pulsar PSR 0531+21

This pulsar is unique in that it is the only pulsar which is known to be pulsing in the optical regime. In the optical, there are two pulses separated by less than half of a rotational period. In the radio, the brighter of these pulses is preceded by a so-called "precursor" pulse at low frequencies, but this disappears at high radio frequencies. This pulsar has also been detected in the infrared, ultraviolet, X-ray and γ-ray regimes. The period of this pulsar is the shortest known, 0.033 second,

and its rate of rotational energy loss is the highest known. It is presumed to power the Crab Nebula which surrounds it.

In the optical, Hegyi et al. (1971) and Horowitz et al. (1972) have shown that all of the observed pulses of the main (or stronger) pulse have the same shape and the same strength, to within the limits of photon statistics. In the radio, it is not known whether all of the ordinary pulses are of the same shape, although it is known that there are occasional "giant" or "jumbo" pulses which are not all alike, in that they may come at different rotational phases within a window of a few milliseconds (Sutton et al., 1971). Although there seem to be giant main pulses and giant interpulses, no giant precursors have been found (Gower and Argyle, 1972, Argyle, 1973). The precursor seems to be modulated less than the other pulses (Backer, 1973).

It is hard to tell exactly what to associate with a sub-pulse in the Crab pulsar. Accordingly, we will try to fit the optical observations with the relativistic vector model, since all of the optical pulses are apparently the same, and since ordinary individual radio pulses are too weak to yield significant results about the change of polarization.

In Figure 153 is shown a theoretical fit of the relativistic vector model to the polarization behavior of the main pulse in a "heart-shaped" diagram as has already been explained in Section I. C. of this dissertation. Figure 154 shows a fit to the secondary or inter-pulse in the optical. The data shown were obtained by Ferguson et al. (1974) with the 229 cm telescope, located on Kitt Peak in Arizona, and owned by Steward Observatory of The University of Arizona. Data gathering and reduction procedures are explained in Ferguson et al. (1974). For the model fits, it was assumed that $P = P_o \sin \phi$.

It should be mentioned that in order to compare theory and observation for the optical radiation from this pulsar, an assumed value for the impressed linear polarization arising from the medium between the pulsar and observer had to be included in the data reduction. As explained in Ferguson et al. (1974), the relativistic vector model could not be valid unless the observed minimum in the pulsar's linear polarization looped about the origin. Allowing this to be so, the relativistic vector model predicts an extrinsic polarization arising in the intervening space of 2.4 to 4.1 per cent at 145° - 180° position angle. A best fit value of 3.6% at 167°.5 position angle has been subtracted from the observations presented herein, in relatively good agreement with an interstellar

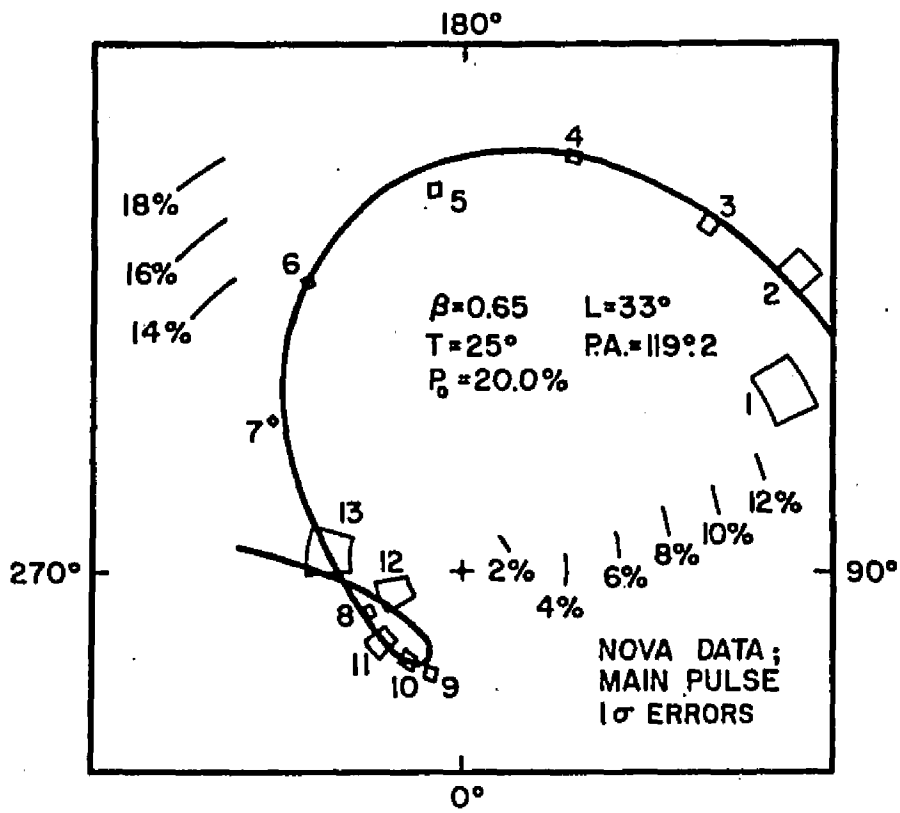

Figure 153. A Theoretical Fit of 2Ψ vs. sin ϕ for the Optical Main Pulse of PSR 0531+21

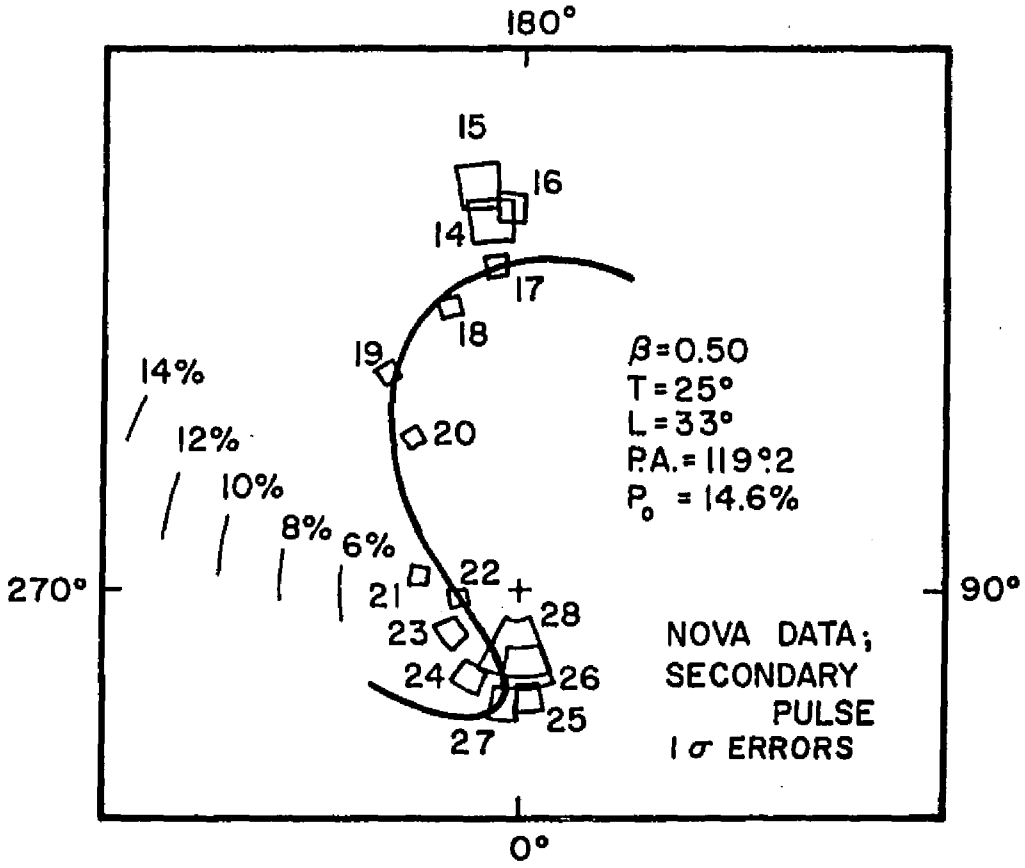

Figure 154. A Theoretical Fit of 2Ψ vs. sin ϕ for the Optical Secondary Pulse of PSR 0531+21

polarization for the Crab Nebula of 2% at 160° measured by P. Martin and J. R. P. Angel (private communication).[1]

In Figures 155 and 156 are shown the time behavior of the polarization for the Crab pulsar main pulse, and for the secondary pulse in Figure 157 and 158. In the theoretical model fits to the observations, the parameter A, the longitudinal deviation of the local magnetic field from the meridian plane in the corotating frame, has been set equal to zero, simply for convenience.

As can be seen, the fits of the model to the observations are very good except for the extreme trailing edge of the secondary pulse, where the model does not accurately reflect the position angle changes with time.

The parameters of the model fits for PSR 0531+21 are given in Table 8 below. P. A. is the position angle of the rotation axis, defined by $0° = \Psi + P.A.$

TABLE 8

Parameters for PSR 0531+21

	Main Pulse	Secondary
β	0.65	0.50
T	25°	25°
A	0°	0°
L	33°	33°
P.A.	119°2	119°2
P_o	20%	14.6%

1. Dr. P. Martin is currently with the Dept. of Astronomy at the Univ. of Toronto and Dr. J. R. P. Angel is at Steward Observatory, The Univ. of Arizona, in Tucson.

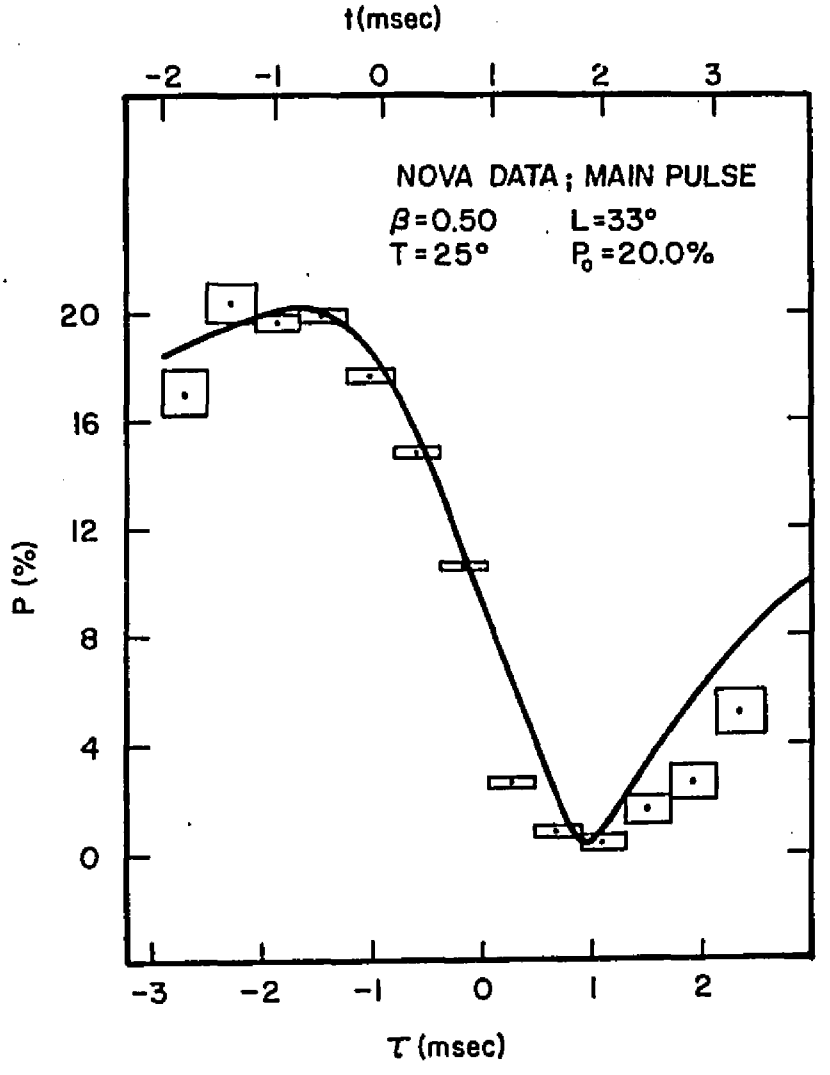

Figure 155. A Theoretical Fit of the Polarization Amt. vs. Time for the Optical Main Pulse of PSR 0531+21

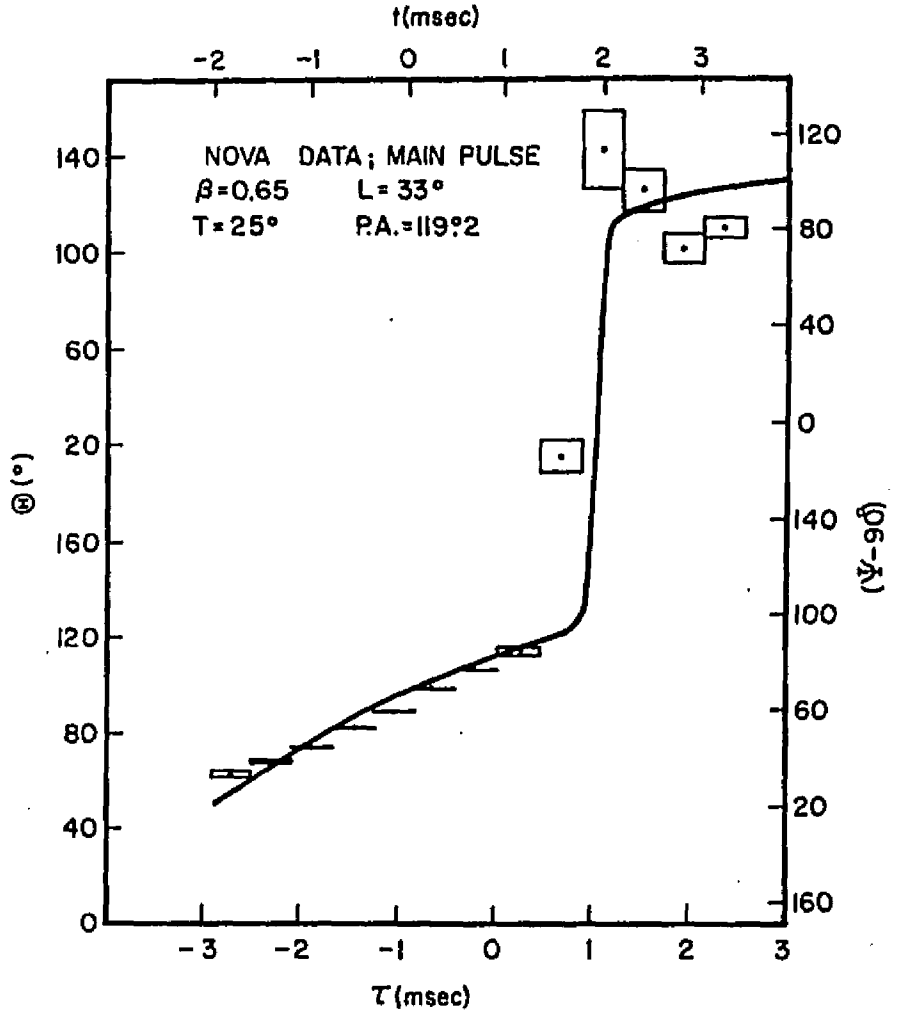

Figure 156. A Theoretical Fit of the Polarization Position Angle vs. Time for the Optical Main Pulse of PSR 0531+21

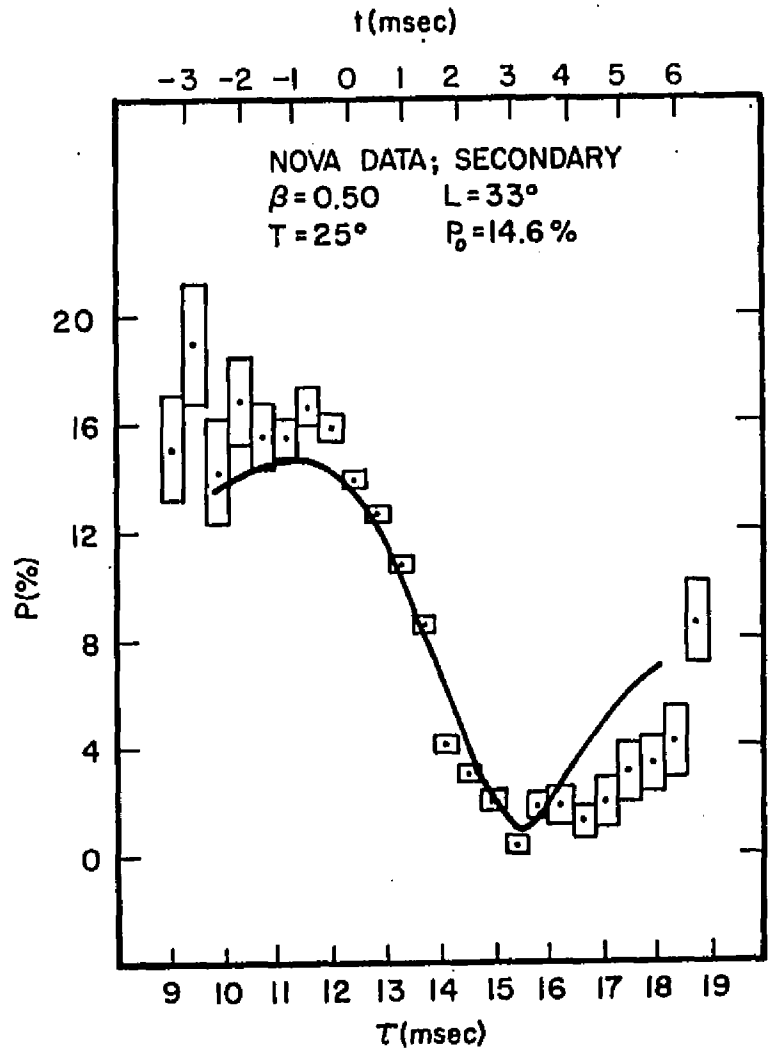

Figure 157. A Theoretical Fit of the Polarization Amt. vs. Time for the Secondary Pulse of PSR 0531+21

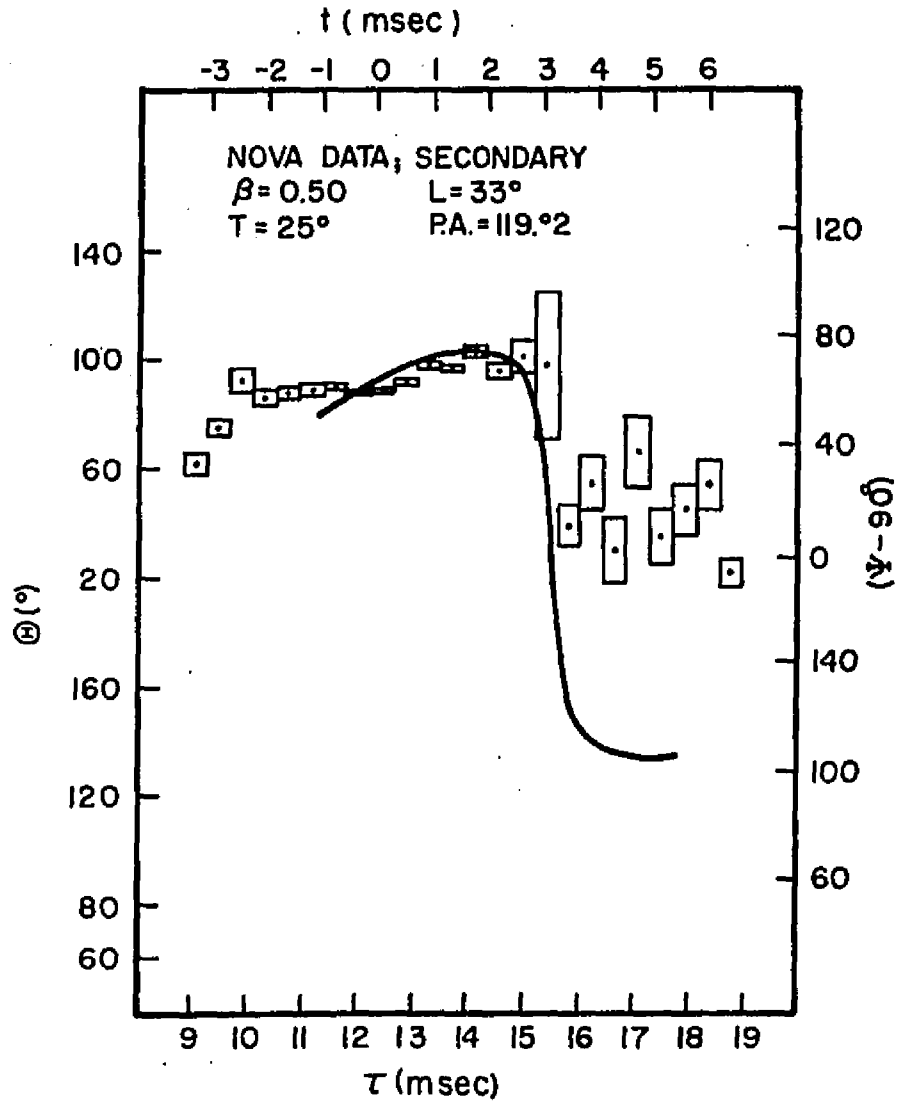

Figure 158. A Theoretical Fit of the Polarization Position Angle vs. Time for the Secondary Pulse of PSR 0531+21

It is reiterated here that the observed polarization variations are not consistent with the non-relativistic single vector model (Cocke et al., 1973). In that paper, it was shown that the fact that the maximum in the linear polarization percentage is coincident with the time of sin ϕ = 1 excludes the possibility of a fit to the observations by the non-relativistic model. Here it will be shown that, in addition, the variation of polarization position angle with rotational phase is inconsistent with the non-relativistic model. In the non-relativistic model, the beaming of radiation along magnetic field lines accounts for the pulses. The main pulse of the Crab pulsar has a peak which is unresolved with a time resolution of 32 μs (Papaliolios et al., 1970). Therefore we can assume that if the radiation is coming from near the stellar surface the peak must come when we are looking very nearly straight down on the magnetic pole, and thus L = T to a high degree of approximation. From Equations (5) and (25.5) of this dissertation, setting L = T, we find that

$$\frac{d\Psi}{d\theta} = \frac{-\sin L(1-\sin\theta)}{\cos^2\theta + \sin^2 L(1-\sin\theta)^2}$$

Setting $(90°-\theta) = \zeta$, so that

$$\sin\theta = \cos\zeta \approx 1 - \frac{\zeta}{2} \quad \text{for} \quad \theta \approx 90°$$

and

$$\cos\theta = \sin\zeta \simeq \zeta$$

and with a little algebra, we find that

$$\frac{d\Psi}{d\delta} = \frac{\sin L}{2 + \sin^2 L(\frac{\zeta^2}{2})} \tag{30}$$

Let f be the fraction of the rotational period, so that $\zeta = 2\pi f$ + constant. We pick the constant so that $f = \zeta = 0$ at the pulse peak. Then

$$\frac{d\Psi}{df} = 2\pi \frac{\sin L}{2 + \sin^2 L(\frac{4\pi^2 f^2}{2})} \tag{31}$$

which is valid for $f<<1$.

From Cocke et al. (1973) and Ferguson et al. (1974) we find that the minimum in $|\frac{d\Psi^\circ}{df}|$ for the Crab pulsar main pulse is at $f \simeq -.07$ where $\frac{\Delta\Psi}{\Delta f} \simeq 400°$/period. Plugging these values in Equation (31) we have

$$\sin L = [2 + \sin^2 L\ (\frac{4\pi^2(.0049)}{2})]\ \frac{1}{360}\ \frac{d\Psi}{df}$$

or

$$\sin L = [2 + \sin^2 L(.097)]\ (0.0028)\ (400)$$

$$= [2 + (.097)\ \sin^2 L]\ (1.1)$$

or

$$\sin L = 2.2 + 0.11 \sin^2 L$$

or

$$\sin L > 2.2 \quad .$$

This is clearly impossible.

If we count ζ and f not from the pulse peak but from the time of maximum position angle sweep rate the result is not much changed. In fact, from (31) we see that for f small, the result is almost independent of f for L = T and is given in Table 9.

TABLE 9

Position Angle Sweep Rate for $\beta=0$, $\theta \simeq 90°$

L = T	$\frac{d\Psi°}{df}$
0	0
30°	90°/period
45°	126
60°	157
90°	180

Of course Table 9 is strictly valid only for L = T, in which case there is an instantaneous position angle jump of 180° at $\zeta = 0$. For the real case, L ≃ T, the results

in Table 9 give only an approximate value which may be used where $\frac{d\Psi}{df}$ is approximately linear. This is a minimum possible $|\frac{d\Psi}{df}|$ if the polarization angle changes monotonically through the pulse (i.e., the line of sight passes above the magnetic field line) and a maximum possible $|\frac{d\Psi}{df}|$ if the polarization angle sweep changes direction in the pulse (i.e., the line of sight passes below the magnetic field line). For the Crab pulsar, the change of polarization position angle is approximately linear with time before the main pulse peak, so our calculation above holds.

So we have seen that neither the behavior of the linear polarization percentage nor of the polarization position angle can be explained by the non-relativistic single vector model, but both are well explained by the relativistic vector model, with the emission coming from about halfway between the neutron star and the speed-of-light cylinder.

Of course, any geometrical model for the polarization variations implies that for emission from any one locality, the polarization variations will be similar at different frequencies. Drake (1971) states that the radio and optical pulse peaks come within 0.2 ms of each other for the main pulse of the Crab Nebula pulsar, if radio dispersion delays are taken into account. This is strongly suggestive that the radio and optical pulse emission

regions are less than $c\Delta t = (3x10^{10})\ (2x10^{-4}) = 6x10^{6}$ cm away from each other. Thus, we should expect, in the relativistic single vector model, for their polarization behaviors to be similar.

Manchester (1971b) found that for the Crab Nebula pulsar, the radio and optical polarizations at the rotational phase of the precursor pulse are orthogonal to each other, but that at the phase of the main pulse peak they may be parallel. However, he did not allow for the effects of interstellar polarization on the optical polarization, an effect which is negligible at the precursor phase due to its relatively high percentage polarization, but which is significant at the pulse peak phase, the percentage linear polarization being nearly zero there. In particular, at a time between 0.24 and 0.65 ms after the main pulse peak, the effect of the correction for an extrinsic polarization may amount to 90° (Ferguson et al., 1974) which would make the optical and radio polarizations orthogonal there also.

Schönhardt (1971), observing with a better time resolution than Manchester, reported a position angle sweep at 408 MHz similar to that observed in the optical. Thus, there is some evidence that the polarization position angle behavior of the Crab pulsar main pulse and precursor may be similar in the radio and optical, but that one is

orthogonal to the other. This is similar in many ways to the existence of orthogonal radio sub-pulses at the same rotational pulse in other pulsars, and may be an indication that in the Crab pulsar, two or more different and orthogonally polarized emission mechanisms are operating at the same place in the magnetosphere. This might also explain the difference between the radio and optical pulse shapes, since different mechanisms could have different beaming characteristics.

Furthermore, in Figure 159 is shown the comparative percentage linear polarizations in the radio and optical. One can see that the behaviors are qualitatively similar, allowing for the fact that the radio polarizations are everywhere about a factor of five greater than the optical. In this Figure, the time axes have been shifted up to 0.2 ms with respect to each other (the maximum allowable). The radio data are taken from Manchester (1971a) corrected for a rotation measure in Manchester (1971b) and the optical data are from Ferguson et al. (1974) corrected for 3.6% extrinsic polarization at 167?5. This similarity in behaviors is very suggestive that the geometrical interpretation afforded by the relativistic vector model is adequate for both the radio and optical. In addition, it may be possible that the radio precursor and main pulse are emitted at the same place in the magnetosphere, and

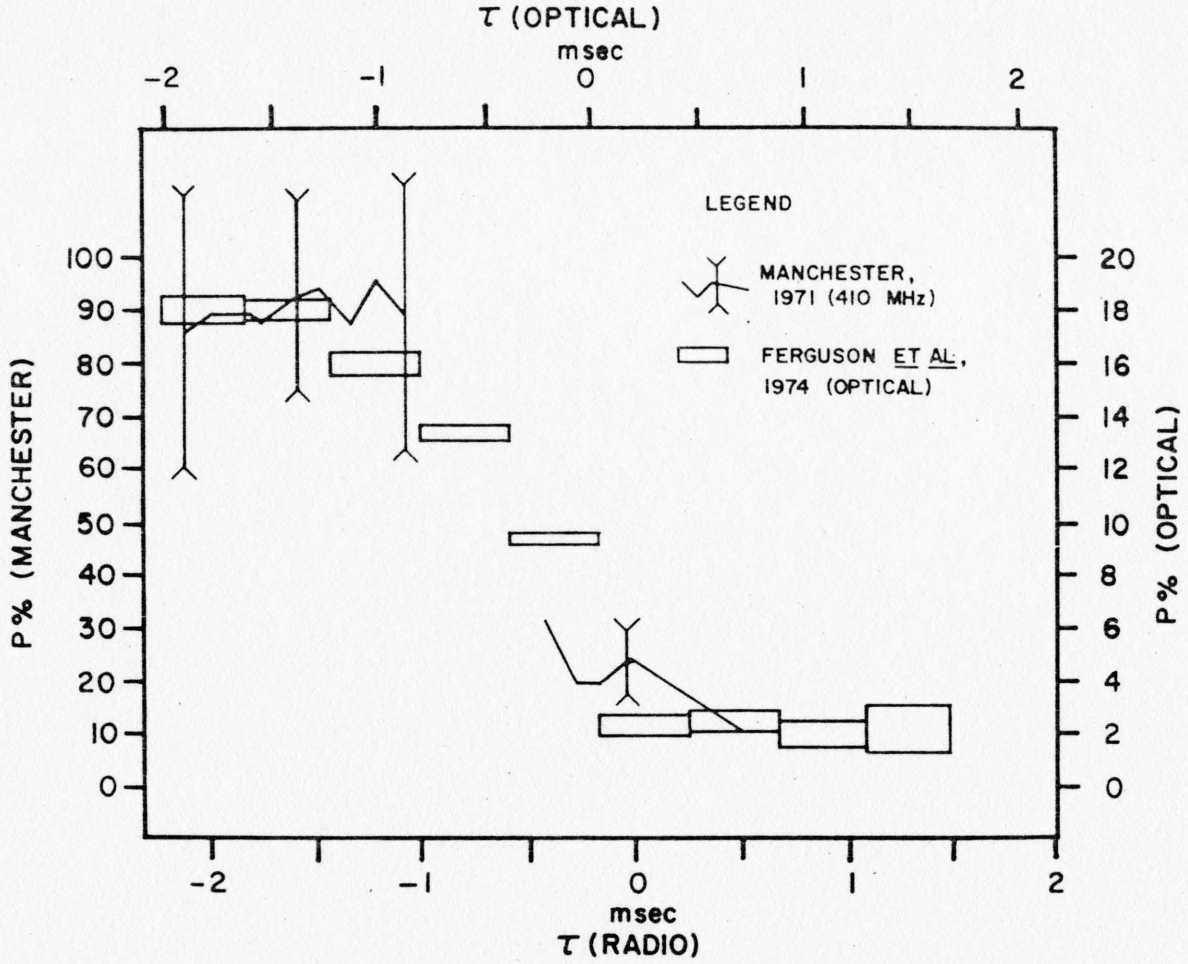

Figure 159. Radio and Optical Polarization Amounts for Main Pulse and Precursor of PSR 0531+21

that their very different properties (pulse shape, modulation, etc.) are due to differences in emission process or coherence producing process, and not to a difference in place of emission.

Much of the foregoing is speculation, but it points out the importance of obtaining better observations of individual radio pulses. If the polarization angle sweep found in the optical is not really there in the radio, our conclusions will be invalid. If the radio individual sub-pulses are very different in width or polarization from the integrated pulse, the conclusions we have made will be invalid. All depends on whether the integrated radio and optical polarizations are indicative of polarizations in the individual radio sub-pulses.

An indication of whether we are correct in assuming that the relativistic vector model applies to the integrated pulses as well as the sub-pulses may be found from the change of observed light curve with color in the Crab pulsar. From Equation (7) and Equation (8) of this dissertation, we see that if the radiation is emitted from a relativistically corotating emission region, the amount of relativistic beaming at each phase in the observed pulse depends on the spectrum of the emission in the emission frame.

Cocke and Ferguson (1974) have analyzed observations of the Crab Nebula pulsar secondary pulse to see if the changes in light curve previously reported by Muncaster and Cocke (1972) could be explained by the relativistic vector model. Observations obtained by Cocke and Ferguson in December, 1973 and January, 1974 with the Steward Observatory 229 cm reflector on Kitt Peak in two different colors, corresponding to the U and V bands of the Johnson photometric system, were examined for light curve differences. Due to timing difficulties, the main pulse data were not of sufficient quality to allow comparisons between the light curves in the two colors. However, the secondary pulse observations were of higher quality. Using the parameters of the relativistic vector model already obtained from earlier polarization observations, Cocke and Ferguson found that the observed light curve color differences were well explained by the relativistic vector model if the difference in spectral index of the optical radiation in the U and V bands was $\Delta\varepsilon \simeq 0.3$, a value not contradicted by observation (Oke, 1969). The fit obtained by the model is shown in Figure 160.

Thus, the optical radiation in the secondary pulse is consistent with its having been emitted from a localized region of the magnetosphere, corotating with the neutron star at a radius one-half that of the

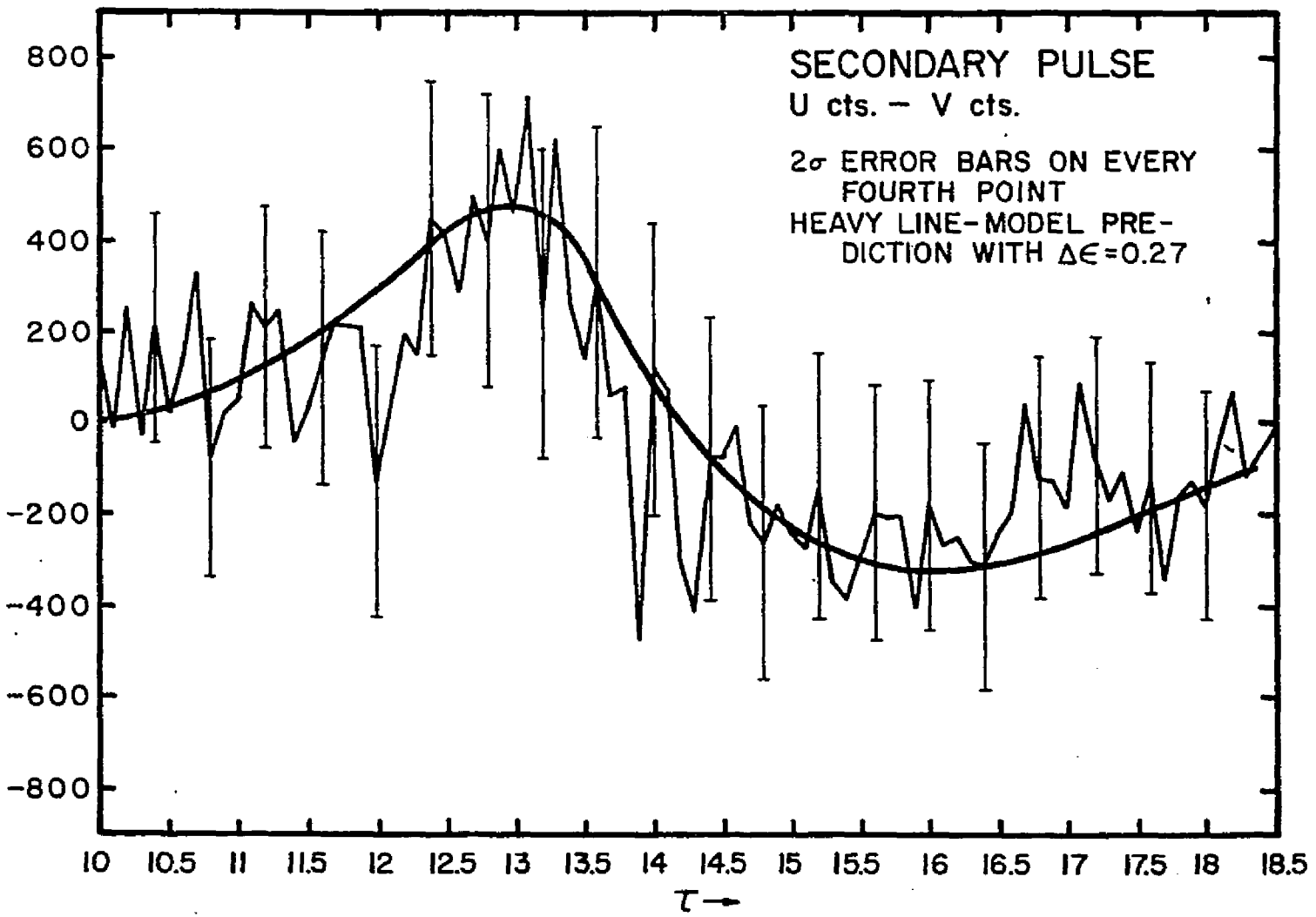

Figure 160. A Theoretical Fit to the Light Curve Changes With Color for the Secondary Pulse of PSR 0531+21

speed-of-light cylinder, and also consistent with the view that the sub-pulses and integrated pulses may be similar or identical in shape.

Such a situation with the integrated pulse and sub-pulses obtains for another very short period pulsar, PSR 0833-45 (Ekers and Moffet, 1969) and thus might not be considered odd for the Crab Nebula pulsar.

It was suggested in Ferguson (1971a) that the effect of relativistic beaming might cause the pulse peaks in the optical to be advanced ahead of the polarization minima for the Crab pulsar. That is, since $I = I' R$, the variation in R through each pulse might cause the maximum intensity, coincident with the polarization minimum in the emission frame, to be advanced ahead of it in our observer's frame. As has been suggested in Section II.C. of this dissertation, such an effect might also occur in the sub-pulses of other pulsars. Here we will investigate the mathematics of such a mechanism in further detail.

Assuming that the spectrum of the pulsar is an approximate power law in the optical,

$$I \underset{\sim}{\propto} \nu^{-\varepsilon}$$

we have from Equation (7), that

$$R \simeq [\gamma(1-\beta \cos \delta)]^{-3-\varepsilon}$$

Now $\cos \delta = \cos \theta \cos T$, so that

$$\ln R \simeq (-3-\varepsilon) \; [\ln \gamma + \ln(1-\beta \cos \theta \cos T)]$$

and

$$\frac{d \ln R}{d\theta} = (-3-\varepsilon) \; \left(\frac{\beta \sin \theta \cos T}{1-\beta \cos \theta \cos T} \right)$$

Recall that $t \simeq (\theta-\beta \sin \theta \cos T) \; p/2\pi$ and using

$$\frac{d \ln R}{dt} = \frac{d \ln R}{d\theta} \frac{d\theta}{dt}$$

we find first that

$$\frac{d\theta}{dt} = \frac{2\pi}{p} \frac{1}{1-\beta \cos \theta \cos T}$$

and then that

$$\frac{d \ln R}{dt} = (-3-\varepsilon) \frac{2\pi}{p} \frac{\beta \sin \theta \cos T}{(1-\beta \cos \theta \cos T)^2} \qquad (32)$$

For $A = 0°$, the minimum linear polarization comes when $\cos \theta = \beta/\cos T$ (Equation 20), so that in this case

$$\frac{d \ln R}{dt} \simeq (-3-\epsilon) \frac{2\pi}{p} \beta \gamma^4 \sqrt{\cos^2 T - \beta^2} \qquad (33)$$

In order to see if the pulsar pulse peak has been shifted, we recall that

$$I = R I'$$

so that

$$\ln I = \ln R + \ln I'$$

or

$$\frac{d \ln I}{dt} - \frac{d \ln R}{dt} = \frac{d \ln I'}{dt}$$

and if

$$\frac{d \ln I}{dt} - \frac{d \ln R}{dt} = 0 \ ,$$

then

$$\frac{d \ln I'}{dt} = 0 \ ,$$

and we have found the intrinsic pulse peak. For our pulse peak region, $\frac{d \ln R}{dt} < 0$ always, so that $\frac{d \ln I}{dt} < 0$ at the time of the intrinsic pulse peak.

Our difficulty with the Crab pulsar arises from the fact that the trailing edge of the main pulse drops very rapidly, so that in order for $\frac{d \ln I'}{dt} > 0$ at that point (before the polarization minimum), $\frac{d \ln R}{dt}$ must be very large and negative. Quantitatively, if the intrinsic pulse peak is to be at the time of linear polarization minimum,

$$\frac{d \ln I}{dt} > \frac{d \ln R}{dt}$$

at the time of the observed pulse peak. From Cocke and Ferguson (1974) we find that the number of photon counts on the trailing edge of the main pulse drops by 14638 from about 100,000 in the time 0.1 ms. This corresponds to

$$\frac{d \ln N}{dt} = \frac{d \ln I}{dt} = -1.46$$

where t is in ms, and where N is the number of counts per data bin. So, we insist that

$$\frac{d \ln R}{dt} < -1.46$$

and find that for $T = 0°$, $\beta = 0.74$ would suffice to shift the main pulse peak assuming $\varepsilon = 0.2$ (Oke, 1969). For

$T = 25°$, $\beta = 0.80$ would be necessary. The fits of the relativistic vector model to the main pulse polarization imply a value of β less than this, but if the emission region is distributed somewhat in radial distance (see Zheleznyakov and Shaposhnikov, 1972) it is not unreasonable that the pulse peak could come from this radial distance.

Performing a similar analysis for the secondary pulse, we find that

$$\frac{d \ln N}{dt} = \frac{d \ln I}{dt} = -0.549$$

(Cocke and Ferguson, 1974) and that if $T = 0°$, $\beta = 0.54$ would be necessary to shift the pulse peak and if $T = 25°$, $\beta = 0.58$ would suffice. These values are very close to the $\beta = 0.50$ found from polarization measurements, and the peak shifting mechanism proposed seems highly possible in this case.

Of course the foregoing discussion is based on $A = 0°$, an assumption which has not been justified. For values of A different from 0, our Equation (32) will have a different form, and will yield somewhat different values of β.

Because of the uncertainties involved in the model fit to the Crab Nebula pulsar it seems premature to try to

find the emission pattern along the locus of the line of sight in the emission frame for this pulsar. However, we can say this much: the emission must be beamed in the emission frame for both the main and secondary pulse emission regions. Otherwise, the pulse peaks would be coincident with and symmetrical about the times t = 0 when the emission regions were traveling most nearly toward us. In reality the main pulse peak comes 0.9 msec after the emission region is most closely approaching us (if A = 0°), and the pulse shape is highly asymmetric. A similar statement can be made about the secondary pulse. Of course, if the emission for each pulse does not come from a localized region, but is spread out in longitude in the magnetosphere, this conclusion is not valid, but neither, in that case, is the fit of the relativistic vector model so that the discussion becomes meaningless.

In concluding the discussion about the model fit to the Crab pulsar observations, I would like to call attention to the work of Zheleznyakov and Shaposhnikov (1972). In that work, it was shown that the observed spectrum of the Crab Nebula pulsar in the optical and X-ray region is consistent with incoherent synchrotron emission from far out in the neutron star magnetosphere. Those authors assume that $\beta = 0.72$, but point out that the length of the emission region would be about 0.3 times

the radius of the speed-of-light cylinder, making their value of β compatible both with the value I derived from polarization characteristics, and with the value necessary to shift the optical main pulse peak. If their hypothesis that synchrotron emission is responsible for the optical and X-ray emission is correct, the possible orthogonality of the radio and optical polarizations might imply that the radio emission is curvature radiation, stimulated linear acceleration radiation, or some other type of radiation which is linearly polarized parallel to the projection of the magnetic field lines in the emission region.

2. A Fit to the Vela Pulsar PSR 0833-45

This pulsar has been reported to be pulsing in the X-ray and γ-ray regions of the spectrum as well as in the radio (Harnden and Gorenstein, 1973, Harnden et al., 1972, Albats et al., 1974). The pulse shape in the radio is simple at low frequencies, but becomes more complex at high frequencies. The period of this pulsar is the second shortest known, 0.089 second, and its rate of rotational energy loss is second only to the Crab pulsar. It is surrounded by the Gum Nebula with which it is generally spatially associated.

For the Vela pulsar, the question of what to identify with the sub-pulse is more clear than for the

Crab pulsar. Ekers and Moffet (1969) reported that PSR 0833-45 has individual pulses identical to the integrated pulse, on the average, at a frequency of 2295 MHz. The rare exception to this is a narrow, circularly polarized component. The integrated pulse is nearly 100% linearly polarized on the leading edge.

An interesting feature of this pulsar was discovered by McCulloch et al. (1972). This is the fact that at very early times on the leading edge of the integrated pulse, the position angle sweeps rapidly through more than 180°, the linear polarization percentage remaining approximately constant at ~50%. We will discuss a possible explanation of this feature somewhat later in this section.

In Figure 161 is shown a theoretical fit of the relativistic vector model to the observations of the integrated pulse polarization obtained by Manchester (1971a) at a frequency of 1665 MHz, and with a time constant of 140 μs, using the 42 meter steerable telescope of NRAO. In this "heart-shaped" diagram, the time behavior is suppressed, and the error bars are approximately 2σ, as indicated by Manchester (1971a). It can be seen that the adopted fit passes through virtually all of the 2σ error bars.

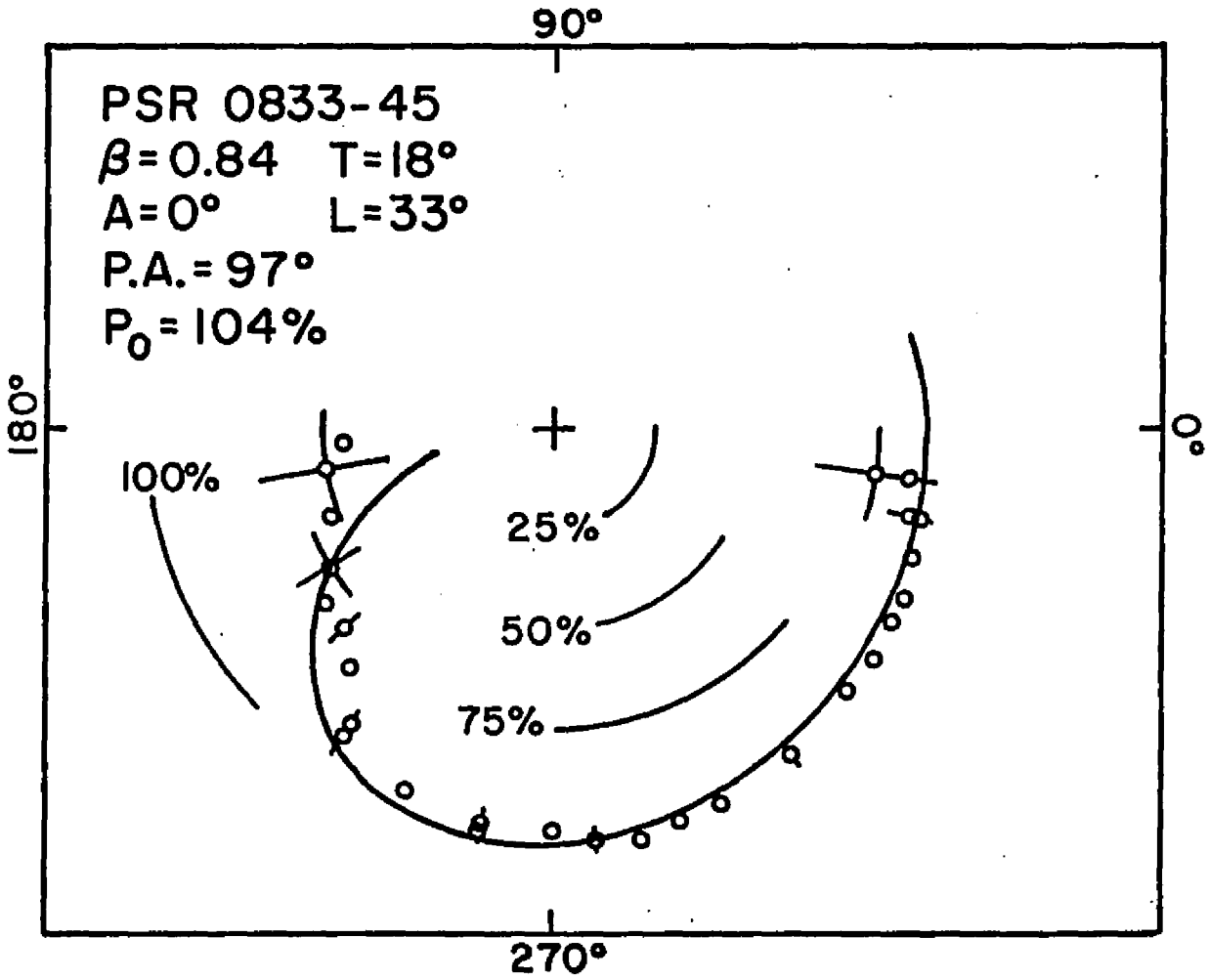

Figure 161. A Theoretical Fit of 2Ψ vs. sin ϕ for PSR 0833-45 at 1665 MHz

In Figures 162 and 163 are shown the time behavior of the same data and the theoretical fit. Here also the fit is good, especially in describing the run of polarization position angle. In these fits, as in all others presented in this dissertation, the value of A was assumed to be zero. Perhaps better fits could be obtained by allowing A to vary, and eventually this must be done to provide a complete specification of conditions within the emission regions, but acceptable fits for A = 0 were found for the pulsars treated in this dissertation, and small variations from this condition will not affect the results too much. Likewise, here it was assumed that $P = P_o \sin \phi$.

The parameters of the model fit to PSR 0833-45 are given in Table 10.

TABLE 10

Parameters for PSR 0833-45

$\beta = 0.84$	$L = 33°$
$T = 18°$	$P_o = 104\%$
$A = 0°$	P?A. $= 97°$

The value of P_o cannot be taken literally, as a polarization greater than 100% is unphysical, but does accurately reflect some degree of systematic error in Manchester's published measurements.

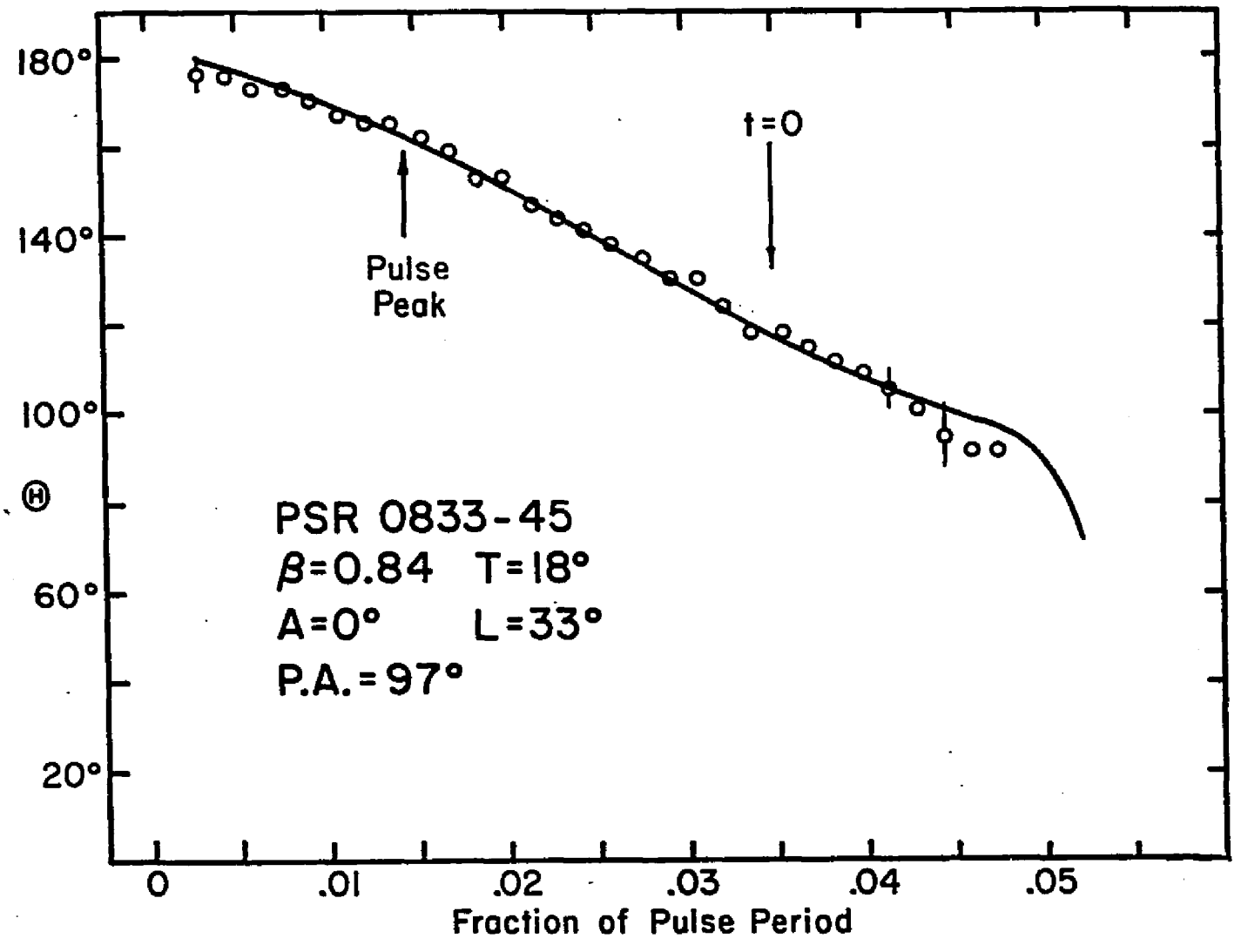

Figure 162. A Theoretical Fit of the Polarization Position Angle vs. Time for PSR 0833-45 at 1665 MHz

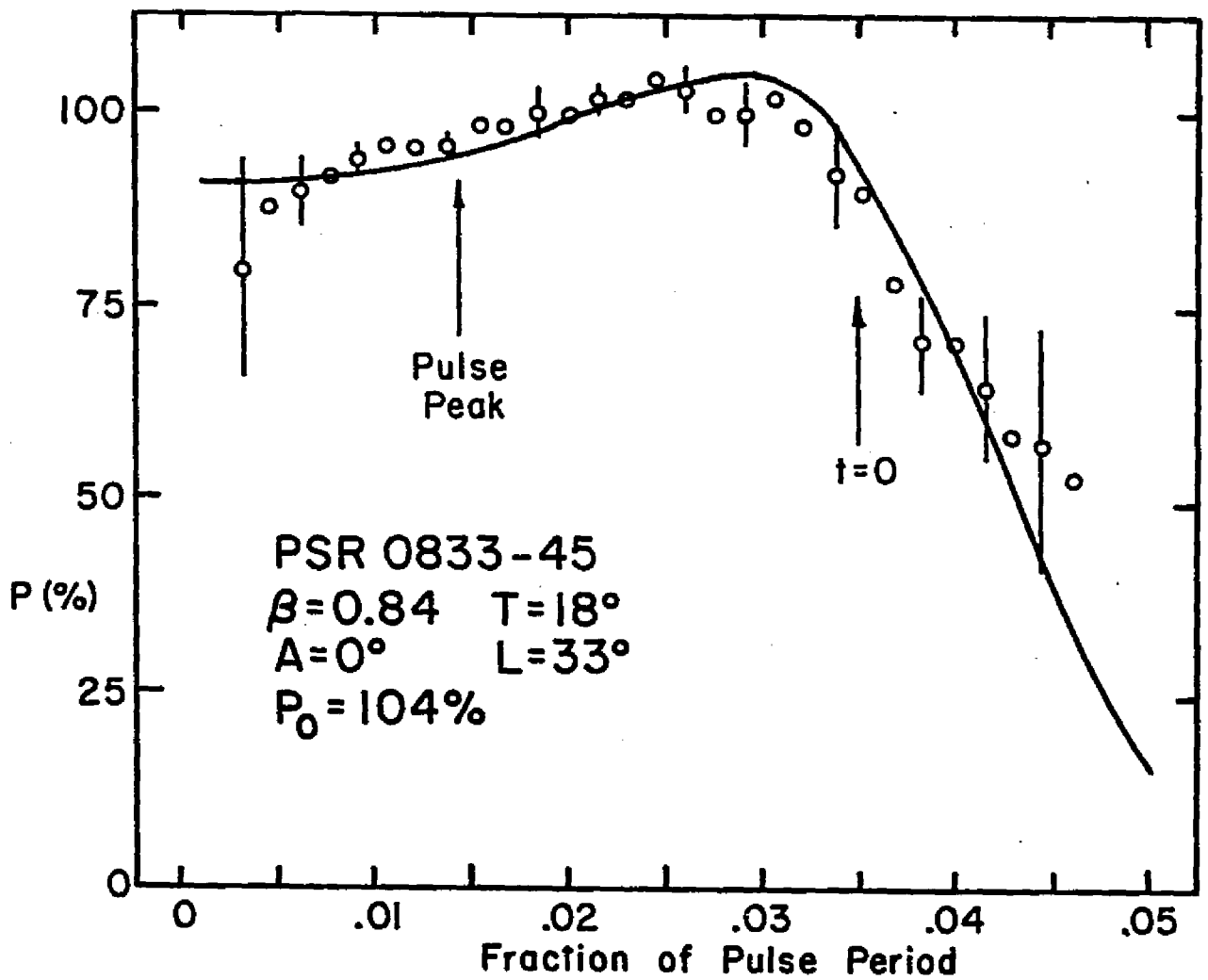

Figure 163. A Theoretical Fit of the Percentage Linear Polarization vs. Time for PSR 0833-45 at 1665 MHz

Manchester does not give polarization position angles nor percentages for times in the pulse where McCulloch et al. (1972) observed the position angle sweep of more than 180° at a frequency of 400 MHz. This feature, if real and as they described it, cannot be due to emission from the same emission region as the main part of the pulse if the relativistic vector model is valid. Strenuous attempts to fit both it and Manchester's measurements which were undertaken by the present author failed miserably. However, if there is another small emission region located far out in the magnetosphere, whose radiation was observed at that rotational phase near the leading edge of the main pulse, it might produce a polarization feature such as is observed.

For example, in Figure 98 is shown the polarization timed behavior for an emission region of $\beta = 0.98$, $T = 37°$, $A = 42°$, $L = -27°$ where such a feature is well exhibited. There, the linear polarization percentage varies only between about 50% and 85%, but the position angle changes by more than 200° within a few percent of the pulsar period. Such behavior is typical for an emission region of high γ, where the magnetic field line passes below our line of sight. There, the relativistic compression of observation times relative to emission times, along with a large aberration of the outgoing light, makes

the changes of polarization parameters very rapid, whether the magnetic field line is close to the line of sight or not.

Of course, the fact that such an effect can be produced by emission from a region very close to the speed-of-light cylinder does not prove that such a region exists. However, I am not aware of how such an effect could be simply produced in any other way. It must be considered a piece of evidence in favor of the hypothesis of relativistically corotating emission regions until another possible explanation is forthcoming.

Predictions based upon the foregoing hypothesis are many. For instance, we would expect the modulation index of this part of the pulse to be very different from the rest, since the contribution of relativistic beaming and the physical conditions present in the emission region would be different. Also, one might expect, in high time resolution studies, to find some structure in intensity at that pulse phase. Komesaroff et al. (1972) have observed an "intensity enhancement" at the proper rotational phase, which they interpret as evidence for a "precursor" pulse similar to that in PSR 0531+21. Whether all precursor pulses are alike, and whether a polarization position angle sweep of over 180° could be produced by the blending of a precursor of constant (or nearly constant)

position angle with a main pulse of changing position angle are topics of importance which should be investigated to provide a possible alternative to the relativistically corotating hypothesis.

At any rate, the simple relativistic vector model can provide an adequate description of the polarization behavior of PSR 0833-45.

In connection with the model fits for PSR 0531+21 and PSR 0833-45, I should like to point out certain similarities in their emission. In the Crab Nebula pulsar, the optical pulses are all similar, as is the case for the radio pulses from the Vela pulsar. Both pulsars exhibit negligible circular polarization in their integrated pulses, although in both there is an occasional narrow pulse of high circular polarization, the "giant" or "jumbo" pulses of the Crab pulsar for example. One is led by such similarities to venture the hypothesis that the emission process is the same in these two pulsars and that it is ordinary synchrotron emission for the radio pulses of PSR 0833-45 and the optical pulses of PSR 0531+21. Such radiation is linearly polarized for a relatively isotropic particle pitch angle distribution. If, however, coherence became greater (through bunching or otherwise) for emitting particles of a particular pitch angle, a spike of highly circularly polarized radiation would be seen when that

pitch angle passed the line of sight. Perhaps such a process could explain the similar polarization properties of the integrated and individual pulses of these two pulsars. A detailed look at the intrinsic polarizations of the regular and rare individual pulses would decide the question.

3. A Fit to the Simple Pulsar PSR 1642-03

This pulsar, of 0.39 second period, has perhaps the simplest integrated pulse shape known. It exhibits a smoothly "Gaussian"-looking integrated pulse shape, with a smooth variation of all polarization parameters through the pulse. There is a non-negligible percentage of circular polarization at most times in the pulse, with a sign reversal at or near the time of maximum linear polarization.

While no good published data exists about the polarizations of individual pulses for this pulsar, the mean sub-pulse width (3.8 ms) is almost as great as the integrated profile width (4.2 ms) so that there can be very little spread in longitude of its sub-pulse emission regions (Taylor et al., 1974). Excluding the possibility that there are some sub-pulses orthogonally polarized to the rest, we may then consider the integrated pulse polarization characteristics to be reasonably representative

of the average sub-pulse, but smeared a small amount in time.

We will fit the theoretical relativistic vector model to observations of the integrated pulse published by Manchester (1971a) obtained at 410 MHz with a timing resolution of 0.4 ms. In Figure 164 is shown the adopted fit in the "heart-shaped" diagram. As before, error bars are approximately 2σ as given by Manchester. One can see that the fit here is reasonably good. Although not all of the error boxes are traversed, the general run of position angle versus linear polarization amount is well reproduced.

Figures 165 and 166 show the fit to the timed polarization behavior. Here the fits are excellent, account being taken of the fact that the 0.4 ms difference between the mean individual pulse width and the integrated pulse width corresponds to 0.001 p. This tends to smear out the polarization percentage behavior especially, since it is rapidly varying through the pulse.

Table 11 gives the parameters of the relativistic vector model fit to PSR 1642-03.

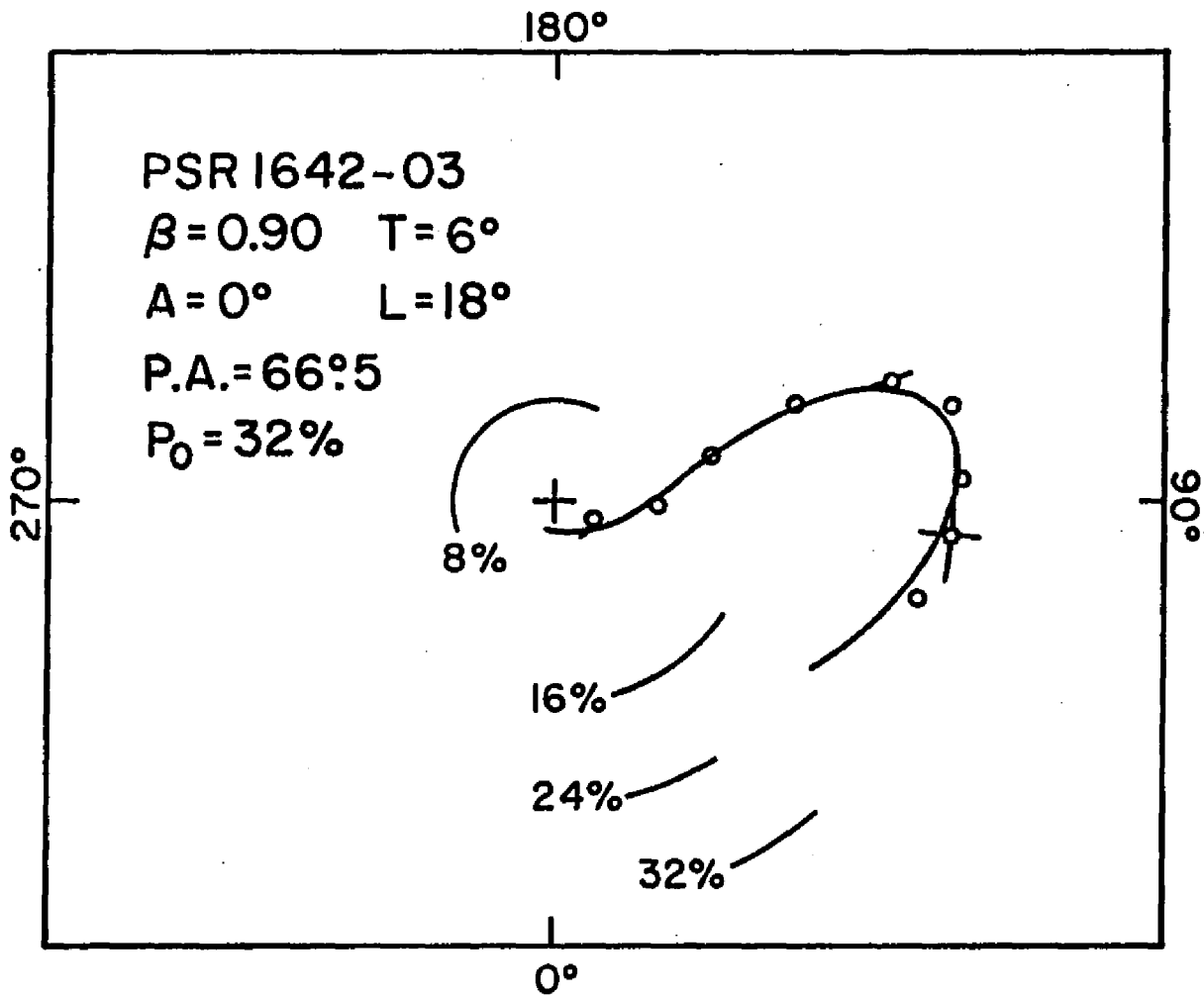

Figure 164. A Theoretical Fit of 2Ψ vs. sin ϕ for PSR 1642-03 at 410 MHz

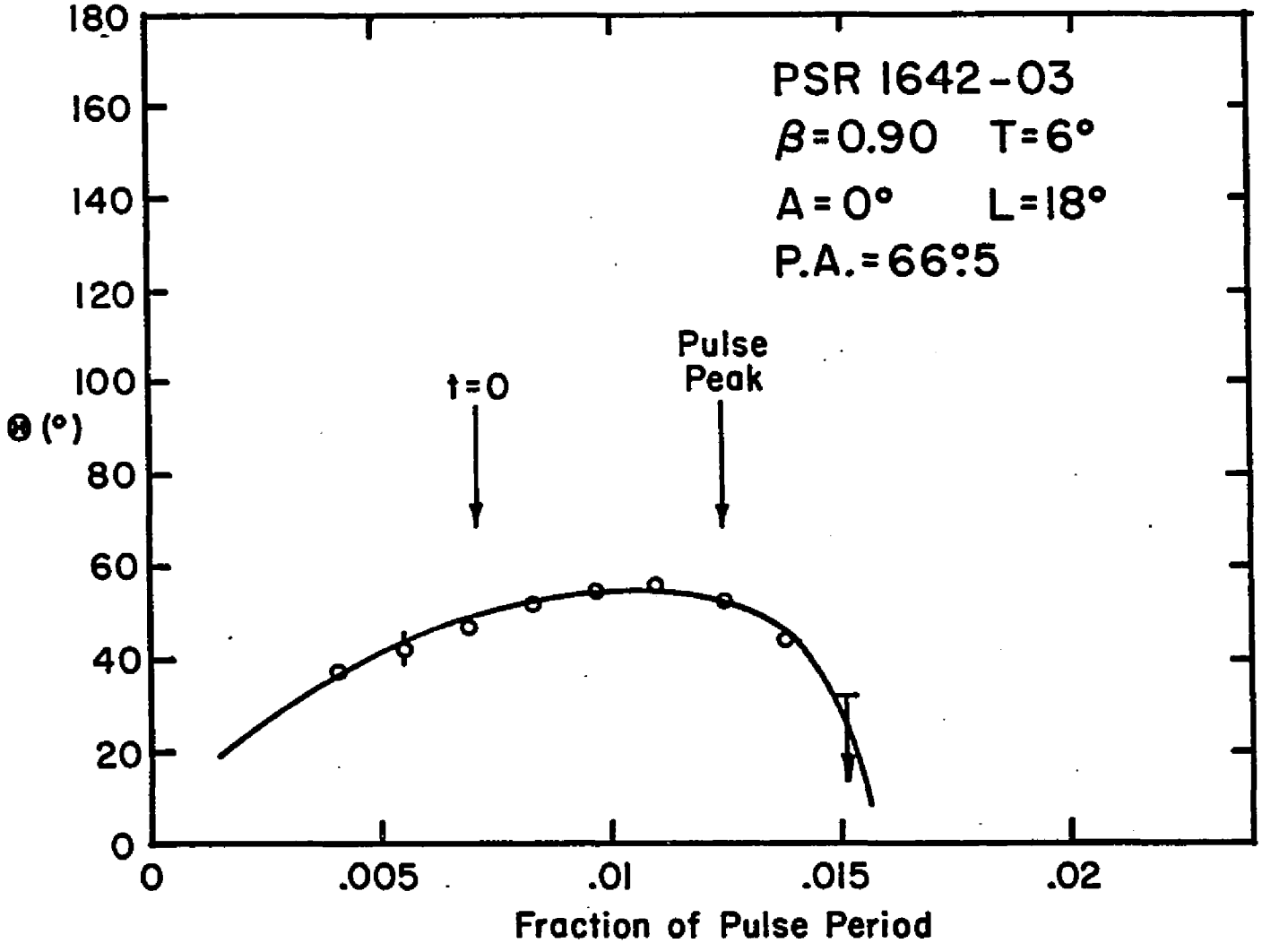

Figure 165. A Theoretical Fit of the Polarization Position Angle vs. Time for PSR 1642-03 at 410 MHz

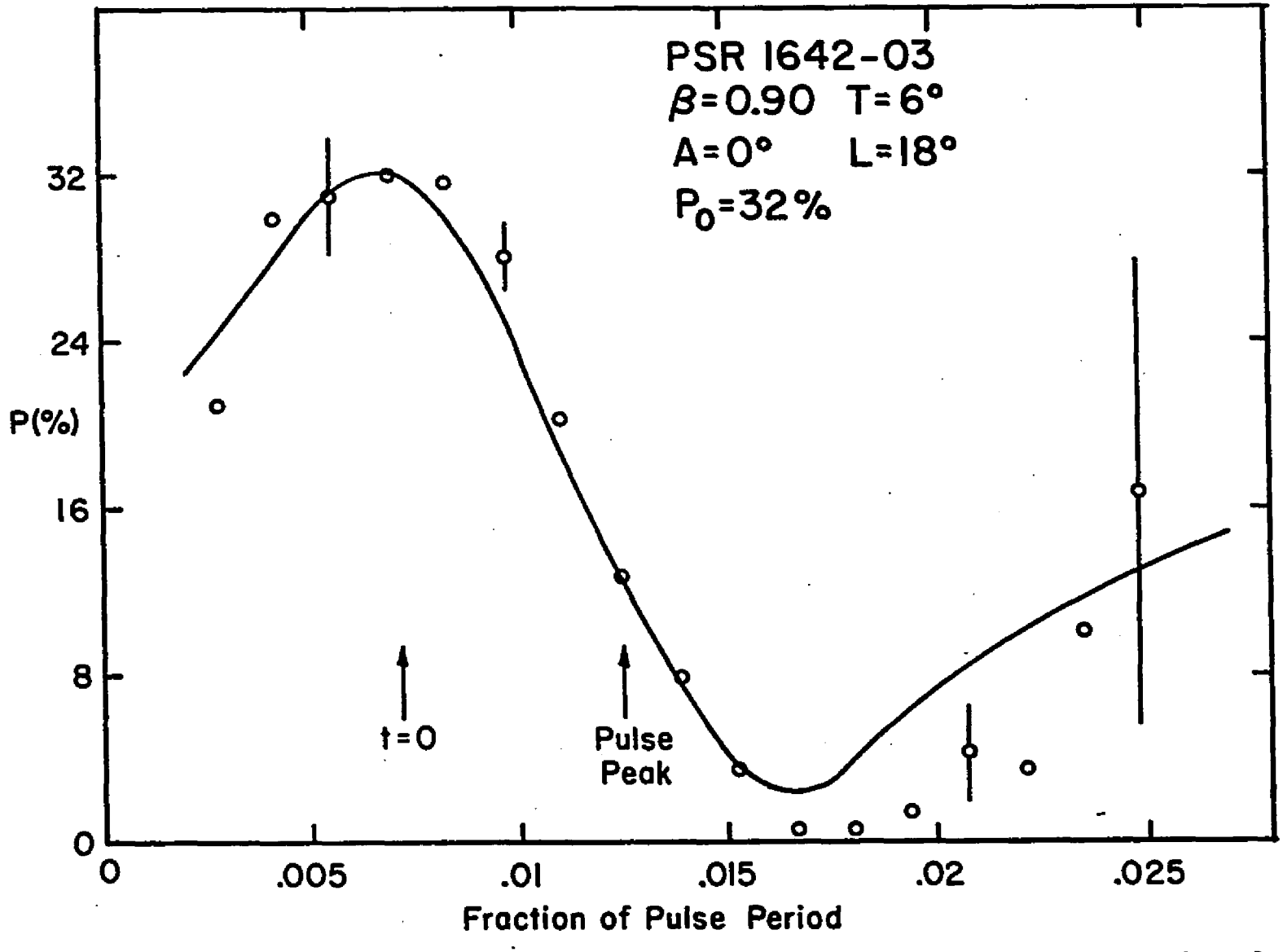

Figure 166. A Theoretical Fit of the Percentage Linear Polarization vs. Time for PSR 1642-03 at 410 MHz

TABLE 11

Parameters for PSR 1642-03

$\beta = 0.90$	$L = 18°$
$T = 6°$	$P_o = 32°$
$A = 0°$	P.A. = 66°.5

This pulsar illustrates the inadequacy of the non-relativistic vector model for describing position angle changes as well as any other pulsar. Here, the maximum rate of change of polarization position angle through the pulse is over 4° in 0.00138 period. This corresponds to $\frac{d\psi^\circ}{df}$ max > 2000°/period, while in Table 9 we see that the maximum the non-relativistic model predicts is 180°/period. Because the direction of sweep of position angle changes within the pulse, our values in Table 9 are valid upper limits to the possible sweep rate on the non-relativistic model. Clearly, the relativistic effects mentioned in Section I.B. are necessary for a fit of a geometrical single-vector model to the observations.

The model fit to PSR 1642-03 also seems to give a good explanation of the variation of the amount of modulation through the pulse. Taylor et al. (1974) show that for PSR 1642-03, the modulation index, defined as

$$m = \sqrt{(\sigma^2 - \sigma_N^2)}/\langle I \rangle \quad ,$$

(where σ_N is the variance of the system noise and σ is the variance of the pulsar signal about its mean level <I>) is greatest near the leading edge of the pulse, and becomes very low near the center of the pulse. In the relativistic model, any variation in the strength of emission will be multiplied by the relativistic beaming factor R, so that all other things being equal, $\sigma \propto R$. In our model fit to PSR 1642-03, the relativistic beaming is greatest near the leading edge of the pulse, and so σ and m will be greatest there in the observer's frame if σ in the emission frame does not vary. Later in the pulse, when the amount of relativistic beaming is less, the modulation index will be smaller. Similar results may obtain for other pulsars whose integrated pulses are similar to their individual pulses. Further work along these lines may be important in our understanding of the modulation of pulsar emission.

4. A Fit to the Simple Pulsar PSR 0329+54

This pulsar is of type S, with weak outriders to the central peak. It has a period of 0.71 seconds. In Section II.C. the individual pulses from this pulsar were used to learn physical information about the location and conditions of its emission regions. In this part, we will fit the relativistic vector model to its individual pulses.

Lyne, Smith and Graham (1971) used individual pulses from this pulsar in support of the contention that the emission from pulsars was cyclotron radiation. They made the point that if the run of polarization were plotted on a Poincaré sphere, all of the sub-pulses showed a traversal of an arc of a great circle which extended more than 180° but which could run at any orientation.

Here we will fit the model to the Stokes average polarization of two pulses shown in Figure 11 of Smith (1972) in order to increase the signal-to-noise ratio. The two pulses are numbers 8 and 9 from the top of that figure. In performing the average, the pulse peaks were shifted so as to be in coincidence, the Stokes parameters were added, the percentage linear polarization calculated from $\sqrt{Q^2+U^2}/I$, and the position angle of polarization from $1/2 \tan^{-1} U/Q$, resolving ambiguities by appeal to the signs of Q and U individually.

In Figure 167 is shown the adopted fit of the model to the published data of Smith (1972) at 408 MHz in the "heart-shaped" diagram. Error bars are estimates of the error in measuring Smith's data from his published plots and do not reflect on the quality of the data. It can be seen that the relativistic vector model affords a very good fit to these sub-pulses. We have assumed again that $P = P_o \sin \phi$.

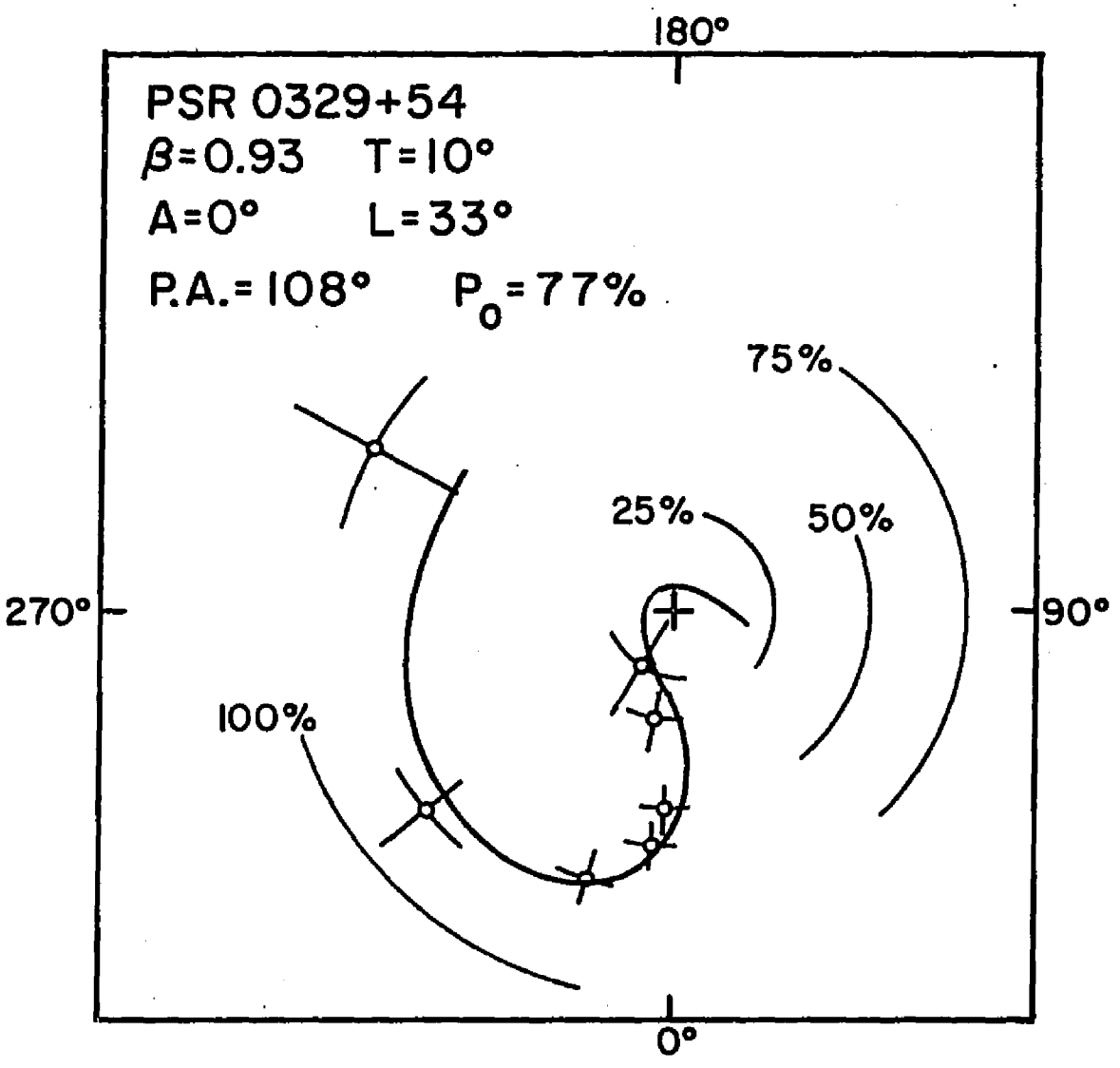

Figure 167. A Theoretical Fit of 2Ψ vs. sin ϕ for PSR 0329+54 at 408 MHz

In Figures 168 and 169 are shown the fit to the time behavior of the linear polarization. Here too the fits are excellent. Table 12 shows the model parameters of the adopted fit.

TABLE 12

Parameters for PSR 0329+54

$\beta = 0.93$	$L = 33°$
$T = 10°$	$P_o = 77\%$
$A = 0°$	P.A. $= 108°$

Since we know from Lyne et al. (1971) that other sub-pulses show a different sort of polarization behavior versus time, we will assume that this is due to differences in A, L and possibly β for different emission regions. However, if the relativistic vector model is correct, they should all follow tracks in the "heart-shaped" diagram (of linear polarization percentage versus twice the position angle) which correspond to roughly the same value of β and exactly the same values of T and P.A. In further work this should definitely be investigated.

The sub-pulses of this pulsar which show a reversal of direction of position angle sweep within the pulse are another proof of the inadequacy of the non-relativistic vector model to describe their behavior. In

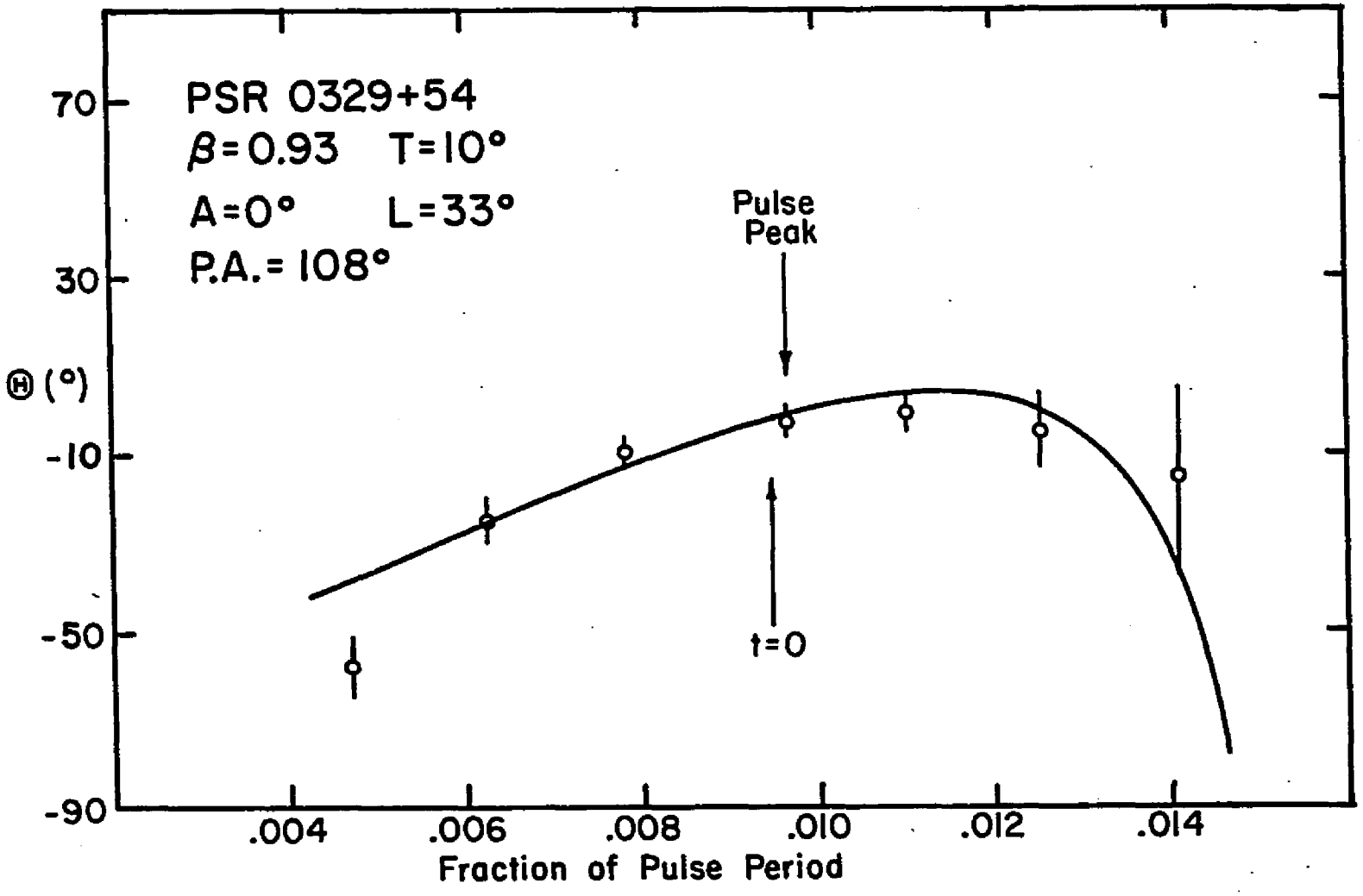

Figure 168. A Theoretical Fit of the Polarization Position Angle vs. Time for PSR 0329+54 at 408 MHz

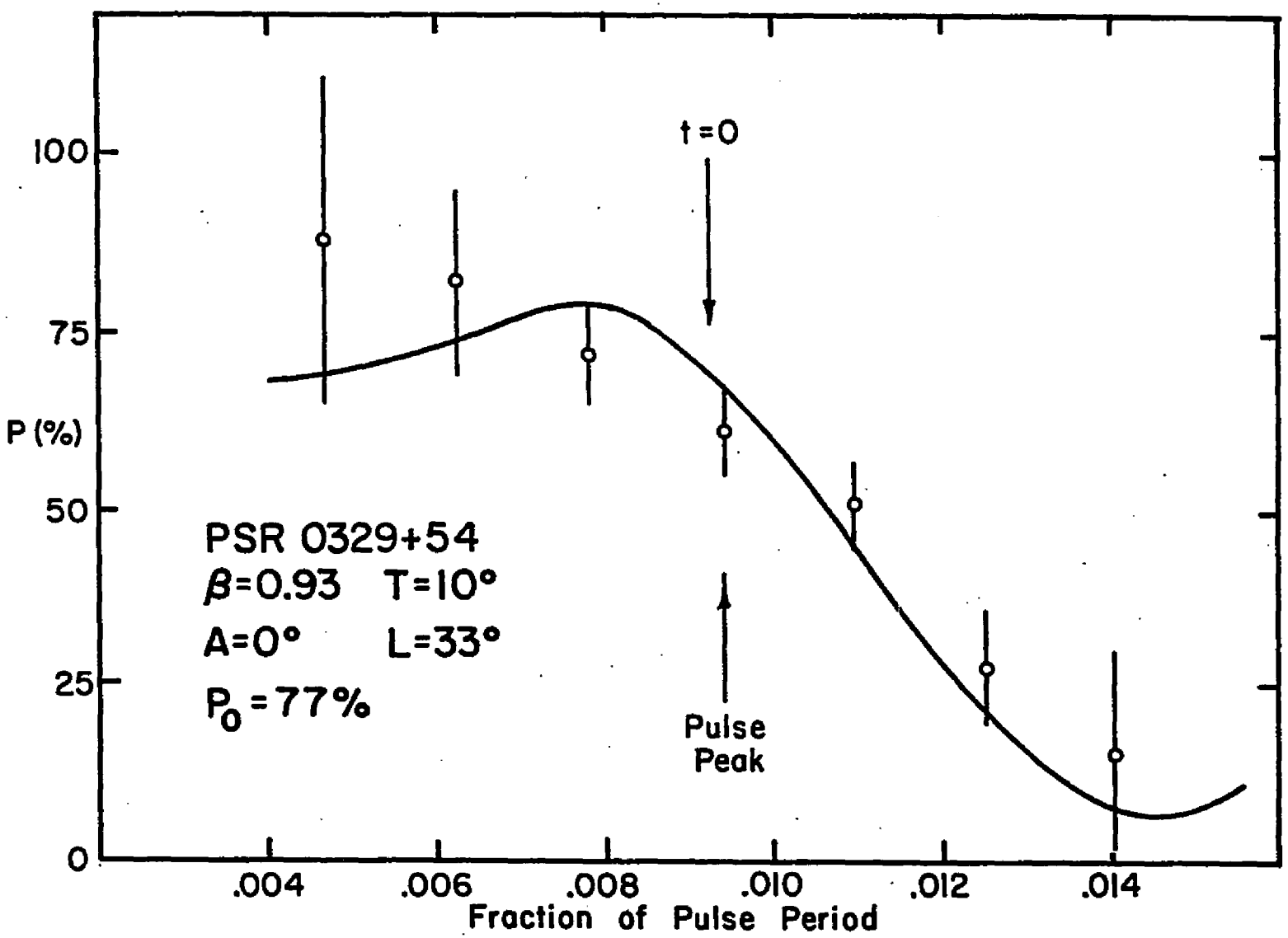

Figure 169. A Theoretical Fit of the Percentage Linear Polarization vs. Time for PSR 0329+54 at 408 MHz

Figure 168 we see that the position angle of polarization changes by at least 20° in 0.0034 period before the direction of sweep reversal. This corresponds to $\frac{\Delta\Psi°}{\Delta f} \simeq 5700°$/ period. From Table 9 we see that this is over thirty times the maximum explainable in terms of the non-relativistic theory. And, in this case, we are dealing solely with sub-pulse observations so that no cry of foul can spring up about using integrated polarization parameters. Manchester et al. (1974) show similar sub-pulse polarization behavior for the abnormal mode of PSR 1237+25 in some sub-pulses.

5. A Model Fit to the "Drifter" PSR 0809+74

Pulsar PSR 0809+74, of period 1.29 second, shows the remarkable drifting sub-pulses of which we made mention in Section II.C. of this dissertation. The drifting pattern repeats every 11 periods, roughly, and there is a good deal of organized change of polarization within the sub-pulses.

Here we will fit the theoretical relativistic vector model to the Stokes average of two synchronous integrations of sub-pulses in PSR 0809+74. The data are taken from Taylor et al. (1971) where sequences of drifting sub-pulses are exhibited, each being the Stokes average of ten drift cycles (measured at a frequency between 230 and

240 MHz) to improve signal-to-noise. To further improve signal to noise, I have performed Stokes averages of their pulses #5 and #16, which show similar polarization behavior of a mean sub-pulse at the same rotational phase, and these are shown in Figures 170, 171, and 172, along with the theoretical model fit, assuming $P = P_o \sin \phi$.

In Figure 170 is shown the adopted model fit to the "heart-shaped" diagram for these data. Error bars again denote uncertainties in measuring their published plots, not in the data themselves. It can be seen that the fit is quite good. Figures 171 and 172 show the time behavior of the linear polarization. Here again the fit is quite good, except near the point where the model predicts a rapid sweep of position angle. Since the time resolution of the data is fully 10 ms, or .008 period, it may be that the rapid sweep was smeared out, making the angle seem to take the "short-route" between two extremes. Parameters of the relativistic vector model fit to the data are given in Table 13.

TABLE 13

Parameters for PSR 0809+74

$\beta = 0.94$	$L = 54°$
$T = 18°$	$P_o = 20\%$
$A = 0°$	P.A. $= 50°$

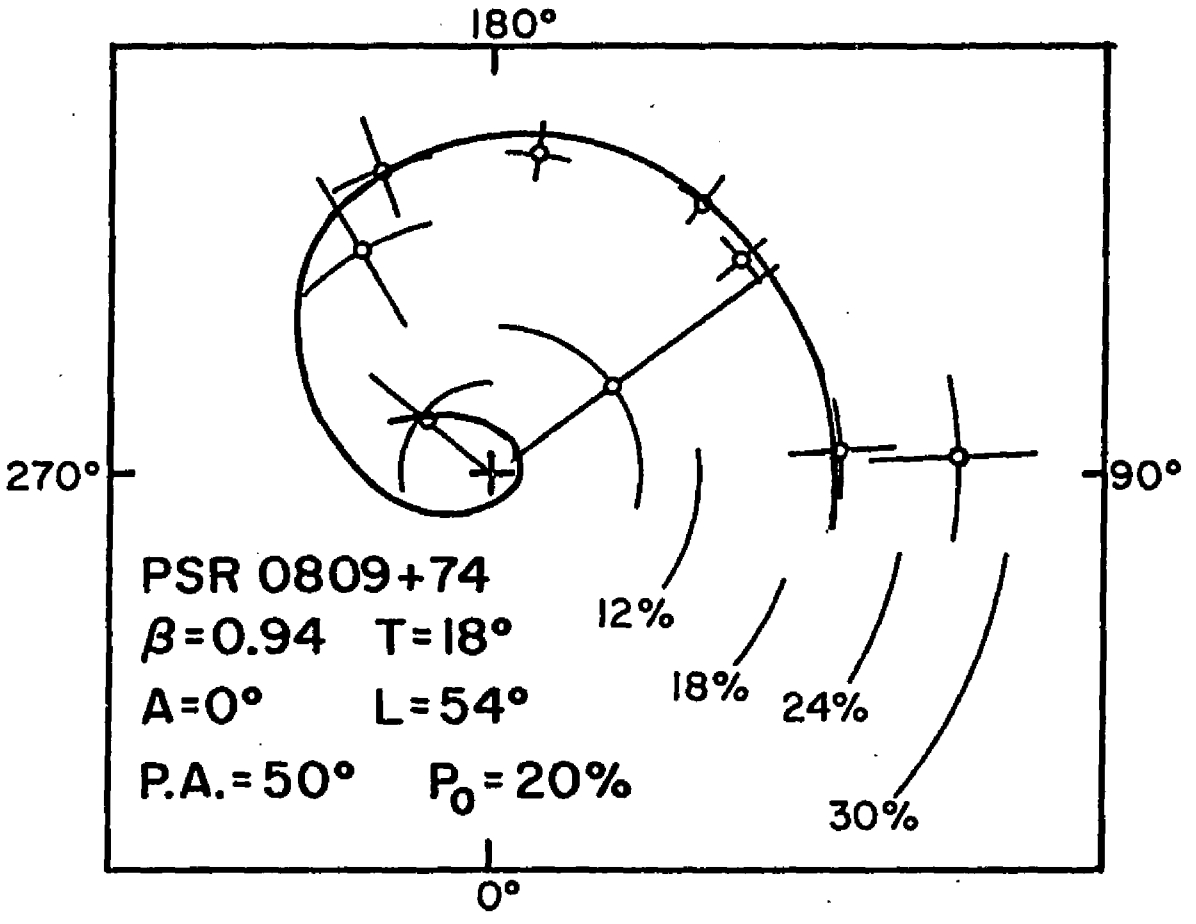

Figure 170. A Theoretical Fit of 2Ψ vs. sin ϕ for PSR 0809+74 at 235 MHz

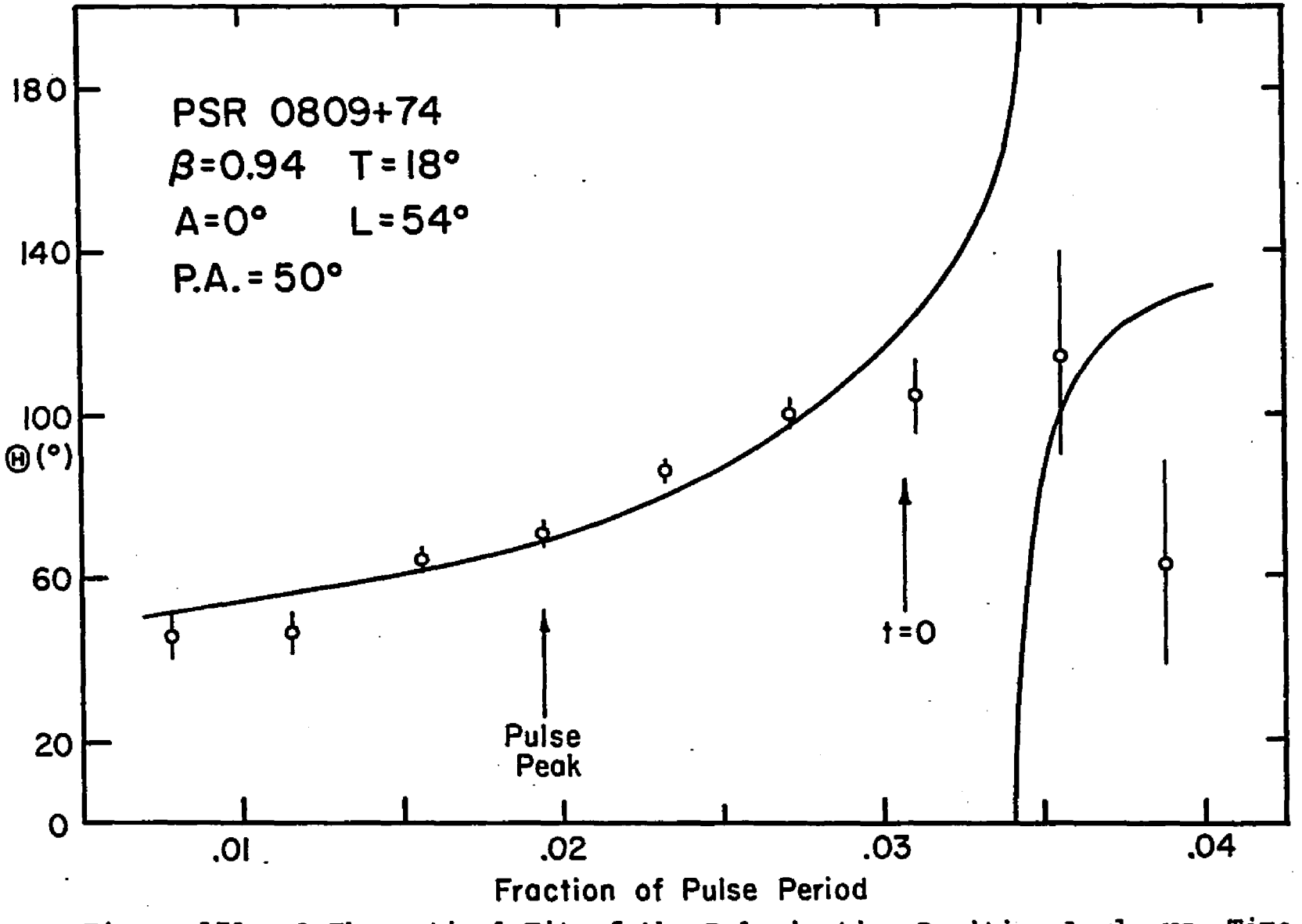

Figure 171. A Theoretical Fit of the Polarization Position Angle vs. Time for PSR 0809+74 at 235 MHz

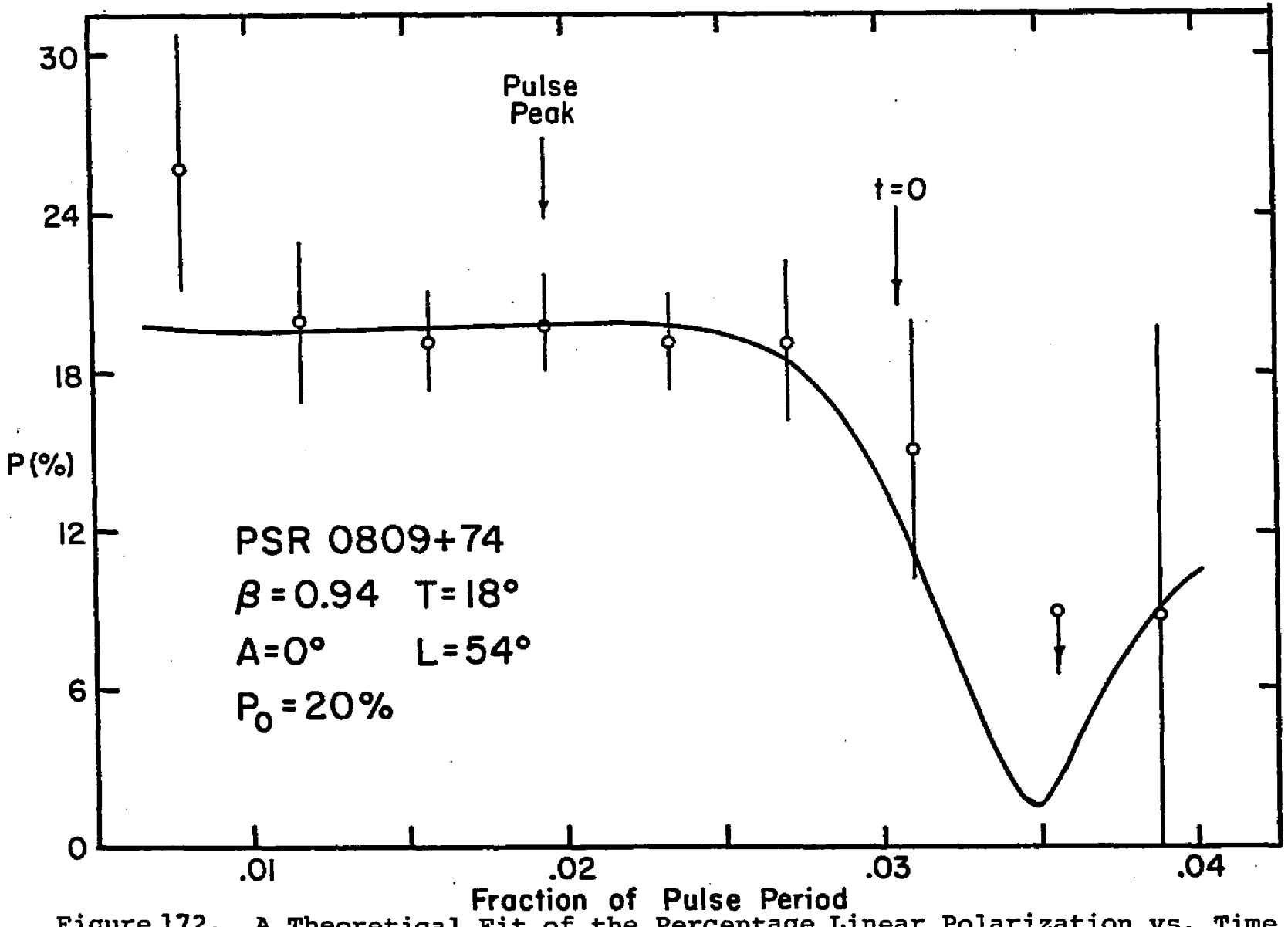

Figure 172. A Theoretical Fit of the Percentage Linear Polarization vs. Time for PSR 0809+74 at 235 MHz

Manchester et al. (1974) published plots of the polarization timed behavior for PSR 0809+74 which have a much greater maximum amount of polarization than those used in our model fit. Also, they found that the position angle goes through a rapid swing near polarization minimum just as our model fit predicts. However, the total swing of position angle they report then is about 90°, rather than the about 180° in our model fit. Presumably, using the new data of Manchester et al. (1974) our model fit would have a few changed parameters. However, the important fit of the parameter β will be changed little if any, since in our fits it depends mainly on the time between polarization maximum and minimum, a value almost unchanged between the two sets of data.

E. Discussion of Results and Restrictions on a Possible Model

It is remarkable that the fits of the relativistic vector model to the observations, which were obtained in Section II.D., all have the percentage linear polarization going nearly to zero at some point in the pulse, or slightly after the pulse fades out in the case of PSR 0833-45. Of course, the assumption made in that section was that $P = P_o \sin \phi$. If really $P = P_o \sin^n \phi$ where n is a number larger than 1, the fact that $P \gtrsim 0$ would not be surprising. The values of the parameters for the

fit in that case would not be greatly changed. However, if $n = 1$, as we have assumed to this point, it would appear that we only see pulses which are going to go through $\sin \phi \approx 0$, even though at the beginning of the pulse, $\sin \phi$ may have any value up to 1. Such a circumstance would seem to either place the observer in a preferred geometrical position for each pulsar, or to imply that something is going on which is not understood in terms of the simple model used.

It may be that $P \approx P_o \sin^3 \phi$, as would be the case for cyclotron radiation, or it may be that the percentage polarization depends on the angular distance of the line of sight from a plane, rather than a vector, as would be the case for curvature radiation. In that case it would be much more probable that any locus of the line of sight would pass through the plane of zero polarization at some time. If the locus of the line of sight were nearly a great circle in the emission frame (i.e., if $T \approx 0°$), the angle between the line of sight and the plane would closely mimic the angle between the line of sight and the point of intersection of the plane and the great circle, to within a multiplicative constant. In either case, the model as it stands would still yield parameters for the location of emission region which were nearly correct.

The values of the parameters β and T used in the model fits are of great interest. Regardless of the values of A or L finally agreed upon, the fits of the model in the "heart-shaped" diagrams would be dependent mainly on β and T, and so these values should survive major modifications in the combination of A and L. We will attempt to relate the values of both β and T to other aspects of the pulsars, such as their periods and types.

Figure 173 shows a plot of the adopted value of $\gamma = (1-\beta^2)^{-1/2}$ for the pulsars fitted, versus the pulsar rotational period in a log-log plot. Error bars are estimated from the uniqueness of the model fits. The four longer period pulsars seem to lie along a straight line of $\gamma = 2.81\ p^{0.174}$, with the Crab pulsar not far away from the line. Using this tentative relation, let us find out what the sub-pulse versus period relation should be for radiation unbeamed in the emission frame and for $T = 0°$.

We start from scratch. According to Equation (7) of this dissertation R is

$$R = [\gamma(1-\beta \cos \delta)]^{-3-\varepsilon}$$

if the spectrum is approximately power law with $I \propto \nu^{-\varepsilon}$. Since $\cos \delta = \cos \theta \cos T$, for $T = 0°$,

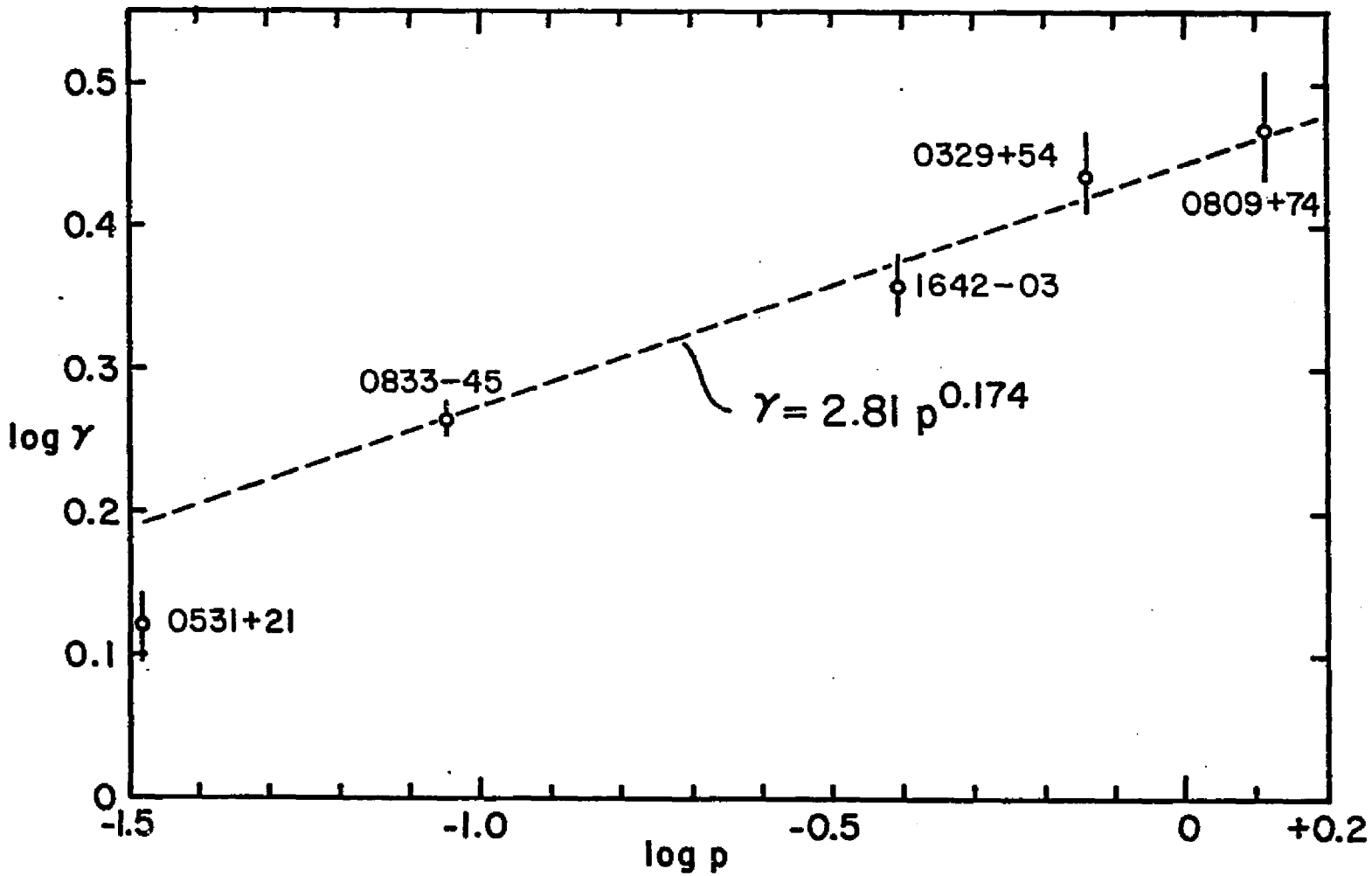

Figure 173. The Tentative Log γ-Log p Relationship

$$R = [\gamma(1-\beta \cos \theta)]^{-3-\varepsilon} .$$

R of course reaches its maximum value at cos θ = 1, and

$$R_{max} = [\gamma(1-\beta)]^{-3-\varepsilon}$$

then. When the value of R is at half its maximum value, we will see the intrinsically unbeamed emission at half strength, or, at $R = \frac{1}{2} R_{max}$,

$$[\gamma(1-\beta \cos \theta)]^{-3-\varepsilon} = \frac{1}{2} [\gamma(1-\beta)]^{-3-\varepsilon}$$

and

$$(1-\beta \cos \theta) = (2)^{\frac{1}{3+\varepsilon}} (1-\beta) ,$$

and

$$\beta \cos \theta = 1 - (2)^{\frac{1}{3+\varepsilon}} (1-\beta) .$$

Now for small θ, cos $\theta = 1 - \theta^2/2$, so we have

$$\beta(1 - \frac{\theta^2}{2}) \simeq 1 - (2)^{\frac{1}{3+\varepsilon}} (1-\beta)$$

and after some algebra

$$\theta \simeq \frac{2(1-\beta)}{\beta} \left(2^{\frac{1}{3+\varepsilon}} - 1\right) .$$

Since

$$\frac{1}{\gamma^2} \simeq 2(1-\beta) \quad \text{for large } \beta ,$$

$$\theta \simeq \frac{1}{\gamma\sqrt{\beta}} \left(2^{\frac{1}{3+\varepsilon}} - 1\right) .$$

For small θ, $\sin\theta \simeq \theta$, and from (8.5) we have

$$t \simeq \theta(1-\beta)/\Omega$$

which gives for the half-power point

$$\frac{2\pi t_{\frac{1}{2}}}{p} \simeq \frac{1-\beta}{\gamma} \frac{1}{\sqrt{\beta}} \left(2^{\frac{1}{3+\varepsilon}} - 1\right)$$

and, reducing $1-\beta = 1/(2\gamma^2)$, we have

$$\frac{2\pi t_{\frac{1}{2}}}{p} \simeq \frac{1}{2\gamma^3} \left(2^{1/(3+\varepsilon)} - 1\right) ,$$

since for $\beta \simeq 1$, $\sqrt{\beta} \simeq 1$, and

$$\frac{2\pi t_{\frac{1}{2}}}{p} \simeq \frac{1}{2\gamma^3} \quad 2^{1/(3+\varepsilon)} - 1 \qquad (34)$$

which is the half-width at half maximum. The full width at half maximum, which we will call W_o, is

$$W_o = 2\ t_{\frac{1}{2}} \simeq \quad (2^{1/(3+\varepsilon)} - 1) \frac{p}{2\pi\gamma^3} \quad .$$

ε for pulsars in the radio range varies from ~0.6 to ~2.5, corresponding to $2^{1/(3+\varepsilon)} - 1$ from ~0.365 to ~0.46. We will take the value of 0.4 to be representative, so that

$$W_o \sim \frac{0.4}{2\pi} \frac{p}{\gamma^3}$$

in agreement with Smith (1971a). Using the relation $\gamma = 2.81\ p^{0.174}$ which we found earlier, we combine the two to find

$$W_o \simeq 0.0029\ p^{0.478} \quad .$$

In Figure 174 is shown an adaptation of Figure 18a from Taylor et al. (1974) whereon are plotted the mean sub-pulse widths for pulsars versus period. As you can see, no pulsar shown has a sub-pulse width as small as our

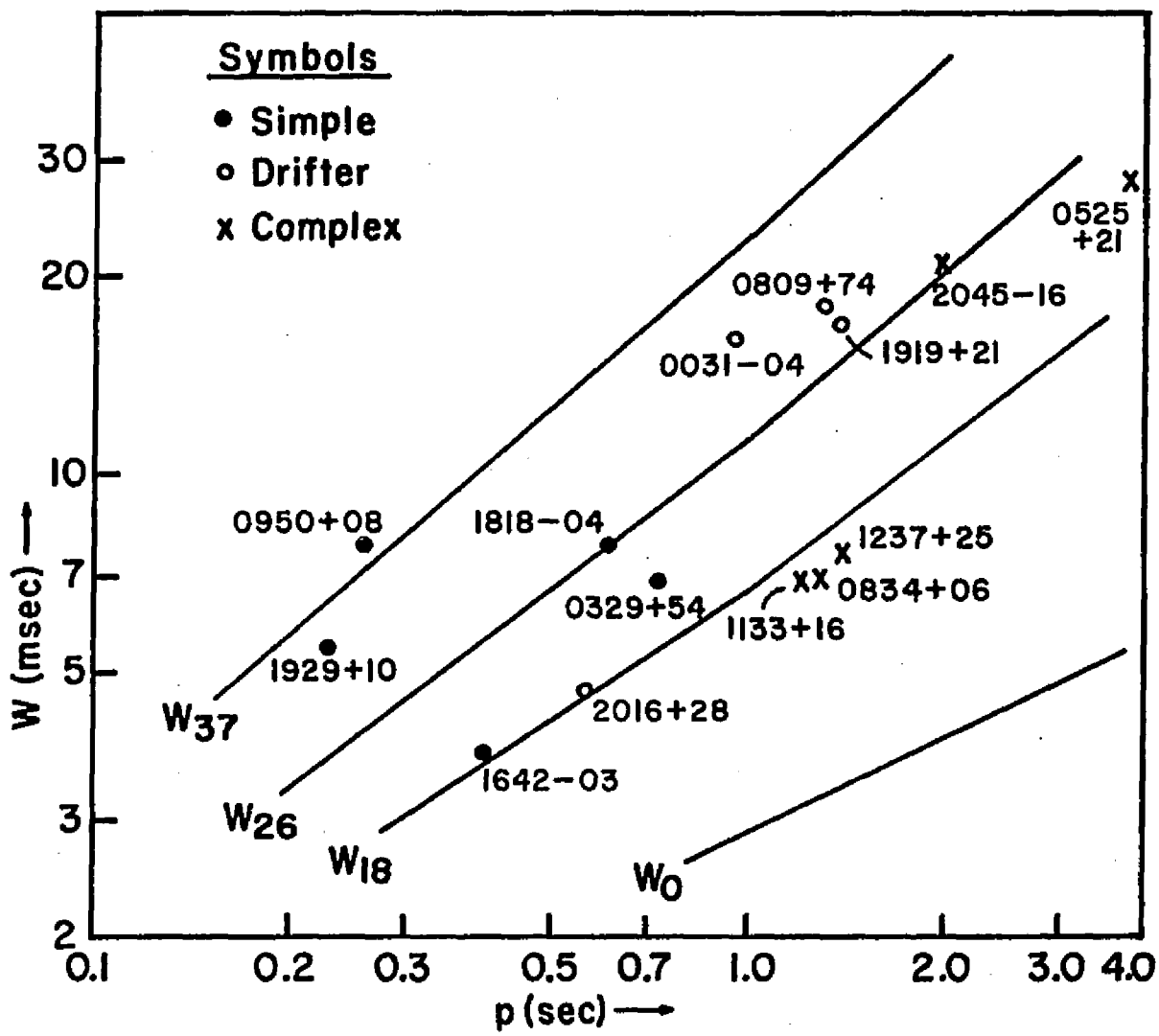

Figure 174. A Theoretical Period-Sub-Pulse-Width Distribution

relation derived above, which is also shown. For a value of $T \neq 0$, Equation (34) becomes

$$\frac{2\pi t_{\frac{1}{2}}}{p} \simeq (1-\beta \cos T)^{3/2} \sqrt{\frac{2}{\beta}} \quad 2^{1/(3+\varepsilon)} - 1 \qquad (35)$$

which is significantly different from Equation (34) for all values of β. The ratio of $t_{\frac{1}{2}}$ from Equation (35) to that from Equation (34) is a steeply increasing function of β, and thus of p. The lines in Figure 174 show the full width at half maximum calculated from Equation (35), W_{18} corresponding to $T = 18°$, W_{26} to $T = 26°$ and W_{37} to $T = 37°$.

This diagram is interesting for many reasons. First of all, one would expect, if there were no beaming in the emission frame, that the pulsars would form a continuous distribution down to the $T = 0°$ line. They do not, however. In fact, a lower limit to their distribution seems to be a line parallel to the W_o line but about 3 times higher.

There are certain kinds of beaming in the emission frame which could produce this result. For instance, if the radiation were beamed along the magnetic field line direction, the intrinsic beaming would generally be high where the relativistic beaming was low and vice versa. This can be seen by inspection of $\sin \phi$ when $t = 0$ for

small values of T in Figures 69 through 121. Such a circumstance will lead to wider sub-pulses than will an isotropic pattern in the emission frame, provided the intrinsic beam pattern is not too narrow.

Another indication that the W_o line is not correctly placed is the model fit to PSR 1642-03, which in the relativistic vector model seems to yield $T = 6°$, not $T \simeq 15°$ as it is placed on the theoretical sub-pulse width versus period diagram.

These considerations are evidence that there may be a degree of beaming intrinsic to the emission reference frame, as well as a component of relativistic beaming.

Secondly, the $T = 0°$ line for full width at half maximum has the dependence

$$W \propto p^{0.478} ,$$

remarkably close to the empirical law for sub-pulse widths which Taylor et al. (1974) derived of

$$W \propto p^{0.5} .$$

Thirdly, there seem to be no pulsars having $T \gtrsim 40°$. This is explainable in terms of the relativistic vector model in the following way. If we only see pulsars

for which our line of sight coincides with the magnetic field line, and A ≈ 0°, this implies (see Section I.B., Equation 21) that

$$\sin L \approx \pm \gamma \sin T \quad .$$

For a typical pulsar γ of about 2, this means that for $\sin T \gtrsim 1/2$, or $T \gtrsim 30°$, no field line will coincide with our line of sight and no pulsar will be seen. This is indirect evidence both that there is intrinsic beaming along field lines, and that $A \neq 90°$ for field lines of pulsar emission, for then, from Equation (24), there is no such restriction on T.

Fourth, pulsars of different classifications occupy different regions of the diagram. We can make these general statements:

(1) All pulsars of period less than about 0.8 seconds are of type S, with the exception of PSR 2016+28. If there is indeed a valid log γ-log p relation, this means that type S pulsars are those in which emission comes from well inside the speed-of-light cylinder where (a) the magnetic field is strong, and (b) inertial forces may not be as disruptive of the field as they would be nearer the speed-of-light cylinder. Both of these facts might help explain the simplicity and lack of periodic

modulation seen in the integrated pulse shape of type S pulsars.

(2) All pulsars of period greater than 0.8 seconds which have relatively high values of T are seen as drifters (type D).

(3) All pulsars of period greater than 0.8 seconds which have relatively low values of T are seen to have complex integrated pulse shapes (type C). This agrees well with the hypothesis advanced in Section II.C. that complex integrated pulse shapes might correspond to low values of T and L, so that a beam which is stronger along the magnetic field line would appear double or triple, with a component corresponding to each time of $\sin \phi \approx 0$ and a possible component from pure relativistic beaming in between.

In conclusion, if the tentative log γ-log p relationship derived from fitting models of polarization is valid, many of the differences between pulsars can be understood in terms of differences in the orientation of the rotation axis with respect to the plane of the sky and differences in the corotational velocities of the emission regions. The period-sub-pulse width distribution is well accounted for if the emission in the emission frame is beamed along the magnetic field line.

The evidence that the emission regions of pulsars are corotating relativistically with their central neutron stars is both straightforward as in the good fits to the polarization properties with the simplest relativistic model, and inferential, as in the inability of non-relativistic models to reproduce the changes in sub-pulse polarization position angle. The evidence that the radiation is beamed along magnetic field lines in the emission frame is both simple, as in the good prediction of the quantitative light curve changes with color in the Crab Nebula pulsar, and complex, as in the interpretation of sub-pulse widths in the period-sub-pulse width diagram as based on a tentative log γ-log p relation. The evidence that there is more than one emission process occuring in some pulsars is both clear, as in the case of pulsars showing sub-pulses of orthogonal polarization at the same rotational phase, and muddled, as in the conjecture that the polarizations of the radio and optical radiation from the Crab Nebula pulsar are orthogonal. Many previously unexplained features of pulsar emission are consistent with all of the above inferences.

Thus, although we fail to provide a physical model to explain the emission, we have seen that much can be explained by the geometry and location of the emission regions. With a few simple assumptions and a lot of hard

labor a true physical model will, I am sure, be arrived at soon. I believe it must incorporate the following features:

(1) The emission regions must be localized, either by making particle emission from the surface a strong function of magnetic field strength, or by other means.

(2) The emission processes must be capable of producing a high degree of circular polarization (in most pulsars).

(3) The radio radiation must be made in a coherent way, either by particle bunching or by stimulated processes.

(4) The emission must come from far out in the magnetosphere, where corotation speeds are a sizable fraction of the speed of light.

(5) The emission must be beamed even in the emission frame, and probably is beamed along the local magnetic field lines.

(6) The value of A is probably not 90°, implying that the field lines on which emission takes place are open field lines, not closed field lines.

Further work with the relativistic vector model may help narrow the specifications of the physical processes. It is hoped that the present dissertation is a

step in the right direction, toward a better understanding of those mysterious pulsars.

LIST OF REFERENCES

Albats, P., Frye, G. M., Tomson, G. B., Hopper, V. D., Mace, O. B., and Thomas, J. A. (1974) Nature, in press.

Argyle, E. (1973) Ap. J. 183, 973.

Backer, D. C. (1973) Ap. J. 182, 245.

Cocke, W. J. (1973) Ap. J. 184, 291.

Cocke, W. J., Ferguson, D. C., and Muncaster, G. W. (1973) Ap. J. 183, 987.

Cocke, W. J., and Holm, D. A. (1972) Nature Phys. Sci. 240, 161.

Cocke, W. J., and Ferguson, D. C. (1974) Ap. J., in press.

Disney, M. J. (1971) Astrophys. Lett. 9, 9.

Drake, F. D. (1971) IAU Symp. No. 46, p. 73.

Eastlund, B. J. (1970) Nature 225, 430.

Ekers, R. D., and Moffet, A. T. (1969) Ap. J. (Letters) 158, L1.

Elitzur, Moshe (1974) Ap. J. 190, 673.

Ferguson, D. C. (1971a) Nature Phys. Sci. 234, 86.

Ferguson, D. C. (1971b) Am. Journ. Phys. 39, 1089.

Ferguson, D. C. (1973) Ap. J. 183, 977.

Ferguson, D. C., Cocke, W. J., and Gehrels, T. (1974) Ap. J. 190, 375.

Gower, J. F. R., and Argyle, E. (1972) Ap. J. (Letters) 171, L23.

Ginzburg, V. L., and Syrovatskii, S. I. (1965) Ann. Rev. Astr. & Ap. 3, 297.

Hankins, T. H. (1971) Ap. J. 169, 487.

Hankins, T. H. (1973) Ap. J. (Letters) 181, L49.

Harnden, F. R., Jr., and Gorenstein, P. (1973), Nature 241, 107.

Harnden, F. R., Jr., Johnson, W. N. III, and Haymes, R. C. (1972) Ap. J. (Letters) 172, L91.

Hegyi, D., Novick, R., and Thaddeus, P. (1971) IAU Symp. No. 46, p. 129.

Horowitz, P., Papaliolios, C., and Carleton, N. P. (1972) Ap. J. (Letters) 172, L51.

Kristian, J., Visvanathan, N., Westphal, J. A., and Snellen, G. A. (1970) Ap. J. 162, 475.

Kemp, J. C., and Wolstencroft, R. D. (1974) MNRAS 166, 1.

Komesaroff, M. M., Hamilton, P. A., and Ables, J. G. (1972) Australian J. Phys. 25, 759.

Lerche, I. (1974) Ap. J. 187, 597.

Lyne, A. G., Smith, F. G., and Graham, D. A. (1971) MNRAS 153, 347.

McCrea, W. H. (1972) MNRAS, 157, 359.

McCrea, W. H. (1973) Nature 241, 423.

McCulloch, P. M., Hamilton, P. A., Ables, J. G., and Komesaroff, M. M. (1972) Astrophys. Letters 10, 163.

Manchester, R. N. (1971a) Ap. J. Suppl. #199, 23, 283.

Manchester, R. N. (1971b) Nature Phys. Sci. 231, 189.

Manchester, R. N., Tademaru, E., Taylor, J. H., and Huguenin, G. R. (1973) Ap. J., 185, 951.

Manchester, R. N., Taylor, J. H., and Huguenin, G. R. (1974) Ap. J., in press.

Muncaster, G. W., and Cocke, W. J. (1972) Ap. J. (Letters) 108, L13.

Oke, J. B. (1969) Ap. J. (Letters) 156, L49.

Pacholczyk, A. G. (1970) Radio Astrophysics (Freeman, San Francisco), p. 131.

Papaliolios, C., Carleton, N. P., and Horowitz, P. (1970) Nature 228, 445.

Radhakrishnan, V., and Cooke, D. J. (1969) Astrophys. Lett. 3, 225.

Radhakrishnan, V., Cooke, D. J., Komesaroff, M. M., and Morris, D. (1969) Nature 221, 443.

Rankin, John M., Campbell, D. B., and Backer, D. C. (1974) Ap. J. 188, 609.

Schönhardt, R. E. (1971) IAU Symp. No. 46, p. 110.

Smith, F. G. (1970) MNRAS 149, 1.

Smith, F. G. (1971a) MNRAS 154, 5P.

Smith, F. G. (1971b) Nature Phys. Sci. 231, 191.

Smith, F. G. (1972) Reports on Progress in Physics 35, 399.

Smith, F. G. (1974) MNRAS 167, 43P.

Sturrock, P. A. (1970) Nature 227, 465.

Sturrock, P. A. (1971) Ap. J. 164, 529.

Sturrock, P. A. (1974) U.S./Australia Specialist Symposium, Stanford U. 1974, Jan. 21-25.

Sutton, J. M., Staelin, D. H., and Price, R. M. (1971) IAU Symp. No. 46, p. 89.

Taylor, J. H., and Huguenin, G. R. (1971) Ap. J. 167, 273.

Taylor, J. H., Huguenin, G. R., Hirsch, R. M., and Manchester, R. N. (1971) Ap. Letters 9, 205.

Taylor J. H., Manchester, R. N., and Huguenin, G. R. (1974) Ap. J., in press.

Wampler, E. J., Scargle, J. D., and Miller, J. S. (1969) Ap. J. (Letters) 57, L1.

Zheleznyakov, V. V. and Shaposhnikov, V. E. (1972), Ap. and Space Sci. 18, 166.